THREE DIMENSIONAL STATIC AND DYNAMIC ANALYSIS OF HYBRID PLATE USING MULTI-TERM MULTI-FIELD EXTENDED KANTOROVICH METHOD

A Thesis Submitted in
Partial Fulfillment of the Requirements
for the Degree of

DOCTOR OF PHILOSOPHY

by

SUSANTA BEHERA
(Roll No: 136103018)

to

DEPARTMENT OF MECHANICAL ENGINEERING
INDIAN INSTITUTE OF TECHNOLOGY GUWAHATI,
GUWAHATI-781039, INDIA
August, 2018

Certificate

This is to certify that the thesis entitled "**THREE DIMENSIONAL STATIC AND DYNAMIC ANALYSIS OF HYBRID PLATE USING MULTI-TERM MULTI-FIELD EXTENDED KANTOROVICH METHOD**" being submitted by **Mr. Susanta Behera** to the Indian Institute of Technology, Guwahati, for the award of the degree of Doctor of Philosophy in Mechanical Engineering is a record of original bonafide research work carried out by him under my supervision and guidance. The thesis work, in my opinion, has reached the requisite standard fulfilling the requirements for the degree of Doctor of Philosophy.

The results contained in this thesis have not been submitted in part or full to any other University or Institute for the award of any degree or diploma.

Dr. Poonam Kumari

Department of Mechanical Engineering

Indian Institute of Technology Guwahati

Guwahati - 781039

Declaration

I, Susanta Behera (Roll no: 136103018) declare that the present written submission is my thoughts in my own words. I have adequately cited and referenced the original sources, where other's ideas have been involved. I also declare that I have adhered to all principles of academic honesty and integrity and have neither fabricated nor falsified any idea/data/fact/source in my submission. I understand that any violation of the above will be cause for disciplinary action by the Institute and can also evoke penal action from the sources which have thus not been properly cited or from whom proper permission has not been taken when needed.

(Susanta Behera)

Date: Roll No. 136103018

Acknowledgements

It is a great pleasure to express my deepest gratitude to Dr Poonam Kumari, my PhD advisor, for her unfading patience and persistent support in carrying out my PhD study and associated research work. Her in-depth research knowledge and sublime work ethics influenced me immensely to work in dedication throughout my PhD tenure which I am proudly taking with me for the rest of my life. She nurtured me to evolve as a researcher and has been a tremendous mentor for me. I am proud to have her as my PhD advisor.

I would like to express my deepest thanks and sincere appreciation to my doctoral committee members Prof. K. S. R. K. Murthy and Prof. Debabrata Chakraborty, *Professors of Mechanical Engineering Department* and Prof. K. D. Singh, *Professor of Civil Engineering Department*, for their valuable time, brilliant comments and suggestions, but also for the hard questions which helped me to refine and widen my research from various perspectives.

I thank my colleagues and fellow researchers especially Agyapal Singh, Shranish Kar and Abhisekh Yadav for their help and support in various academic and non-academic activities.

Finally, I would like to thank my parents for their love, care, patience, support and firm faith on me which kept me motivated throughout my PhD period and my life in general.

Susanta Behera

Abstract

Laminated composite structures are extensively used in aerospace vehicles, marine applications, automotive and various other industries for their high specific strength, design flexibility and requiring low maintenance. These structures with embedded or surface bonded piezoelectric layers often called as smart or intelligent or hybrid structures offer additional advantage of sensing and control apart from their primary structural responsibility. The smart structures are extensively used in structural health monitoring, shape and vibration control applications, but the presence of geometric and material inhomogeneity across the layers introduce complex electromechanical couplings inducing sharp stress variations near the non-simply supported edges. So, the analysis of such structures with high accuracy demand special tools with greater computational efficiency. Three dimensional (3D) analytical solutions are the most efficient tools for analysis of smart or hybrid laminated structures which can compute the global as well as local responses more accurately. In this thesis, three dimensional extended Kantorovich method (3D EKM) is used to obtain the static and free vibration elasticity/piezoelasticity solution of hybrid rectangular laminated plates and results from two dimensional (2D) zig-zag and third order theory are assessed with respect to the 3D solutions.

The generalized coupled three-dimensional piezoelasticity solution for multi-layered composite plates integrated with piezoelectric layers subjected to Levy-type boundary conditions is presented using the mixed-field multi-term extended Kantorovich method (EKM) and Fourier series expansion. A mixed formulation approach in which displacement as well as stresses are taken as state variables in the solution domain is followed. The initial functions are not required to satisfy the essential or natural boundary conditions and the solution converges very fast. The convergence and accuracy of this method is established by comparing the results with the 3D exact solution, wherever available, and with the 3D finite element (FE) solution for the rest

for both pressure and potential loading cases. The anomalies and pitfalls of the FE solution in predicting stress responses at or near to the edges are pointed out. The effect of adhesive layer between the face and elastic substrate is also investigated and found that it eases out the sharp stress variations at the layer interface. The method is further extended to the free vibration analysis of finite dimensional elastic laminated plates. Results are presented for various laminate lay-ups and boundary conditions and are extensively validated by comparing with the results of other theories and 3D FE results. Benchmark natural frequencies and mode shapes are presented for laminated composite and sandwich plates. It is found that single term solution is sufficient enough for obtaining accurate natural frequencies, but stresses near the clamped edge are accurately predicted by multi-term (n=2) solution. The effect of span-to-thickness ratio and in-plane modulus ratio on the natural frequency is also studied. The effect of adhesive modulus, density and layer thickness on the free vibration behaviour of elastic laminated plates is also investigated. The 3D EKM has also been extended to investigate the free vibration behaviour of Levy-type hybrid laminated composite and sandwich plates integrated with piezoelectric actuators and sensors. The accuracy and efficacy of this method is verified thoroughly by comparing it with the existing results in the literature and FE solutions. The numerical results are presented for bimorph, hybrid composites and sandwich plates. Effect of piezo-layer thickness, electric circuit conditions and plate aspect ratios on the natural frequency are also investigated. Effect of adhesive layer on the free vibration characteristics of a bimorph plate is also investigated.

Apart from the above 3D analysis, analytical solutions for the free vibration of Levy-type rectangular elastic laminated plates based on efficient layerwise 2D zig-zag theory and the third order theory (TOT) are also presented. The 2D results are assessed in comparison with the 3D elasticity solution to estimate its accuracy. Further, the analysis is extended for the piezoelasticity static and free vibration solution of hybrid rectangular plates. The improved zig-zag theory (IZIGT) and its smeared counterpart, the improved third order theory (ITOT) are developed to obtain the results and are assessed for the accuracy with respect to the 3D piezoelasticity solution of 3D EKM.

Contents

List of Figures

List of Tables

Chapter 1

INTRODUCTION

1.1 PREFACE

With the advancement of technology, one of the major ambitions in any modern technological fields like aerospace and automobile industries, is to make the systems ultra-reliable with a near-zero incidence of failure and to fulfill stringent performance requirements under challenging environments. So being capable of detecting the damage or failure in advance is the key step in this direction. This has led to the concept of advanced high-performance control systems and multi-functional structures wherein multiple properties of materials are exploited in such a way that besides its major designated functionality, the same structural components can accomplish at least one more task of the host structure, such as active vibration control, health monitoring etcetera. Composites and sandwich laminates with embedded or surface-mounted piezoelectric sensors and actuators (hereafter called as smart hybrid plates and smart hybrid sandwich plates) form a very important part of this new generation of smart structures for active vibration control, acoustic control, shape control, damage identification and compensation (health monitoring) applications. The term hybrid denotes to the heterogeneous nature of laminated plates. Recent developments of the piezoelectric fibre reinforced composite (PFRC) with high strength (maximum strain of 2300 microstrain), toughness, operating range (-1500 to 2800 V) and life (200 million cycles), conformability to curved shell surfaces and broadband have widened the scope of its use as distributed piezoelectric sensors and actuators in smart structures [1].

Many structural elements in aerospace vehicles, automobiles, ships, submarines and process equipment can be modelled as beams, rectangular plates, and cylindrical shells. Analytical three-dimensional (3D) piezoelasticity solutions of hybrid beams, rectangular plates, and cylindrical

shells are mostly available for simply-supported boundary conditions, in which case an assumed series expansion in the in-plane coordinates which satisfy the boundary conditions (BCs) at the edges identically, converts the partial differential equations (PDEs) into ordinary differential equations (ODEs). Consequently, the advanced two-dimensional (2D) laminate theories are commonly assessed for their accuracy in comparison with 3D solutions for simply supported boundary conditions. however, such an assessment can at best provide an incomplete picture since no special effects known as boundary effects are observed on the simply-supported edges [2] as opposed to clamped (C) and free (F) edges. So, to accurately predict the stress fields near the non-simply supported edges analytical solutions are most proficient the importance of which has been shown by Pipes and Pagano [3]. In most practical applications, piezoelectric materials as thin layers are surface mounted on a host structure as distributed sensors and actuators for control and sensing purpose. In such smart hybrid plates, the edge effect is more complex due to the presence of electromechanical coupling and can lead to the loss of actuation and sensing authority of the piezoelectric layers. A 3D finite element analysis (FEA) results in large problem size in proportion to the number of layers which often become computationally intractable and also encounters challenges when the piezoelectric layers are thin compared to the elastic substrate. Accurate estimation of the free edge stress field of both hybrid elastic and smart hybrid piezoelectric composite and sandwich plates is thus an essential component in composite and smart structure engineering, for achieving the reliable design of these structures. In spite of the fact that the determination of interlaminar stresses at the free edges has been one of the key issues of research since the year 1967 [4], no analytical 3D elasticity solution satisfying all boundary and interface conditions at the free edges existed so far. This research work proposes the development of accurate analytical 3D piezoelasticity solutions for smart hybrid-rectangular plates integrated with monolithic piezoelectric/PFRC sensors and actuators, subjected to arbitrary boundary conditions under electromechanical loading using a powerful extended Kantorovich method (EKM). It is also proposed to develop 3D piezoelectric solutions for the dynamic response of the same. Dynamic solution based on efficient and accurate zigzag theory is also developed for Levy-type rectangular hybrid plates so as to assess the theory for predicting dynamic response and boundary effects. The general hybrid rectangular plate configuration considered for analysis in the present work is as shown in Fig. 1.1. The plate has dimensions $(a \times b \times h)$ as width, length and thickness, respectively and consists of L orthotropic

layer with cross-ply (0^0 or 90^0) lay-up.

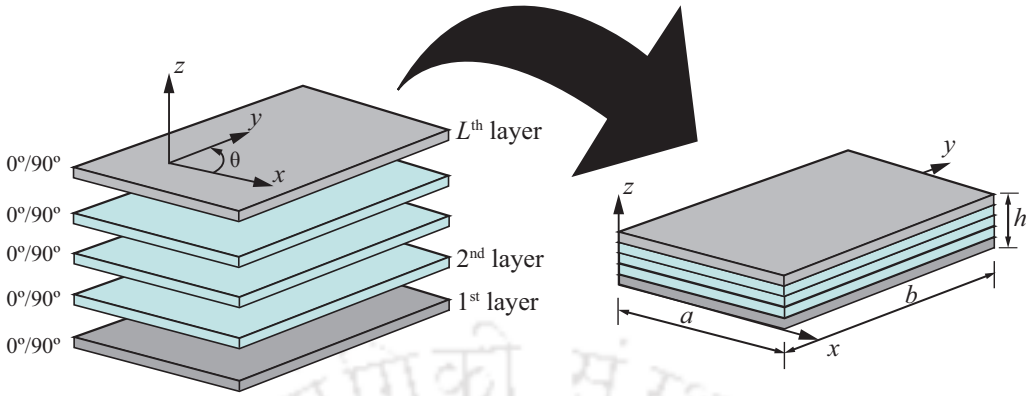

Figure 1.1: General configuration of a rectangular hybrid plate.

1.2 HISTORICAL BACKGROUND OF EKM

In Ritz or Galerkin method, an approximate solution is usually assumed as series of products of unknown coefficients and a bi-variable function chosen along the coordinates where the functions are assumed in such a way that it satisfies the kinematic boundary conditions in Ritz case while both kinematic and kinetic boundary conditions in Galerkin case. Therefore, the solution accuracy and convergence highly depend on the initial choice of functions. To eliminate this dependence, the Russian mathematician and economist Leonid Vitaliyevich Kantorovich (joint winner of Nobel Memorial Prize in economic sciences, 1975) proposed a method in the year 1936 in his remarkable book *Approximate Methods of Higher Analysis* [5] with co-author Vladimir Ivanovich Krylov, the English version [6] of which was published in 1958. In this method, a bivariate function $\phi_m(x, y)$ is assumed in the form as, $\phi_m(x, y) = f_1(x) \cdot g_1(y)$, where $f_1(x)$ is unknown function of x and $g_1(y)$ is a priori known function of y. Upon substitution in variational equation and using the fundamental Lemms of variational calculus, an ordinary differential equation along x-axis is obtained which is solved by satisfying the boundary conditions exactly. Therefore, solution accuracy depends upon the initial choice of function along y-direction only. This technique is known as Kantorovich method.

In year 1968, Kerr [7] modified the Kantorovich method by introducing the concept of iterative step calculation to further eliminate the dependence along y-axis. In this technique, instead of stopping the calculation after the other part of the function unknown is obtained, the obtained function from the first step is taken as known a priori function for the next calculation

step. This calculation steps continue iteratively until a desired convergence is achieved. Afterwards this method is known as extended Kantorovich method (EKM). In this method the initial chosen function is not required to satisfy the boundary conditions of the problem and hence can be selected arbitrarily. Besides the above advantage of EKM, the convergence in solution is achieved very fast which is examined in the present work in successive Chapters.

1.3 LITERATURE REVIEW

A brief survey of literature concerning the specific analysis type is presented in this section and in the succeeding subsections addressing the advancement of work done up to the date. Based on the nature of displacement field approximation along the thickness, piezoelasticity solutions of smart structures can be divided into two main categories: (a) two-dimensional theories and (b) three-dimensional theories. The 2D theories though can predict results well in acceptable accuracy for thin plates and shells only with low computational complexity, but for high accuracy and for thick plates and shells, 3D theories are the foremost tools.

Some extensive reviews on different 2D and 3D theories for beams, plates, and shells can be looked through the articles [8–11] for elastic and [12–20] for hybrid piezoelectric case, adding with them the most recent review article [21] on bending, buckling, vibration, and 3D stress analysis by extended Kantorovich method. A review of the literature on the free vibration analysis of elastic laminates can be found in the recent review article presented by Sayyad and Ghugal [22]. In the succeeding subsections, literature relevant to the scope of this work is presented.

1.3.1 Pioneered Researchers in the Field of Piezoelasticity

Ever since the brothers Jacques and Pierre Curie discovered piezoelectricity, in the year 1880, which is the phenomenon of internal generation of electricity resulting from applied mechanical pressure, the research on piezoelectric materials and its applications have come a long way though still remained a major research focus. This phenomenon of piezoelectricity is exploited in a number of useful applications in modern technology, such as piezoelectric inkjet printing, sound navigation and ranging (SONAR), vibration control, structural damage detection and health monitoring, to name a few. Accordingly, various theories are developed accommodating the intermingling of elastic and electric effects of piezoelectricity. The research

on piezoelectric smart structures are few decades old. Here, in this section, a list of the pioneering works on smart structural applications of piezoelectric materials especially as composite beam/plate structures integrated with piezoelectric layers are presented. For active control of structural vibration Hanagud et al. [23] and Baz and Poh [24] developed methods of numerical simulations for a cantilevered elastic beam surface-bonded with piezoelectric actuators. By using the displacement based layer-wise theory Robbins and Reddy [25] analysed piezoelectrically actuated beams. Tauchert [26] studied piezothermoelastic behavior of a laminated plate. The vibration behaviour of smart plates are presented by Chandra and Agarwal [27] and Batra et al. [28] whereas for shells Tzou and Zhong [29]. Ray et al. [30, 31] contributed the 2D exact static analysis of smart laminated plate structures whereas Bisegna and Maceri [32] presented 3D exact solution for rectangular piezoelectric plates. The following Table 1.1 lists some more number of pioneered researchers and their contribution to smart structural research.

Table 1.1: Authors pioneered in smart structure research

Author	Contribution
Chandra and Chopra [33]	Analytical and experimental investigation of composite beams with induced-strain actuators.
Heyliger [34]	Static analysis of laminated elastic/piezoelectric plates.
Tzou and Fu [35]	Distributed vibration sensing and control of continua using segmented distributed piezoelectric sensors and actuators.
Ghosh and Batra [36]	Shape control of plates using piezoceramic elements.
Xu et al. [37]	Thermoelectroelastic response of multilayered plates (3D solution).
Saravanos and Hopkins [38]	Local stresses in smart composite plates using discrete-layer theory.
Ashida and Noda [39]	Control of thermally induced normal elastic displacement of piezolaminated isotropic plate.
Dumir et al. [40]	Exact piezoelastic solution of circular cylindrical panel
Kapuria and Kumari [41]	First time extended EKM to 3D piezoelasticity case

1.3.2 Piezoelasticity Solution for Static Analysis of Smart Hybrid Plates

The localized stresses occurring within a short distance from the edges of laminated structures, caused by the widely different material properties in adjacent layers and the geometric discontinuity, are often responsible for the initiation of delamination and crack in these structures. The concentrated stresses are also critical for the fatigue life of structures. This so-called boundary layer stress field is truly three-dimensional (3D) in nature, and can not be predicted accurately by the simple two-dimensional laminate theories. The need for obtaining accurate analytical solutions for this 3D boundary layer stress field has been felt ever since Pagano and Pipes [3, 42] showed its importance on the integrity of these laminates. In many smart structural applications, thin layers of piezoelectric materials are surface-bonded to or embedded in the composite laminates to be used as distributed sensors and actuators, for achieving high-performance objectives such as active vibration control, acoustic control, shape control, and damage detection. In such smart hybrid plates, the edge effect is more complex due to electromechanical coupling and can lead to debonding of the piezoelectric sensors and actuators. An accurate understanding of the strain/stress transfer mechanism between the piezoelectric actuator/sensor and the host structure is also essential for the development and validation of simplified models for the same [43, 44].

Near the clamped/free edges, the stress field changes sharply. For such cases, the general purpose displacement based finite element may not be reliable in the vicinity of the edges [45, 46]. The limitations of the general finite element solution for addressing the edge effects have also been pointed out in a recent review article by Mittelstedt and Becker [47]. Analytical/semi-analytical three-dimensional solutions of piezoelectric plates with clamped/free support conditions can help to understand the edge effects and effect of electromechanical coupling on the same [47].

Few approximate analytical solutions of the 3D elasticity/piezoelasticity solutions have been reported for the elastic and piezoelectric laminated plates with non-simply supported edges, but in all of them, the boundary and interfacial continuity conditions are satisfied in an approximate sense.

Vel and Batra presented series solution using the Eshelby-Stroh formalism for the cylindrical bending [48] and general bending [49] of hybrid piezoelectric plates with arbitrary boundary

conditions. However, the boundary and interface conditions were satisfied in the sense of Fourier series, leading to an infinite system of equations, and its truncation even after a large number of terms (∼400), was seen to yield extra oscillations in the through-thickness variations of the out-of-plane stresses near the edge. Recently, Tahani and Andakhshideh [50] presented a 3D elasticity solution using the extended Kantorovich method for the general bending of rectangular laminated plates under arbitrary edge conditions. However, since they consider displacements as the primary variables, all boundary and interface conditions involving stresses are satisfied only in a weak integrated sense over the surface, and not exactly at all points. Since the stress field in the vicinity of the boundaries, which is of particular interest here, is highly sensitive to any such approximation, its prediction can not be reliable and therefore, this solution is not suitable for boundary layer stress field prediction. Very recently, a stress function based equivalent single-layer theory approach [51] has been employed to analyze the free edge interlaminar stresses of symmetrical hybrid laminated panels under symmetrical applied electric potential, without considering two-way electromechanical coupling [52]. Once again, the out-of-plane stress distributions showed undesired oscillations and were not predicted accurately.

The EKM, proposed by Kerr [7, 53], is a very powerful and elegant semi-analytical method for solving partial differential equations (PDEs). In this method, the PDEs of a bivariate problem is converted into two sets of ordinary differential equations (ODEs) in two directions, by approximating the solution as a series of products of two separable functions. The ODE in a given direction is obtained by assuming the functions in the other direction as known from initial guess or previous iteration. The iterative process converges fast (generally in two/three iterations), even when the initial trial functions do not satisfy the boundary conditions, and unlike in Ritz's and Galerkin's methods, the accuracy of the final solution is independent of the initial guess. The method has been shown to yield accurate results for several problems of elastic single layer [54, 55] and multi-layer plates [56–61], and shells [62, 63] subjected to arbitrary boundary conditions. In the recent past, it has been successfully applied to obtain the bending response of rectangular piezo-laminated plates using the classical laminate theory [64], and the first order shear deformation theory [65] without considering the two-way electromechanical coupling. The common feature of all these EKM solutions is that they are all based on 2D plate/shell theories and not on the 3D elasticity theory, and involve only homogeneous boundary conditions.

Kapuria and Kumari presented first a single-term EKM solution [66] and later a multi-term EKM solution [41] based on the 3D elasticity, for the cylindrical bending of anisotropic laminated panels subjected to arbitrary boundary conditions. A mixed formulation approach was followed, considering both displacements and some stresses as primary variables, which not only allows for the exact satisfaction of all homogeneous and nonhomogeneous boundary conditions, as well as interface continuity conditions at all points but also ensure the same order of accuracy for both displacements and stresses. It was shown in comparison with other available 3D elasticity solution and detailed 3D finite element analysis that the multi-term solution yields accurate results for all response entities including the stress field near the edges, with just two to three terms in the solution. The method has been extended to multi-field problem of 3D piezoelasticity solution for the cylindrical bending of hybrid piezolaminated panels with edge effects, considering full electromechanical coupling [67]. Kumari et al. [68] applied the multi-term EKM solution in conjunction with Fourier series to obtain the general bending response of elastic rectangular laminated plates subjected to Levy-type boundary conditions.

The lack of a coupled 3D piezoelasticity solution by EKM for Levy-type hybrid-rectangular plates, as reviewed from the literature, presented an opportunity to develop an accurate 3D piezoelasticity solution for hybrid piezolaminated rectangular plates with Levy-type boundary conditions under electromechanical loading using the mixed-field multi-term EKM is presented.

1.3.3 3D Elasticity Solution for Dynamic Analysis of Elastic Plates

The literature on free vibration of plates can be categorized into two broad categories as per the type of theories i.e. 2D solution and 3D elasticity solution. In the earlier stages of research, equivalent single layer models such as classical laminate [69], Mindlin plate [70, 71] and first order shear deformation [72–74] and third order shear deformation [75–77] theories were used to analyse the free vibration of composite plates. Navier and Levy approaches were used to obtain the natural frequencies and mode shapes of the composite plates. A comprehensive review of literature can be found in the recent review article presented by Sayyad and Ghugal [22]. These theories overestimate the natural frequencies and are valid for only thin sections. To overcome these issues, other layer-wise models are developed by researchers. But analytical solutions can be developed only for simply supported boundary conditions. Therefore a large number

of approximate (Ritz, Chebyshev Polynomials, Legendre Polynomials) and numerical solutions (FEM, DQM) are also developed, details of which can be found in Ref. [22, 78, 79]. But these numerical solutions have low efficiency, insufficient accuracy and slow convergence [80].

Recently, free vibration analysis of composite plate using dynamic stiffness method (DSM) which take the advantage of both analytical and numerical technique is presented by Fazzolari et al. [81] based on HSDT. Boscolo and Banerjee [82] presented free vibration analysis of laminated composite plates extending the DSM with the use of first order layer-wise theory based on Carrera unified formulation (CUF). Since it is a displacement based formulation and further natural boundary conditions are satisfied in the average sense, therefore boundary layer effect or stress variation near the clamped/free edge can not be predicted accurately. Very recently, Zuo et al. [80] presented free vibration analysis of laminated plates based on higher order shear deformation theory (HSDT) using wavelet finite element method. This method gives high accuracy, but results are presented for simply supported boundary conditions only.

Three-dimensional (3D) solutions can provide more accurate local and global behaviour of vibrating plates as compared to 2D methods [82–84]. Three-dimensional exact analysis for vibration of rectangular plates and laminate composites are presented for isotropic [85], orthotropic [86] and anisotropic composite plates [87, 88] which served as benchmark solution for assessing 2D theories and numerical solutions. The above 3D models are valid only for simply supported laminates. The boundary layer effects or the edge effects are absent for simply supported case. The edge effects significantly affect the vibrating response of laminated plates and further initiates the crack/damage to the structure. Therefore 3D analytical closed-form solutions are required not only to address the above concern but also act as benchmark solution for assessing the 2D approximate and 3D numerical solutions. Messina [89] presented 3D free vibration of isotropic and laminated rectangular plates using multi-segmented approach. Displacement based approach is used by satisfying essential boundary conditions along the mid-plane. Chen and Lü [90] presented the 3D vibration of Levy-type cross-ply laminated plates using state space method (SSM) in combination with the differential quadrature method (DQM) combinedly known as SSDQM. Using the same SSDQM, Lü et al. [91] carried out free vibration analysis for generally laminated plates. Zhang et al. [92] presented a free vibration analysis of composite laminates for simply supported and clamped boundary conditions by using the 3D

theory of elasticity and the DQ discretization method. Very recently, Eftekhari and Jafari [93] employing the DQM mixed with finite element method (FEM) presented the free vibration analysis of rectangular and skew Mindlin plates with general boundary conditions. However, DQM is known to have limitations in handling complex boundary conditions and irregular geometries pertaining to its global approach.

Very recently, Qu et al. [84] developed 3D free and transient vibration analysis of composite laminated and sandwich rectangular parallelepipeds. Multilevel partitioning hierarchy is employed to obtain the governing equations in terms of displacements. The functions are expanded in terms of polynomial along x, y and z axis. Very informative detailed discussion about the development of 3D free vibration solutions is given in this paper also. Hanukah and Givli [94] presented a 3D free vibration analysis of isotropic elastic skewed parallelepiped using Tailor's multi variable expansion.

Initially, Kantorovich [6] developed a method to remove the inherent limitation of Ritz and Galerkin methods i.e. satisfaction of natural and essential boundary conditions. This method gives exact solution along one direction whereas it depends on the initial choice of the function along second direction. Kapuria and Kumari [41] first time extended this method to the 3D elasticity case, before that it was limited to two-dimensional case only. Kumari et al. [68] further extended this method to develop 3D elasticity solution for laminated composite and sandwich plates. Recently, Kapuria and Dhanesh [95] developed 3D solution for composite laminated panels with interfacial imperfections. Bespalova [96] presented 3D free vibration analysis of isotropic parallelepiped using the extended Kantorovich method. Very recently, Huang et al. [97] studied the local stress concentrations at the vicinity of free edges in symmetrically layered composite laminates subjected to uniaxial tensile load using EKM.

As per the author's knowledge, 3D closed form free vibration analysis for composite and sandwich plates subjected to arbitrary boundary conditions is not available [84]. Apart from this, the following loopholes exist in the literature:

1. Fundamental lowest frequency is reported in the majority of works (numerical/analytical). For practical designing of structures, at least three consecutive frequencies should be known.

2. Majorly results were presented for composite plates. Sandwich plate results are not available for different boundary conditions. Even in the very recent article presented by Qu et al. [84], results for moderately thick simply supported sandwich plates are presented. No results exist for thick sandwich plates under arbitrary boundary conditions.

3. Mode shapes of laminated plates with arbitrary supports are not presented completely.

4. Bending and shear stresses due to the unit amplitude of motion are not presented. This information is very important for fatigue and fracture design of laminates.

1.3.4 3D Piezoelasticity Solution for Dynamic Analysis of Smart Hybrid Plates

The behaviour of hybrid structures is very complex and pose a difficult challenge for analysis because of coupling between electromechanical entities and stress concentration at interfaces which causes delamination failure in such structures used in different applications where these are subjected to heavy static and dynamic loads. Hence, an efficient tool is necessary to predict the behaviour of such structures with great accuracy. The 3D piezoelasticity solution can predict accurately the complex behaviour of piezoelectric laminated plates and also act as a benchmark for assessing various approximate 2D theories and further, can help in making suitable kinematics or kinetics assumptions for the development of 2D theories [18, 98]. A detailed review of 3D mathematical modelling and solution techniques for laminated piezoelectric plates and shells can be found in Ref. [15, 18–20].

Xu et al. [99] presented the vibration of initially stressed thermoelectroelastic multilayered plates. Pan and Heyliger [100] presented the free vibration of multilayered magneto-electro-elastic plates. Kapuria and Achary [101] developed a 3D harmonic analysis of piezoelectric plate and Kumari et al. [102] presented the harmonic analysis of hybrid piezoelectric and magnetoelastic angle-ply panels. The above 3D analyses were applied to analyze the all-round simply supported plates. There are very limited articles reported about the development of 3D analysis of piezoelectric plates subjected to arbitrary boundary conditions [20].

Some articles are presented for the vibration analysis of hybrid plates based on different numerical approaches i.e. 3D finite element [103], 3D differential quadrature [104] and 3D meshless methods [105, 106]. Numerical techniques are very time consuming and do not provide contin-

uous transverse stresses across the thickness of multi-layered structures and predict artificially high natural frequencies [107]. Recently, Feri et al. [108], presented 3D static and free vibration of piezo-layered cross-ply laminated plate using a DQM. Cupial [109] presented 3D natural vibration solution of piezoelectric simply supported rectangular plates using perturbation technique. Messina [110] presented 3D free vibration analysis of multilayered piezoelectric plates using adaptive global piecewise-smooth function. Kulikov and Plotnikova [111] presented a 3D exact analysis of piezoelectric laminated plates via sampling surfaces method. Apart from EKM being applied largely for rectangular plate configurations, has it been tried for other plate configurations? Yes, it has also been employed for analyzing different other plate configurations by various researchers. Bespalova [112] presented the bending vibrations of polygonal (L-shaped) plates with different shapes and boundary conditions using Kantorovich-Vlasov methods. Joodaky and co-researchers [113, 114] studied the static behaviour of thin skew plates on various foundations like on Winkler and Pasternak foundations. Shufrin et al. [112] studied the nonlinear analysis of trapezoidal plates. Aghdam et al. [115] used EKM for static analysis of thick FGM sector plates. Fallah and Khakbaz [116] and [117] used EKM for the static analysis of functionally graded annular sector plates. To the best of the author's knowledge, 3D piezoelasticity solution for the free vibration analysis of hybrid composite and sandwich plates for arbitrary boundary conditions using multi-term EKM does not exist.

1.3.5 Advanced 2D Laminate Theories for Static and Dynamic Analysis of Elastic and Smart Hybrid Plates

The 2D theories are preferred for design and optimization of smart structures as it is relatively simple and easy to execute in comparison to 3D solutions with reasonable accuracy. In recent years there has been much interest in higher order theories of plates. In the review articles [19, 118–120] elaborate reviews of 2D plate theories are presented considering various computational methods on static as well as free vibration analysis of different laminated elastic/piezoelectric composite and sandwich structures.

Analytical solutions are preferred over numerical solutions for better accuracy and simplicity. Leissa and his coworkers [121, 122] presented the free vibration analysis of plate based on the classical laminate plate theory (CLPT), which is based on Kirchhoff's hypothesis, where the transverse normal and shearing effects are neglected. Hence, the CLPT provides good results for

thin plates, while on the other hand it over-predicts the natural frequencies and under-predicts the deflections for moderately thick isotropic/composite plates. Then, the first order shear deformation theory (FSDT) is proposed for moderately thick plates [123, 124] to overcome the deficiency of CLPT. The FSDT does not satisfy the shear traction free conditions at the top and bottom surfaces of the plates, therefore a shear correction factor is required in FSDT in order to satisfy the transverse shear traction free conditions on the top and bottom surfaces of the plate. Analytical solutions for elastic rectangular laminated plates with Levy-type boundary conditions have been presented for the static response of symmetric cross-ply [125], antisymmetric angle-ply plates [126] and vibration response of laminated composite plates [127–133] based on FSDT.

Though FSDT is good in predicting the vibration responses with reasonable accuracy for thin and moderately thick plates, its dependence on the appropriate choice of shear correction factor makes it inconvenient for accurate analysis of thick plates. The limitations of FSDT are overcome by the development of higher order shear deformation theories (HSDT) which involves the transverse shear stress function. The HSDT is applied to study the behaviour of laminated composite and sandwich plates for buckling and vibration [87, 134–139] cases. Brank [140] studied the boundary layer effect in an isotropic Levy-type plate using Mindlin plate model. Levy-type solutions of the FSDT and TOT for rectangular cross-ply laminated plates under sinusoidal loading have been presented by Khdeir and Reddy [141]. Abdelnaser and Sing [142] presented a levy type solution for the forced vibration response of antisymmetric angle-ply rectangular plates under random loading using the third order theory (TOT). Based on a global HSDT, Matsunaga presented the free vibration analysis of cross-ply [77] and angle-ply [143] laminated composite plates taking into account the effects of shear deformations and rotary inertia. However, the above advanced two-dimensional (2D) laminate theories were assessed for their accuracy against the 3D solutions of plates subjected to Navier-type supports (all round simply supported boundary conditions). Such an assessment can not provide the complete evaluation of theories because boundary effects are absent for the simply-supported edges [2]. Very limited research articles have been published for both static and dynamic analysis of laminated plates considering the Levy-type support conditions. Tahani and Nosier [144] presented a Levy-type solution for uniformly loaded rectangular composite plates using a layerwise theory (LWT) and studied the edge effects at the traction free edges of such laminates. Umasree [145] presented

an analytical infinite series solution for a clamped rectangular cross-ply plate using the zig-zag theory (ZIGT).

The dynamic analysis of functionally graded plate by using FSDT, TOT and Fourier-Laplace transform method was presented by Akbarzadeh et al. [146] considering thermomechanical loading. But they have presented results only for the simply supported case. Izadi and Tahani [147] studied the edge effect in Levy-type piezolaminated plates using a second order shear deformation plate theory, again without considering the electromechanical coupling due to the direct piezoelectric effect. All Levy-type solutions presented above for smart piezoelectric rectangular plates are based on the ESL theories and do not consider the two-way electromechanical coupling.

The coupled efficient layerwise zigzag theory (ZIGT) proposed by Kapuria and coworkers [148, 149] for hybrid plates structures, has emerged as the best possible compromise between the accuracy and computation efficiency. The in-plane displacements in this theory are assumed to have a layerwise linear variation with a global third order variation across the thickness. But the number of displacement variables is reduced to only five, as in the smeared theory like the first order shear deformation theory (FSDT) and third order theory (TOT), by enforcing the conditions of transverse shear stress continuity at layer interfaces and zero shear traction at the top and bottom surfaces. The electric potential is assumed to follow a quadratic variation across the piezoelectric layer. The accuracy of the theory has been assessed by comparing its analytical solutions for simply supported rectangular plates with the available exact 3D piezoelasticity solutions [101]. Such assessment can at best provide an incomplete picture since no boundary layer effects are observed on the simply-supported edges [2] as opposed to clamped and free edges. The boundary layer effect also known as the edge effect, is often responsible for the initiation of delamination damage in laminated structures. This theory has been applied by Kapuria and Kumari [150] to get a Levy type solution for the rectangular elastic plate and piezoelectric plate considering two-way electromechanical coupling under static bending. There is no dynamic solution available for elastic/piezoelectric plate considering two-way electromechanical coupling using higher order theory.

1.4 OBJECTIVES OF THE PRESENT WORK

Based on the literature survey, the following objectives were identified for the present research work:

1. To develop 3D piezoelasticity solutions of cross-ply rectangular smart hybrid laminated plates integrated with PFRC layers subjected to Levy-type boundary conditions using multi-term multi-field extended Kantorovich method (EKM) under electromechanical excitation.
2. To investigate the effect of boundary layer stresses for the adhesively bonded piezolaminated plates and study the effect of aspect ratio and span-to thickness ratio on the boundary layer effect in the inplane and interlaminar stresses.
3. To develop a closed form solution for dynamic analysis of cross-ply elastic laminates subjected to Levy-type boundary conditions using multi-term EKM.
4. To investigate the effect of adhesive layer thickness, elastic modulus and density on the natural frequency of adhesive bonded laminated plate using multi-term EKM
5. To further extend multi-term 3D EKM to develop the dynamic analysis of piezolaminated plates subjected to Levy-type boundary conditions considering two-way electro-mechanical coupling.
6. To investigate the effect of adhesive thickness on the free vibration behaviour of adhesively bonded piezoelectric bimorph and assess the effect of adhesive layer thickness, elastic modulus and adhesive density on the plate natural frequencies.
7. To present an analytical solution of an advanced efficient layerwise 2D theory for Levy-type rectangular elastic/smart hybrid plates for free vibration analysis and to assess its accuracy in comparison with the 3D elasticity/piezoelasticity solutions.

1.5 ORGANISATION OF THE THESIS

The complete work presented in this thesis has been organized into seven chapters. Chapter 1 is devoted to the literature survey and the proposed objectives of the present work. An overview

of the contents of the remaining six chapters is presented below.

Chapter 2 presents a coupled 3D piezoelasticity solution for edge effects in the static analysis of Levy-type rectangular hybrid composite and sandwich plates using mixed field extended Kantorovich method (EKM). The effect of adhesive layers for the static response of smart hybrid sandwich plates have also been investigated. The method is derived using Reissner's variational principle following a mixed formulation approach which takes displacements as well as stresses into account as primary variables. In this method, the boundary and interface conditions are exactly satisfied at all points ensuring the same order of accuracy for all the displacement and stress variables. The accuracy in predicting the order of free edge stress singularity has been verified. Numerical results are presented for thick single layer piezoelectric, smart hybrid composite and sandwich plates subjected to the various type of boundary conditions. The convergence and accuracy of the present method have been substantiated by direct comparison with the 3D exact elasticity solution and 3D FE solution of ABAQUS. It is observed that two/three term in the solution is sufficient enough to predict stresses accurately near the edges.

The 3D EKM developed in Chapter 2 for the static piezoelasticity solution of laminated hybrid composite and sandwich rectangular plates is extended to the free vibration analysis of elastic laminated plates in Chapter 3. In Chapter 3, the 3D EKM has been used to present the free vibration analysis of elastic composite and sandwich plates along with the effect of adhesive characteristics on the free vibration behaviour of composite plates have been investigated. The accuracy and efficacy of the present method have been established by comparing the results with the results from other theories published previously and with the 3D FE results of ABAQUS wherever no other results are available. Benchmark natural frequencies and mode shapes are presented for composite and sandwich plates for different types of boundary conditions.

In Chapter 4, the generalized 3D EKM presented in Chapter 3 for the dynamic analysis of elastic laminated plates has been extended to develop the free vibration solution of bimorph, smart hybrid composite and sandwich plates. The accuracy of the present solution is verified in comparison with the results from other theories and with the 3D FE solutions of ABAQUS. The effect of adhesive layer on the natural frequency of bimorph plate has also been investigated. Benchmark natural frequencies are presented for bimorph, composite sandwich and smart hybrid sandwich plates. Mode shapes for smart hybrid composite and sandwich plates for various

boundary conditions are presented.

In Chapter 5, the formulation for exact Levy-type free vibration piezoelectric solution is presented for rectangular plates using an efficient zigzag theory (ZIGT) and the third order theory (TOT). The inplane displacements (u_x, u_y), in this theory, are approximated as a combination of third order variation in z across the thickness and a layerwise linear variation of slopes $(u_{x,z},\ u_{y,z})$ at the interface. The field variables in the solution scope are expanded in Fourier series along the normal to the simply supported edge. The mixed formulation approach is followed in deriving the solution process. This solution methodology can be used to obtain the static and free vibration response of elastic/piezoelectric laminated composite plates.

The piezoelasticity exact Levy solution methodology using ZIGT and TOT presented in Chapter 5 is used in Chapter 6 to predict the free vibration of elastic laminated plates as well as static and free vibration response of smart hybrid laminated rectangular plates. The accuracy of the 2D theories i.e. ZIGT and TOT are assessed with the 3D elasticity solution based on EKM and in some cases with the 3D FE solution from ABAQUS.

Finally, the major conclusions of this work and suggestions for future research are summarized in Chapter 7.

Chapter 2

3D Piezoelasticity Solution for Static Analysis of Smart Hybrid Rectangular Plates by Extended Kantorovich Method

2.1 INTRODUCTION

A coupled three-dimensional static piezoelasticity solution [151] for rectangular piezolaminated plates with Levy-type boundary conditions is presented in this chapter using the mixed-field multi-term extended Kantorovich method (EKM) and Fourier series expansion. The piezoelectric or PFRC layers are embedded or surface bonded on the elastic laminated substrates with poling along the thickness direction. The formulation considers full electromechanical coupling, and the piezoelectric layers can be modeled as both actuators and sensors. The solution considers two-way electromechanical coupling, and satisfies all the essential and natural boundary conditions as well as the continuity conditions at the interface exactly at all points.

In Sec. 2.2, modified constitutive relations of piezoelasticity are deduced and subsequently expanded using the strain-displacement and electric field-potential relations. The solution methodology is laid out in Sec. 2.3 following a mixed formulation approach expressing the governing equations with the help of mechanical (displacement and stress) and electrical (potential and displacement) state variables. The state variables and the electromechanical loading functions are expressed in terms of Fourier series in the span coordinate which satisfy the simply-supported boundary condition on the pair of edges along the span direction. The variational principle is implemented along the inplane (x) and thickness (z) directions which furnish $8n$ ODEs with

constant coefficients and $5n$ algebraic equations in terms of x. In the first iteration step, the trial function are assumed along the x-direction and are solved for the z-functions which in turn serves as a priori function in the next step to determine the functions in x-direction. The processes is repeated until a desired convergence is warranted. It is perceived that, in this method, convergence in the results is achieved very fast just in two to three terms of the Fourier expansion in the iteration process.

The objective in this analysis is to accurately characterize the edge effects and the effects of adhesive in finite dimensional piezolaminated plates under mechanical and actuation potential loading, and also to provide a benchmark for assessing the accuracy of the two-dimensional laminate theories. The efficacy and eminence of the present method is ascertained by comparing the present results with other previous results and with the 3D FE solution obtained from ABAQUS and are presented in Sec. 2.4. At first the accuracy in predicting the order of stress singularity is examined taking long dissimilar bi-material strips and then results for rectangular hybrid and sandwich plates are presented. Results of piezoelectric plates with F-F boundary condition under electric potential loading are presented and effect of b/a on the interlaminar stresses has been studied. The effect of electromechanical coupling and the electric boundary conditions on the boundary layer effect is studied providing interesting insight into the behavior of smart plates. The effect of adhesive thickness on the interlaminar stresses are also investigated.

2.2 GOVERNING EQUATIONS

A rectangular smart hybrid plate (Fig. 2.1) of length a along x-axis, width b along y axis and thickness h along z-axis is considered for the study. There are L orthotropic layers in the laminate, which can be made of elastic or piezoelectric materials of class mm2 symmetry with poling along the thickness direction z. The piezoelectric layers can be used as distributed actuators as well as sensors. A perfect bonding is assumed at the layer interfaces. The presence of electrodes on piezoelectric layers and its effect are neglected. The plate is subjected to Levy-type boundary conditions with two opposite edges at $y = 0$ and b being simply-supported and the other two edges under arbitrary boundary conditions. The thickness of the kth layer and the z-coordinate of its upper surface are denoted as t^k and z_k, respectively. The layer index k over the entities is dropped, unless required for clarity.

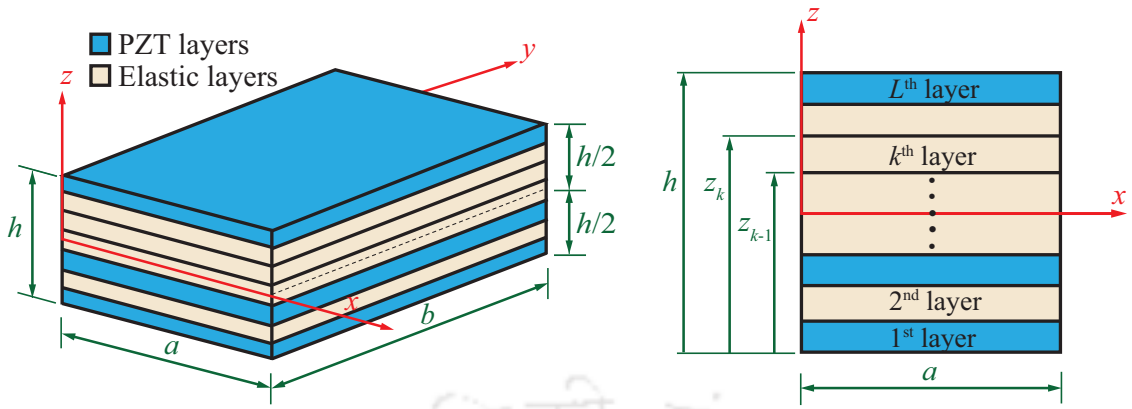

Figure 2.1: Geometry and coordinate system of a L-layer smart hybrid plate.

The normal strains ε_i, shear strains γ_{ij}, and the electric field components E_i $(i, j = x, y, z)$ are related to the displacements u, v and w, and the electric potential ϕ by

$$\varepsilon_{ij} = \frac{1}{2}(u_{i,j} + u_{j,i}), \qquad E_i = -\phi_{,i} \tag{2.1}$$

where a subscript comma followed by i, for example, denotes the partial differentiation with respect to x_i. The linear 3D piezoelasticity constitutive equations for an orthorhombic/orthotropic (for elastic layers) lamina are given by

$$\begin{aligned}
&\varepsilon_x = s_{11}\sigma_x + s_{12}\sigma_y + s_{13}\sigma_z + d_{31}E_z, \quad \gamma_{yz} = s_{44}\tau_{yz} + d_{24}E_y, \quad D_x = d_{15}\tau_{zx} + \epsilon_{11}E_x \\
&\varepsilon_y = s_{12}\sigma_x + s_{22}\sigma_y + s_{23}\sigma_z + d_{32}E_z, \quad \gamma_{zx} = s_{55}\tau_{zx} + d_{15}E_x, \quad D_y = d_{24}\tau_{yz} + \epsilon_{22}E_y \\
&\varepsilon_z = s_{13}\sigma_x + s_{23}\sigma_y + s_{33}\sigma_z + d_{33}E_z, \quad \gamma_{xy} = s_{66}\tau_{xy}, \quad D_z = d_{31}\sigma_x + d_{32}\sigma_y + d_{33}\sigma_z + \epsilon_{33}E_z
\end{aligned} \tag{2.2}$$

where σ_i, τ_{ij} and D_i denote the normal stress, shear stress and electric displacement components, respectively. The elastic compliances s_{ij}, piezoelectric strain constants d_{ij} and dielectric permittivities ϵ_{ij} (at constant stress field) can be expressed in terms of the engineering material constants as given below:

$$\begin{aligned}
&s_{11} = 1/Y_1, && s_{44} = 1/G_{23}, && s_{12} = -\nu_{21}/Y_2 = -\nu_{12}/Y_1 \\
&s_{22} = 1/Y_2, && s_{55} = 1/G_{13}, && s_{13} = -\nu_{31}/Y_3 = -\nu_{13}/Y_1 \\
&s_{33} = 1/Y_3, && s_{66} = 1/G_{12}, && s_{23} = -\nu_{32}/Y_3 = -\nu_{23}/Y_2 \\
&\epsilon_{11} = \eta_{11} + e_{15}d_{15}, && \epsilon_{22} = \eta_{22} + e_{24}d_{24}, && \epsilon_{33} = \eta_{33} + e_{31}d_{31} + e_{32}d_{32} + e_{33}d_{33}
\end{aligned} \tag{2.3}$$

where

$$[\,e_{31}\quad e_{32}\quad e_{33}\,] = [\,d_{31}\quad d_{32}\quad d_{33}\,]\begin{bmatrix} s_{11} & s_{12} & s_{13} \\ s_{12} & s_{22} & s_{23} \\ s_{13} & s_{23} & s_{33} \end{bmatrix}^{-1}$$
$$e_{24} = d_{24}/s_{44}, \qquad e_{15} = d_{15}/s_{55} \tag{2.4}$$

where Y_i, G_{ij} and ν_{ij} denote Young's moduli, shear moduli and major Poisson's ratios, respectively.

To ensure numerical stability in the solution process all entities are expressed in non-dimensional forms as given in Ref. [67], which are obtained in such a way that, on substitution of the dimensionless entities, the resulting governing equations appear identical to original equations and are reproduced below for ready reference.

$$\begin{aligned}
&S = a/h, && (\sigma_x^*, \sigma_y^*, \sigma_z^*, \tau_{yz}^*, \tau_{zx}^*, \tau_{xy}^*, p_\alpha^*) = (\sigma_x, \sigma_y, \sigma_z, \tau_{yz}, \tau_{zx}, \tau_{xy}, p_\alpha)S/Y_0 \\
&\bar{s}_{ij}^* = \bar{s}_{ij}Y_0, && (\varepsilon_x^*, \varepsilon_y^*, \varepsilon_z^*, \gamma_{yz}^*, \gamma_{zx}^*, \gamma_{xy}^*) = (\varepsilon_x, \varepsilon_y, \varepsilon_z, \gamma_{yz}, \gamma_{zx}, \gamma_{xy})S \\
&(u^*, v^*, w^*) = (u, v, w)/h, && (G_{ij}^*,\, Y_i^*) = (G_{ij},\, Y_i)/Y_0 \\
&[h^*, t^{*(k)}] = [h, t^{(k)}]/a, && \epsilon_{ij}^* = \epsilon_{ij}/Y_0 d_0^2 \\
&(E_x^*, E_y^*, E_z^*) = (E_x, E_y, E_z)d_0 S, && (D_x^*, D_y^*, D_z^*, D_\alpha^*, \tau_q^*) = (D_x, D_y, D_z, D_\alpha, \tau_q)S/Y_0 d_0 \\
&(\phi^*, \phi_\alpha^*, \Phi_q^*) = (\phi, \phi_\alpha, \Phi_q)d_0/h
\end{aligned} \tag{2.5}$$

where Y_0 and d_0 denote the value of the chosen Young's modulus and the piezoelectric constant used for non-dimensionalisation. In subsequent equations the above dimensionless forms are used dropping the superscript * for simplicity.

Using the relation for D_z in Eq. (2.2) in the relations for ε_x, ε_y, ε_z in the same equation, we obtain

$$\begin{aligned}
&\varepsilon_x = \bar{s}_{11}\sigma_x + \bar{s}_{12}\sigma_y + \bar{s}_{13}\sigma_z + \bar{d}_{31}D_z, && \varepsilon_y = \bar{s}_{12}\sigma_x + \bar{s}_{22}\sigma_y + \bar{s}_{23}\sigma_z + \bar{d}_{32}D_z \\
&\varepsilon_z = \bar{s}_{13}\sigma_x + \bar{s}_{23}\sigma_y + \bar{s}_{33}\sigma_z + \bar{d}_{33}D_z, && E_z = -\bar{d}_{31}\sigma_x - \bar{d}_{32}\sigma_y - \bar{d}_{33}\sigma_z + \bar{\epsilon}_{33}D_z
\end{aligned} \tag{2.6}$$

where, $\bar{\epsilon}_{33} = 1/\epsilon_{33}$, $\bar{s}_{ij} = s_{ij} - d_{3i}\bar{d}_{3j}$, $\bar{d}_{3i} = d_{3i}/\epsilon_{33}$, for $(i, j) = 1, 2, 3$. Similarly, the relations for γ_{yz}, γ_{zx}, E_x and E_y in Eq. (2.2) can be rewritten as

$$\begin{aligned}
&\gamma_{yz} = \bar{s}_{44}\tau_{yz} + \bar{d}_{24}D_y, && \gamma_{zx} = \bar{s}_{55}\tau_{zx} + \bar{d}_{15}D_x, && E_x = \bar{\epsilon}_{11}D_x - \bar{d}_{15}\tau_{zx} \\
&E_y = \bar{\epsilon}_{22}D_y - \bar{d}_{24}\tau_{yz}, && \bar{s}_{44} = s_{44} - d_{24}\bar{d}_{24}, && \bar{s}_{55} = s_{55} - d_{15}\bar{d}_{15}
\end{aligned} \tag{2.7}$$

where

$$\bar{\epsilon}_{11} = 1/\epsilon_{11}, \qquad \bar{\epsilon}_{22} = 1/\epsilon_{22}, \qquad \bar{d}_{24} = d_{24}/\epsilon_{22}, \qquad \bar{d}_{15} = d_{15}/\epsilon_{11}.$$

The Reissner-type variational principle [41] for the static analysis of the piezoelectric plate, without any body force, can be expressed as

$$\int_a\int_b\int_h[\delta u(\sigma_{x,x}+\tau_{xy,y}+\tau_{zx,z})+\delta v(\tau_{xy,x}+\sigma_{y,y}+\tau_{yz,z})+\delta w(\tau_{zx,x}+\tau_{yz,y}+\sigma_{z,z})$$
$$+\delta\sigma_x(\varepsilon_x-u_{,x})+\delta\sigma_y(\varepsilon_y-v_{,y})+\delta\sigma_z(\varepsilon_z-w_{,z})+\delta\tau_{yz}(\gamma_{yz}-v_{,z}-w_{,y})+\delta\tau_{zx}(\gamma_{zx}-u_{,z}$$
$$-w_{,x})+\delta\tau_{xy}(\gamma_{xy}-v_{,x}-u_{,y})+\delta\phi(D_{x,x}+D_{y,y}+D_{z,z})-\delta D_x(E_x+\phi_{,x})-\delta D_y(E_y$$
$$+\phi_{,y})-\delta D_z(E_z+\phi_{,z})]\mathrm{d}z\mathrm{d}y\mathrm{d}x=0,\quad\forall\ \delta u_i,\ \delta\phi,\ \delta\sigma_i,\ \delta\tau_{ij},\ \delta D_i \tag{2.8}$$

Equation (2.8) implies the following boundary conditions are satisfied exactly at surface boundaries

(a) where surface tractions $\bar{T}_i^n$ are specified: $\sigma_{ij}n_j-\bar{T}_i^n=0$

(b) where displacements $\bar{u}_i$ are specified: $u_i-\bar{u}_i=0$

(c) where electric displacement $\bar{D}_i^n$ are specified: $D_in_i-\bar{D}_n=0$

(d) where $\bar{\phi}$ is specified: $\phi-\bar{\phi}=0$

The surface is denoted by its outward normal $\bar{n}=n_i\hat{e}_i$, where $\hat{e}_i$ $(i=1,2,3)$ are the unit vectors along x, y and z directions. Substituting the expressions of the strain and electric components from Eqs. (2.6) and (2.7) into Eq. (2.8) yields

$$\int_a\int_b\int_h[\delta u(\tau_{xz,z}+\sigma_{x,x}+\tau_{xy,y})+\delta v(\tau_{yz,z}+\tau_{xy,x}+\sigma_{y,y})+\delta w(\sigma_{z,z}+\tau_{zx,x}+\tau_{yz,y})$$
$$+\delta\phi(D_{x,x}+D_{y,y}+D_{z,z})+\delta\sigma_x(\bar{s}_{11}\sigma_x+\bar{s}_{12}\sigma_y+\bar{s}_{13}\sigma_z+\bar{d}_{31}D_z-u_{,x})+\delta\sigma_y(\bar{s}_{12}\sigma_x$$
$$+\bar{s}_{22}\sigma_y+\bar{s}_{23}\sigma_z+\bar{d}_{32}D_z-v_{,y})-\delta\sigma_z(w_{,z}-\bar{s}_{13}\sigma_x-\bar{s}_{23}\sigma_y-\bar{s}_{33}\sigma_z-\bar{d}_{33}D_z)$$
$$-\delta\tau_{yz}(v_{,z}+w_{,y}-\bar{s}_{44}\tau_{yz}-\bar{d}_{24}D_y)-\delta\tau_{zx}(u_{,z}+w_{,x}-\bar{s}_{55}\tau_{zx}-\bar{d}_{15}D_x)+\delta\tau_{xy}(s_{66}\tau_{xy}$$
$$-v_{,x}-u_{,y})-\delta D_x(\phi_{,x}+\bar{\epsilon}_{11}D_x-\bar{d}_{15}\tau_{zx})-\delta D_y(\phi_{,y}+\bar{\epsilon}_{22}D_y-\bar{d}_{24}\tau_{yz})-\delta D_z(\phi_{,z}$$
$$-\bar{d}_{31}\sigma_x-\bar{d}_{32}\sigma_y-\bar{d}_{33}\sigma_z+\bar{\epsilon}_{33}D_z)]\mathrm{d}z\mathrm{d}y\mathrm{d}x=0,\quad\forall\ \delta u_i,\ \delta\phi,\ \delta\sigma_i,\ \delta\tau_{ij},\ \delta D_i \tag{2.9}$$

Dimensionless inplane coordinates ξ_1, ξ_2 and a local thickness coordinate $\zeta^{(k)}$ for the kth layer are introduced, which vary from 0 to 1:

$$\xi_1=x/a,\qquad\xi_2=y/b\qquad\zeta^{(k)}=(z-z_{k-1})/t^{(k)} \tag{2.10}$$

The bottom and top surfaces of the plate are subjected to applied pressure p_1 and p_2, respectively, with zero shear traction. If the piezoelectric layer is used as an actuator, ϕ is prescribed (close

circuit condition) and if it is used as a sensor, D_z is prescribed (open circuit condition) at the outer surfaces. Thus, the boundary conditions at $z = \mp h/2$ are

$$\begin{aligned} &\text{at} \quad z = -h/2: \quad \sigma_z = -p_1, \quad \tau_{yz} = 0, \quad \tau_{zx} = 0, \quad \phi = \phi_1 \ \text{ or } \ D_z = D_1 \\ &\text{at} \quad z = h/2: \quad \sigma_z = -p_2, \quad \tau_{yz} = 0, \quad \tau_{zx} = 0, \quad \phi = \phi_2 \ \text{ or } \ D_z = D_2 \end{aligned} \tag{2.11}$$

For perfect bonding, the continuity conditions at the interface between kth and $(k+1)$th layers are given by:

$$[(u,\, v,\, w,\, \sigma_z,\, \tau_{yz},\, \tau_{zx},\, \phi,\, D_z)|_{\zeta=1}]^{(k)} = [(u,\, v,\, w,\, \sigma_z,\, \tau_{yz},\, \tau_{zx},\, \phi,\, D_z)|_{\zeta=0}]^{(k+1)} \tag{2.12}$$

for $k = 1, \ldots, L-1$. The interfaces of the piezoelectric layers with the adjacent elastic layers are taken as grounded ($\phi = 0$) for effective actuation/sensing. At these interfaces, D_z is discontinuous, and the continuity condition for D_z in Eq. (2.12) is replaced by the condition

$$[\phi|_{\zeta=1}]^{(n_q)} = 0, \qquad q = 1, \ldots, L_a \tag{2.13}$$

where L_a is the interface where electric potential is prescribed (actuation potential).

The mechanical boundary conditions at the edges $\xi_1 = 0$ and 1 can be prescribed for a given support type, for example,

$$\begin{aligned} &\text{Simply supported (S):} \quad \sigma_x = 0, \quad v = 0, \quad w = 0 \\ &\text{Clamped (C):} \quad u = 0, \quad v = 0, \quad w = 0 \\ &\text{Free (F):} \quad \sigma_x = 0, \quad \tau_{xy} = 0, \quad \tau_{xz} = 0 \end{aligned} \tag{2.14}$$

Electrically, the ends may be subjected to closed circuit (CC) condition with prescribed potential or open circuit (OC) condition with known D_x (=0). The boundary conditions at the simply supported edges at $\xi_2 = 0$ and 1 are considered as

$$u = 0, \qquad \sigma_y = 0, \qquad w = 0, \qquad \phi = 0 \tag{2.15}$$

2.3 FOURIER SERIES-GENERALIZED EKM SOLUTION

The solution is expressed in terms of Fourier series in y, which identically satisfies the boundary conditions (2.15) at two simply-supported edges $y = 0, b$.

$$(u,\, w,\, \sigma_x,\, \sigma_y,\, \sigma_z,\, \tau_{zx},\, \phi,\, D_x,\, D_z) = \sum_{m=1}^{\infty} (u,\, w,\, \sigma_x,\, \sigma_y,\, \sigma_z,\, \tau_{zx},\, \phi,\, D_x,\, D_z)_m \sin m\pi\xi_2,$$

$$(v,\, \tau_{xy},\, \tau_{yz},\, D_y) = \sum_{m=1}^{\infty} (v,\, \tau_{xy},\, \tau_{yz},\, D_y)_m \cos m\pi\xi_2, \tag{2.16}$$

where $(\ )_m$ denotes the mth Fourier component. The Fourier coefficients are functions of x and z. The applied electromechanical loading functions, $p_i(\xi_1, \xi_2)$, $\phi_i(\xi_1, \xi_2)$ and $D_i(\xi_1, \xi_2)$ are also similarly expanded in Fourier series in ξ_2 direction as

$$[p_i(\xi_1,\, \xi_2),\, \phi_i(\xi_1,\, \xi_2),\, D_i(\xi_1,\, \xi_2)] = \sum_{m=1}^{\infty} [p_{im}(\xi_1),\, \phi_{im}(\xi_1),\, D_{im}(\xi_1)] \sin m\pi\xi_2 \quad (i = 1,\, 2) \tag{2.17}$$

where

$$[p_{im}(\xi_1),\, \phi_{im}(\xi_1),\, D_{im}(\xi_1)] = 2\int_0^1 [p_i(\xi_1, \xi_2),\, \phi_i(\xi_1, \xi_2),\, D_i(\xi_1, \xi_2)] \sin m\pi\xi_2\, d\xi_2 \tag{2.18}$$

Substituting the expression from Eq. (2.16) into the variational Eq. (2.9), and using the orthogonality properties of $\cos m\pi\xi_2$ and $\sin m\pi\xi_2$ for $m = 1, 2, ..., \infty$, we obtain, for each Fourier term m

$$\begin{aligned}
\int_a \int_h [&\delta u_m(\tau_{xzm,z} + \sigma_{xm,x} - \bar{m}\tau_{xym}) + \delta v_m(\tau_{yzm,z} + \tau_{xym,x} + \bar{m}\sigma_{ym}) + \delta w_m(\sigma_{zm,z} + \tau_{zxm,x} \\
&-\bar{m}\tau_{yzm}) + \delta\phi_m(D_{xm,x} - \bar{m}D_{ym} + D_{zm,z}) + \delta\sigma_{xm}(\bar{s}_{11}\sigma_{xm} + \bar{s}_{12}\sigma_{ym} + \bar{s}_{13}\sigma_{zm} + \bar{d}_{31}D_{zm} \\
&-u_{m,x}) + \delta\sigma_{ym}(\bar{s}_{12}\sigma_{xm} + \bar{s}_{22}\sigma_{ym} + \bar{s}_{23}\sigma_{zm} + \bar{d}_{32}D_{zm} + \bar{m}v_m) - \delta\sigma_{zm}(w_{m,z} - \bar{s}_{13}\sigma_{xm} \\
&-\bar{s}_{23}\sigma_{ym} - \bar{s}_{33}\sigma_{zm} - \bar{d}_{33}D_{zm}) - \delta\tau_{yzm}(v_{m,z} + \bar{m}w_m - \bar{s}_{44}\tau_{yzm} - \bar{d}_{24}D_{ym}) - \delta\tau_{zxm}(u_{m,z} \\
&+w_{m,x} - \bar{s}_{55}\tau_{zxm} - \bar{d}_{15}D_{xm}) + \delta\tau_{xym}(s_{66}\tau_{xym} - v_{m,x} - \bar{m}u_m) - \delta D_{xm}(\phi_{m,x} + \bar{\epsilon}_{11}D_{xm} \\
&-\bar{d}_{15}\tau_{zxm}) - \delta D_{ym}(\bar{m}\phi_m + \bar{\epsilon}_{22}D_{ym} - \bar{d}_{24}\tau_{yzm}) - \delta D_{zm}(\phi_{m,z} - \bar{d}_{31}\sigma_{xm} - \bar{d}_{32}\sigma_{ym} \\
&-\bar{d}_{33}\sigma_{zm} + \bar{\epsilon}_{33}D_{zm})]\mathrm{d}z\mathrm{d}x = 0, \quad \forall \quad \delta u_{im}, \delta\phi_m, \delta\sigma_{im}, \delta\tau_{ijm}, \delta D_{im}
\end{aligned} \tag{2.19}$$

where $\bar{m} = m\pi/b$.

The solution of Eq. (2.19) is obtained using the mixed-field multi-term EKM proposed by Kapuria and Kumari [67]. In this method, the field variables

$$\mathbf{X} = [\, u \quad v \quad w \quad \sigma_x \quad \sigma_y \quad \sigma_z \quad \tau_{xy} \quad \tau_{yz} \quad \tau_{zx} \quad \phi \quad D_x \quad D_y \quad D_z\,]_m^{\mathrm{T}} \tag{2.20}$$

are expressed as the sum of n terms consisting of products of separable functions of ξ_1 and ζ. These functions $f_l^i(\xi_1)$ and $g_l^i(\zeta)$ are determined so as to satisfy the homogeneous boundary conditions. To satisfy the non-homogeneous boundary condition for σ_z and ϕ as given by Eq. (2.11), additional terms are added to the above solution. Thus, the solution of the lth

variable X_l of $\mathbf{X}$ for the kth layer takes the form:

$$X_l(\xi_1,\zeta) = \sum_{i=1}^{n} f_l^i(\xi_1) g_l^i(\zeta) + \underline{\delta_{l6}[p_a + z p_d]} + \underline{\delta_{l,10}\bar{g}_{10}} \quad \text{for} \quad l = 1, 2, \ldots, 13 \tag{2.21}$$

where the repeated index l does not mean summation here. The underlined terms are used to satisfy the non-homogeneous boundary conditions for σ_z and ϕ, where δ_{lp} is Kroneckor's delta, $p_a = -(p_{1m} + p_{2m})/2$, $p_d = -(p_{2m} - p_{1m})/h$, and $\bar{g}_{10}$ is given by

$$\bar{g}_{10} = \begin{cases} \phi_1(1-\zeta) & \text{for} \quad k = 1 \\ \phi_2 \zeta & \text{for} \quad k = L \end{cases} \tag{2.22}$$

Functions $f_l^i(\xi_1)$ are valid for all layers, whereas $g_l^i(\zeta)$ correspond to kth layer. These are determined iteratively as follows.

2.3.1 First Iteration Step

In the first step, functions $f_l^i(\xi_1)$ are considered as known, while $g_l^i(\zeta)$ are determined for each layer. As mentioned earlier, in the EKM, the initial trial functions are not required to satisfy the prescribed boundary conditions. Here, in the first iteration, we assume f_l^i as

$$\begin{aligned} &f_2^i(\xi_1) = f_3^i(\xi_1) = f_4^i(\xi_1) = f_5^i(\xi_1) = f_6^i(\xi_1) = f_8^i(\xi_1) = f_{10}^i(\xi_1) = f_{12}^i(\xi_1) = f_{13}^i(\xi_1) = \sin i\pi\xi_1 \\ &f_1^i(\xi_1) = f_7^i(\xi_1) = f_9^i(\xi_1) = f_{11}^i(\xi_1) = \cos i\pi\xi_1. \end{aligned} \tag{2.23}$$

In the subsequent iteration, f_l^i are taken as obtained from the second step (Sec. 2.3.1) of the previous iteration. From Eq. (2.21), the variation δX_l in this case is obtained as

$$\delta X_l = \sum_{i=1}^{n} f_l^i(\xi_1) \delta g_l^i \tag{2.24}$$

Functions $g_l^i(\zeta)$ are divided into two groups

$$\begin{aligned} \bar{\mathbf{G}} &= [\, g_1^1 \ldots g_1^n \quad g_2^1 \ldots g_2^n \quad g_3^1 \ldots g_3^n \quad g_6^1 \ldots g_6^n \quad g_8^1 \ldots g_8^n \quad g_9^1 \ldots g_9^n \quad g_{10}^1 \ldots g_{10}^n \quad g_{13}^1 \ldots g_{13}^n \,]^{\mathrm{T}} \\ \hat{\mathbf{G}} &= [\, g_4^1 \ldots g_4^n \quad g_5^1 \ldots g_5^n \quad g_7^1 \ldots g_7^n \quad g_{11}^n \ldots g_{11}^n \quad g_{12}^n \ldots g_{12}^n \,]^{\mathrm{T}} \end{aligned} \tag{2.25}$$

where $\bar{\mathbf{G}}$ contains the $8n$ primary variables that appear in Eqs. (2.11)-(2.12), while $\hat{\mathbf{G}}$ contains the remaining $5n$ dependent variables. After substituting Eqs. (2.21) and (2.24) into the variational expansion Eq. (2.19), its dependence on ξ_1 is eliminated by performing the integration over ξ_1 direction on the known functions of ξ_1. Since the variations δg_l^i are arbitrary, the coefficients of

δg_l^i in the resulting expression must vanish individually. This process yields $8n$ ODEs of first order and $5n$ linear algebraic equations for g_l^i for the kth layer:

$$\mathbf{M}\bar{\mathbf{G}}_{,\zeta} = \bar{\mathbf{A}}\bar{\mathbf{G}} + \hat{\mathbf{A}}\hat{\mathbf{G}} + \bar{\mathbf{Q}}_\mathbf{p} \tag{2.26}$$

$$\mathbf{K}\hat{\mathbf{G}} = \tilde{\mathbf{A}}\bar{\mathbf{G}} + \tilde{\mathbf{Q}}_\mathbf{p} \tag{2.27}$$

where $\mathbf{M}$, $\bar{\mathbf{A}}$, $\hat{\mathbf{A}}$, $\mathbf{K}$ and $\tilde{\mathbf{A}}$ are $8n \times 8n$, $8n \times 8n$, $8n \times 5n$, $5n \times 5n$ and $5n \times 8n$ matrices. The load vectors $\bar{\mathbf{Q}}_\mathbf{p}$ and $\tilde{\mathbf{Q}}_\mathbf{p}$ of size $8n$ and $5n$, respectively, are linear functions of ζ. Defining $\langle \ldots \rangle_a = a\int_0^1 (\ldots) d\xi_1$, the nonzero terms of above mentioned matrices are given by

$$
\begin{aligned}
&M_{i_1j_1} = M_{j_6i_6} = \langle f_9^i f_1^j \rangle_a, && M_{i_2j_2} = M_{j_5i_5} = \langle f_8^i f_2^j \rangle_a, && M_{i_3j_3} = M_{j_4i_4} = \langle f_6^i f_3^j \rangle_a \\
&M_{i_7j_7} = M_{j_8i_8} = \langle f_{13}^i f_{10}^j \rangle_a, && \bar{A}_{i_1j_3} = \tfrac{-t}{a}\langle f_9^i f_{3,\xi_1}^j \rangle_a, && \bar{A}_{i_1j_6} = t\bar{s}_{55}\langle f_9^i f_9^j \rangle_a \\
&\hat{A}_{i_1j_4} = t\bar{d}_{15}\langle f_9^i f_{11}^j \rangle_a, && \bar{A}_{i_2j_3} = -\bar{m}t\langle f_8^i f_3^j \rangle_a, && \bar{A}_{i_2j_5} = t\bar{s}_{44}\langle f_8^i f_8^j \rangle_a \\
&\hat{A}_{i_2j_5} = t\bar{d}_{24}\langle f_8^i f_{12}^j \rangle_a, && \bar{A}_{i_3j_4} = t\bar{s}_{33}\langle f_6^i f_6^j \rangle_a, && \bar{A}_{i_3j_8} = t\bar{d}_{33}\langle f_6^i f_{13}^j \rangle_a \\
&\hat{A}_{i_3j_1} = t\bar{s}_{13}\langle f_6^i f_4^j \rangle_a, && \hat{A}_{i_3j_2} = t\bar{s}_{23}\langle f_6^i f_5^j \rangle_a, && \bar{A}_{i_4j_5} = \bar{m}t\langle f_3^i f_8^j \rangle_a \\
&\bar{A}_{i_4j_6} = \tfrac{-t}{a}\langle f_3^i f_{9,\xi_1}^j \rangle_a, && \hat{A}_{i_5j_2} = -\bar{m}t\langle f_2^i f_5^j \rangle_a, && \hat{A}_{i_5j_3} = \tfrac{-t}{a}\langle f_2^i f_{7,\xi_1}^j \rangle_a \\
&\hat{A}_{i_6j_1} = \tfrac{-t}{a}\langle f_1^i f_{4,\xi_1}^j \rangle_a, && \hat{A}_{i_6j_3} = \bar{m}t\langle f_1^i f_7^j \rangle_a, && \bar{A}_{i_7j_4} = t\bar{d}_{33}\langle f_{13}^i f_6^j \rangle_a \\
&\bar{A}_{i_7j_8} = -t\bar{\epsilon}_{33}\langle f_{13}^i f_{13}^j \rangle_a, && \hat{A}_{i_7j_1} = t\bar{d}_{31}\langle f_{13}^i f_4^j \rangle_a, && \hat{A}_{i_7j_2} = t\bar{d}_{32}\langle f_{13}^i f_5^j \rangle_a \\
&\hat{A}_{i_8j_4} = \tfrac{-t}{a}\langle f_{10}^i f_{11,\xi_1}^j \rangle_a, && \hat{A}_{i_8j_5} = t\bar{m}\langle f_{10}^i f_{12}^j \rangle_a, && K_{i_1j_1} = \bar{s}_{11}\langle f_4^i f_4^j \rangle_a \\
&K_{i_1j_2} = \bar{s}_{12}\langle f_4^i f_5^j \rangle_a, && K_{j_2i_1} = K_{i_1j_2}, && K_{i_2j_2} = \bar{s}_{22}\langle f_5^i f_5^j \rangle_a, \\
&K_{i_3j_3} = s_{66}\langle f_7^i f_7^j \rangle_a, && K_{i_4j_4} = \bar{\epsilon}_{11}\langle f_{11}^i f_{11}^j \rangle_a, && K_{i_5j_5} = \bar{\epsilon}_{22}\langle f_{12}^i f_{12}^j \rangle_a \\
&\tilde{A}_{i_1j_1} = \tfrac{1}{a}\langle f_4^i f_{1,\xi_1}^j \rangle_a, && \tilde{A}_{i_1j_4} = -\bar{s}_{13}\langle f_4^i f_6^j \rangle_a, && \tilde{A}_{i_1j_8} = -\bar{d}_{31}\langle f_4^i f_{13}^j \rangle_a \\
&\tilde{A}_{i_2j_2} = -\bar{m}\langle f_5^i f_2^j \rangle_a, && \tilde{A}_{i_2j_4} = -\bar{s}_{23}\langle f_5^i f_6^j \rangle_a, && \tilde{A}_{i_2j_8} = -\bar{d}_{32}\langle f_5^i f_{13}^j \rangle_a, \\
&\tilde{A}_{i_3j_1} = \bar{m}\langle f_7^i f_1^j \rangle_a, && \tilde{A}_{i_3j_2} = \tfrac{1}{a}\langle f_7^i f_{2,\xi_1}^j \rangle_a, && \tilde{A}_{i_4j_6} = \bar{d}_{15}\langle f_{11}^i f_9^j \rangle_a \\
&\tilde{A}_{i_4j_7} = -\tfrac{1}{a}\langle f_{11}^i f_{10,\xi_1}^j \rangle_a, && \tilde{A}_{i_5j_5} = \bar{d}_{24}\langle f_{12}^i f_8^j \rangle_a, && \tilde{A}_{i_5j_7} = -\bar{m}\langle f_{12}^i f_{10}^j \rangle_a \\
&\bar{Q}_{p_i4} = -t\langle f_3^i \rangle_a p_d, && \bar{Q}_{p_i3} = t\bar{s}_{33}\langle f_6^i \rangle_a (p_a^k + \zeta t p_d), && \bar{Q}_{p_i7} = t\bar{d}_{33}\langle f_{13}^i \rangle_a (p_a^k + \zeta t p_d) \\
&\tilde{Q}_{p_i1} = -\bar{s}_{13}\langle f_4^i \rangle_a (p_a^k + \zeta t p_d), && \tilde{Q}_{p_i2} = -\bar{s}_{23}\langle f_5^i \rangle_a (p_a^k + \zeta t p_d)
\end{aligned}
\tag{2.28}
$$

$$\bar{Q}_{e_{i7}} = \begin{cases} \langle f_{13}^i \rangle_a \phi_1 & \text{for } k=1 \\ -\langle f_{13}^i \rangle_a \phi_2 & \text{for } k=L \\ 0 & \text{otherwise} \end{cases} \qquad \tilde{Q}_{e_{i5}} = \begin{cases} -\bar{m}\langle f_{12}^i \rangle_a \phi_1 (1-\zeta) & \text{for } k=1 \\ -\bar{m}\langle f_{12}^i \rangle_a \phi_2 \zeta & \text{for } k=L \\ 0 & \text{otherwise} \end{cases} \tag{2.29}$$

where $i_p = n(p-1)+i$, $j_q = n(q-1)+j$ for $p,q = 1,2,\ldots,13$, and $p_a^k = p_a + p_d z_{k-1}$. Since f_l^i are known analytical functions consisting of exponential and trigonometric functions, the integrations $\langle \ldots \rangle_a$ in the above elements have been evaluated in close form.

Eliminating $\hat{\mathbf{G}}$ from Eq. (2.26) using Eq. (2.27) yields

$$\bar{\mathbf{G}}_{,\zeta} = \mathbf{A}\bar{\mathbf{G}} + \mathbf{Q_p} \tag{2.30}$$

where $\mathbf{A} = \mathbf{M}^{-1}[\bar{\mathbf{A}} + \hat{\mathbf{A}}\mathbf{K}^{-1}\tilde{\mathbf{A}}]$ and $\mathbf{Q_p} = \mathbf{M}^{-1}[\bar{\mathbf{Q}}_\mathbf{p} + \hat{\mathbf{A}}\mathbf{K}^{-1}\tilde{\mathbf{Q}}_\mathbf{p}]$. The general solution of the system of first order ODEs with constant coefficients given by Eq. (2.30) is obtained, using the procedure described in Ref. [66] in terms of real constants $C_i^{(k)}$ (i=1,2,....$8n$) as

$$\bar{\mathbf{G}}(\zeta) = \sum_{i=1}^{8n} \mathbf{F}_i(\zeta) C_i^{(k)} + \mathbf{U_0} + \zeta \mathbf{U_1} \tag{2.31}$$

where the elements of the column vector $\mathbf{F}_i(\zeta)$ are expressed using the exponential and trigonometric functions of ζ in terms of the ith eigenvalue and eigenvector of $\mathbf{A}$. $\mathbf{U_0}$ and $\mathbf{U_1}$ are the particular solution vectors, corresponding to the constant and linear loading terms, respectively. The boundary and interface conditions for $g_l^i(\zeta)$ are obtained from Eqs. (2.11)-(2.12) as

$$\text{for } k=1, \quad \text{at } \zeta = 0: \quad g_6^i = 0, \quad g_8^i = 0, \quad g_9^i = 0, \quad g_{10}^i \text{ or } g_{13}^i$$

$$\text{for } k=L, \quad \text{at } \zeta = 1: \quad g_6^i = 0, \quad g_8^i = 0, \quad g_9^i = 0, \quad g_{10}^i \text{ or } g_{13}^i \tag{2.32}$$

$$[(g_1^i,\, g_2^i,\, g_3^i,\, g_6^i,\, g_8^i,\, g_9^i,\, g_{10}^i,\, g_{13}^i)|_{\zeta=1}]^{(k)} = [(g_1^i,\, g_2^i,\, g_3^i,\, g_6^i,\, g_8^i,\, g_9^i,\, g_{10}^i,\, g_{13}^i)|_{\zeta=0}]^{(k+1)} \tag{2.33}$$

for $i = 1,2,\ldots,n$. The $8n \times L$ constants $C_i^{(k)}$ for L layers, are determined using the $8n$ boundary conditions (2.32) and $8n \times (L-1)$ interface continuity conditions.

2.3.2 Second Iteration Step

Now that g_l^i's have been obtained in the previous step, these are considered as known, and new estimates of f_l^i are determined. In this case, the variation $\delta\mathbf{X}$ is obtained from Eq. (2.21) as

$$\delta X_l = \sum_{i=1}^{n} g_l^i(\zeta)\delta f_l^i \tag{2.34}$$

Similar to the thickness direction, $f_l^i(\xi_1)$ are divided into two groups : (i) $\bar{\mathbf{F}}$ containing $8n$ primary variables that appear in the boundary conditions (2.15), and (ii) $\hat{\mathbf{F}}$ containing the remaining $5n$ variables:

$$\bar{\mathbf{F}} = [\, f_1^1 \dots f_1^n \quad f_2^1 \dots f_2^n \quad f_3^1 \dots f_3^n \quad f_4^1 \dots f_4^n \quad f_7^1 \dots f_7^n \quad f_9^1 \dots f_9^n \quad f_{10}^1 \dots f_{10}^n \quad f_{11}^1 \dots f_{11}^n \,]^{\mathrm{T}}$$
$$\hat{\mathbf{F}} = [\, f_5^1 \dots f_5^n \quad f_6^1 \dots f_6^n \quad f_8^1 \dots f_8^n \quad f_{12}^1 \dots f_{12}^n \quad f_{13}^1 \dots f_{13}^n \,]^{\mathrm{T}} \tag{2.35}$$

Equations (2.21) and (2.34) are substituted into Eq. (2.19), and this time, it is integrated over the thickness direction ζ. Since the variations δf_l^i are arbitrary, their coefficients are individually equated to zero, which yields the following system of differential-algebraic equations for f_l^i:

$$\mathbf{N}\bar{\mathbf{F}}_{,\xi_1} = \bar{\mathbf{B}}\bar{\mathbf{F}} + \hat{\mathbf{B}}\hat{\mathbf{F}} + \bar{\mathbf{P}}_{\mathbf{m}} \tag{2.36}$$

$$\mathbf{L}\hat{\mathbf{F}} = \tilde{\mathbf{B}}\bar{\mathbf{F}} + \tilde{\mathbf{P}}_{\mathbf{m}} \tag{2.37}$$

where $\mathbf{N}$, $\bar{\mathbf{B}}$, $\hat{\mathbf{B}}$, $\mathbf{L}$ and $\tilde{\mathbf{B}}$ are matrices of size $8n \times 8n$, $8n \times 8n$, $8n \times 5n$, $5n \times 5n$ and $5n \times 8n$, respectively, and $\bar{\mathbf{P}}_{\mathbf{m}}$ and $\tilde{\mathbf{P}}_{\mathbf{m}}$ are $8n \times 1$ and $5n \times 1$ load vectors. Using the notation $\langle \dots \rangle_h = \sum_{k=1}^{L} t^{(k)} \int_0^1 (\dots)^{(k)}\, d\zeta$ for integration across the laminate thickness, the nonzero elements of matrices $\mathbf{N}$, $\bar{\mathbf{B}}$, $\hat{\mathbf{B}}$, $\mathbf{L}, \tilde{\mathbf{B}}$, $\bar{\mathbf{P}}_{\mathbf{m}}$ and $\tilde{\mathbf{P}}_{\mathbf{m}}$ of Eqs. (2.36)-(2.37) are given below

$$N_{i_1 j_1} = N_{j_4 i_4} = \langle g_4^i g_1^j \rangle_h, \quad N_{i_2 j_2} = N_{j_5 i_5} = \langle g_7^i g_2^j \rangle_h, \; N_{i_3 j_3} = N_{j_6 i_6} = \langle g_9^i g_3^j \rangle_h$$

$$N_{i_7 j_7} = N_{j_8 i_8} = \langle g_{10}^i g_{11}^j \rangle_h, \; \bar{B}_{i_1 j_4} = a\langle \bar{s}_{11} g_4^i g_4^j \rangle_h, \qquad \hat{B}_{i_1 j_1} = a\langle \bar{s}_{12} g_4^i g_5^j \rangle_h$$

$$\hat{B}_{i_1 j_2} = a\langle \bar{s}_{13} g_4^i g_6^j \rangle_h, \qquad \hat{B}_{i_1 j_5} = \langle \bar{d}_{31} g_4^i g_{13}^j \rangle_h, \qquad \bar{B}_{i_2 j_1} = -a\bar{m}\langle g_7^i g_1^j \rangle_h$$

$$\bar{B}_{i_2 j_5} = a\langle s_{66} g_7^i g_7^j \rangle_h, \qquad \bar{B}_{i_3 j_1} = -a\langle g_9^i \tfrac{g_{1,\zeta}^j}{t} \rangle_h, \qquad \bar{B}_{i_3 j_6} = a\langle \bar{s}_{55} g_9^i g_9^j \rangle_h$$

$$\bar{B}_{i_3 j_8} = a\langle \bar{d}_{15} g_9^i g_{11}^j \rangle_h, \qquad \bar{B}_{i_4 j_5} = a\bar{m}\langle g_1^i g_7^j \rangle_h, \qquad \bar{B}_{i_4 j_6} = a\langle \tfrac{g_{1,\zeta}^i}{t} g_9^j \rangle_h$$

$$\hat{B}_{i_5 j_1} = -a\bar{m}\langle g_2^i g_5^j \rangle_h, \qquad \hat{B}_{i_5 j_3} = a\langle \tfrac{g_{2,\zeta}^i}{t} g_8^j \rangle_h, \qquad \hat{B}_{i_6 j_2} = -a\langle g_3^i \tfrac{g_{6,\zeta}^j}{t} \rangle_h$$

$$\hat{B}_{i_6 j_3} = a\bar{m}\langle g_3^i g_8^j \rangle_h, \qquad \bar{B}_{i_7 j_8} = -a\langle \bar{\epsilon}_{11} g_{11}^i g_{11}^j \rangle_h, \; \bar{B}_{i_7 j_6} = a\langle \bar{d}_{15} g_{11}^i g_9^j \rangle_h$$

$$\hat{B}_{i_8 j_4} = a\bar{m}\langle g_{10}^i g_{12}^j \rangle_h, \qquad \hat{B}_{i_8 j_5} = -a\langle g_{10}^i \tfrac{g_{13,\zeta}^j}{t} \rangle_h, \qquad L_{i_1 j_1} = \langle \bar{s}_{22} g_5^i g_5^j \rangle_h$$

$$L_{i_1 j_2} = \langle \bar{s}_{23} g_5^i g_6^j \rangle_h, \qquad L_{i_1 j_5} = \langle \bar{d}_{32} g_5^i g_{13}^j \rangle_h, \qquad L_{j_2 i_1} = L_{i_1 j_2}$$

$$L_{i_2 j_2} = \langle \bar{s}_{33} g_6^i g_6^j \rangle_h, \qquad L_{i_2 j_5} = \langle \bar{d}_{33} g_6^i g_{13}^j \rangle_h, \qquad L_{i_3 j_3} = \langle \bar{s}_{44} g_8^i g_8^j \rangle_h$$

$$
\begin{aligned}
&L_{i_3j_4} = \langle \bar{d}_{24} g^i_8 g^j_{12} \rangle_h, \quad L_{i_4j_3} = L_{i_3j_4}, \qquad\qquad L_{i_4j_4} = -\langle \bar{\epsilon}_{22} g^i_{12} g^j_{12} \rangle_h \\
&L_{i_5j_1} = \langle \bar{d}_{32} g^i_{13} g^j_5 \rangle_h, \quad L_{i_5j_2} = \langle \bar{d}_{33} g^i_{13} g^j_6 \rangle_h, \quad L_{i_5j_5} = -\langle \bar{\epsilon}_{33} g^i_{13} g^j_{13} \rangle_h \\
&\tilde{B}_{i_1j_2} = -\bar{m} \langle g^i_5 g^j_2 \rangle_h, \quad \tilde{B}_{i_1j_4} = -\langle \bar{s}_{12} g^i_5 g^j_4 \rangle_h, \quad \tilde{B}_{i_2j_3} = \langle g^i_6 \tfrac{g^j_{3,\zeta}}{t} \rangle_h, \\
&\tilde{B}_{i_2j_4} = -\langle \bar{s}_{13} g^i_6 g^j_4 \rangle_h, \; \tilde{B}_{i_3j_3} = \bar{m} \langle g^i_8 g^j_3 \rangle_h, \qquad \tilde{B}_{i_3j_2} = \langle g^i_8 \tfrac{g^j_{2,\zeta}}{t} \rangle_h \\
&\tilde{B}_{i_4j_7} = \bar{m} \langle g^i_{12} g^j_{10} \rangle_h, \quad \tilde{B}_{i_5j_4} = -\langle \bar{d}_{31} g^i_{13} g^j_4 \rangle_h, \; \tilde{B}_{i_5j_7} = \langle g^i_{13} \tfrac{g^j_{10,\zeta}}{t} \rangle_h
\end{aligned}
\tag{2.38}
$$

$$
\begin{aligned}
&\bar{P}_{m_{i1}} = a \langle \bar{s}_{13} g^i_4 (p^k_a + p_d t\zeta) \rangle_h, \qquad \bar{P}_{m_{i6}} = -a \langle p_d g^i_3 \rangle_h, \; \tilde{P}_{m_{i1}} = -\langle s_{23} g^i_5 (p^k_a + p_d t\zeta) \rangle_h \\
&\tilde{P}_{m_{i2}} = -\langle s_{33} g^i_6 (p^k_a + p_d t\zeta) \rangle_h, \qquad \tilde{P}_{m_{i4}} = \bar{m} \langle g^i_{12} \bar{g}_{10} \rangle_h \\
&\tilde{P}_{m_{i5}} = \tfrac{1}{t} \langle g^i_{13} \bar{g}_{10,\zeta} \rangle_h - \langle \bar{d}_{33} g^i_{13} (p^k_a + p_d t\zeta) \rangle_h
\end{aligned}
\tag{2.39}
$$

Equations (2.36) and (2.37) are of the same nature as Eqs. (2.26)-(2.27), and are solved following the same procedure. The solution involves $8n$ constants, which are determined from the boundary conditions given by Eq. (2.14), expressed in terms of f^i_l.

The two steps described in Sec. 2.3.1 and Sec. 2.3.2 complete one iteration. The iterations are continued till the desired level of convergence is achieved.

2.4 NUMERICAL RESULTS AND DISCUSSIONS

2.4.1 Stress Field at the Interface of Long Bi-material Strip

To establish the accuracy of the present method in predicting the stresses near the edges, a long bi-material strip under uniform tension (Fig. 2.2) is analysed for which the analytical expressions for the order of singularity in stress components at the interfacial point on the free edge have been provided by Akisanya and Fleck [152]. Two groups of isotropic materials are considered for the study, having a mismatch in the two Young's moduli of elastic stiffness 3 and 100 times. The material properties are listed in Table 2.1. It has been analysed as plain strain problem with infinite length along y-direction. The breadth is taken as h=10a so that the stresses at the interface are independent of h. The singular stress distribution has been analytically predicted in Ref. [152] as:

$$\sigma_z = H r^{\lambda - 1} \tag{2.40}$$

where r is the distance from the free edge interface, H is the intensity of the singularity and $(\lambda - 1)$ is the order of the stress singularity.

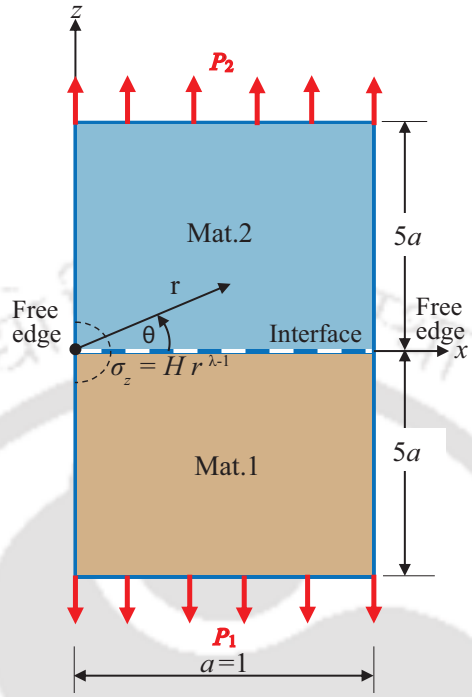

Figure 2.2: Geometry of bi-material strip.

Table 2.1: Material properties

Material group [153]		Mat.1	Mat.2
1	Y(GPa), ν	206, 0.3	70.3, 0.345
2	Y(GPa), ν	100, 0.3	1, 0.3

The distribution of the normal stress ($\bar{\sigma}_z$) along the interface ($z = 0$) obtained from the solution is plotted in Fig. 2.3 for material groups 1 and 2. Converged results are obtained by taking four terms in the trial function. It is seen in Fig. 2.3 that the normal stress is greater than the applied traction load over the range $0 < r/a \leq 0.04$ which can cause delamination near the interface. The order of singularity in the stress distribution is calculated by fitting a power law curve over the plot upto r/a=0.05, and these are compared in Table 2.2 with their theoretical values computed from Eq. (A.9) of Ref. [152]. The coefficient of variation (R^2) is also mentioned in the Table 2.2 and it is nearly equal to 1 for both cases, indicating a good fit to the power law. The comparison shows that the order of stress singularity near the free

edge obtained from the present solution is in excellent agreement with the reference analytical solution. Having established the accuracy of the mixed-field multiterm EKM for edge stresses, we now present results for edge effects in piezoelectric and smart hybrid laminated plates.

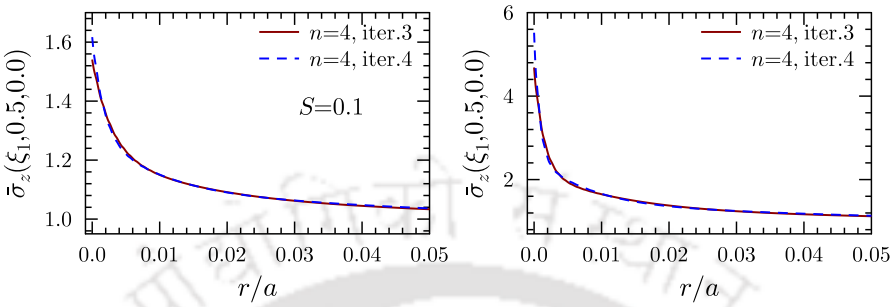

Figure 2.3: Stress distribution along the interface of bi-material strip

Table 2.2: Comparison of order of stress singularity $(\lambda - 1)$.

Material group	Analytical [152]	Present (from Fig. 2.3)
1	-0.0930	-0.096 (R^2 = .9939)
2	-0.2770	-0.271(R^2 = .9928)

2.4.2 Edge Effects in Piezoelectric and Smart Hybrid Laminated Plates

Numerical results are presented for (a) a single layer piezoelectric plate of PZT-5A, for sensory applications, and (b) a smart hybrid soft-core sandwich plate integrated with piezoelectric fiber reinforced composites (PFRC) layers at the top and bottom surfaces, as shown in Fig. 2.4. The interfaces between the PFRC layers with the host laminate in the hybrid plate are grounded ($\phi = 0$). The material properties are listed in Table 2.3.

The following electromechanical load cases are considered.

Load case 1. Pressure $p_2 = p_0 \sin \pi\xi_2$ applied on the top surface.

Load case 2. Actuation potentials applied to top and bottom piezoelectric surfaces, $\phi_1 = \phi_2 = \phi_0 \sin \pi\xi_2$.

The results are presented in nondimensionalised form as given below:

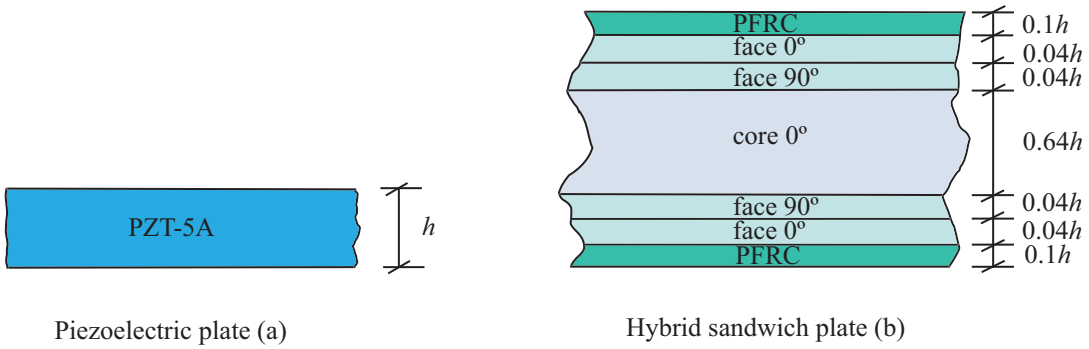

Piezoelectric plate (a) Hybrid sandwich plate (b)

Figure 2.4: Configurations of (a) piezoelectric plate and (b) smart hybrid sandwich plate.

Table 2.3: Material constants.

Material	Y_1	Y_2	Y_3	G_{23}	G_{13}	G_{12}	ν_{12}	ν_{13}	ν_{23}
Face†	181.0	10.3	10.3	2.87	7.17	7.17	0.28	0.28	0.33
Core†	0.276	0.276	3.45	0.414	0.414	0.1104	0.25	0.02	0.02
PZT-5A†	61.0	61.0	53.2	21.1	21.1	22.6	0.35	0.38	0.38
PFRC†	38.87	13.68	13.20	3.0148	4.3541	4.3699	0.31080	0.41796	0.20079
Adhesive	4.2	4.2	4.2	1.59	1.59	1.59	0.32	0.32	0.32
Material	d_{31}	d_{32}	d_{33}	d_{24}	d_{15}	η_{11}	η_{22}	η_{33}	
PZT-5A†	-171	-171	374	584	584	15.3	15.3	15.0	
PFRC†	-263	-224	485	0	0	29.769	29.769	24.403	

Units: Young's moduli Y_i and shear moduli G_{ij} in GPa; piezoelectric strain coefficients d_{ij} in pm/V; electric permittivities η_{ij} in nF/m; †Ref. [67]

Load case 1:

$$(\bar{u}, \bar{w}, \bar{\phi}) = 100(Su,\ w,\ 10^2\phi d_0 S^2)Y_0/p_0 hS^4, \quad (\bar{D}_x,\ \bar{D}_y,\ \bar{D}_z) = (D_x/S,\ D_y/S,\ D_z)/d_0 p_0$$

$$(\bar{\sigma}_x,\ \bar{\sigma}_y,\ \bar{\tau}_{xy},\ \bar{\tau}_{zx},\ \bar{\tau}_{yz}) = (\sigma_x,\ \sigma_y,\ 10\tau_{xy},\ S\tau_{zx},\ S\tau_{yz})/p_0 S^2$$

Load case 2:

$$(\bar{u}, \bar{w}) = (uS,\ w)/S^2 d_0\phi_0, \qquad (\bar{D}_x,\ \bar{D}_y,\ \bar{D}_z) = (SD_x, SD_y, D_z)h/Y_0 d_0^2\phi_0$$

$$(\bar{\sigma}_x,\ \bar{\sigma}_y,\ \bar{\sigma}_z,\ \bar{\tau}_{xy},\ \bar{\tau}_{zx},\ \bar{\tau}_{yz}) = (\sigma_x,\ \sigma_y,\ S^2\sigma_z,\ \tau_{xy},\ S\tau_{zx},\ S\tau_{yz})h/Y_0 d_0\phi_0$$

where $S = a/h$, $Y_0 = 10.3$ GPa, and $d_0 = 374.0 \times 10^{-12}$ m/V for the PZT plate and $d_0 = 100.0 \times 10^{-12}$ m/V for the hybrid plate.

The plates are designated in terms of their mechanical boundary conditions at the edges at $\xi_1 = 0, 1$. For example, a plate which is clamped (C) at $\xi_1 = 0$ and free (F) at $\xi_1 = 1$, is called a C-F plate. The response of the piezoelectric plate is obtained for the pressure load case 1, while the smart hybrid sandwich plate is analysed for both pressure and potential load cases. The EKM results are compared with the 3D exact piezoelasticity solution of Kapuria et al. [154] for simply supported (S-S) plates under CC conditions, and with 3D FE solution obtained using the FE software ABAQUS [155], for all other boundary conditions.

The 20-node hexahedral piezoelectric (C3D20RE) and elastic (C3D20R) solid elements with reduced integration are used for the FE modeling. The converged FE results are obtained by discretizing the piezoelectric plate with a 160 (length) $\times$40 (width) $\times$16 (thickness) mesh, and the multi-layered hybrid plate with a 160 (length) $\times$40 (width) $\times$20 (thickness) mesh. A typical convergence study for the 3D FE is shown in Fig. 2.12 by comparing the results obtained using 80 and 160 elements along the length. The results show excellent convergence at all locations except at the edges.

2.4.3 Single-Layer Piezoelectric Plate

Figure 2.5 presents the response of a thick PZT-5A square plate with $S = 5$ with simply supported ends (S-S) that are electrically under OC condition ($D_x = 0$). The top surface of the plate is under OC condition ($D_z = 0$), while the bottom surface is grounded. The longitudinal variations of displacements $\bar{u}$ and $\bar{w}$, stresses $\bar{\sigma}_x$, $\bar{\tau}_{xy}$, $\bar{\tau}_{zx}$, $\bar{\tau}_{yz}$, sensory potential $\bar{\phi}$, and electrical displacements $\bar{D}_x$, $\bar{D}_y$ and $\bar{D}_z$, at z-locations where they are large, are plotted for one ($n = 1$) and two terms in the trial functions. The 3D FE results are also plotted for comparison. It is observed that the two-term EKM solution is in excellent agreement with 3D FE solution for all the response entities, and even the one-term is very accurate for the S-S plate. Both one-term and two-term solution converge in just two iterations.

Similar results for the plate under clamped-clamped (C-C) boundary conditions are presented in Fig. 2.6. It is observed that the single-term solution is not so accurate for this non-simply supported boundary conditions. The two-term solution, however, matches very well with the 3D FE solution except at the clamped edges specifically for some entities like $\bar{\sigma}_x$ and $\bar{\sigma}_y$. The reason of this mismatch will be explained through Fig. 2.7. The two term solution converges

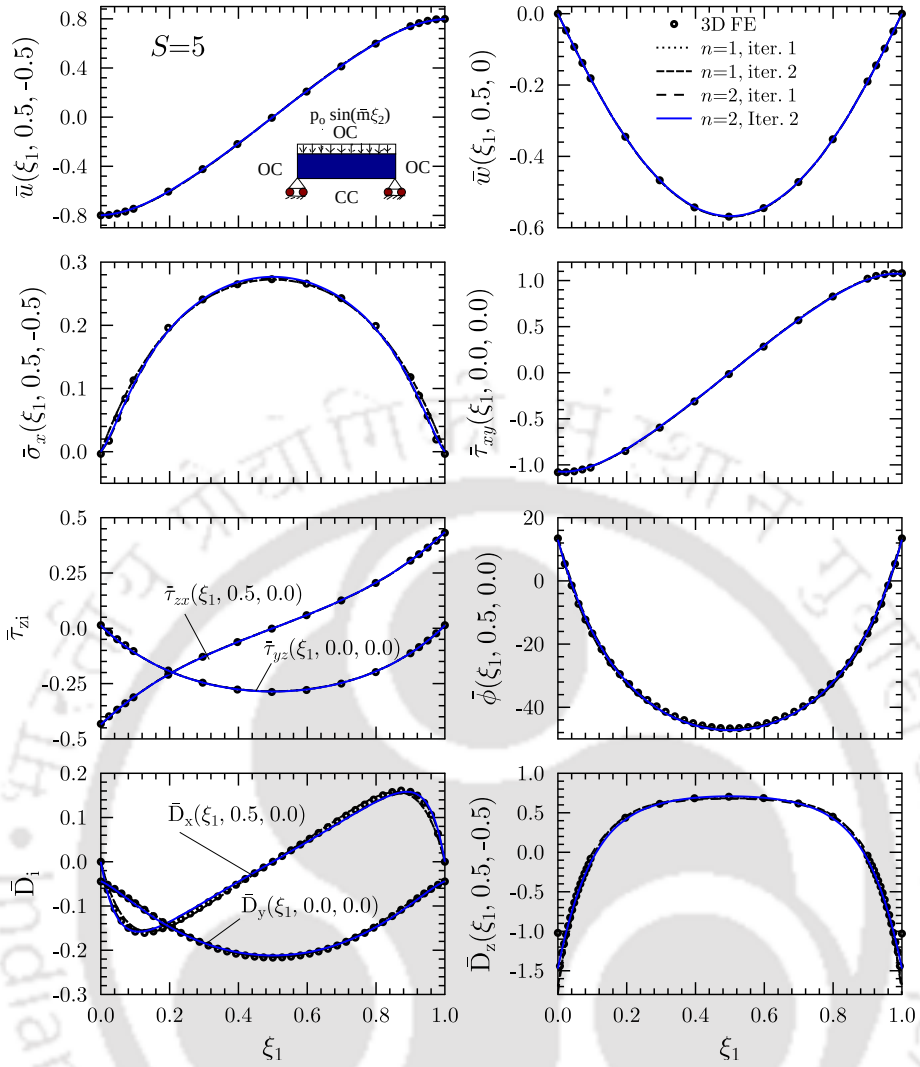

Figure 2.5: Longitudinal variations of displacements, stresses, electric potential and electric displacements for square simply-supported (S-S) piezoelectric plate under pressure loading.

in two iterations.

The through-thickness distributions of $\bar{\sigma}_x$, $\bar{\sigma}_y$, $\bar{\tau}_{zx}$, $\bar{\tau}_{yz}$, $\bar{\phi}$ and $\bar{\sigma}_z$ at various locations along span direction x of the C-C plate are plotted in Fig. 2.7. The nature of the distributions changes from near the support to the interior. For comparison, 3D FE results at the support ($\xi_1 = 0.0$) and slightly away from the support ($\xi_1 = 0.05$) are also plotted in the figure. The plate is subjected to the transverse pressure loading p_z of magnitude -1 at the top of the plate and there is no shear loading applied on the top and bottom surface of the plate. But it can be clearly seen in Fig. 2.7 that the converged 3D FE solution does not satisfy the boundary conditions of $\bar{\sigma}_z$ and $\bar{\tau}_{zx}$ at the clamped edge. The through-thickness variation is highly nonlinear for this case. The displacement based finite element solution can not capture this behaviour due to sharp

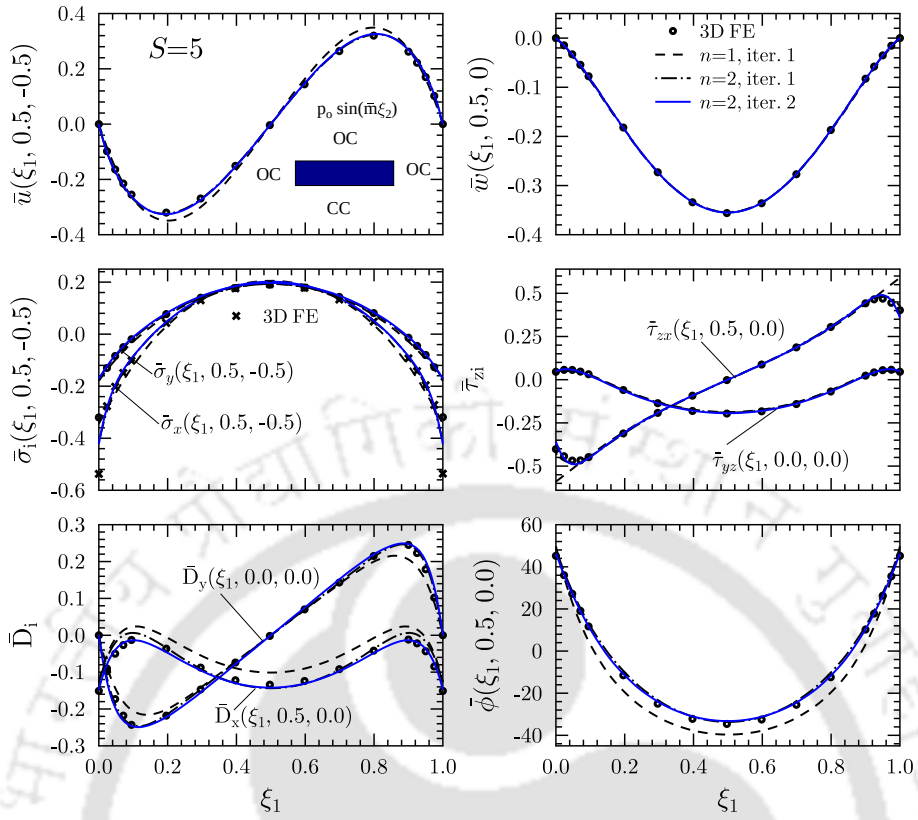

Figure 2.6: Longitudinal variations of displacements, stresses, electric potential and electric displacements for square piezoelectric plate with C-C boundary condition under pressure loading.

gradients across the thickness. The results confirm the limitations of the FE solution reported in literature [45–47]

The through-thickness variations of stresses $\bar{\sigma}_x$, $\bar{\sigma}_y$, $\bar{\tau}_{zx}$ and electrical potential $\bar{\phi}$ in the vicinity of the clamped edge of the C-C PZT plate are presented in Fig. 2.8 for five values of $b/a = 1.0$, 1.5, 2, 4 and 6. As the b/a ratio increases from 1 to 1.5, there is significant increase in the magnitude of all entities. The nature of the distributions of the inplane stresses show appreciable change with the aspect ratio (b/a). It can be seen in Fig. 2.8 that as the ratio b/a increases, results become independent of b/a due to cylindrical bending effect.

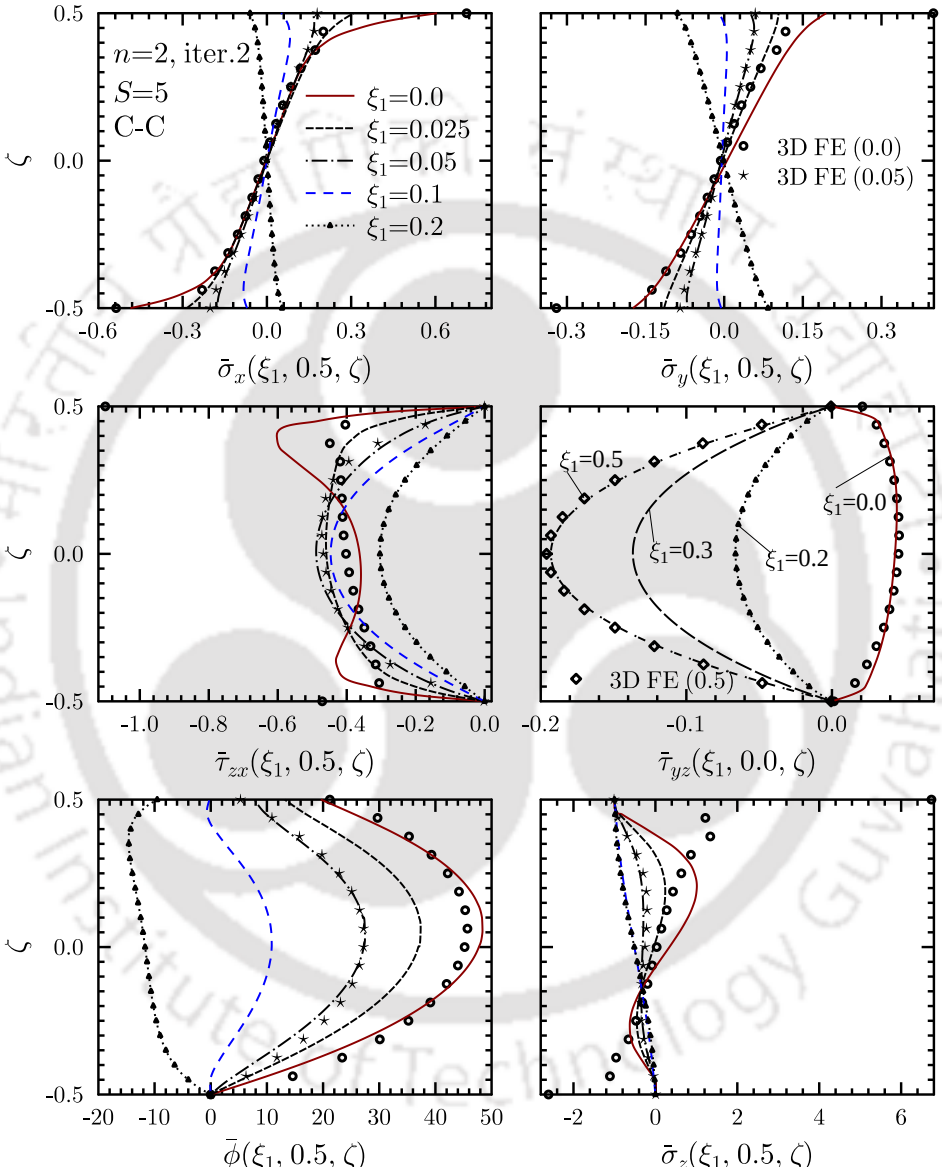

Figure 2.7: Through-thickness distributions of stresses and electric potential for square piezoelectric plate with C-C boundary condition under pressure loading.

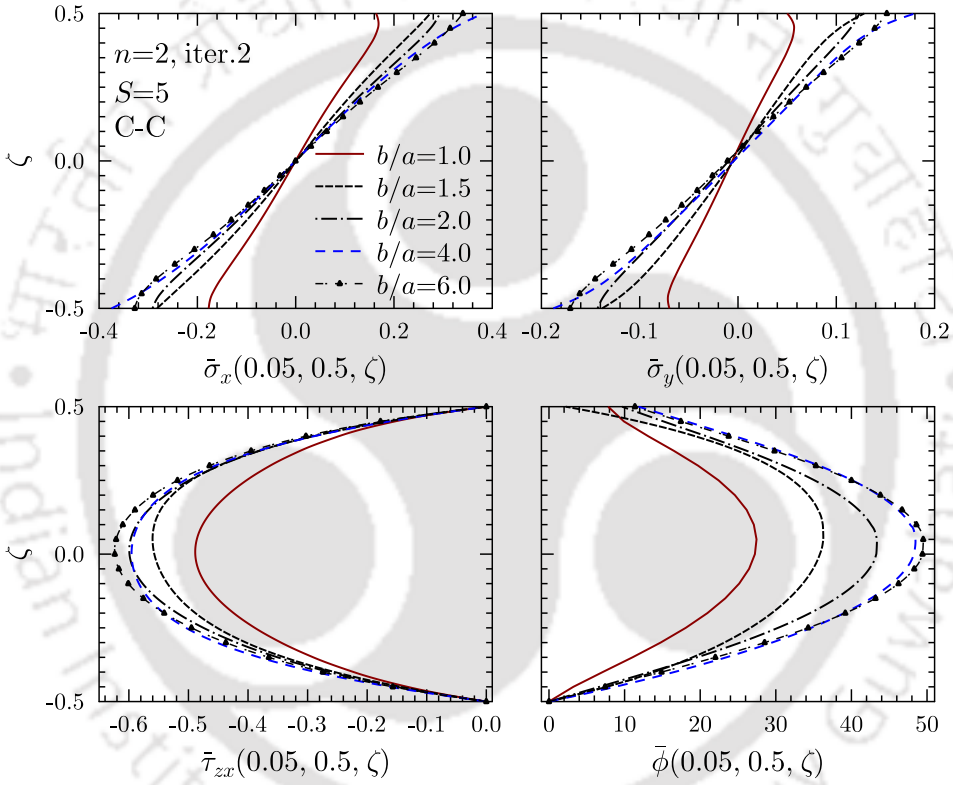

Figure 2.8: Effect of b/a on through-thickness variations of stresses and electric potential for square piezoelectric plate with C-C boundary condition under pressure loading.

2.4.4 Smart Hybrid Sandwich Plate

A simply supported square smart hybrid sandwich plate with CC electric condition at the edges is analyzed next. For such boundary conditions, exact analytical 3D piezoelasticity solutions are available [156, 157]. Since Heyliger [156] presented results only for bi-sinusoidal pressure and potential loadings, the results for the present loading have been obtained using the computer program developed by Kapuria et al. [157] for the thermoelectromechanical analysis. For converged results, 49 non-zero terms are taken in the Fourier series along the ξ_1-direction, in the exact 3D solution. The top and bottom surfaces of the plate are considered under CC condition. The longitudinal variations of deflection $\bar{w}$, stresses $\bar{\sigma}_x$, $\bar{\tau}_{zx}$ and electric displacement $\bar{D}_z$ under the pressure and potential loading are plotted in Fig. 2.9, and compared with the 3D exact solution. It is observed that a two-term (n=2) solution is sufficient enough for accurately predicting the response for the pressure load case, while three terms ($n = 3$) are needed for accurately predicting sharp variations of stresses near the support, for the potential load case. The present results are in excellent agreement with the 3D exact solution for both pressure and potential load cases, where 49 non-zero terms were needed to obtain converged results. It is revealed that under the actuation potential, the load transfer from the actuated piezoelectric layer to the host structure occurs through the interlaminar shear stresses over a small region near the ends of the actuator. The high interlaminar shear stresses at the interfaces may cause debonding near the edges of the piezoelectric actuator, and its accurate prediction has been the subject of many studies since long [43].

Figure 2.10 shows the longitudinal variations of the deflection, stresses and electric displacement in a thick (S=5) square smart hybrid sandwich plate with C-F and C-S boundary conditions under pressure loading. The EKM solution converges in two or three terms with one or two iterations, even though the initial trial functions do not satisfy the given boundary conditions. The EKM results are in very good agreement with FE results except at the clamped edge.

The longitudinal variations of the response entities for the square smart hybrid plate under potential excitation are presented in Figs. 2.11 and 2.12, for C-F, C-S and F-F boundary conditions, respectively. It is observed that for this load case, a three-term solution is able to yield accurate prediction of the response entities, including the sharp variations of $\bar{\sigma}_x$ and $\bar{\tau}_{zx}$

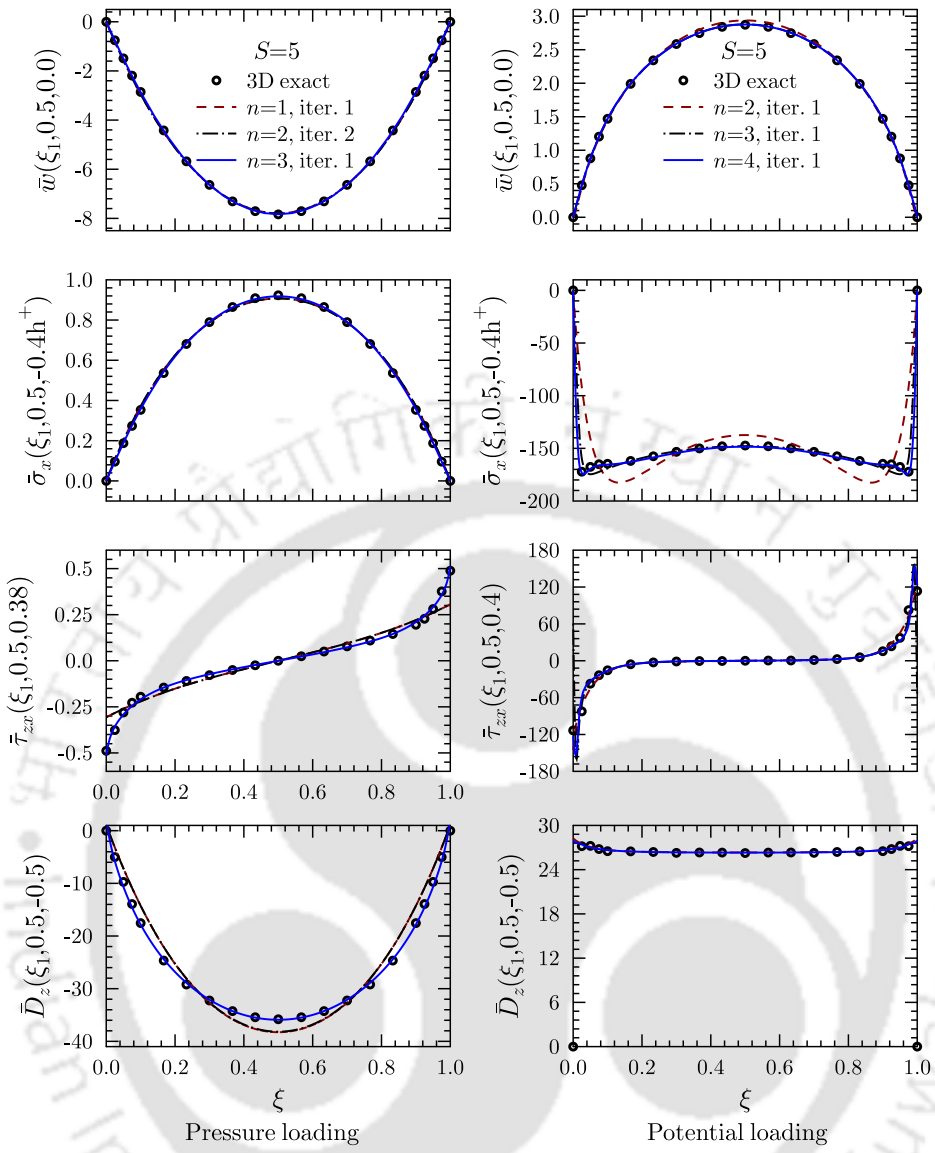

Figure 2.9: Longitudinal variations of displacements, stresses and electric displacement for simply-supported (S-S) sandwich plate under pressure and potential loading.

in the vicinity of clamped and free edges. The nature of distribution of the interlaminar shear stress $\bar{\tau}_{zx}$ at the actuator interface is similar for simply-supported and free edges, and is different from the clamped edge where a stress singularity occurs at the support, which is similar to the pin-force model commonly used for the load transfer mechanism [158]. Here too, the predicted response is in excellent agreement with the FE solution except at the boundary. This mismatch is because the FE solution does not satisfy the condition of zero shear traction at the top and bottom surfaces, and interfacial continuity of transverse shear stresses at the clamped edge, and the condition of $\sigma_x = 0$ and $\tau_{zx} = 0$ at the free edge.

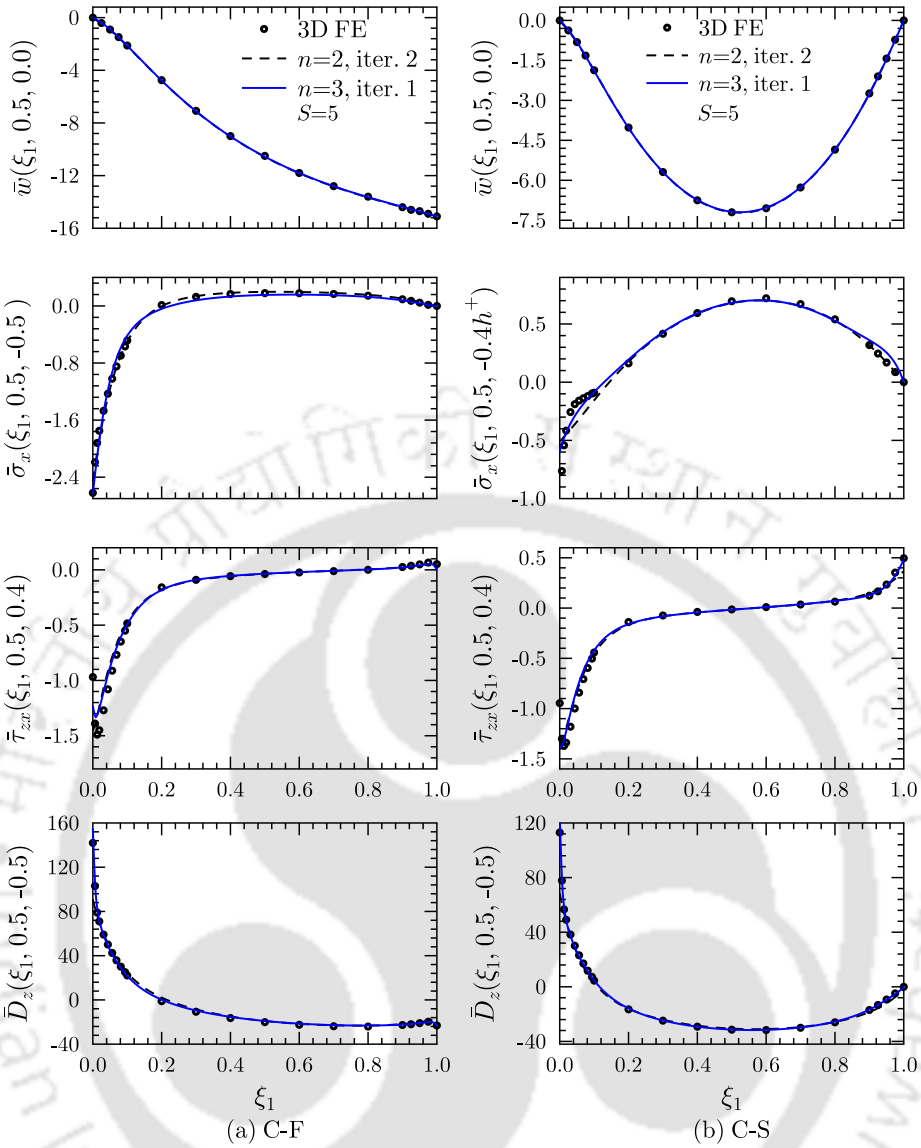

Figure 2.10: Longitudinal variations of deflection, stresses and electric displacement for smart hybrid sandwich plate with C-F and C-S boundary conditions under pressure loading.

2.4.5 Effect of x-Location, Aspect Ratio and Thickness Ratio on the Response Profiles

The through-thickness distributions of $\bar{\tau}_{zx}$ and $\bar{\tau}_{yz}$ at various locations along the span direction x are plotted in Fig. 2.13 for the square smart hybrid plate with F-F boundary condition for the potential load case. It is revealed that nature of the shear stress distribution in the piezoelectric or face layers changes from near the supports to the interior.

Figure 2.14 shows the longitudinal and through-thickness variations of the peeling stress $\bar{\sigma}_z$ for different boundary conditions of the square smart hybrid sandwich plate under potential

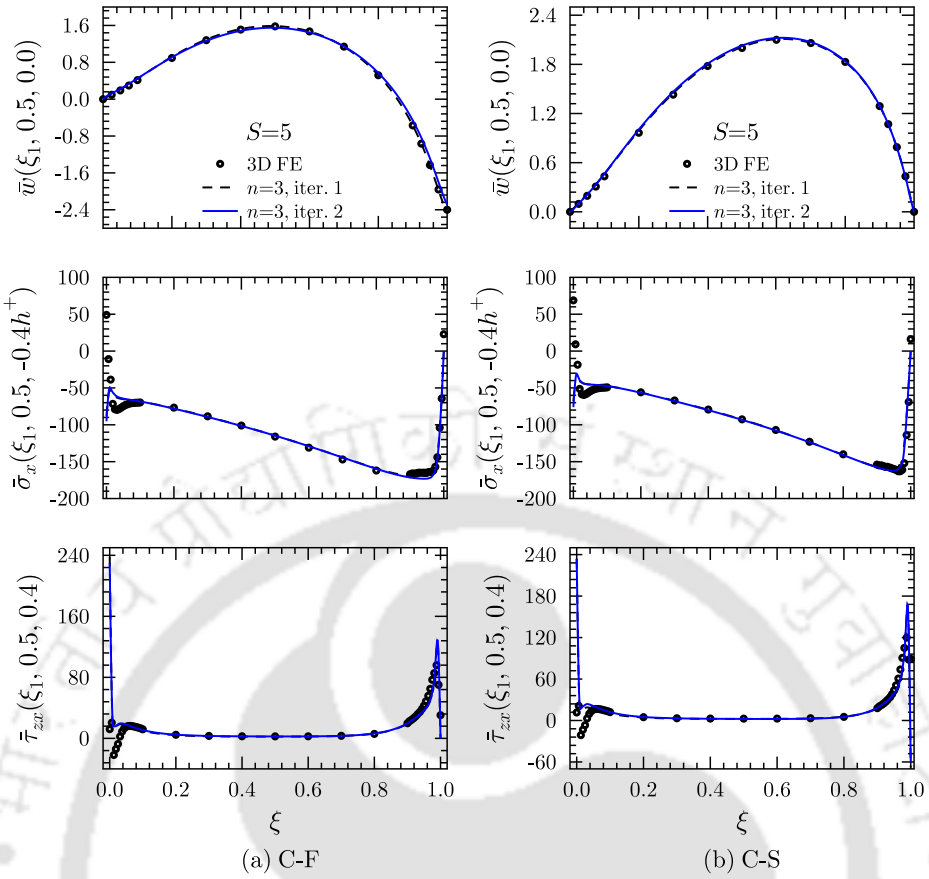

Figure 2.11: Longitudinal variations of deflection and stresses for square smart hybrid plate with C-F and C-S boundary conditions under potential loading.

loading. For better clarity of the edge effects, the longitudinal variation is plotted only for half span. It is observed that there is a singularity in $\bar{\sigma}_z$ at the free and simply supported edge conditions, which does not happen for the clamped support. The maximum $\bar{\sigma}_z$ under the actuation potential loading occurs at the face-core interface, which can initiate debonding at the free and simply-supported edges. For simply supported and free edge boundary conditions, normal stress σ_{xx} must vanish at the edge. Due to this sudden change of inplane normal stress at the boundary, material particles are free to glide at this boundary and move in transverse direction therefore other component of transverse stresses specifically peel stress σ_{zz} may become very high.

Figure 2.15 shows the effect of span-to-thickness ratio S on the nature of through-thickness distributions of transverse shear stress for the square C-F smart smart hybrid sandwich plate under pressure and potential load cases. The variation of stress under the pressure load case is asymmetrical along the mid-surface and the asymmetry is greater in a thicker plate. For the

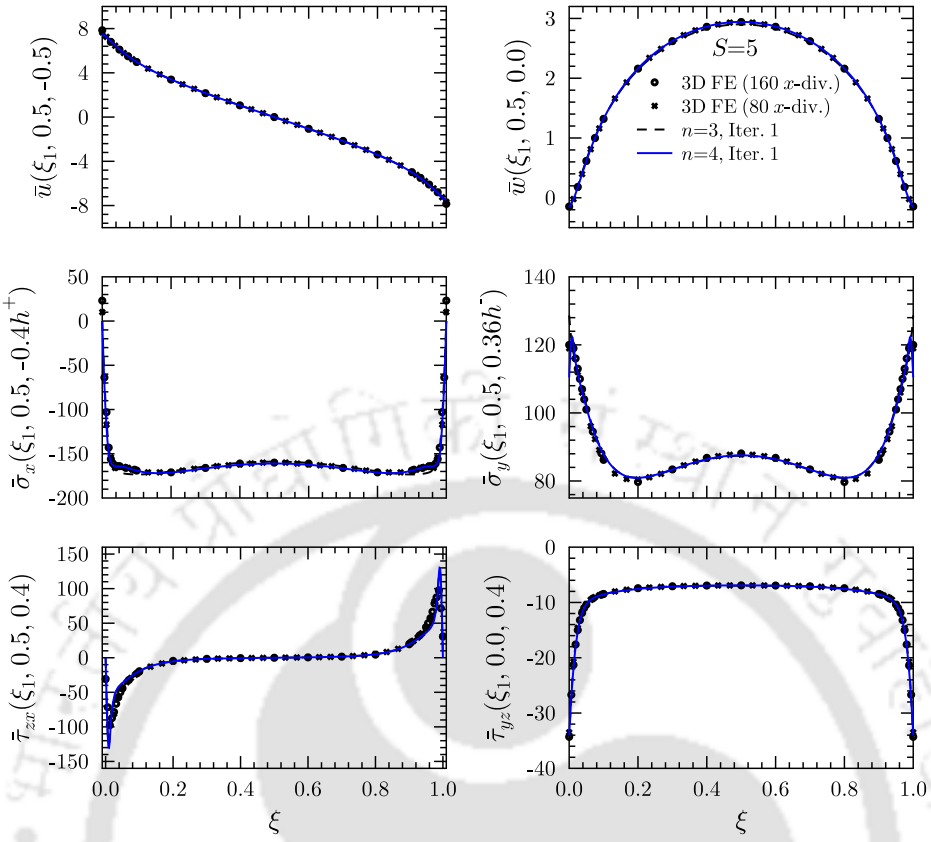

Figure 2.12: Longitudinal variations of deflection and stresses for sandwich plate (b) with free-free (F-F) boundary condition under potential loading.

symmetrically applied potential loading, the through-thickness distributions are always symmetrical. Thick plate ($S = 4$) has a higher value of $\bar{\tau}_{zx}$ at the piezo-elastic interface and it decreases significantly with an increment of S but the central value of $\bar{\tau}_{zx}$ increases with S for both pressure and potential loadings. The sign of $\bar{\tau}_{zx}$ is same throughout the laminate for both thick to thin plate under pressure loading whereas it changes sign (compressive to tensile in the central zone of laminate) for potential case.

The effect of width to length ratio b/a on the through-thickness distributions of the inplane displacement and transverse shear stresses is shown in Fig. 2.16 for a thick smart smart hybrid sandwich plate with C-F boundary condition, under pressure and potential loadings. While the magnitudes of $\bar{u}$ and $\bar{\tau}_{zx}$ increase with the increase in the b/a ratio until $b/a \leq 4$ for both pressure and electric potential load cases, the magnitude of $\bar{\tau}_{yz}$ decreases as the b/a ratio increases. For $b/a > 4$, there is little change in the response with the b/a ratio, as it approaches the cylindrical bending case. But, the nature of through-thickness variations does not seem to change with b/a

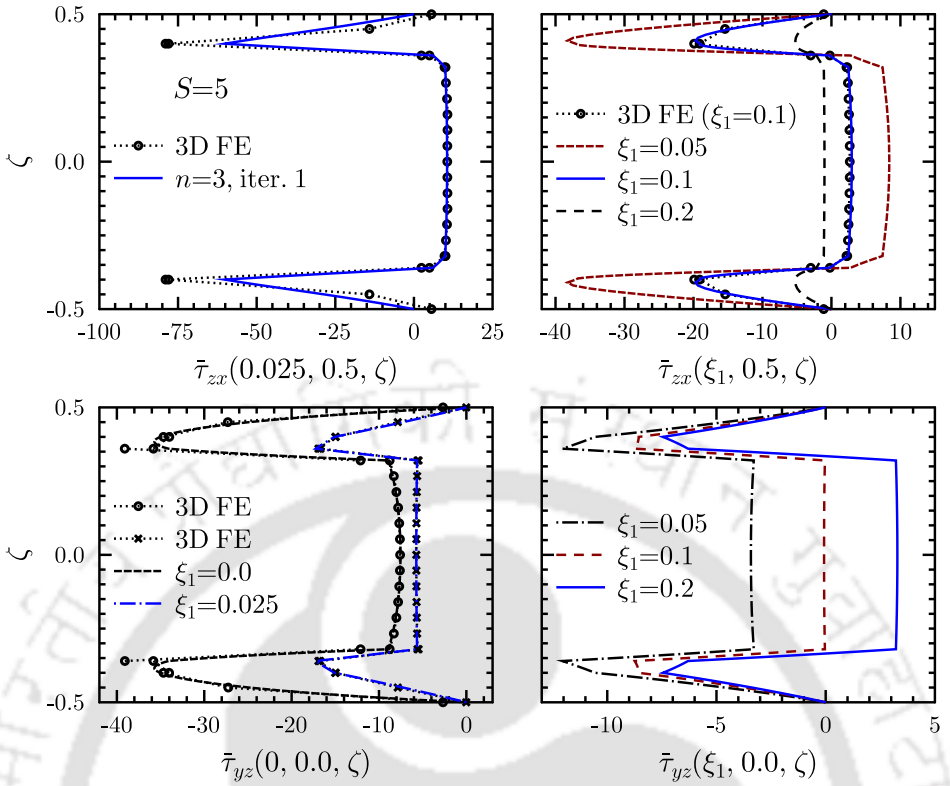

Figure 2.13: Through-thickness variations of stresses for F-F boundary condition at different ξ_1 locations of square sandwich plate under potential loading.

ratio. The effect of b/a on the longitudinal distribution of interlaminar shear stress $\bar{\tau}_{zx}$ at the piezoelectric layer-host laminate interface is shown in Fig. 2.17 for an F-F smart hybrid plate with $S = 5$ under electric potential loading. It is observed that the longitudinal variation of $\bar{\tau}_{zx}$ is independent of b/a. The effect of the actuator thickness on the nature of longitudinal profile of $\bar{\tau}_{zx}$ is also examined in Fig. 2.17 for the same smart smart hybrid plate, by changing the actuator thickness to total thickness ratio (h_p/h) while keeping the face thickness unchanged. It is observed that the shear stress distribution gets sharper near the edge for lower actuator thickness.

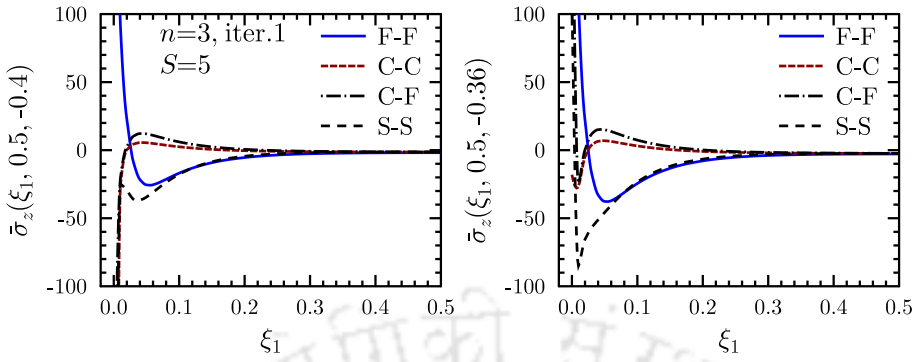

(a) Longitudinal distribution

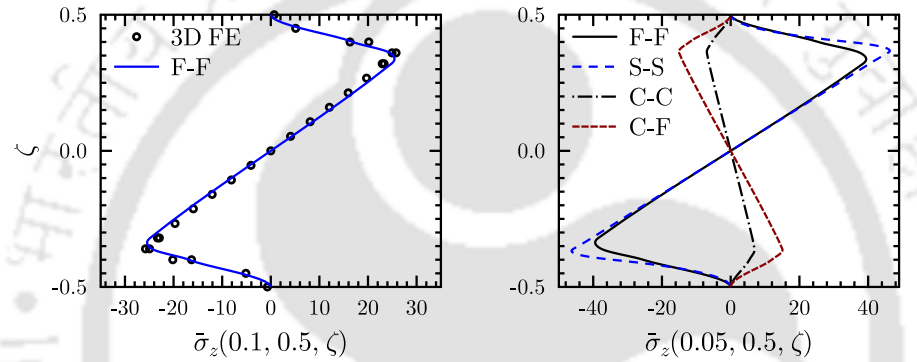

(b) Through-thickness distribution

Figure 2.14: Effect of boundary conditions on $\bar{\sigma}_z$ under potential loading.

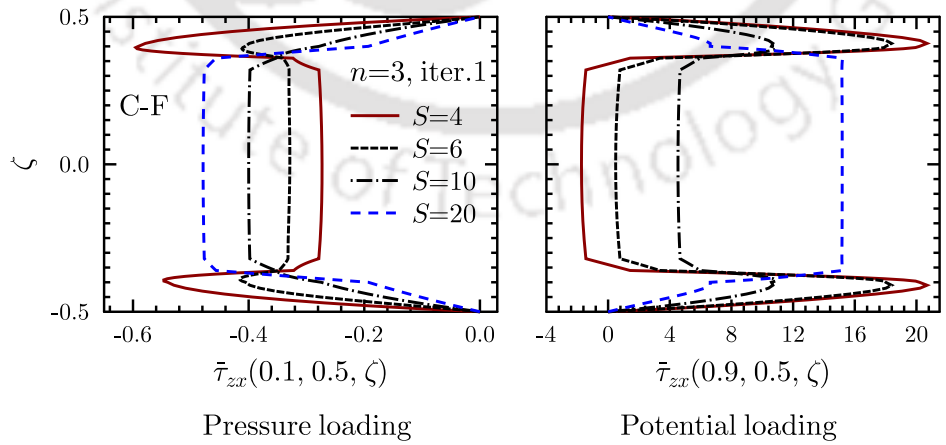

Figure 2.15: Effect of thickness on the through-thickness variations of $\bar{\tau}_{zx}$ for C-F smart hybrid sandwich plate under pressure and and potential loadings.

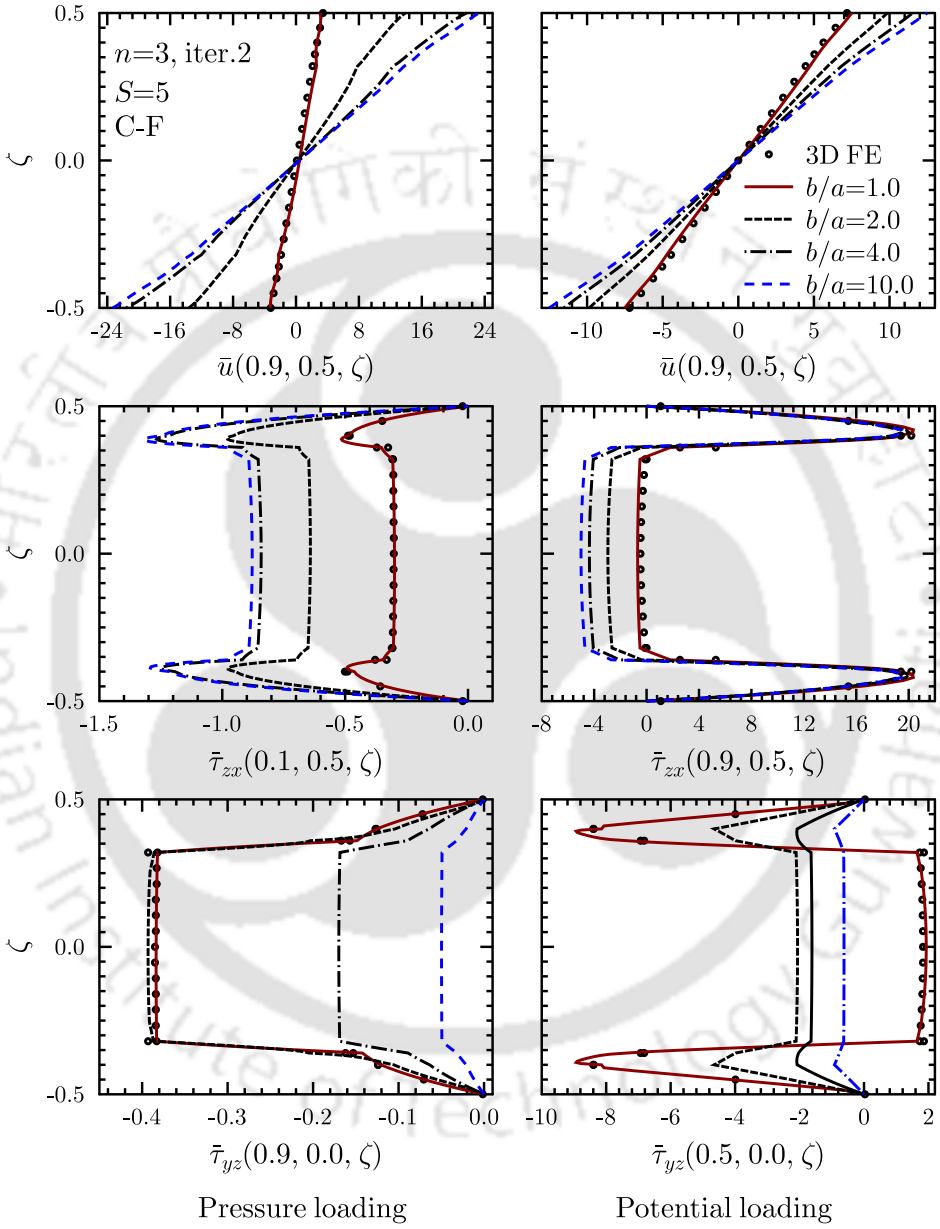

Figure 2.16: Effect of b/a on the through-thickness variations of inplane displacement and shear stresses for C-F smart hybrid sandwich under (a) pressure and (b) potential loadings.

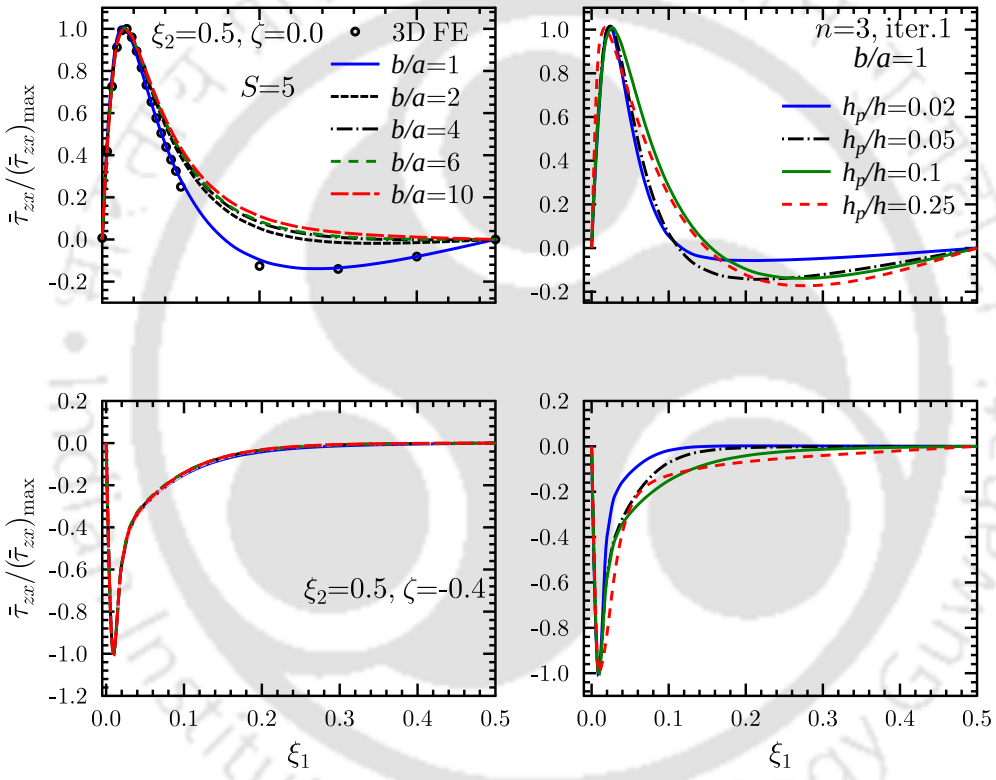

Figure 2.17: Effect of b/a and actuator thickness on the longitudinal variation of interlaminar shear stress for F-F smart hybrid plate under actuation potential

2.4.6 Accurate Estimation of Interlaminar Stresses for the Adhesive Bonded Smart Hybrid Sandwich Plates

The effect of adhesive layer on the interlaminar stresses of a smart hybrid soft-core sandwich plate as shown in Fig. 2.18 is investigated here. The PFRC layers are surface bonded on the top and bottom surfaces of the underneath face layers with the help of adhesive layers of thickness, t_a. Here, $t_a = 0$ indicates the absence of adhesive layers. The interfaces between the PFRC layers with the host sandwich laminate or the adhesive layers in the hybrid plate are grounded ($\phi = 0$). The material properties for this test plate are given in Table 2.3.

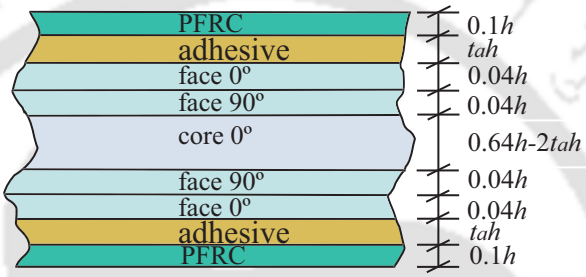

Figure 2.18: Configuration of adhesive bonded smart hybrid sandwich plate.

Figure 2.19 presents the effect of adhesive layer thickness (t_a = 0.0, 0.02, 0.04) on the through-thickness variation of different interlaminar stresses for C-C and C-F boundary conditions under pressure loading. It is observed that for all the response entities ($\bar{\sigma}_x$, $\bar{\tau}_{zx}$, $\bar{\tau}_{yz}$), an increased adhesive layer thickness suppressed the sharp stress variations at the layer interfaces which is visibly more pronounced for the case of $\bar{\tau}_{zx}$. Similar analysis for the potential loading case is presented in Fig. 2.21, but the effect of the adhesive layer thickness on the interlaminar stresses is less pronounced unlike pressure loading case.

In Fig. 2.20 the variation of peeling stress $\bar{\sigma}_z$ for C-C boundary condition under potential loading at two locations i.e. one on the edge and other at the vicinity of that edge is presented. It is to be observed that stress singularity occurs on the edge and the effect of adhesive layer is not prominent but little away (x=0.05) from the edge it is quite convincingly suppressed the stress concentration.

In Fig. 2.22 the longitudinal and through-thickness variation $\bar{\tau}_{zx}$ both for pressure and potential loading is presented with different elastic stiffness of adhesive for C-C boundary condition.

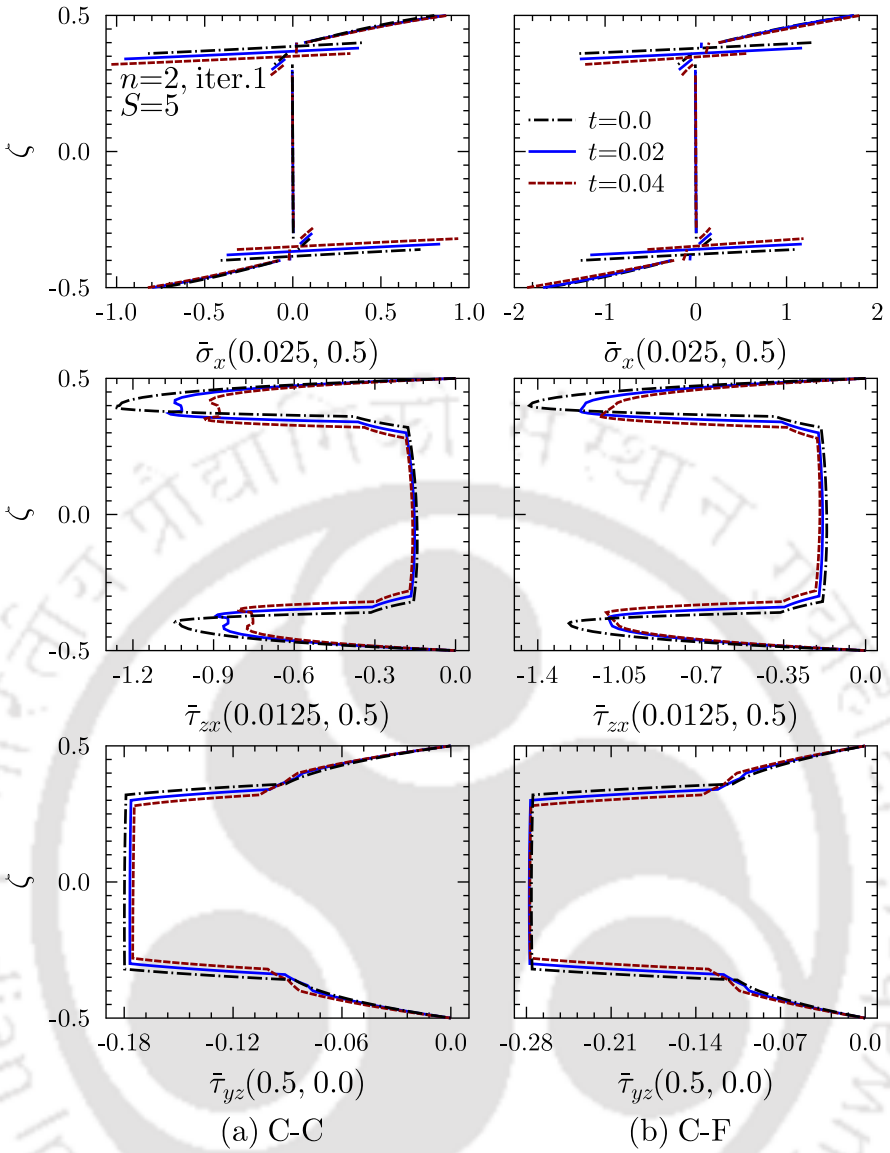

Figure 2.19: Effect of adhesive layer thickness on the through-thickness variation of stresses under pressure loading.

From the plot it is clearly observed that when the elastic stiffness of the adhesive is increased, counter-intuitively the stress concentration at the layer interface is increased, which is due to the fact that increased stiffness has an adverse effect on the binding property of the adhesive.

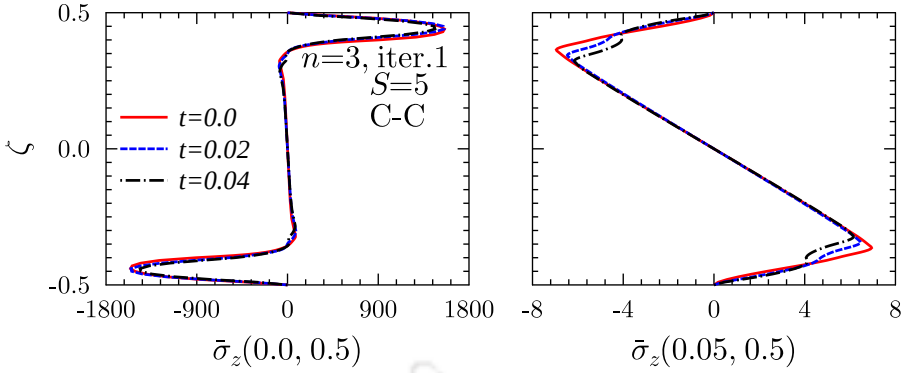

Figure 2.20: Effect of adhesive layer thickness on the through-thickness variation of $\bar{\sigma}_z$ under potential loading.

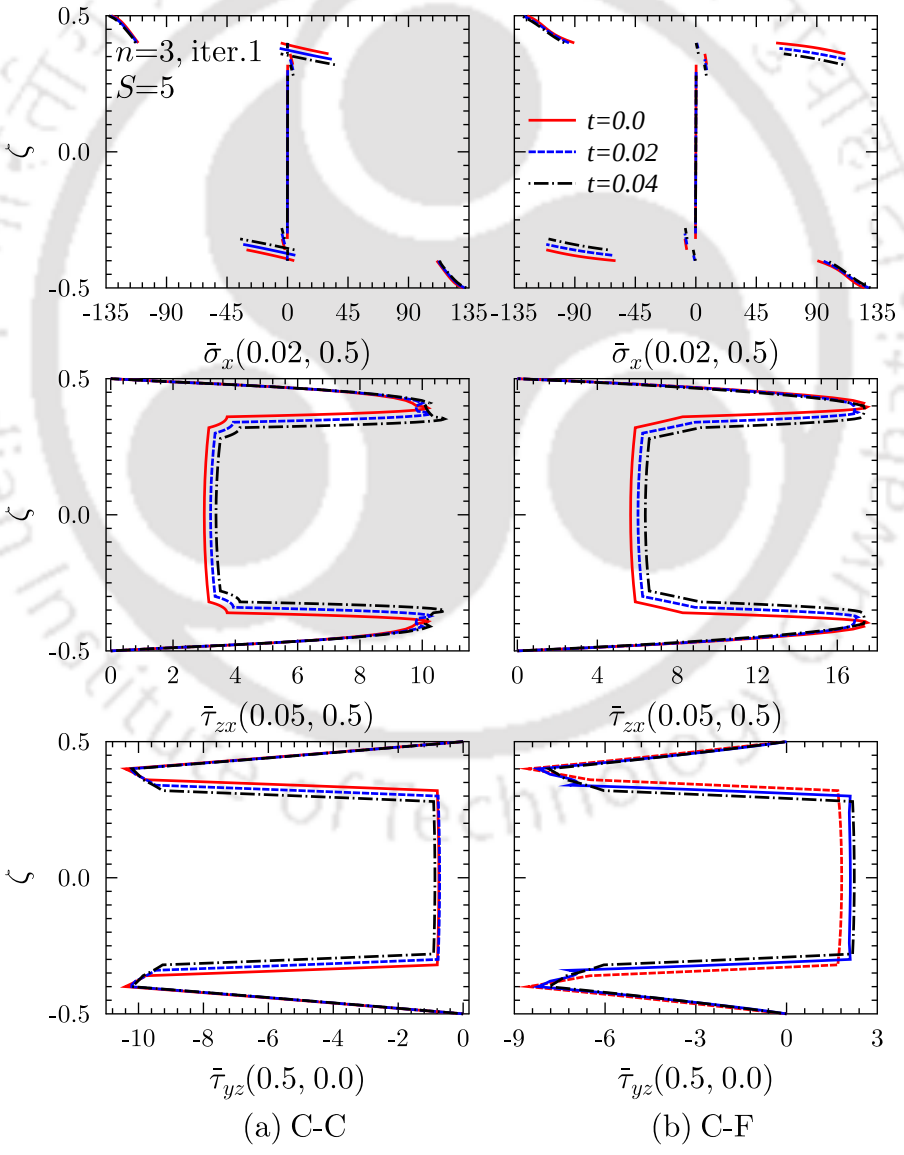

Figure 2.21: Effect of adhesive layer thickness on the through-thickness variation of stresses under potential loading.

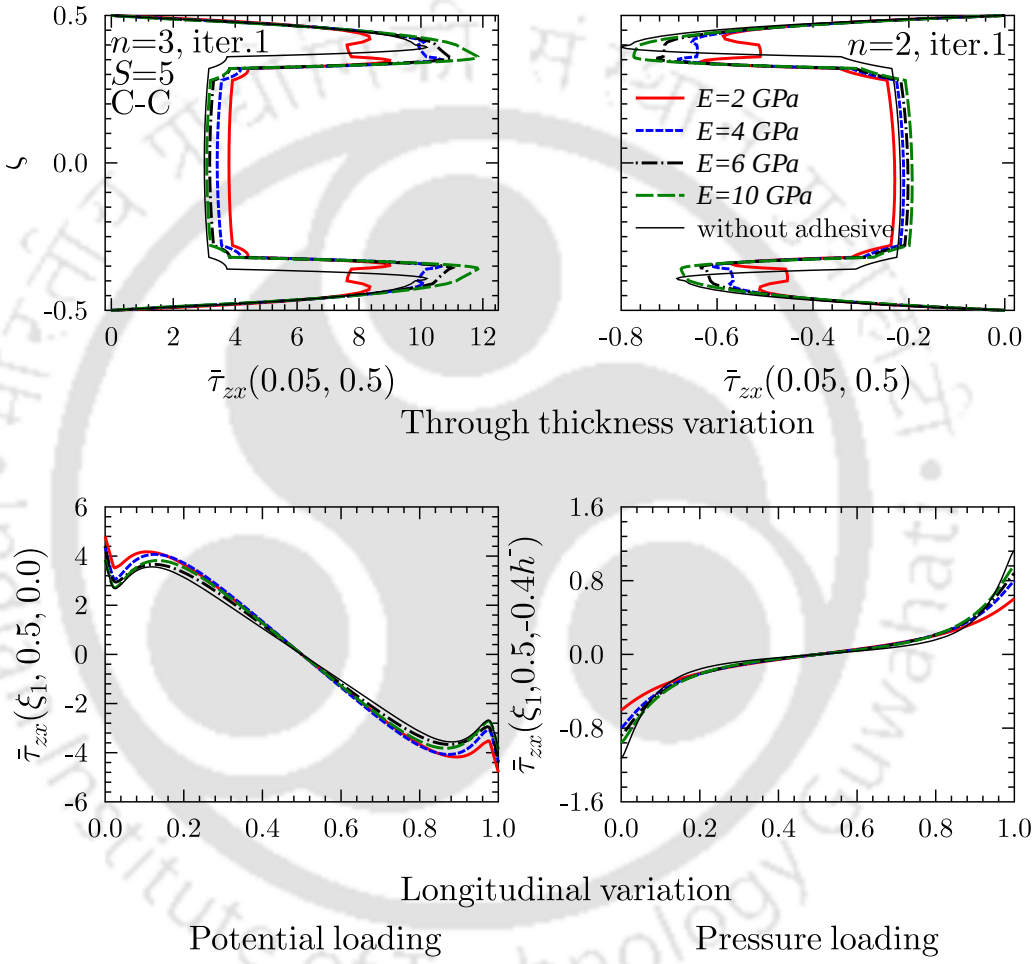

Figure 2.22: Effect of elastic modulus on the interlaminar stress.

2.5 CONCLUSIONS

An accurate 3D piezoelasticity solution for rectangular piezolaminated plates with Levy-type boundary conditions is presented using the mixed-field multi-term EKM, with a view to study the edge effects and the effects of adhesive in finite dimensional plates under pressure as well as electric potential loading. The accuracy of the method for stresses near the edge is established by comparing the order of singularity obtained from the present solution at the interface of a bi-material long strip with the available analytical solution. The solution would also serve as a useful benchmark for assessing the accuracy of the 2D plate theories in predicting such boundary layer effects in piezolaminated plates. The numerical study reveals that:

- The EKM solution converges within just two/three terms in the trial functions, for both single layer piezoelectric plates and hybrid plates under electromechanical loading. A single-term solution, though, is unable to predict the stresses near the edges accurately. It is also shown that for a given value of n, the solution accurately converges generally within two iteration cycles, for all boundary conditions studied.

- The nature of through-thickness distributions of displacements and stresses changes depending on the x-location and thickness ratio. The distribution of in-plane stresses in the piezoelectric layer is dependent on the aspect ratio (b/a).

- The solution provides an accurate means to understand the load transfer mechanism from an actuator to the host structure under applied actuation potential. It is revealed that the load transfer takes place over a small range from the edge of the actuator, leading to a very large interlaminar shear stress near the edge. The nature of its variation along the interface is similar for the simply-supported and free edge conditions. This distribution clearly departs from the pin-force model usually adopted for perfectly bonded actuators, wherein the shear transfer is assumed to take place only at the actuator edges. For the clamped edge, however, a singularity of shear stress is observed, which is similar to the pin-force model. On the other hand, the simply supported and the free edges show a singularity in the peel stress $\bar{\sigma}_z$ which may lead to debonding, whereas the clamped edge does not show the same behaviour.

- It is observed that the use of adhesive as binding layers in piezolaminated composites

helped to smoothen the interlaminar stress concentrations for pressure loading

- But for potential loading case, the interfacial and central values of interlaminar stresses slightly increase with adhesive layer thickness
- Lower elastic modulus gives significant reduction in interlaminar stresses for both pressure and potential load cases

Chapter 3

3D Elasticity Dynamic Solution of Laminated Plates by Extended Kantorovich Method

3.1 INTRODUCTION

A closed form 3D free vibration solution [159] for Levy-type rectangular elastic laminated composite and sandwich plates is developed first time in this chapter using recently developed extended Kantorovich method (EKM). The momentum, strain-displacement and constitutive equations are used to developed the mixed formulation in terms of displacements and stresses as primary variables with the help of extended Hamilton's principle as explained in Sec. 3.2. The partial differential equations (PDEs) in this method are successively reduced to ordinary differential equations (ODEs) and are solved exactly. The solution is built taking the initial functions as a product of two separable functions along the inplane (x) and thickness (z) directions and are expanded satisfying the surface traction free boundary conditions at top and bottom of the plate as shown in Sec. 3.3. The application of variational principle produces a system of $6n$ ODEs and $3n$ linear algebraic equations. The algebraic equations are solved in closed form satisfying the interface continuity and/or the other edge boundary conditions taking the initial trial functions in x-direction and solving in z and x-direction iteratively until appropriate convergence. The coefficient matrix of the $6n$ ODEs contains the frequency (ω) which is obtained by first bracketing the root and then using the bi-section method. It is found that single term solution is sufficient enough for obtaining accurate natural frequencies.

The accuracy of the 3D EKM is established by extensive comparison study with results from other theories and with the 3D FE solution of ABAQUS. The natural frequencies and mode shapes are presented for various configuration and lay-ups. Benchmark natural frequencies are tabulated for composite and sandwich laminates (first time) for different boundary conditions. Effect of span-to-thickness (S) and in-plane modulus ratios on the natural frequencies are also studied. The present solution will serve as a benchmark for assessing two-dimensional (2D) theories and 3D numerical solutions.

3.2 THEORETICAL FORMULATIONS

A generally laminated plate of cross-ply lay-up with dimensions ($a \times b \times h$) as shown in Fig. 3.1, is considered for the present analysis. The laminate has L perfectly bonded orthotropic layers. The k^{th} layer (counted from the bottom) has a thickness of $t_k = z_k - z_{k-1}$, where z_k and z_{k-1} are the thickness coordinate (i.e. z-coordinate) of the upper and lower surfaces of the layer. Henceforth, the layer index k is dropped unless required for clarity. Displacement components at any point in the rectangular laminated plate along x-, y- and z-axis are denoted as u, v and w, respectively which are functions of x, y, z and t, where t is a time variable. The plate is subjected to Levy-type boundary conditions, i.e., simply supported at a pair of opposite edges at $y = 0$ and b. The other pair of edges at $x = 0$ and a, are subjected to arbitrary support conditions.

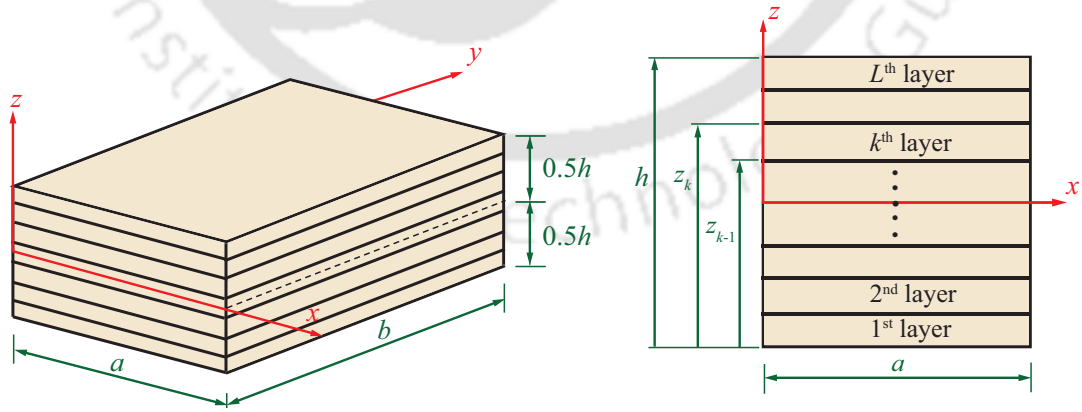

Figure 3.1: Geometry and coordinate system of the laminated plate.

The strain tensor $\varepsilon_{ij}(i, j = x, y, z)$ is related to the displacement component u_i by

$$\varepsilon_{ij} = 0.5(u_{i,j} + u_{j,i}) \tag{3.1}$$

where a comma followed by index j denotes partial differentiation with respect to the position x_j. The 3D linear constitutive equations for a transversely isotropic cross-ply lamina can be written as:

$$\begin{Bmatrix} \varepsilon_x \\ \varepsilon_y \\ \varepsilon_z \\ \gamma_{yz} \\ \gamma_{zx} \\ \gamma_{xy} \end{Bmatrix} = \begin{bmatrix} s_{11} & s_{12} & s_{13} & 0 & 0 & 0 \\ s_{12} & s_{22} & s_{23} & 0 & 0 & 0 \\ s_{13} & s_{23} & s_{33} & 0 & 0 & 0 \\ 0 & 0 & 0 & s_{44} & 0 & 0 \\ 0 & 0 & 0 & 0 & s_{55} & 0 \\ 0 & 0 & 0 & 0 & 0 & s_{66} \end{bmatrix} \begin{Bmatrix} \sigma_x \\ \sigma_y \\ \sigma_z \\ \tau_{yz} \\ \tau_{zx} \\ \tau_{xy} \end{Bmatrix} \tag{3.2}$$

where $[s]$, $\{\varepsilon\}$ and $\{\sigma\}$ denote the elastic compliances, strain vector and stress vector, respectively. For an orthotropic cross-ply lamina the compliance matrix contains only nine independent elastic coefficients. The nine independent elastic compliances and their relations to the engineering material constants are given in Ref. [160].

The modified Hamilton's principle for rectangular elastic plate, without any body force, can be expressed as:

$$\int_t \int_V [(\sigma_{ij,j} - \rho \ddot{u}_i)\delta u_i + (\varepsilon_{ij} - 0.5(u_{i,j} + u_{j,i}))\delta\sigma_{ij}] \mathrm{d}V \mathrm{d}t = 0, \qquad \forall \delta u_i,\ \delta\sigma_{ij}, \tag{3.3}$$

with the variationally consistent boundary conditions at surface boundaries where displacements u_i are prescribed: $u_i - \bar{u_i} = 0$. Here $V(= a \times b \times h)$ is the volume of the plate. With the help of Eq. (3.2), Eq. (3.3) can further be modified to yield

$$\int_t \int_V [(\sigma_{ij,j} - \rho \ddot{u}_i)\delta u_i + ([s]\,\sigma_{ij} - 0.5(u_{i,j} + u_{j,i}))\delta\sigma_{ij}] \mathrm{d}V \mathrm{d}t = 0, \quad \forall\ \delta u_i,\ \delta\sigma_{ij} \tag{3.4}$$

In-plane non-dimensional parameters (ξ_1, ξ_2) are defined as $\xi_1 = x/a$ and $\xi_2 = y/b$, where ξ_1 and ξ_2 varies from 0 to 1. Local thickness parameter $\zeta^{(k)}$ is defined as $\zeta^{(k)} = (z - z_{k-1})/t_k$, where in k^{th} layer $\zeta^{(k)}$ varies from 0 to 1. The top and bottom surfaces of the plate are shear traction free. The boundary conditions on bounding surfaces at edges, $\xi_2 = 0$ and 1 are simply supported ($u = w = \sigma_y = 0$). The plate is subjected to arbitrary support conditions (simply supported, clamped and free) at edges $\xi_1 = 0$ and 1. The interface continuity conditions at the k^{th} interface between k^{th} and $(k+1)^{th}$ layers are:

$$[(u,\, v,\, w,\, \sigma_z,\, \tau_{yz},\, \tau_{zx})|_{\zeta=1}]^{(k)} = [(u,\, v,\, w,\, \sigma_z,\, \tau_{yz},\, \tau_{zx})|_{\zeta=0}]^{(k+1)} \tag{3.5}$$

3.3 FOURIER SERIES-GENERALIZED EKM SOLUTION

The solution of the field variables for the k^{th} layer is expressed in terms of Fourier series in y direction so as to satisfy the simply-supported boundary conditions at edges $y = 0$ and b, is given as:

$$\begin{aligned}(u, w, \sigma_x, \sigma_y, \sigma_z, \tau_{zx}) &= \sum_{m=1}^{\infty} \Re\left[(u, w, \sigma_x, \sigma_y, \sigma_z, \tau_{zx})_m e^{i\omega t}\right] \sin m\pi\xi_2 \\ (v, \tau_{xy}, \tau_{yz}) &= \sum_{m=1}^{\infty} \Re\left[(v, \tau_{xy}, \tau_{yz})_m e^{i\omega t}\right] \cos m\pi\xi_2 \end{aligned} \tag{3.6}$$

where $(...)_m$ denote the m^{th} Fourier term and is a function of x and z. $\Re[\ldots]$ is the real part of the complex number $(\ldots)$. On substitution of the expansions given in Eq. (3.6) into the variational Eq. (3.4), and noting that sine and cosine series functions are orthogonal, Eq. (3.4) reduces to

$$\begin{aligned}\int_t \int_A [&\delta u_m(\tau_{xz_m,z} + \sigma_{x_m,x} - \bar{m}\tau_{xy_m} - \rho\omega^2 u_m) + \delta v_m(\tau_{yz_m,z} + \tau_{xy_m,x} + \bar{m}\sigma_{y_m} - \rho\omega^2 v_m) \\ &+\delta w_m(\sigma_{z_m,z} + \tau_{zx_m,x} - \bar{m}\tau_{yz_m} - \rho\omega^2 w_m) + \delta\sigma_{x_m}(s_{11}\sigma_{x_m} + s_{12}\sigma_{y_m} + s_{13}\sigma_{z_m} - u_{m,x}) \\ &+\delta\sigma_{y_m}(s_{12}\sigma_{x_m} + s_{22}\sigma_{y_m} + s_{23}\sigma_{z_m} + \bar{m}v_m) - \delta\sigma_{z_m}(w_{m,z} - s_{13}\sigma_{x_m} - s_{23}\sigma_{y_m} - s_{33}\sigma_{z_m}) \\ &-\delta\tau_{yz_m}(v_{m,z} + \bar{m}w_m - s_{44}\tau_{yz_m}) - \delta\tau_{zx_m}(u_{m,z} + w_{m,x} - s_{55}\tau_{zx_m}) + \delta\tau_{xy_m}(s_{66}\tau_{xy_m} \\ &-v_{m,x} - \bar{m}u_m)]\mathrm{d}A\mathrm{d}t = 0, \qquad \forall \quad \delta u_{i_m}, \delta\sigma_{i_m}, \delta\tau_{ij_m}\end{aligned} \tag{3.7}$$

for each Fourier term m, where $\bar{m} = m\pi/b$. Here $A(= a \times h)$ is the side area of the plate on xz-plane. The solution of Eq. (3.7) for the field variables

$$\mathbf{X} = [\,u \quad v \quad w \quad \sigma_x \quad \sigma_y \quad \sigma_z \quad \tau_{xy} \quad \tau_{yz} \quad \tau_{zx}\,]_m^{\mathrm{T}} \tag{3.8}$$

for the m^{th} Fourier term is obtained using the multi-term EKM proposed by Kapuria and Kumari [41]. It is assumed in multi-term series of the products of separable functions in the two coordinates ξ_1 and ζ. The solution of the l^{th} variable X_l of $\mathbf{X}$ for the k^{th} layer is thus taken in the form:

$$X_l(\xi_1, \zeta) = \sum_{i=1}^{n} f_l^i(\xi_1) g_l^i(\zeta) \quad \text{for} \quad l = 1, 2, \ldots, 9 \tag{3.9}$$

where $f_l^i(\xi_1)$ and $g_l^i(\zeta)$ are functions of ξ_1 and ζ respectively, for the i^{th} term of the n-term series solution. While functions $f_l^i(\xi_1)$ are valid for all layers, functions $g_l^i(\zeta)$ are determined for each layer separately. These functions are to be determined iteratively, satisfying all homogenous boundary conditions.

3.3.1 Solution Along Thickness Direction (z)

For this case, functions $f_l^i(\xi_1)$ are taken as known, while functions $g_l^i(\zeta)$ are determined. In the first iteration, f_l^i are assumed as

$$\begin{aligned}
&\left[f_1^i(\xi_1), \quad f_7^i(\xi_1), \quad f_9^i(\xi_1)\right] = \cos i\pi\xi_1 \\
&\left[f_2^i(\xi_1), \quad f_3^i(\xi_1), \quad f_4^i(\xi_1), \quad f_5^i(\xi_1), \quad f_6^i(\xi_1), \quad f_8^i(\xi_1)\right] = \sin i\pi\xi_1
\end{aligned} \tag{3.10}$$

which corresponds to the simply supported boundary conditions at $\xi_1 = 0, 1$. The trial functions are not required to satisfy the prescribed boundary conditions. Since f_l^i are known, the variation δX_i is obtained as

$$\delta X_l = \sum_{i=1}^{n} f_l^i(\xi_1)\delta g_l^i, \qquad l = 1, 2, \ldots, 9. \tag{3.11}$$

Only six variables can be solved at a time using the boundary and interface conditions. Functions $g_l^i(\zeta)$ are divided into two sets i.e.

$$\begin{aligned}
\bar{\mathbf{G}} &= [\, g_1^1 \ldots g_1^n \quad g_2^1 \ldots g_2^n \quad g_3^1 \ldots g_3^n \quad g_6^1 \ldots g_6^n \quad g_8^1 \ldots g_8^n \quad g_9^1 \ldots g_9^n \,]^{\mathrm{T}} \\
\hat{\mathbf{G}} &= [\, g_4^1 \ldots g_4^n \quad g_5^1 \ldots g_5^n \quad g_7^1 \ldots g_7^n \,]^{\mathrm{T}}
\end{aligned} \tag{3.12}$$

where $\bar{\mathbf{G}}$ contains the $6n$ variables that appear in boundary and interface along the z direction, while $\hat{\mathbf{G}}$ contains the rest $3n$ variables. Equation (3.11) is substituted in Eq. (3.7), and the integration is performed over ξ_1 direction on the known functions of ξ_1. Since the variations δg_l^i are arbitrary, the coefficients of δg_l^i $(l = 1, ..., 9)$ in the resulting left hand side expression are equated to zero individually. This process yields the following $6n$ first order non-homogeneous ODEs and $3n$ linear algebraic equations for g_l^i for the k^{th} layer:

$$\mathbf{M}\bar{\mathbf{G}}_{,\zeta} = \bar{\mathbf{A}}\bar{\mathbf{G}} + \hat{\mathbf{A}}\hat{\mathbf{G}} \tag{3.13}$$

$$\mathbf{K}\hat{\mathbf{G}} = \tilde{\mathbf{A}}\bar{\mathbf{G}} \tag{3.14}$$

where $\mathbf{M}$, $\bar{\mathbf{A}}$, $\hat{\mathbf{A}}$, $\mathbf{K}$ and $\tilde{\mathbf{A}}$ are $6n \times 6n$, $6n \times 6n$, $6n \times 3n$, $3n \times 3n$ and $3n \times 6n$ matrices. Defining $\langle \ldots \rangle_a = a \int_0^1 (\ldots) d\xi_1$, the nonzero terms of the above described matrices of Eqs. (3.13)-(3.14) are given as follows:

$$
\begin{aligned}
&M_{i_1j_1} = M_{j_6i_6} = \langle f_9^i f_1^j \rangle_a,\ M_{i_2j_2} = M_{j_5i_5} = \langle f_8^i f_2^j \rangle_a,\ M_{i_3j_3} = M_{j_4i_4} = \langle f_6^i f_3^j \rangle_a \\
&\bar{A}_{i_1j_3} = \tfrac{-t}{a}\langle f_9^i f_{3,\xi_1}^j \rangle_a, \qquad \bar{A}_{i_1j_6} = ts_{55}\langle f_9^i f_9^j \rangle_a, \qquad \bar{A}_{i_2j_3} = -\bar{m}t\langle f_8^i f_3^j \rangle_a \\
&\bar{A}_{i_2j_5} = ts_{44}\langle f_8^i f_8^j \rangle_a, \qquad \bar{A}_{i_3j_4} = ts_{33}\langle f_6^i f_6^j \rangle_a, \qquad \hat{A}_{i_3j_1} = ts_{13}\langle f_6^i f_4^j \rangle_a \\
&\hat{A}_{i_3j_2} = ts_{23}\langle f_6^i f_5^j \rangle_a, \qquad \bar{A}_{i_4j_5} = \bar{m}t\langle f_3^i f_8^j \rangle_a, \qquad \bar{A}_{i_4j_6} = \tfrac{-t}{a}\langle f_3^i f_{9,\xi_1}^j \rangle_a \\
&\hat{A}_{i_5j_2} = -\bar{m}t\langle f_2^i f_5^j \rangle_a, \qquad \hat{A}_{i_5j_3} = \tfrac{-t}{a}\langle f_2^i f_{7,\xi_1}^j \rangle_a, \qquad \hat{A}_{i_6j_1} = \tfrac{-t}{a}\langle f_1^i f_{4,\xi_1}^j \rangle_a, \\
&\hat{A}_{i_6j_3} = \bar{m}t\langle f_1^i f_7^j \rangle_a, \qquad K_{i_1j_1} = s_{11}\langle f_4^i f_4^j \rangle_a, \qquad K_{j_2i_1} = s_{12}\langle f_4^i f_5^j \rangle_a \\
&K_{j_2i_1} = K_{i_1j_2}, \qquad K_{i_2j_2} = s_{22}\langle f_5^i f_5^j \rangle_a, \qquad K_{i_3j_3} = s_{66}\langle f_7^i f_7^j \rangle_a \\
&\tilde{A}_{i_1j_1} = \tfrac{1}{a}\langle f_4^i f_{1,\xi_1}^j \rangle_a, \qquad \tilde{A}_{i_1j_4} = -s_{13}\langle f_4^i f_6^j \rangle_a, \qquad \tilde{A}_{i_2j_2} = -\bar{m}\langle f_5^i f_2^j \rangle_a \\
&\tilde{A}_{i_2j_4} = -s_{23}\langle f_5^i f_6^j \rangle_a, \qquad \tilde{A}_{i_3j_1} = \bar{m}\langle f_7^i f_1^j \rangle_a, \qquad \tilde{A}_{i_3j_2} = \tfrac{1}{a}\langle f_7^i f_{2,\xi_1}^j \rangle_a \\
&\bar{A}_{i_4j_3} = -\rho\omega^2 t\langle f_3^i f_3^j \rangle_a, \qquad \bar{A}_{i_5j_2} = -\rho\omega^2 t\langle f_2^i f_2^j \rangle_a, \qquad \bar{A}_{i_6j_1} = -\rho\omega^2 t\langle f_1^i f_1^j \rangle_a
\end{aligned}
\tag{3.15}
$$

where $i_p = (p-1)n + i$, $j_q = (q-1)n + j$ for $p, q = 1, 2, \ldots, 9$. Since f_l are known analytical functions, elements of the matrices defined above have been evaluated in close form.

Equation (3.14) is solved for $\hat{\mathbf{G}}$, which is substituted back into Eq. (3.13) to yield

$$\bar{\mathbf{G}}_{,\zeta} = \mathbf{A}\bar{\mathbf{G}} \tag{3.16}$$

where $\mathbf{A} = \mathbf{M}^{-1}[\bar{\mathbf{A}} + \hat{\mathbf{A}}\mathbf{K}^{-1}\tilde{\mathbf{A}}]$. Equation Eq. (3.16) represents a system of $6n$ homogeneous first order ODEs with constant coefficients. Its complementary solution is of the form $\bar{\mathbf{G}}_{\mathbf{c}}(\zeta) = e^{\lambda\zeta}\mathbf{Y}$, which on substitution in the homogeneous part of Eq. (3.16) yields an eigenvalue problem

$$\mathbf{A}\mathbf{Y} = \lambda\mathbf{Y} \tag{3.17}$$

Hence, the exponent λ and $\mathbf{Y}$ are the $6n$ eigenvalue and eigenvector pairs of matrix $\mathbf{A}$. The eigenvalues λ can be either real or occur in complex conjugate pairs. The general solution of Eq. (3.16) is

$$\bar{\mathbf{G}}(\zeta) = \sum_{i=1}^{6n} \mathbf{F}_i(\zeta) C_i \tag{3.18}$$

where $\mathbf{F}_i(\zeta)$ are column vector of functions corresponding to the eigenpair λ_i and Y_i. After applying the traction free boundary condition at the top and bottom of the plate and satisfying the interface continuity conditions, equation Eq. (3.18) yields

$$\sum_{i=1}^{6n} \mathbf{K_d}_i(\zeta) C_i = \mathbf{0} \tag{3.19}$$

where, the coefficient matrix $\mathbf{K_d}$ depends on $\omega = \omega_n$. For non-trivial solution, it's determinant is zero and ω can be obtained by finding roots of the equation $|det(\mathbf{K_d})|$=0 using bisection method. The undamped natural frequencies $\omega_{01} = \omega_n$ are obtained using the procedure of Kapuria and Achary [101].

3.3.2 Solution Along In-plane Direction (x)

The solution of $g_l^i(\zeta)$ obtained in Sec. 3.3.1 is now taken as known a priori, whereas f_l^i are considered unknown. The variation $\delta\mathbf{X}$ for this case is given by

$$\delta X_l = \sum_{i=1}^{n} g_l^i(\zeta)\delta f_l^i, \qquad l=1, 2, \ldots, 9. \tag{3.20}$$

Similar to the previous solution, the functions $f_l^i(\xi_1)$ are grouped into two sets : (i) vector $\bar{\mathbf{F}}$ of $6n$ primary variables that appear in the arbitrary boundary conditions, and (ii) vector $\hat{\mathbf{F}}$ of the remaining $3n$ variables:

$$\begin{aligned}
\bar{\mathbf{F}} &= [\, f_1^1 \ldots f_1^n \quad f_2^1 \ldots f_2^n \quad f_3^1 \ldots f_3^n \quad f_4^1 \ldots f_4^n \quad f_7^1 \ldots f_7^n \quad f_9^1 \ldots f_9^n \,]^{\mathrm{T}} \\
\hat{\mathbf{F}} &= [\, f_5^1 \ldots f_5^n \quad f_6^1 \ldots f_6^n \quad f_8^1 \ldots f_8^n \,]^{\mathrm{T}}
\end{aligned} \tag{3.21}$$

Equation (3.20) is substituted into the variational equation Eq. (3.7). This time, the integration is performed over the thickness direction ζ, as functions $g_l^i(\zeta)$ are known. Applying the integration by parts over ξ_1, wherever necessary, and equating the coefficients of δf_l^i to zero, since the variations are arbitrary, we obtain the following system of differential-algebraic equations for f_l^i:

$$\mathbf{N}\bar{\mathbf{F}}_{,\xi_1} = \bar{\mathbf{B}}\bar{\mathbf{F}} + \hat{\mathbf{B}}\hat{\mathbf{F}} \tag{3.22}$$

$$\mathbf{L}\hat{\mathbf{F}} = \tilde{\mathbf{B}}\bar{\mathbf{F}} \tag{3.23}$$

where $\mathbf{N}$, $\bar{\mathbf{B}}$, $\hat{\mathbf{B}}$, $\mathbf{L}$ and $\tilde{\mathbf{B}}$ are matrices of size $6n \times 6n$, $6n \times 6n$, $6n \times 3n$, $3n \times 3n$ and $3n \times 6n$, respectively. Using the notation $\langle \ldots \rangle_h = \sum_{k=1}^{L} t^{(k)} \int_0^1 (\ldots)^{(k)}\, d\zeta$ for integration across the laminate thickness, the nonzero elements of the matrices of Eqs. (3.22)-(3.23) are given as follows:

$$
\begin{aligned}
&N_{i_1j_1} = N_{j_4i_4} = \langle g_4^i g_1^j \rangle_h,\ N_{i_2j_2} = N_{j_5i_5} = \langle g_7^i g_2^j \rangle_h,\ N_{i_3j_3} = N_{j_6i_6} = \langle g_9^i g_3^j \rangle_h \\
&\bar{B}_{i_1j_4} = \langle s_{11} g_4^i g_4^j \rangle_h, \quad \hat{B}_{i_1j_1} = \langle s_{12} g_4^i g_5^j \rangle_h, \quad \hat{B}_{i_1j_2} = \langle s_{13} g_4^i g_6^j \rangle_h \\
&\bar{B}_{i_2j_1} = -\bar{m}\langle g_7^i g_1^j \rangle_h, \quad \bar{B}_{i_2j_5} = \langle s_{66} g_7^i g_7^j \rangle_h, \quad \bar{B}_{i_3j_1} = -\langle g_9^i \tfrac{g_{1,\zeta}^j}{t} \rangle_h \\
&\bar{B}_{i_3j_6} = \langle s_{55} g_9^i g_9^j \rangle_h, \quad \bar{B}_{i_4j_5} = \bar{m}\langle g_1^i g_7^j \rangle_h, \quad \bar{B}_{i_4j_6} = \langle \tfrac{g_{1,\zeta}^i}{t} g_9^j \rangle_h \\
&\hat{B}_{i_5j_1} = -\bar{m}\langle g_2^i g_5^j \rangle_h, \quad \hat{B}_{i_5j_3} = \langle \tfrac{g_{2,\zeta}^i}{t} g_8^j \rangle_h, \quad \hat{B}_{i_6j_2} = -\langle g_3^i \tfrac{g_{6,\zeta}^j}{t} \rangle_h \\
&\hat{B}_{i_6j_3} = \bar{m}\langle g_3^i g_8^j \rangle_h, \quad L_{i_1j_1} = \langle s_{22} g_5^i g_5^j \rangle_h, \quad L_{i_1j_2} = \langle s_{23} g_5^i g_6^j \rangle_h \\
&L_{i_2j_2} = \langle s_{33} g_6^i g_6^j \rangle_h, \quad L_{j_2i_1} = L_{i_1j_2}, \quad L_{i_3j_3} = \langle s_{44} g_8^i g_8^j \rangle_h \\
&\tilde{B}_{i_1j_2} = -\bar{m}\langle g_5^i g_2^j \rangle_h, \quad \tilde{B}_{i_1j_4} = -\langle s_{12} g_5^i g_4^j \rangle_h, \quad \tilde{B}_{i_2j_3} = \langle g_6^i \tfrac{g_{3,\zeta}^j}{t} \rangle_h \\
&\tilde{B}_{i_2j_4} = -\langle s_{13} g_6^i g_4^j \rangle_h, \quad \tilde{B}_{i_3j_3} = \bar{m}\langle g_8^i g_3^j \rangle_h, \quad \tilde{B}_{i_3j_2} = \langle g_8^i \tfrac{g_{2,\zeta}^j}{t} \rangle_h \\
&\bar{B}_{i_4j_1} = a\rho\omega^2\langle g_1^i g_1^j \rangle_h, \quad \bar{B}_{i_5j_2} = a\rho\omega^2\langle g_2^i g_2^j \rangle_h, \quad \bar{B}_{i_6j_3} = a\rho\omega^2\langle g_3^i g_3^j \rangle_h
\end{aligned}
\tag{3.24}
$$

Since the functions $g_l(\zeta)$ are known in close form, the above integrations are computed in close form. Using Eq. (3.23), $\hat{\mathbf{F}}$ is eliminated from Eq. (3.22) to yield

$$
\bar{\mathbf{F}}_{,\xi} = \mathbf{B}\bar{\mathbf{F}} \tag{3.25}
$$

with $\mathbf{B} = \mathbf{N}^{-1}[\bar{\mathbf{B}} + \hat{\mathbf{B}}\mathbf{L}^{-1}\tilde{\mathbf{B}}]$. The same procedure is used for obtaining the natural frequency $\omega_{01} = \omega_n$ as in Sec. 3.3.1. In this case, Eq. (3.25) is of the same nature as Eq. (3.16) and is solved similarly satisfying the boundary conditions at $\xi_1 = 0, 1$. The two solution steps described in Secs. 3.3.1 and 3.3.2 complete one iteration. These are repeated till the converged natural frequency is obtained. The similar treatment for handling the large positive eigenvalues is adopted here as used in Ref. [41].

3.4 RESULTS AND DISCUSSION

In this section, the proposed analytical method is employed to analyse the free vibration of Levy-type rectangular composite and sandwich plates. An exhaustive comparison of present results with results available in literature is presented first. Since limited analytical solution exists, therefore present results are compared with the three-dimensional finite element (3D FE)

solutions obtained from FE software ABAQUS [161]. For this purpose, the 20-noded (C3D20R) solid elements with reduced integration is used. The converged FE results are obtained by discretizing the plate with a [50(length) × 50(width) × 20(thickness)] mesh for both composite and sandwich plates.

The natural frequency $\bar{\omega}_m$, the modal displacements and stresses are non-dimensionalized as:

$$\bar{\omega}_m = \omega a S \sqrt{\rho_0 / Y_2} \tag{3.26}$$

$$(\bar{u},\, \bar{v},\, \bar{w}) = (u, v, w)/\max(u, v, w) \tag{3.27}$$

$$(\bar{\sigma}_x,\, \bar{\sigma}_y,\, \bar{\sigma}_z,\, \bar{\tau}_{yz},\, \bar{\tau}_{zx}) = (\sigma_x,\, \sigma_y,\, \sigma_z,\, \tau_{yz},\, \tau_{zx}) S\, h/Y_2 \max(u, v, w)$$

where $S = a/h$. The plates are denoted in terms of their boundary conditions at the edges at ξ_1(or x)=0, 1(or a). For example, a clamped-free (C-F) plate is clamped at ξ_1(or x)=0 and free at ξ_1(or x)=1(or a) where as the other pair of edges (ξ_2=0, 1) are constantly simply supported.

3.4.1 Free Vibration Analysis of Cross-ply Laminated Plates

3.4.1.1 Validation

The orthotropic material parameters considered in the present study in dimensionless forms are as follows: $Y_1/Y_2 = 40, Y_2 = Y_3 = 6.9\,\text{GPa}, G_{12} = G_{13} = 0.6Y_2, G_{23} = 0.5Y_2, \nu_{23} = \nu_{13} = \nu_{12} = 0.25$. Any modification to the above material constants are mentioned in the respective places. All the laminas under investigation have the same thickness and mass density, where the value of density ρ_0=1000 kg/m^3.

The accuracy of the present method has been established by comparing the fundamental frequency parameter $\bar{\omega}_n$, for simply-supported square laminates with the un-symmetric and symmetric schemes of [0°/90°] and [0°/90°/90°/0°] as listed in Table 3.1. The present results are in excellent agreement with the results from the literature even for thick laminates having span-to-thickness ratio, $S(= a/h)$=2. It is also observed that for both the cases an increase in laminate thickness lowers the bending fundamental frequencies. It is also observed that for various span-to-thickness ratios S, the present predictions(n=1, iter.=1) match exactly with the 3D exact solution.

Dimensionless natural frequencies are compared with Boscolo and Banerjee [82] for different boundary conditions in Table 3.2 for thick (S=5) composite plate of lay-up [0°/90°] with in-plane modulus ratio Y_1/Y_2=30 except for SS case where additional results for Y_1/Y_2=3 are also presented. For simply supported case present approach is exactly matching with 3D elasticity solution of Noor and Burton [73]. The present results match excellently with Ref. [82] for all boundary conditions.

Table 3.1: Comparison of the fundamental frequency parameter, $\bar{\omega}$ for simply-supported (S-S) cross-ply laminated composite plate

Lay-up scheme	Theory	S					
		2	5	10	20	50	100
[0°/90°]	Present, $n = 1$	4.953	8.526	10.336	11.036	11.263	11.297
	Present, $n = 2$	4.952	8.544	10.341	11.048	11.271	11.284
	3D Exact [101]	4.953	8.526	10.336	11.036	11.263	11.297
	Chen and Lü [90]	4.953	8.526	10.336	11.036	11.263	11.297
	Nosier et al. [162]	4.953	8.518	10.333	11.036	11.263	11.297
	Matsunaga [77]	4.956	8.530	10.337	11.037	11.263	11.297
	Wu and Chen [76]	4.959	8.527	10.337	11.037	11.264	11.300
	Cho et al. [163]	4.810	8.388	10.270	11.016	11.260	11.296
[0°/90°/90°/0°]	Present, $n = 1$	5.314	10.682	15.068	17.635	18.669	18.835
	3D Exact [101]	5.314	10.682	15.068	17.635	18.669	18.835
	Chen and Lü [90]	5.314	10.682	15.068	17.635	18.670	18.835
	Matsunaga [77]	5.321	10.687	15.072	17.636	18.670	18.835
	Wu and Chen [76]	5.317	10.682	15.069	17.636	18.670	18.835
	Cho et al. [163]	5.923	10.673	15.066	17.535	18.670	18.835

Table 3.2: Comparison of first five dimensionless frequencies $\bar{\omega}_m = \omega h\sqrt{\rho_0/Y_2}$ for a two layer $[0°/90°]$ laminated composite plate with material parameters: $Y_1/Y_2 = 30, G_{12}/Y_2 = G_{13}/Y_2 = 0.5, G_{23}/Y_2 = 0.35, \nu_{12} = \nu_{13} = 0.3, \nu_{23} = 0.49$

BCs	Theory	Mode sequences				
		1	2	3	4	5
S-S(Y_1/Y_2=3)	Present	0.2392	0.5262	0.5262	0.7420	0.8980
	3D Exact [73]	0.2392	-	-	-	-
	DSM [82]	0.2398	-	-	-	-
S-S	Present	0.3117	0.6361	0.6361	0.8532	1.0185
	3D Exact [73]	0.3117	-	-	-	-
	DSM [82]	0.3135	-	-	-	-
C-C	Present	0.3782	0.6664	0.6772	0.8819	1.0345
	DSM [82]	0.3830	0.6706	0.6908	0.8924	1.0400
	3D FE	0.3822	0.6689	0.6890	0.8886	1.0371
C-F	Present	0.2328	0.4260	0.5942	0.7107	0.7784
	DSM [82]	0.2336	0.4313	0.5964	0.7153	0.7813
	3D FE	0.2332	0.4305	0.5948	0.7138	0.7794
S-F	Present	0.2179	0.3984	0.4320	0.5893	0.6970
	DSM [82]	0.2183	0.3998	0.4322	0.5909	0.6996
	3D FE	0.2179	0.3993	0.4321	0.5893	0.6981
F-F	Present	0.2073	0.2438	0.4120	0.5138	0.5763
	DSM [82]	0.2077	0.2446	0.4123	0.5144	0.5825
	3D FE	0.2073	0.2442	0.4123	0.5135	0.5809

The effect of span-to-thickness ratio (S) on the fundamental frequency parameters ($\bar{\omega}_n$) for arbitrary boundary conditions is presented in Table 3.3 for symmetric laminate [0°/90°/0°]. In this table, present results are compared with 2D analytical solution based on higher order plate theory [75]. 3D FE results are also presented for comparison. It is observed that higher order shear deformation theory [75] underpredicts the natural frequencies for C-C, S-C and S-S supports, whereas it overpredicts the natural frequencies for F-C, F-S and F-F supports. Present results are in good agreement with 3D FE.

Table 3.3: Comparison of dimensionless fundamental frequency ($\bar{\omega}$) of a three layer [0°/90°/0°] laminated composite plate

Theory	S	C-C	S-C	S-S	F-C	F-S	F-F
Present, $n = 1$	2	5.332	5.203	5.183	3.456	3.067	2.712
Present, $n = 2$		5.331	5.201	5.192	3.481	3.072	2.715
Khdeir and Librescu [75]		5.198	5.163	5.158	3.577	3.214	2.910
3D FE		5.341	5.241	5.183	3.473	3.076	2.713
Present, $n = 1$	5	11.467	10.670	10.245	5.827	4.414	3.906
Present, $n = 2$		11.426	10.679	10.246	5.810	4.401	3.911
Khdeir and Librescu [75]		11.164	10.576	10.240	5.897	4.518	4.025
3D FE		11.518	10.759	10.246	5.862	4.421	3.907
Present, $n = 1$	10	19.697	17.118	14.703	7.283	4.872	4.260
Present, $n = 2$		19.660	17.108	14.702	7.135	4.876	4.241
Khdeir and Librescu [75]		19.500	17.069	14.725	7.310	4.906	4.334
3D FE		19.817	17.204	14.703	7.304	4.877	4.299

In Table 3.4 the effect of in-plane modulus ratio (Y_1/Y_2) on the fundamental frequency parameter $\bar{\omega}_n = \omega h\sqrt{\rho_0/Y_2}$ is investigated for different sets of boundary conditions of moderate thickness (S=10) un-symmetric cross-ply square laminate. The present results are compared with Chen and Lü [90] and Qu et al. [84]. For this case also present results are in excellent agreement for all boundary conditions and modulus ratios. It is worth to observe from the table that as the in-plane modulus ratio (Y_1/Y_2) increased (keeping Y_2 constant) the frequency parameter increase significantly because the overall plate stiffness increases.

Table 3.4: Comparison of the effect of in-plane modulus ratio, (Y_1/Y_2) on the fundamental frequency parameter $(\bar{\omega}_m = \omega h\sqrt{\rho_0/Y_2})$ of un-symmetric cross-ply laminates $[0°/90°/0°/90°]$ with different sets of boundary conditions:(S=10, $\upsilon_{23} = 0.49$)

Y_1/Y_2	Theory	S-S	C-C	C-S	C-F
40	Present (n=1, iter.=2)	0.14501	0.18652	0.16490	0.10875
	Chen and Lü [90]	0.14501	0.18800	0.16554	0.10925
	Qu et al. [84]	0.14501	0.18752	0.16550	0.10885
20	Present (n=1, iter.=2)	0.11653	0.16088	0.13738	0.08638
	Chen and Lü [90]	0.11653	0.16161	0.13757	0.08265
	Qu et al. [84]	0.11653	0.16123	0.13752	0.08611
10	Present (n=1, iter.=2)	0.09438	0.13627	0.11337	0.06869
	Chen and Lü [90]	0.09439	0.13638	0.11334	0.06889
	Qu et al. [84]	0.09438	0.13602	0.11326	0.06820
2	Present (n=1, iter.=2)	0.06719	0.09641	0.07992	0.04628
	Chen and Lü [90]	0.06719	0.09552	0.07952	0.04264
	Qu et al. [84]	0.06719	0.09495	0.07928	0.04476

The first eight bending frequencies are compared in Table 3.5 of a three layer symmetric square laminate with $S = 10$ and 20. The non-dimensional frequency parameter $\bar{\omega}_m = (\omega a^2/\pi^2)\sqrt{\rho_0 h/D}$, where $D = E_2h^3/12(1 - \nu_{12}\nu_{21})$. The results are presented for SS and CC boundary conditions. First order shear deformation theory [71] predicts natural frequencies for lower modes accurately while erroneous predictions for higher modes. Three-dimensional FE results are also presented for comparison and it is observed that present results are in excellent match with 3D FE. In the subsequent sections, results are obtained by taking n=1, iter. 2.

3.4.1.2 Cross-ply Laminated Plate

The composite plate (a), as shown in Fig. 3.2, made of graphite-epoxy with four layer of equal thickness $0.25h$ with symmetric layup $[0°/90°/90°/0°]$ is considered for study in this section. The graphite-epoxy composite properties are given as: $Y_1 = 181\,\text{GPa}, Y_2 = Y_3 = 10.3\,\text{GPa}, G_{12} = G_{13} = 7.17\,\text{GPa}, G_{23} = 2.87\,\text{GPa}, \nu_{12} = \nu_{13} = 0.28$, $\nu_{23} = 0.33$, $\rho_0 = 1578\,\text{kg/m}^3$. The non-dimensional frequency parameter, $\bar{\omega}_m = \omega a S\sqrt{\rho_0/Y_2}$. The results for sandwich plate (b) and composite plate (c) with an adhesive layer are presented in Sec. 3.4.2 and Sec. 3.4.3, respectively.

Table 3.6 presents the first five flexural frequencies for $m = 1$ and the lowest four flexural frequencies for m= 2 and 3, respectively. The lowest flexural frequencies (m=1) are significantly

Table 3.5: Comparison of dimensionless natural frequencies, $\bar{\omega}_m = (\omega a^2/\pi^2)\sqrt{\rho_0 h/D}$ for a three ply [0°/90°/0°] laminated plate

			Mode sequences							
BC	S	Theory	1	2	3	4	5	6	7	8
S-S	10	Present (n=1, iter.=2)	5.154	7.606	12.276	13.100	14.355	17.399	18.087	21.355
		FSDT (Liew [71])	5.166	7.757	12.915	13.049	14.376	17.788	19.502	21.051
		3D FE	5.151	7.581	12.233	13.098	14.343	17.370	18.040	21.355
	20	Present (n=1, iter.=2)	6.131	8.841	14.845	19.320	20.618	23.287	24.202	30.426
		FSDT (Liew [71])	6.138	8.888	15.110	19.354	20.665	24.070	24.344	31.028
		3D FE	6.131	8.837	14.833	19.321	20.617	23.269	24.158	30.413
C-C	10	Present (n=1, iter.=2)	5.796	9.019	13.363	13.830	15.147	18.521	19.487	21.535
		FSDT (Liew [71])	5.871	9.454	13.340	14.878	15.340	19.229	21.231	21.275
		3D FE	5.790	9.046	13.361	13.944	15.155	18.591	19.722	21.515
	20	Present (n=1, iter.=2)	6.867	11.040	18.001	19.578	21.675	26.230	26.827	33.205
		FSDT (Liew [71])	6.890	11.246	18.664	19.619	21.801	26.689	28.260	34.348
		3D FE	6.862	11.050	18.053	19.578	21.675	26.256	26.952	33.292

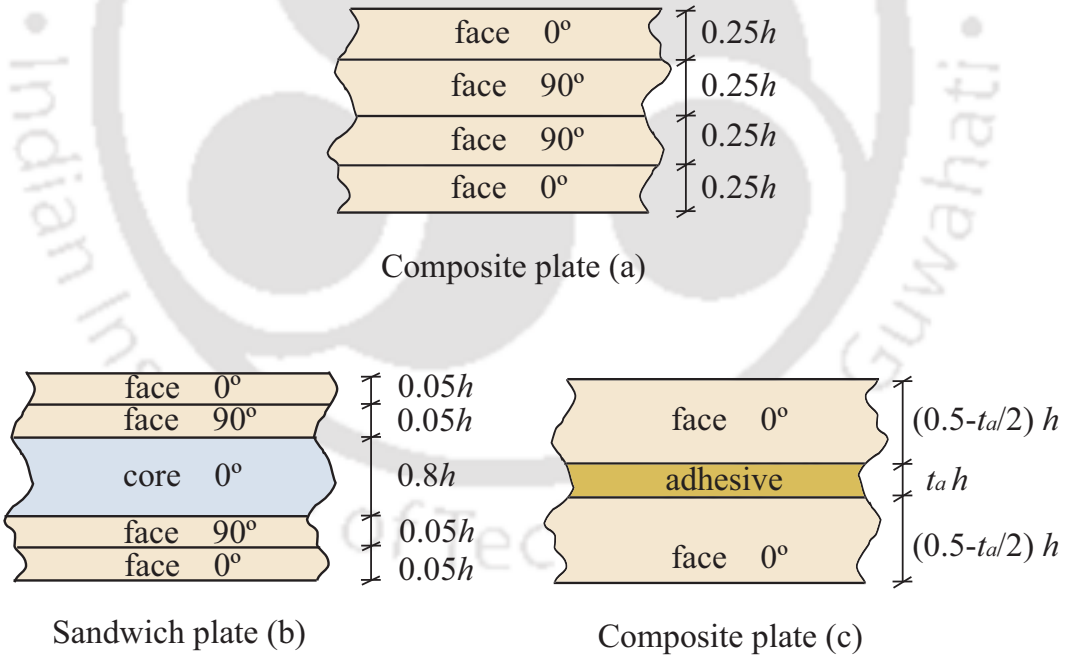

Figure 3.2: Configurations of composite and sandwich plates.

affected by boundary conditions for both thick and thin plates. For present case, first flexural frequency for F-F boundary condition is reduced by 48.68% with respect to S-S boundary condition. The reduction factor further reduces to 13.7%, 5.7% for higher modes m=2 and 3

respectively. For C-C and C-S case frequency increases slightly as compared with S-S case. The boundary conditions have little effect on the flexural frequencies for higher modes.

Table 3.6: Benchmark dimensionless natural frequencies ($\bar{\omega}_m$) of symmetric thick (S=5) composite plate (a) under five different boundary conditions (n=1, iter.=2)

(m)	S-S	C-C	C-S	C-F	F-F
1	8.561	9.739	9.003	5.526	4.398
	17.508	18.046	17.763	11.773	6.010
	27.440	28.247	27.652	21.509	15.625
	37.889	38.254	38.067	31.550	24.361
	48.599	48.890	48.739	42.385	35.724
2	15.879	16.346	16.036	14.194	13.692
	22.231	22.552	22.388	18.129	15.066
	30.813	31.186	30.976	25.608	21.083
	40.512	40.821	40.662	33.613	28.718
3	25.616	25.800	25.672	24.466	24.152
	30.077	30.260	30.166	27.215	25.260
	36.965	37.237	37.083	32.745	29.397
	45.452	45.702	45.574	40.139	35.185

The first three bending mode shapes are presented for five (S-S, C-C, C-S, C-F, F-F) boundary conditions in Fig. 3.3 for a thick (S=5) laminated composite plate. Plate vibrates in symmetric modes for S-S, C-C, C-S and F-F cases, whereas asymmetric mode for C-F case.

As there are no analytical results available in the literature, so 3D FE results obtained by using ABAQUS software [161] are plotted for comparison of the displacements and stresses. The plot in Fig. 3.4 shows the longitudinal variation of the displacements ($\bar{u}, \bar{w}$) and stresses ($\bar{\sigma}_y$, $\bar{\tau}_{yz}$) of first two flexural modes for C-F boundary condition. The present graph matches well with the 3D FE results.

In Fig. 3.5, the longitudinal variation of field variables ($\bar{u}, \bar{w}, \bar{\sigma}_y, \bar{\tau}_{yz}$) is shown for F-F boundary condition. No significant edge effects are observed for this plate (a). The through-thickness variation of stresses $\bar{\sigma}_z$ and $\bar{\tau}_{yz}$ for C-F and F-F boundary conditions are presented in Fig. 3.6 for the first mode. The normal transverse stress $\bar{\sigma}_z$ is maximum at the interface for both the cases near the free edge ($\xi_1 = 0.9$), which can incite delamination damage in laminated plate subjected to vibration. The distribution of shear stress $\bar{\tau}_{yz}$ at three different locations are shown for both the cases and are observed to be maximum at mid-interface.

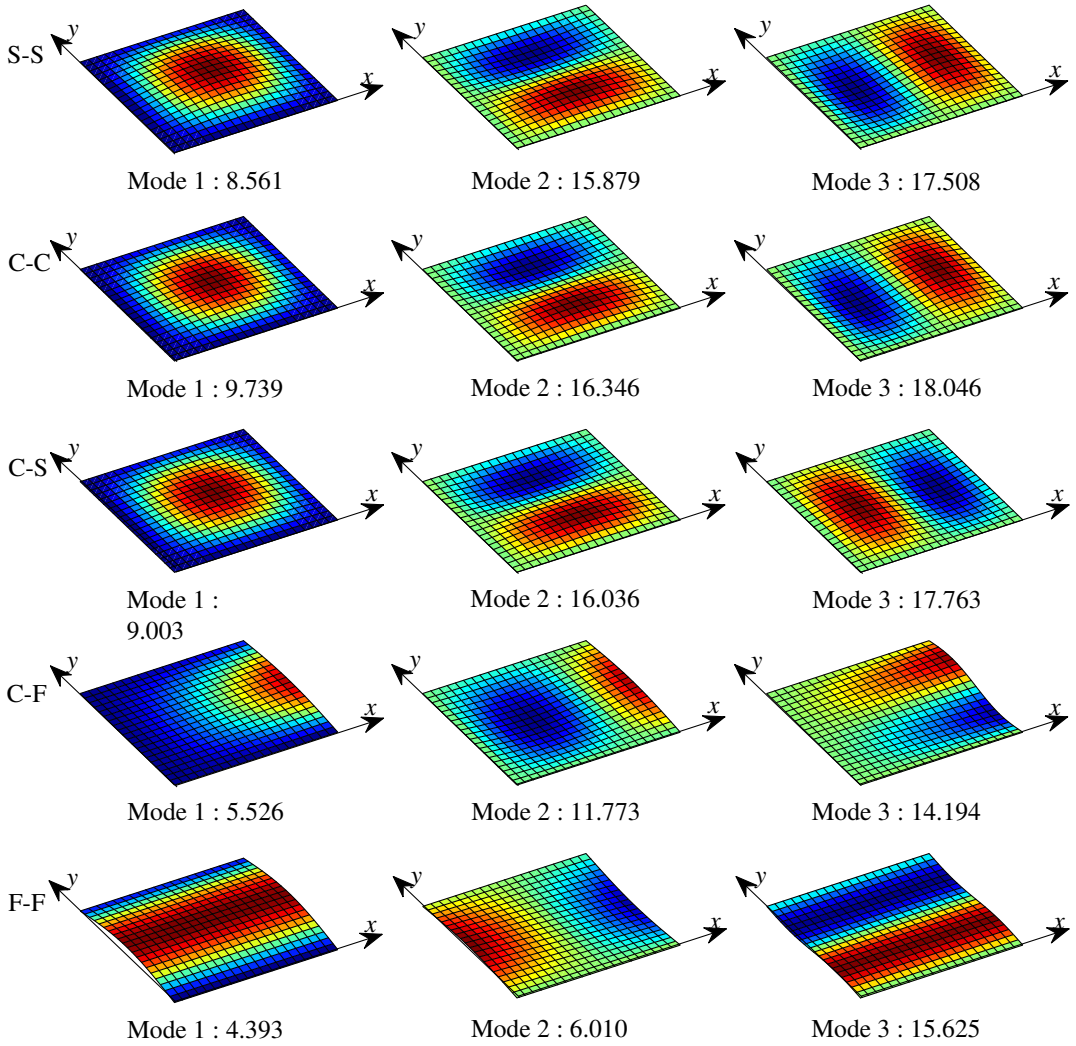

Figure 3.3: First three flexural mode shapes with the frequencies for thick (S=5) composite plate (a) subjected to arbitrary boundary conditions (S-S, C-C, C-S, C-F, F-F).

3.4.2 Free Vibration Analysis of Soft Core Sandwich Plate

A five layered [0°/90°/Core/90°/0°] symmetric soft-core sandwich plate (b) as shown in Fig. 3.2 is considered for analysis in this section. The following material properties are considered for face and core as, Face: $Y_1 = 181\,\text{GPa}, Y_2 = Y_3 = 10.3\,\text{GPa}, G_{12} = G_{13} = 7.17\,\text{GPa}, G_{23} =$

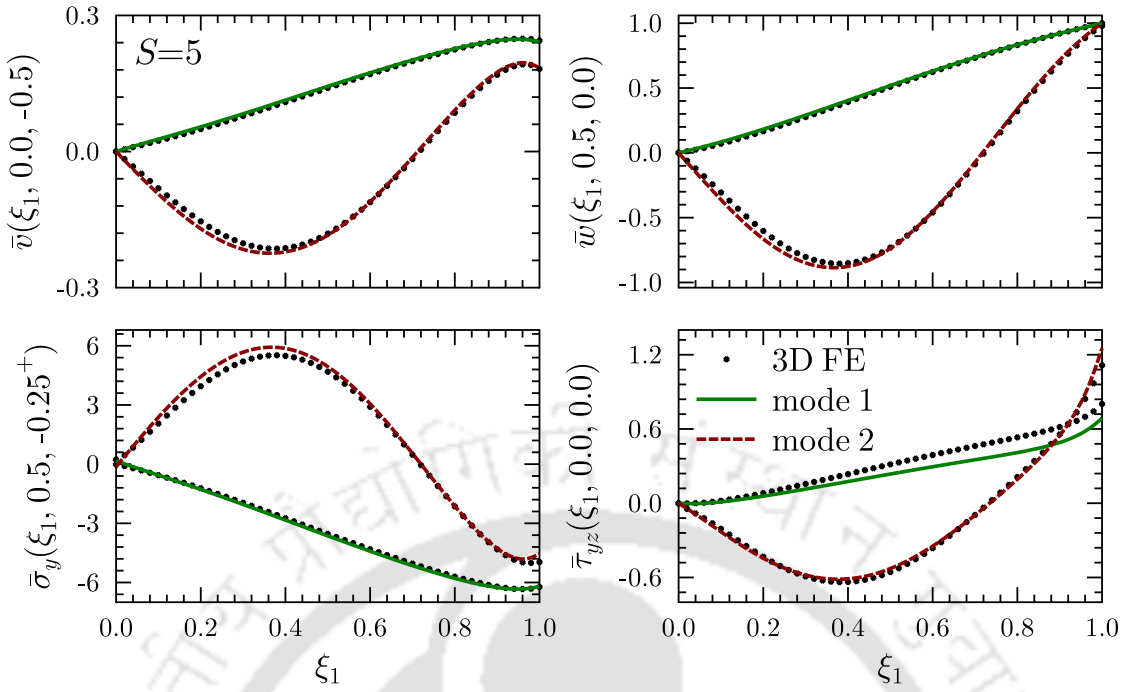

Figure 3.4: Longitudinal variation of displacements and stresses of first two modes for thick (S=5) composite plate (a) under C-F boundary condition.

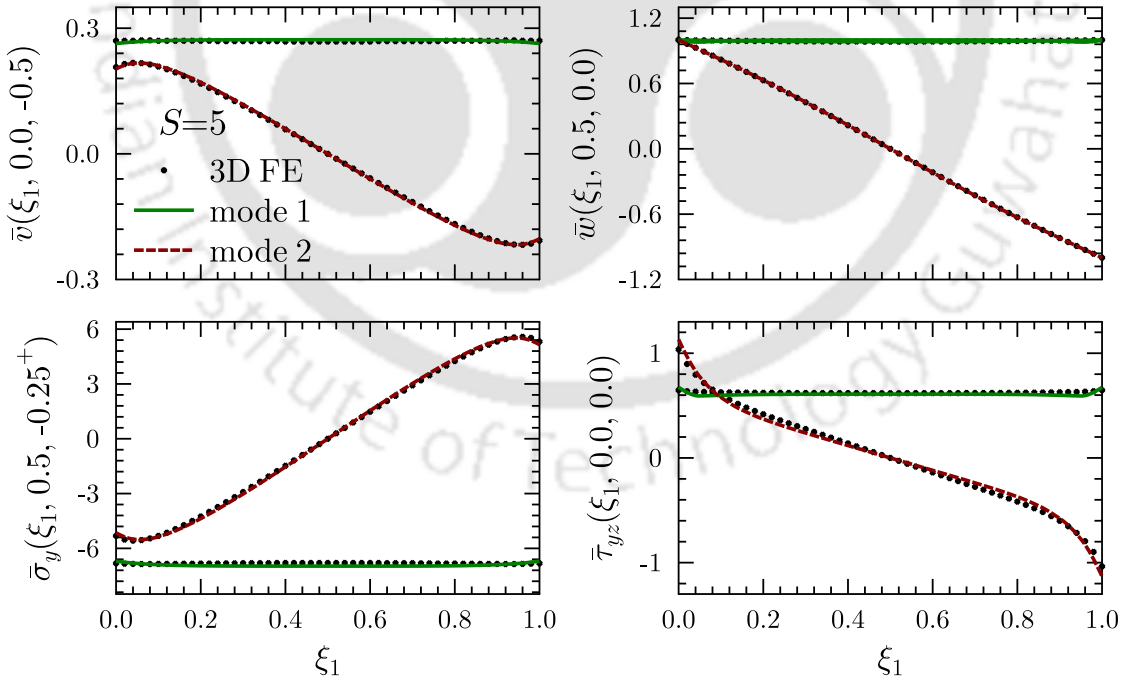

Figure 3.5: Longitudinal variation of displacements and stresses of first two modes for thick (S=5) composite plate (a) under F-F boundary condition.

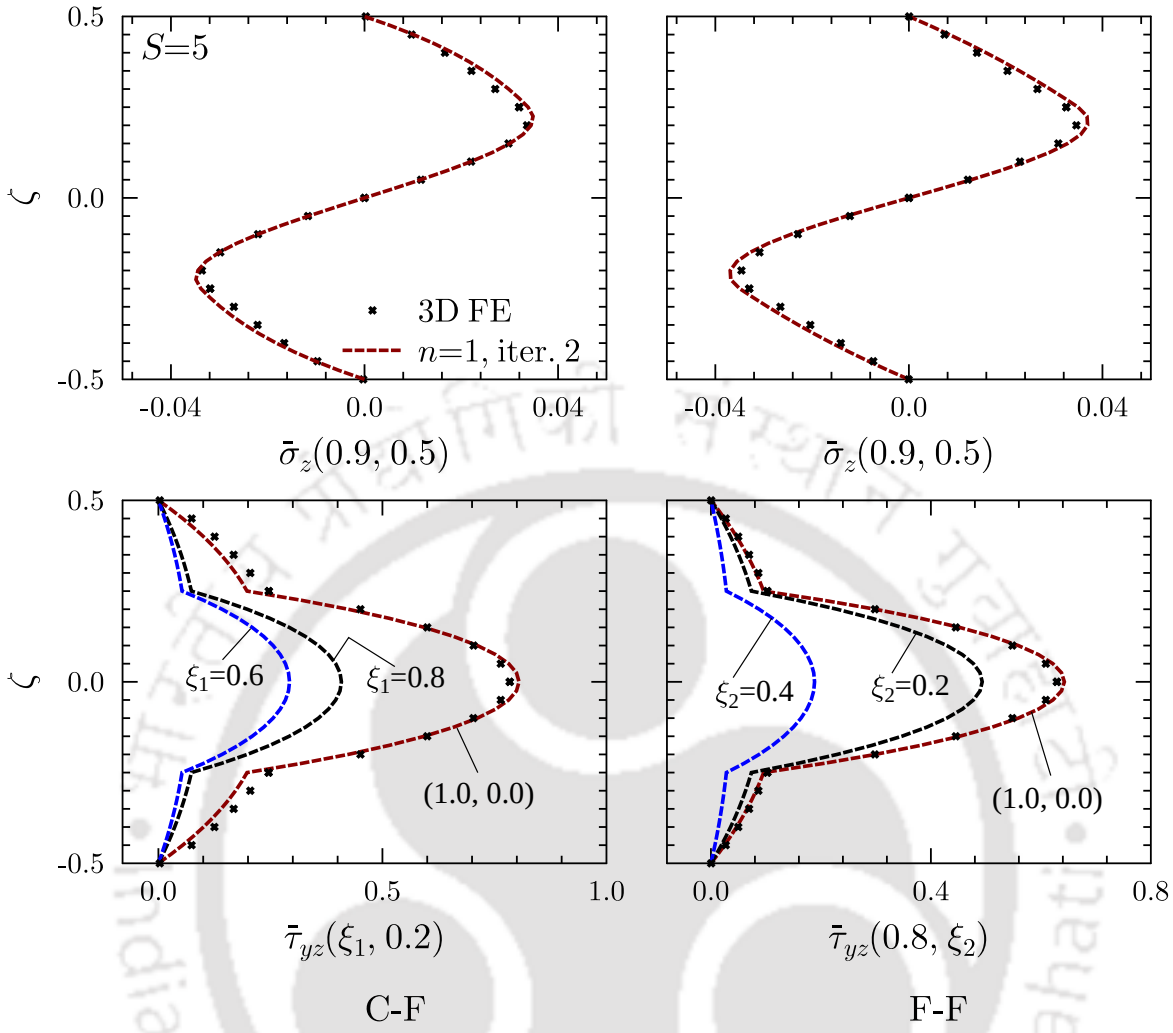

Figure 3.6: Through-thickness distributions of $\bar{\sigma}_z$ and $\bar{\tau}_{yz}$ in the first flexural mode of composite plate (a) under C-F and F-F boundary conditions.

2.87 GPa, $\nu_{12} = \nu_{13} = 0.28, \nu_{23} = 0.33, \rho = 1578\,\text{kg/m}^3$, Core: $Y_1 = Y_2 = 0.276 \quad GPa, Y_3 = 3.45 \quad GPa, G_{13} = G_{23} = 0.414 \quad GPa, G_{12} = 0.1104 \quad GPa, \quad \nu_{12} = 0.25, \quad \nu_{13} = \nu_{23} = 0.02$ and $\rho = 1000\,\text{kg/m}^3$. The frequency parameter $\bar{\omega}_m = \omega a S\sqrt{\rho_0/Y_2}$, where $\rho_0 = 1578\,\text{kg/m}^3$ and $Y_2 = 10.3\,\text{GPa}$.

The first ten flexural frequencies are calculated for S value of 5, 10 and 20 for five sets of boundary conditions and are presented in Table 3.7. It is observed that as the S value is increased from 5 to 20 (thick to thin plate) the frequencies also increased significantly for all type of boundary conditions. The lower mode frequencies are significantly affected by boundary conditions for thick, moderately thick and thin plates, while its diminishing effect is observed at higher modes. For instance, the fundamental frequency for F-F boundary condition is reduced by

Table 3.7: Benchmark dimensionless frequency parameter($\bar{\omega}_m$) of sandwich plate (b) under five different boundary conditions (n=1, iter.=2)

		Mode sequences									
S	BCs	1	2	3	4	5	6	7	8	9	10
5	S-S	4.807	7.921	8.367	10.479	11.505	12.316	13.417	13.855	15.357	16.225
	C-C	5.041	8.036	8.397	10.507	11.564	12.360	13.447	13.894	15.389	16.262
	C-S	4.876	7.958	8.388	10.497	11.525	12.323	13.433	13.865	15.369	16.239
	C-F	3.605	6.162	7.232	8.890	10.079	11.019	11.925	12.248	14.322	14.615
	F-F	3.181	3.829	6.997	7.637	7.972	10.220	10.848	11.406	11.578	13.257
10	S-S	7.677	14.164	15.078	19.228	21.437	23.130	25.084	26.026	28.860	30.607
	C-C	8.821	14.702	15.469	19.508	21.726	23.333	25.285	26.191	29.026	30.740
	C-S	8.201	14.406	15.296	19.381	21.567	23.222	25.192	26.102	28.934	30.669
	C-F	5.597	10.323	13.005	15.915	18.388	20.663	21.994	22.743	26.471	27.328
	F-F	4.951	5.791	12.728	13.146	13.486	17.998	20.421	21.136	21.313	24.338
20	S-S	9.849	21.707	23.314	30.711	36.632	39.807	42.807	44.720	51.994	53.813
	C-C	13.453	23.338	26.275	32.819	37.517	41.570	44.208	46.173	52.538	54.938
	C-S	11.569	22.460	24.875	31.811	37.031	40.707	43.527	45.459	51.994	54.383
	C-F	7.009	14.973	20.240	24.870	29.958	35.630	36.232	38.814	46.425	47.063
	F-F	6.193	7.249	17.551	19.823	20.765	27.061	34.086	35.303	36.156	40.142

33.82% with respect to S-S boundary condition, while the reduction is 18.29% in the tenth mode for thick plate. In a similar manner, it is 35.50% and 20.48% for moderately thick plate ($S = 10$) and for thin plate ($S = 20$) it is 37.12% and 25.40% at the first and tenth mode respectively. For C-C and C-S case, a gradual increment in frequencies are observed in comparison to other boundary conditions. The boundary conditions have little effect on the flexural frequencies in higher modes. The first lowest eight frequencies for m=1 of thick sandwich plate for different boundary conditions are presented in Table 3.8 to explore the thickness stretching effects. It has been observed that the thickness stretching occurs generally at higher modes. For this typical case, 8th mode is the thickness stretching mode for all the boundary conditions except for F-F case where it is the 7th mode. The percentage decrement variation in natural frequencies of sandwich plate (b) for F-F boundary condition against S-S and C-F boundary conditions is presented in Fig. 3.7. he maximum decrement in the frequency is observed for second mode and it decreases with the increase of mode sequences. This information is very helpful in design and construction of components made of sandwich laminate with more reliability.

Table 3.8: Lowest eight frequencies of sandwich plate for m=1 and S=5

(m)	S-S	C-C	C-S	C-F	F-F
1	4.807	5.041	4.877	3.606	3.182
	18.818	19.479	19.474	19.173	18.353
	19.919	20.648	20.469	19.980	19.132
	34.694	36.218	35.825	33.955	32.312
	36.664	37.926	37.607	35.260	34.540
	48.458	50.434	49.251	39.975	35.225
	50.249	51.337	51.258	48.696	47.365
	52.869	52.716	53.563	50.277	49.277

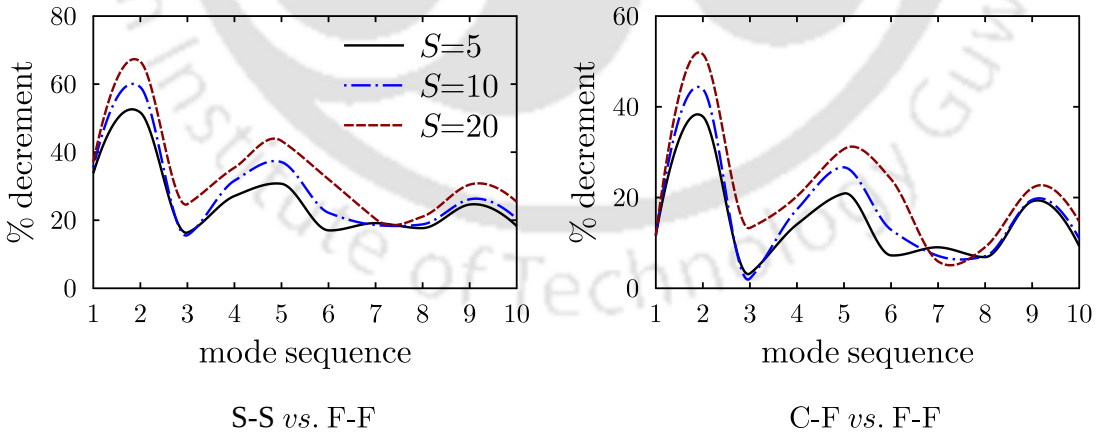

Figure 3.7: Percentage decrement variation in natural frequencies of sandwich plate (b) for F-F boundary condition against S-S and C-F boundary conditions.

The first three flexural mode shapes with frequencies of thick sandwich plate (S=5) for different boundary conditions are presented in Fig. 3.8. The sandwich plate also vibrates in the symmetric mode for S-S, C-C, C-S and F-F case, while antisymmetric mode for C-F case. Here also, longitudinal and through-thickness variations of entities are compared with 3D FE results.

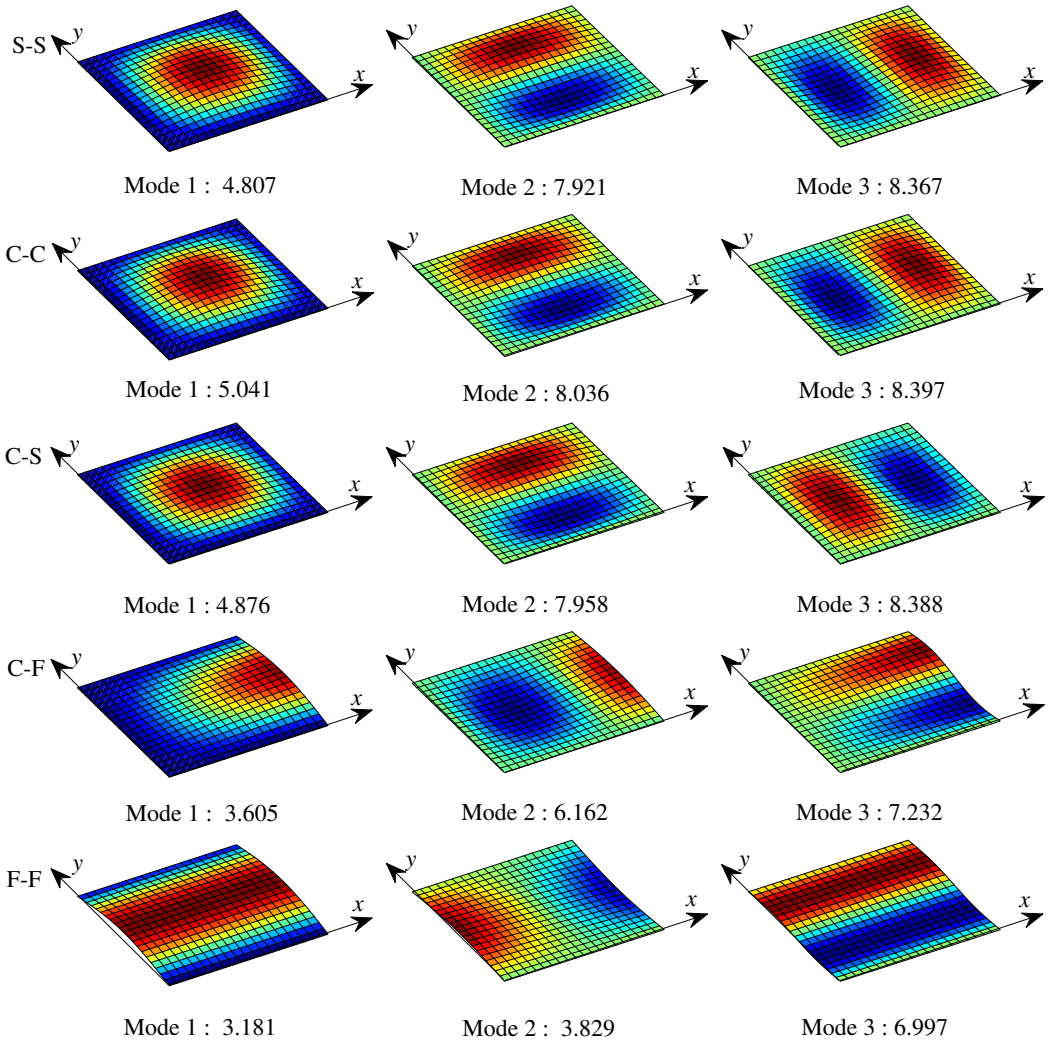

Figure 3.8: First three flexural mode shapes with the frequencies for thick (S=5) sandwich plate (b) subjected to arbitrary boundary conditions (S-S, C-C, C-S, C-F, F-F).

The longitudinal variation of displacements $\bar{v}$ and $\bar{w}$, normal stress $\bar{\sigma}_y$ and shear stress $\bar{\tau}_{yz}$ are presented in Fig. 3.9 and Fig. 3.10 for thick sandwich plate (S=5) under C-F and F-F case, respectively. Converge results of single term 3D EKM with iter.=2 are in excellent agreement with 3D FE results for both mode shapes and boundary conditions. Boundary effect is observed near the free edge in the variation of $\bar{\sigma}_y$ for both C-F and F-F cases.

The through-thickness variation of transverse stresses $\bar{\sigma}_z$ and $\bar{\tau}_{yz}$ for the first mode is presented in Fig. 3.11 for C-F and F-F cases. For this case also, present results are in good agreement with 3D FE. Maximum transverse normal stress ($\bar{\sigma}_z$) is observed at the core-face interfaces for both the C-F and F-F cases.

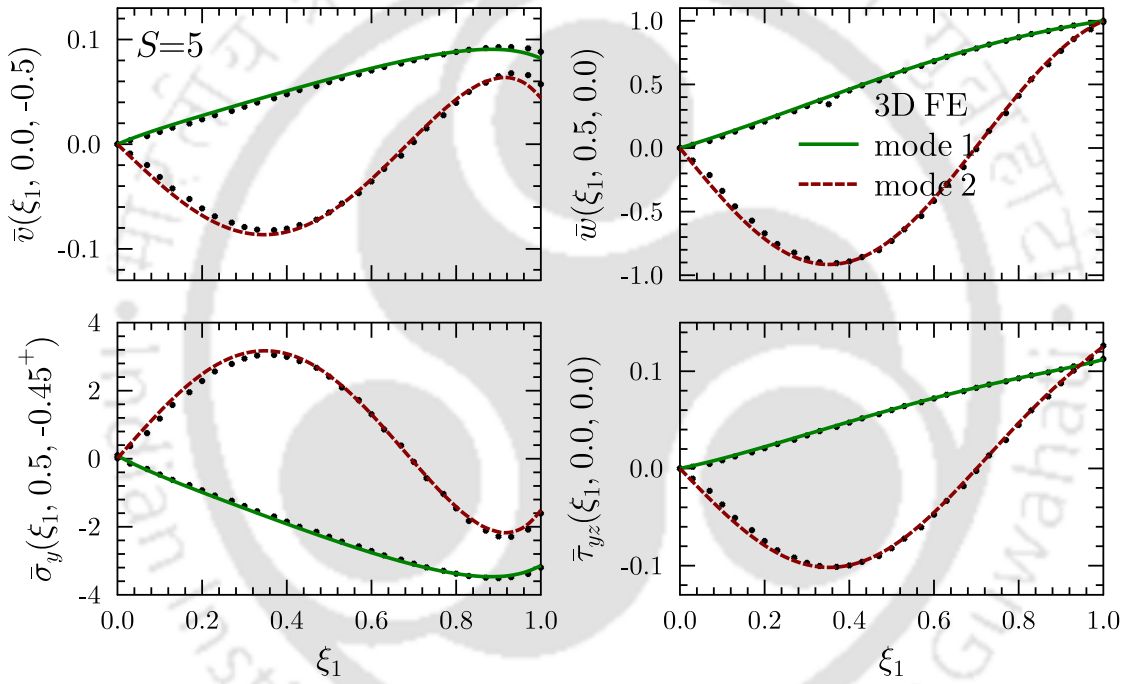

Figure 3.9: Longitudinal variation of displacements and stresses of first two modes for thick (S=5) sandwich plate (b) under C-F boundary condition.

Typical through-the-thickness distributions of modal displacements $\bar{u}$, $\bar{v}$ and $\bar{w}$ are plotted in Fig. 3.12 for thick (S=5) sandwich plate under S-S and C-C boundary conditions for the lowest eight modes for $m = 1$. The mode shapes indicate that the 1st mode is a bending mode for both S-S and C-C case. The second mode is a higher order shear mode along x-axis for S-S case and along y-axis for C-C case. The third mode is a higher order shear mode along x- and y-axis for S-S case; it is along x-axis for C-C case. The fourth mode is a thickness shear mode in x- and y-axis for S-S while it is in y-axis for C-C case. The fifth mode is a thickness shearing mode in x-axis for both. The sixth and seventh modes are also thickness shear modes in x-

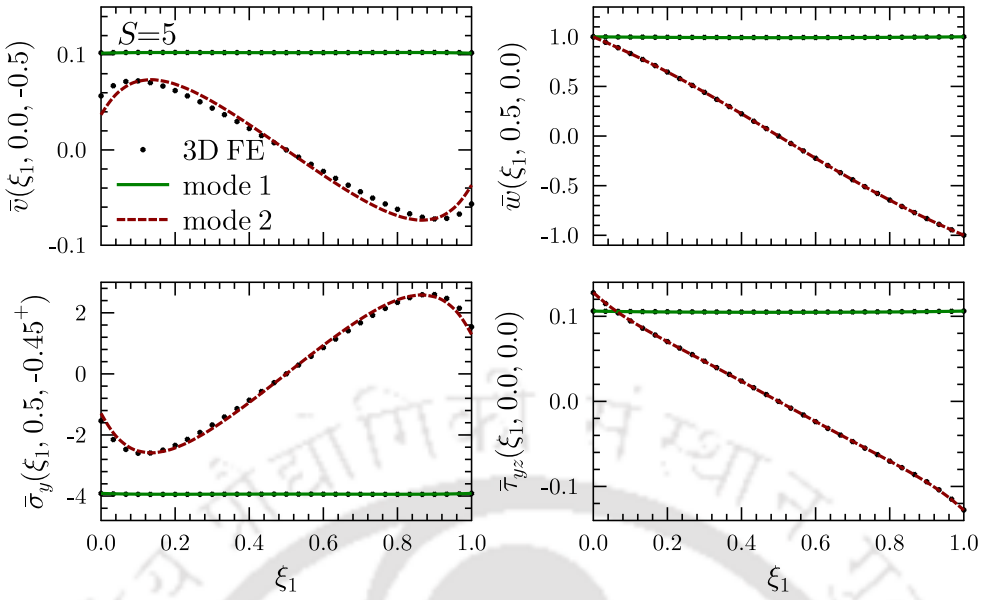

Figure 3.10: Longitudinal variation of displacements and stresses of first two modes for thick (S=5) sandwich plate (b) under F-F boundary condition.

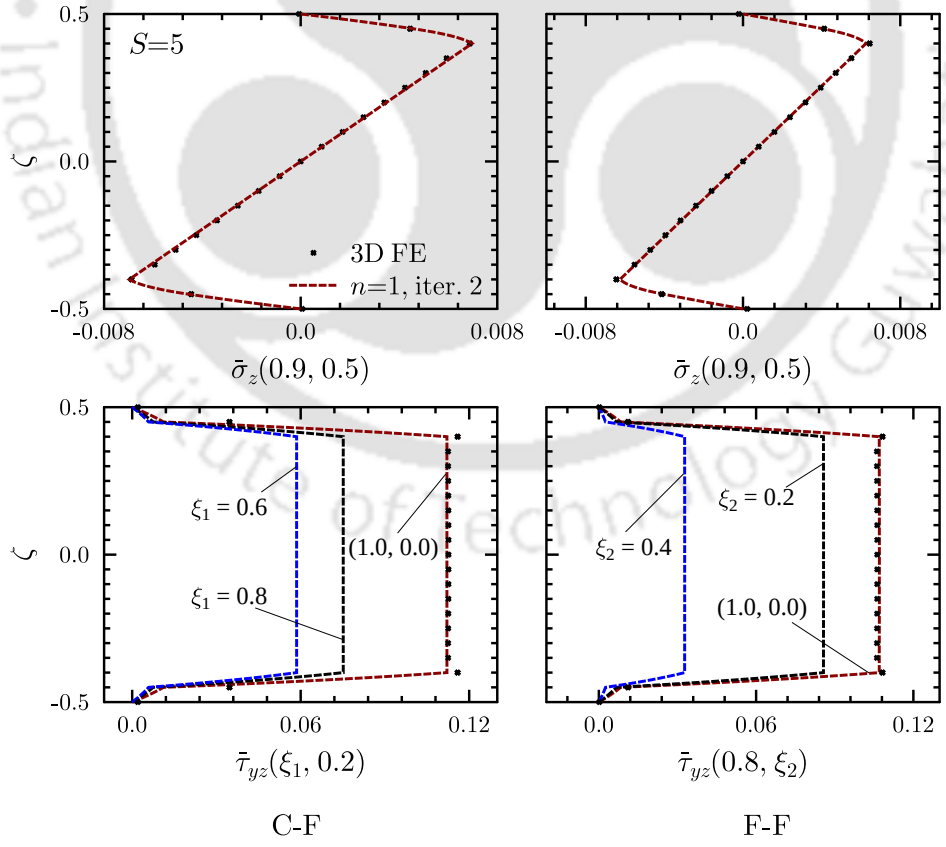

Figure 3.11: Through-thickness distributions of $\bar{\sigma}_z$ and $\bar{\tau}_{yz}$ in the first flexural mode of sandwich plate (b) under C-F and F-F boundary conditions.

and y-axis for S-S case. For C-C case the sixth one is thickness shearing mode in x-axis and the seventh one is higher order shear mode also in x-axis. The eighth mode for both the cases correspond to thickness stretching.

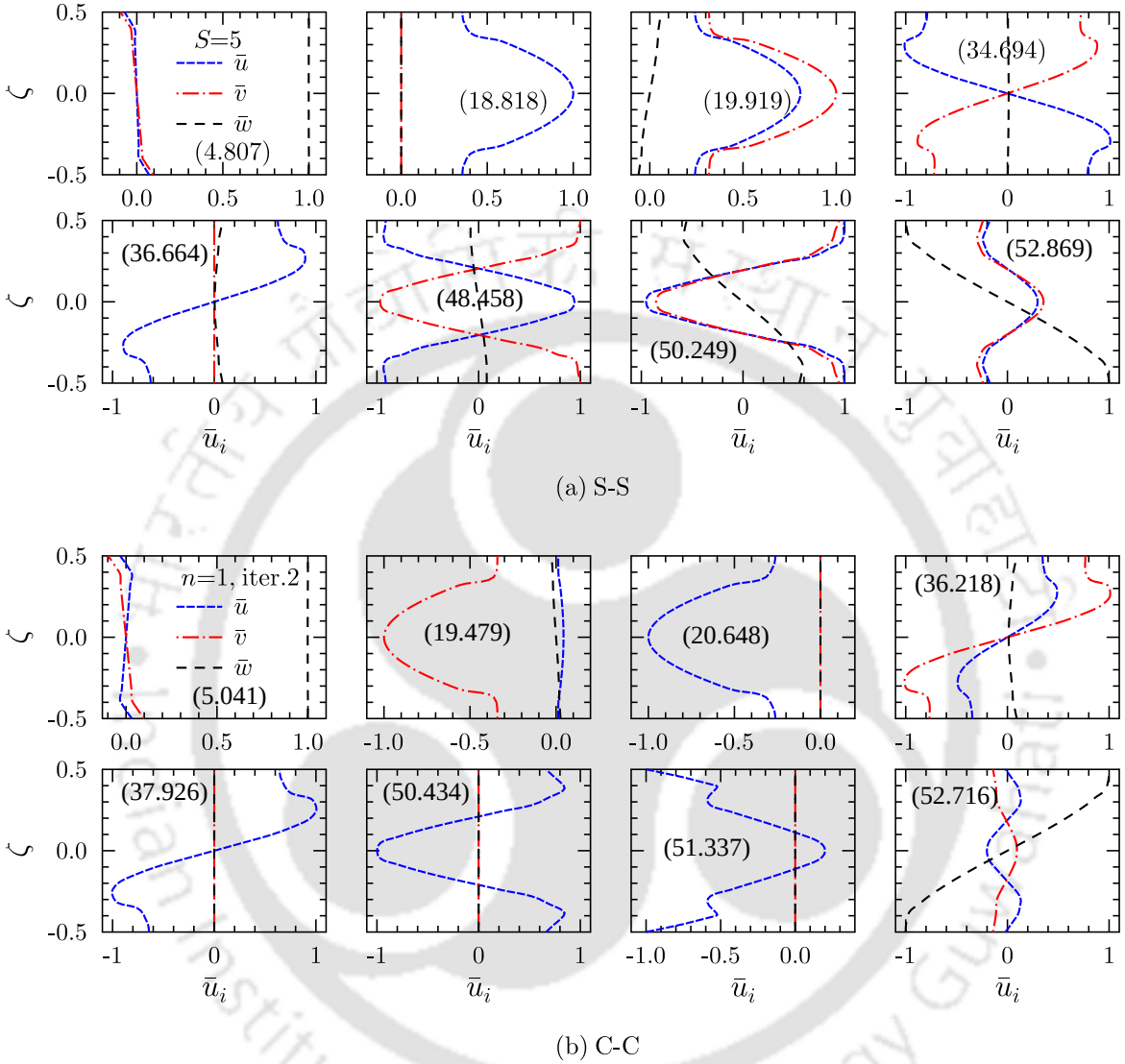

Figure 3.12: Through-thickness distributions of $\bar{u}$, $\bar{v}$ and $\bar{w}$ in the lowest eight frequencies of sandwich plate under (a) S-S and (b) C-C boundary conditions for m=1 (numbers in parenthesis are the corresponding frequencies).

3.4.3 Accurate Estimation of the Influence of Adhesive Bonding on the Free Vibration of Laminated Plates

The influence of adhesive layer sandwiching between the layers of laminated composite plate (c), as shown in Fig. 3.2, is presented and discussed here. The adhesive property considered here is as given in Table 2.3 of Chapter 2. In the Table 3.9, first eight natural flexural frequencies for different boundary conditions are presented for adhesive thicknesses t_a= 0.0, 0.02 and 0.04. The same data are illustrated in graphical structure in the Fig. 3.13. It can be observed from the table or from the figure that as the adhesive thickness increases, the frequency of the plate decreases for all type of boundary conditions and the decrement is significant at higher modes. There is a maximum decrement of 5.43% observed for S-S case for t_a=0.04 at $4th$ mode, a maximum of 5.42% at $1st$ and $3rd$ mode for C-C case, 5.29% for C-F case at $8th$ mode and 4.60% for F-F case at $6th$ mode. The percentage difference is calculated with respect the frequency of plate without an adhesive layer (t_a=0).

Table 3.9: Natural flexural frequencies of plate (c) for different boundary conditions for the adhesive thickness, t_a=0.0, 0.02 and 0.04

	S-S			C-C			C-F			F-F		
Mode	t_a=0	0.02	0.04	t_a=0	0.02	0.04	t_a=0	0.02	0.04	t_a=0	0.02	0.04
1	9.410	9.205	9.030	11.537	11.269	10.912	4.786	4.726	4.678	2.639	2.644	2.648
2	13.358	13.167	13.007	14.637	14.351	14.149	10.057	10.000	9.950	4.976	4.972	4.969
3	19.759	19.558	19.388	20.432	20.179	19.993	14.079	13.672	13.362	8.917	8.906	8.896
4	22.174	21.481	20.971	22.891	22.219	21.771	17.422	17.156	16.788	11.338	11.279	11.218
5	24.354	23.697	23.215	24.907	24.265	23.833	17.557	17.329	17.247	16.666	16.609	16.557
6	27.232	26.996	26.794	27.614	27.351	27.145	23.055	22.693	22.401	18.768	18.302	17.906
7	28.536	27.953	27.475	28.940	28.339	27.929	25.455	25.307	25.175	18.773	18.658	18.557
8	34.230	33.652	33.222	34.530	33.961	33.563	27.379	26.536	25.930	21.830	21.350	21.422

Figure 3.14 illustrates the percentage variation of natural frequencies of $2.1Y$ and $3Y$ with respect to the Y. It can be observed from the figure that as the elastic modulus of adhesive increases the percentage difference plate natural frequency also increases and it is higher for S-S and C-C cases. At higher modes for all types of boundary conditions, the percentage difference is higher. In Figure 3.15, the percentage variation of natural frequencies of 1.5ρ and 2.5ρ is illustrated. As can be seen from the figure that increasing the adhesive density decreases the plate natural frequency and is seen maximum on the fundamental frequency. For higher modes the % difference remain almost constant.

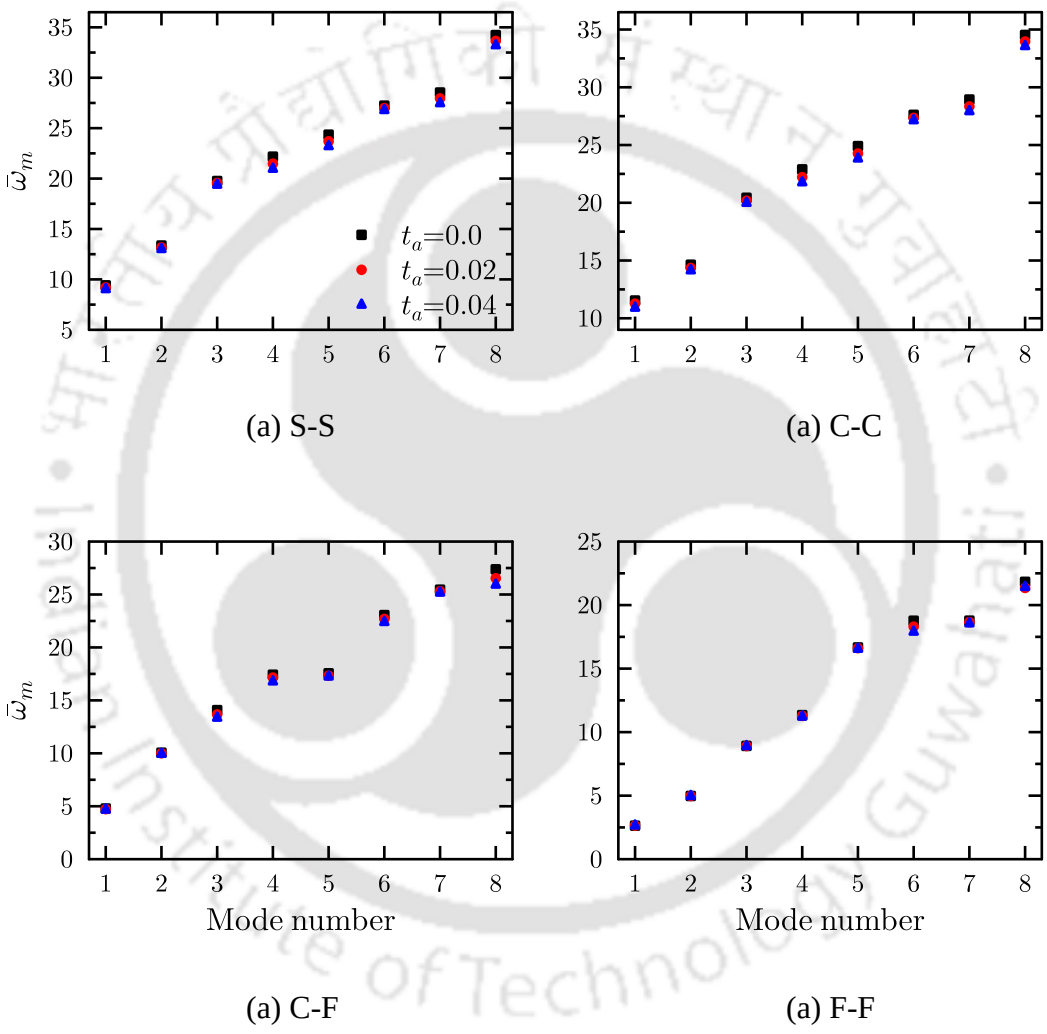

Figure 3.13: The effect of adhesive layer thickness (t_a=0.0, 0.02, 0.04) on the flexural natural frequencies of plate (c) for different boundary conditions

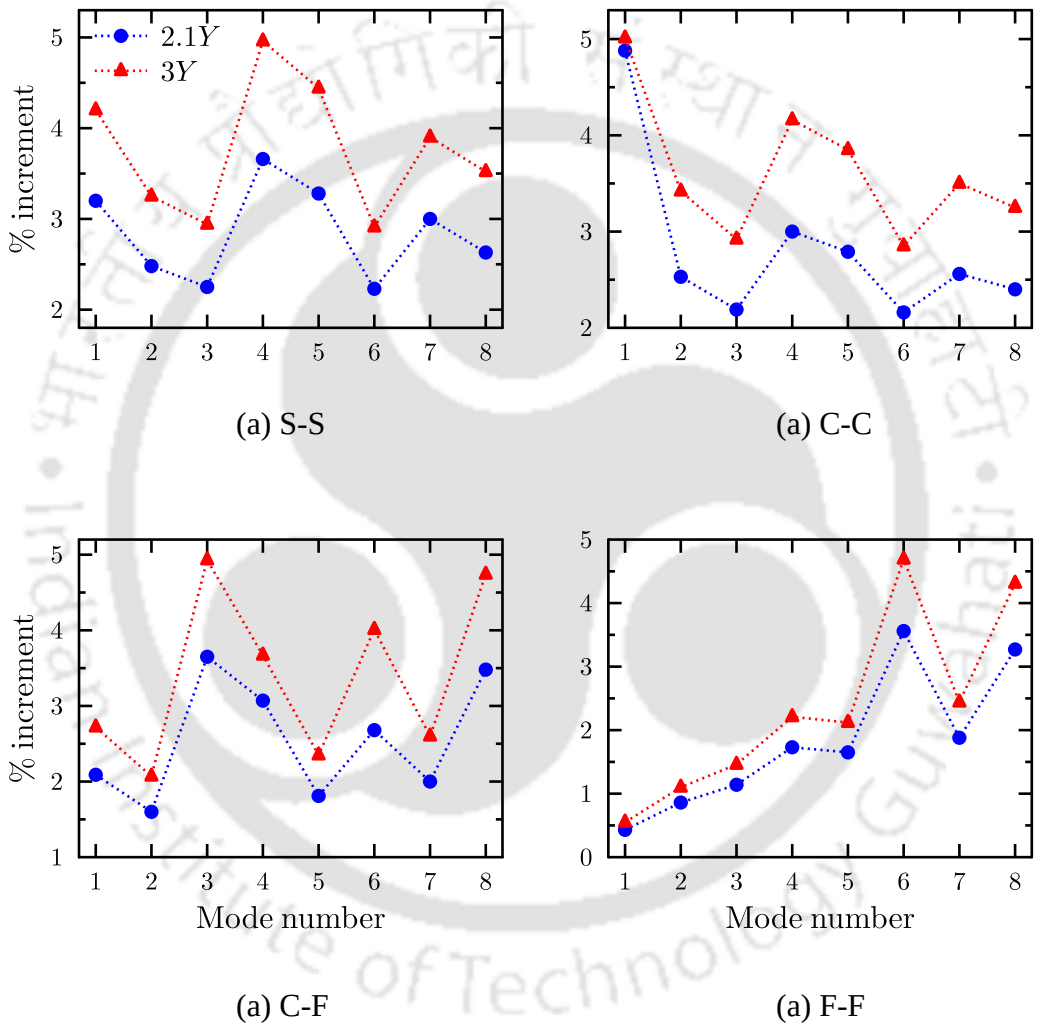

Figure 3.14: Percentage increment of natural frequency for adhesive elastic modulus of $2.1Y$ and $3Y$ for S-S, C-C, C-F and F-F boundary conditions.

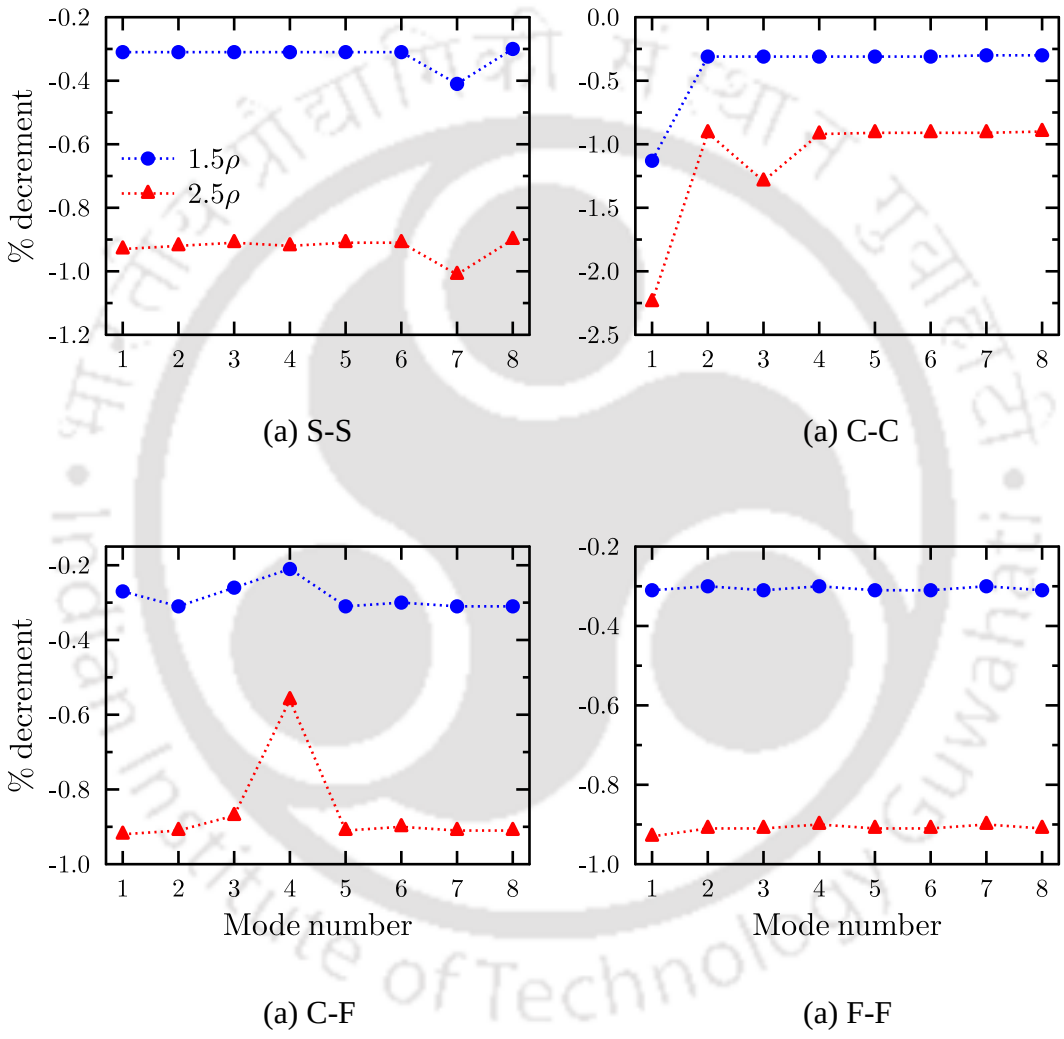

Figure 3.15: Percentage decrement of natural frequency for adhesive density of 1.5ρ and 2.5ρ for S-S, C-C, C-F and F-F boundary conditions.

3.5 CONCLUSIONS

In this chapter, the free vibration analysis of rectangular laminated composite and sandwich plates, of which a pair of opposite edges are subjected to Levy-type boundary conditions and the other pair subjected to arbitrary boundary conditions, is presented using 3D EKM. The effect of adhesive parameters on the natural frequency is also studied. Natural frequencies predicted by single term EKM solution are in excellent match with literature.

- First time, lowest ten flexural frequencies for cross-ply laminated composite and sandwich plates are presented for different sets of boundary conditions. Longitudinal and through-thickness variation of stresses is also presented for C-F and F-F case. Present solution can serve as benchmark to assess the other 2D and numerical results.
- Increasing the in-plane modulus ratio Y_1/Y_2 (keeping Y_2 constant) increases the plate natural frequency.
- Using adhesives as binding agent reduces the frequency response of laminated plates. As the adhesive thickness increases, the frequency of the plate decreases. There is significant decrement in the natural frequencies of the plate for higher modes
- Increasing the adhesive modulus increases the frequency response of laminated plates and the increment is more pronounced in case of C-C boundary condition.
- The density increment of adhesives have a minor decreasing effect on the frequency response of adhesive bonded laminated plates.

Chapter 4

3D Extended Kantorovich Method for Free Vibration Analysis of Piezolaminated Plates

4.1 INTRODUCTION

The generalized mixed-field multi-term extended Kantorovich method (EKM) for piezoelasticity solution for static case developed in Chapter 2 is further extended to 3D piezoelasticity solution for free vibration [164] of Levy-type laminated plate integrated with piezoelectric actuators and sensors in this chapter. The governing partial differential equations for the dynamic case are reduced to ordinary differential equations in the thickness (z) and in-plane (x) directions by applying the multi-term multi-field EKM in conjunction with Fourier series along y-direction which satisfies the Levy-type support conditions along the y-axis. In this chapter, the multi-term 3D EKM has been used for the free vibration analysis of single layer piezoelectric and bimorph plates and also for multi-layered composite and sandwich plates with integrated piezoelectric layers at top and bottom. The formulation enables to provide independently both close circuit (CC) and open circuit (OC) electric conditions at the outer and inner surfaces satisfying the interface continuity. After thorough validation, some new benchmark results are presented for both smart composite and sandwich plates investigating the influence of plate aspect ratio, various mechanical and electric boundary conditions and face thickness on the natural frequency and stresses. The effect of adhesive layer thickness on the natural frequency of a bimorph plate is also investigated. The present results can serve as benchmark versus various approximate numerical or closed-form 2D piezolaminated solutions.

4.2 THEORETICAL FORMULATION

For mathematical modelling a cross-ply laminated rectangular plate integrated with piezoelectric layers (Fig. 4.1) of dimensions ($a \times b \times h$) is considered. The displacement components (u, v, w) and the electrical potential (ϕ) are the functions of x, y, z and t where t is the time variable. The laminate has L orthotropic layers made up of elastic and piezoelectric materials of class mm2 symmetry with poling along the z direction. Presence of electrodes on piezoelectric layers and its influence on response parameters are neglected. The plate is subjected to Levy-type boundary conditions along y axis ($y = 0, b$) and arbitrary support conditions along x axis. The thickness of the kth layer and the z-coordinate of its upper surface are denoted as t_k and z_k, respectively. The layer index k over the entities is dropped, unless required for clarity.

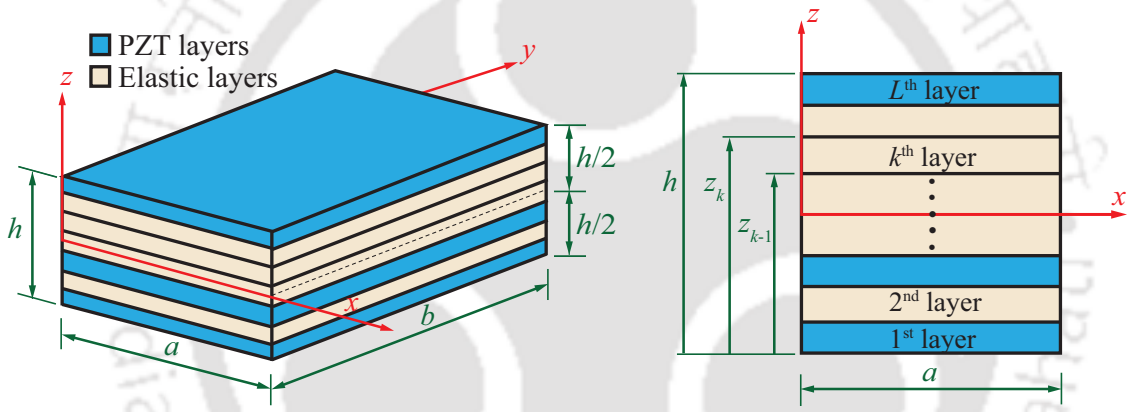

Figure 4.1: Geometry and coordinate system of a L-layer piezo-laminated plate.

The strain-displacement relation for infinitesimal deformations and the electrical field-potential relation in the rectangular cartesian coordinates is given by

$$\{\varepsilon\} = \frac{1}{2}(\nabla \mathbf{u} + (\nabla \mathbf{u})^T), \quad \mathbf{E} = -\nabla\phi \tag{4.1}$$

where $\{\varepsilon\}$ is the strain tensor, $\mathbf{u}$ is the displacement vector, $\mathbf{E}$ is the electric field vector for the kth layer and ∇ the gradient operator.

The linear 3D piezoelasticity constitutive relations for an orthorhombic/orthotropic (for elastic layers) lamina are given by

$$\{\varepsilon\} = [\mathbf{S}]\{\sigma\} + [\mathbf{d}]\{\mathbf{E}\}, \quad [\mathbf{D}] = [\mathbf{d}]\{\sigma\} + [\epsilon]\{\mathbf{E}\} \tag{4.2}$$

or in expanded form

$$\begin{bmatrix} \varepsilon_x \\ \varepsilon_y \\ \varepsilon_z \\ \gamma_{yz} \\ \gamma_{zx} \\ \gamma_{xy} \end{bmatrix} = \begin{bmatrix} s_{11} & s_{12} & s_{13} & 0 & 0 & 0 \\ s_{12} & s_{22} & s_{23} & 0 & 0 & 0 \\ s_{13} & s_{23} & s_{33} & 0 & 0 & 0 \\ 0 & 0 & 0 & s_{44} & 0 & 0 \\ 0 & 0 & 0 & 0 & s_{55} & 0 \\ 0 & 0 & 0 & 0 & 0 & s_{66} \end{bmatrix} \begin{bmatrix} \sigma_x \\ \sigma_y \\ \sigma_z \\ \tau_{yz} \\ \tau_{zx} \\ \tau_{xy} \end{bmatrix} + \begin{bmatrix} 0 & 0 & d_{31} \\ 0 & 0 & d_{32} \\ 0 & 0 & d_{33} \\ 0 & d_{24} & 0 \\ d_{15} & 0 & 0 \\ 0 & 0 & 0 \end{bmatrix} \begin{bmatrix} E_x \\ E_y \\ E_z \end{bmatrix}, \tag{4.3}$$

$$\begin{bmatrix} D_x \\ D_y \\ D_z \end{bmatrix} = \begin{bmatrix} 0 & 0 & 0 & 0 & d_{15} & 0 \\ 0 & 0 & 0 & d_{24} & 0 & 0 \\ d_{31} & d_{32} & d_{33} & 0 & 0 & 0 \end{bmatrix} \begin{bmatrix} \sigma_x \\ \sigma_y \\ \sigma_z \\ \tau_{yz} \\ \tau_{zx} \\ \tau_{xy} \end{bmatrix} + \begin{bmatrix} \epsilon_{11} & 0 & 0 \\ 0 & \epsilon_{22} & 0 \\ 0 & 0 & \epsilon_{33} \end{bmatrix} \begin{bmatrix} E_x \\ E_y \\ E_z \end{bmatrix} \tag{4.4}$$

where

$$\begin{aligned} &s_{11} = 1/Y_1, && s_{44} = 1/G_{23}, && s_{12} = -\nu_{21}/Y_2 = -\nu_{12}/Y_1 \\ &s_{22} = 1/Y_2, && s_{55} = 1/G_{13}, && s_{13} = -\nu_{31}/Y_3 = -\nu_{13}/Y_1 \\ &s_{33} = 1/Y_3, && s_{66} = 1/G_{12}, && s_{23} = -\nu_{32}/Y_3 = -\nu_{23}/Y_2 \\ &\epsilon_{11} = \eta_{11} + e_{15}d_{15}, && \epsilon_{22} = \eta_{22} + e_{24}d_{24}, && \epsilon_{33} = \eta_{33} + e_{31}d_{31} + e_{32}d_{32} + e_{33}d_{33} \end{aligned} \tag{4.5}$$

with

$$\begin{aligned} &[\, e_{31} \quad e_{32} \quad e_{33} \,] = [\, d_{31} \quad d_{32} \quad d_{33} \,] \begin{bmatrix} s_{11} & s_{12} & s_{13} \\ s_{12} & s_{22} & s_{23} \\ s_{13} & s_{23} & s_{33} \end{bmatrix}^{-1} \\ &e_{24} = d_{24}/s_{44}, \qquad e_{15} = d_{15}/s_{55} \end{aligned} \tag{4.6}$$

where [**S**] is the compliance matrix, {**E**} and [**D**] are the electric field and electrical displacement in the piezoelectric layer, respectively, [**d**] and [ϵ] are the piezoelectric strain constants and dielectric permittivities (at constant stress field), respectively and $\{\sigma\}$ is the stress vector. Y_i, G_{ij} and ν_{ij} denote Young's moduli, shear moduli and major Poisson's ratios, respectively.

To ensure numerical stability in the solution process all entities are expressed in non-dimensional forms which are obtained in such a way that, on substitution of the dimensionless entities, the resulting governing equations appear identical to original equations. Using the relation for D_z in Eq. (4.4) in the relations for ε_x, ε_y, ε_z in the Eq. (4.3), we obtain

$$\begin{aligned} &\varepsilon_x = \bar{s}_{11}\sigma_x + \bar{s}_{12}\sigma_y + \bar{s}_{13}\sigma_z + \bar{d}_{31}D_z, && \varepsilon_y = \bar{s}_{12}\sigma_x + \bar{s}_{22}\sigma_y + \bar{s}_{23}\sigma_z + \bar{d}_{32}D_z \\ &\varepsilon_z = \bar{s}_{13}\sigma_x + \bar{s}_{23}\sigma_y + \bar{s}_{33}\sigma_z + \bar{d}_{33}D_z, && E_z = -\bar{d}_{31}\sigma_x - \bar{d}_{32}\sigma_y - \bar{d}_{33}\sigma_z + \bar{\epsilon}_{33}D_z \end{aligned} \tag{4.7}$$

where

$$\bar{\epsilon}_{33} = 1/\epsilon_{33}, \qquad \bar{s}_{ij} = s_{ij} - d_{3i}\bar{d}_{3j}, \quad \bar{d}_{3i} = d_{3i}/\epsilon_{33}, \quad \text{for} \quad (i,j) = 1,2,3$$

Similarly, the relations for γ_{yz}, γ_{zx}, E_x and E_y in Eq. (4.4) can be rewritten as

$$\begin{aligned} &\gamma_{yz} = \bar{s}_{44}\tau_{yz} + \bar{d}_{24}D_y, \qquad \gamma_{zx} = \bar{s}_{55}\tau_{zx} + \bar{d}_{15}D_x, \qquad E_x = \bar{\epsilon}_{11}D_x - \bar{d}_{15}\tau_{zx} \\ &E_y = \bar{\epsilon}_{22}D_y - \bar{d}_{24}\tau_{yz}, \qquad \bar{s}_{44} = s_{44} - d_{24}\bar{d}_{24}, \qquad \bar{s}_{55} = s_{55} - d_{15}\bar{d}_{15} \end{aligned} \tag{4.8}$$

where

$$\bar{\epsilon}_{11} = 1/\epsilon_{11}, \qquad \bar{\epsilon}_{22} = 1/\epsilon_{22}, \qquad \bar{d}_{24} = d_{24}/\epsilon_{22}, \qquad \bar{d}_{15} = d_{15}/\epsilon_{11}.$$

Using the modified Hamilton's principle for piezoelasticity case, the free vibration analysis for piezoelectric medium without any body force and charge source, the governing equation of piezo-laminated plate can be expressed as

$$\begin{aligned} \int_t \int_V [(\sigma_{ij,j} - \rho\ddot{u}_i)\delta u_i + (\varepsilon_{ij} - 0.5(u_{i,j} + u_{j,i}))\delta\sigma_{ij} + D_{i,i}\delta\phi \\ -(E_i + \phi_{,i})\delta D_i]\mathrm{d}V\,\mathrm{d}t = 0, \qquad \forall\delta u_i,\ \delta\sigma_{ij},\ \delta\phi_i,\ \delta D_i \end{aligned} \tag{4.9}$$

where V stands for the volume $(a \times b \times h)$ of the plate. Equation (4.9) implies the following boundary conditions are satisfied exactly at surface boundaries

(a) where displacements $\bar{u}_i$ are specified: $u_i - \bar{u}_i = 0$

(b) where electric displacement $\bar{D}_i^n$ are specified: $D_i n_i - \bar{D}_n = 0$

(c) where $\bar{\phi}$ is specified: $\phi - \bar{\phi} = 0$

The surface is denoted by its outward normal $\bar{n} = n_i\hat{e}_i$, where $\hat{e}_i$ $(i = 1,2,3)$ are the unit vectors along x, y and z directions. Substituting the expressions of the strain and electric components from Eqs. (4.7) and (4.8) into Eq. (4.9) yields

$$\begin{aligned} &\int_t\int_a\int_b\int_h [\delta u(\tau_{xz,z} + \sigma_{x,x} + \tau_{xy,y} - \rho\ddot{u}) + \delta v(\tau_{yz,z} + \tau_{xy,x} + \sigma_{y,y} - \rho\ddot{v}) + \delta w(\sigma_{z,z} + \tau_{zx,x} \\ &+\tau_{yz,y} - \rho\ddot{w}) + \delta\phi(D_{x,x} + D_{y,y} + D_{z,z}) + \delta\sigma_x(\bar{s}_{11}\sigma_x + \bar{s}_{12}\sigma_y + \bar{s}_{13}\sigma_z + \bar{d}_{31}D_z - u_{,x}) \\ &+\delta\sigma_y(\bar{s}_{12}\sigma_x + \bar{s}_{22}\sigma_y + \bar{s}_{23}\sigma_z + \bar{d}_{32}D_z - v_{,y}) - \delta\sigma_z(w_{,z} - \bar{s}_{13}\sigma_x - \bar{s}_{23}\sigma_y - \bar{s}_{33}\sigma_z - \bar{d}_{33}D_z) \\ &-\delta\tau_{yz}(v_{,z} + w_{,y} - \bar{s}_{44}\tau_{yz} - \bar{d}_{24}D_y) - \delta\tau_{zx}(u_{,z} + w_{,x} - \bar{s}_{55}\tau_{zx} - \bar{d}_{15}D_x) + \delta\tau_{xy}(s_{66}\tau_{xy} - v_{,x} \\ &-u_{,y}) - \delta D_x(\phi_{,x} + \bar{\epsilon}_{11}D_x - \bar{d}_{15}\tau_{zx}) - \delta D_y(\phi_{,y} + \bar{\epsilon}_{22}D_y - \bar{d}_{24}\tau_{yz}) - \delta D_z(\phi_{,z} - \bar{d}_{31}\sigma_x \\ &-\bar{d}_{32}\sigma_y - \bar{d}_{33}\sigma_z + \bar{\epsilon}_{33}D_z)]\mathrm{d}z\mathrm{d}y\mathrm{d}x\mathrm{d}t = 0, \quad \forall\ \delta u_i,\ \delta\phi,\ \delta\sigma_i,\ \delta\tau_{ij},\ \delta D_i \end{aligned} \tag{4.10}$$

Dimensionless inplane coordinates ξ_1, ξ_2 and a local thickness coordinate $\zeta^{(k)}$ for the kth layer are introduced, which vary from 0 to 1:

$$\xi_1 = x/a, \qquad \xi_2 = y/b \qquad \zeta^{(k)} = (z - z_{k-1})/t^{(k)} \tag{4.11}$$

The bottom and top surfaces of the plate are shear traction free. If the piezoelectric layer is used as an actuator, ϕ is prescribed (close circuit condition) and if it is used as a sensor, D_z is prescribed (open circuit condition) at the outer surfaces. Thus, the boundary conditions at $z = \mp h/2$ are

$$\text{at} \quad z = \mp h/2: \quad \sigma_z = 0, \quad \tau_{yz} = 0, \quad \tau_{zx} = 0, \quad \phi = 0 \ \text{ or } \ D_z = 0 \tag{4.12}$$

For perfect bonding, the continuity conditions at the interface between kth and $(k+1)$th layers are given by:

$$[(u,\, v,\, w,\, \sigma_z,\, \tau_{yz},\, \tau_{zx},\, \phi,\, D_z)|_{\zeta=1}]^{(k)} = [(u,\, v,\, w,\, \sigma_z,\, \tau_{yz},\, \tau_{zx},\, \phi,\, D_z)|_{\zeta=0}]^{(k+1)} \tag{4.13}$$

for $k = 1, \ldots, L-1$. The interfaces of the piezoelectric layers with the adjacent elastic layers are taken as grounded ($\phi = 0$) for effective actuation/sensing. At these interfaces, D_z is discontinuous, and the continuity condition for D_z in Eq. (4.13) is replaced by the condition

$$[\phi|_{\zeta=1}]^{(n_q)} = 0, \qquad q = 1, \ldots, L_a \tag{4.14}$$

where L_a is the interface where electric potential is prescribed (actuation potential).

The mechanical boundary conditions at the edges $\xi_1 = 0$ and 1 can be prescribed for a given support type, for example,

$$\begin{aligned}
&\text{Simply supported (S):} && \sigma_x = 0, && v = 0, && w = 0 \\
&\text{Clamped (C):} && u = 0, && v = 0, && w = 0 \\
&\text{Free (F):} && \sigma_x = 0, && \tau_{xy} = 0, && \tau_{xz} = 0
\end{aligned} \tag{4.15}$$

The ends may be subjected to closed circuit (CC) condition with prescribed potential or open circuit (OC) condition with known D_x (=0). The boundary conditions at the simply supported edges at $\xi_2 = 0$ and 1 are considered as

$$u = 0, \qquad \sigma_y = 0, \qquad w = 0, \qquad \phi = 0 \tag{4.16}$$

4.3 FOURIER SERIES-GENERALIZED EKM SOLUTION

The solution is expressed in terms of Fourier series along y, which identically satisfies the boundary conditions (4.16) at two simply-supported edges $y = 0, b$.

$$(u,\, w,\, \sigma_x,\, \sigma_y,\, \sigma_z,\, \tau_{zx},\, \phi,\, D_x,\, D_z) = \sum_{m=1}^{\infty} (u,\, w,\, \sigma_x,\, \sigma_y,\, \sigma_z,\, \tau_{zx},\, \phi,\, D_x,\, D_z)_m \cos\omega t \sin m\pi\xi_2,$$
$$(v,\, \tau_{xy},\, \tau_{yz},\, D_y) = \sum_{m=1}^{\infty} (v,\, \tau_{xy},\, \tau_{yz},\, D_y)_m \cos\omega t \cos m\pi\xi_2, \tag{4.17}$$

Substituting the expression from Eq. (4.17) into the variational equation (4.10), and using the orthogonality properties of $\cos m\pi\xi_2$ and $\sin m\pi\xi_2$ for $m = 1, 2, ..., \infty$, we obtain, for each Fourier term m

$$\int_t \int_a \int_h [\delta u_m(\tau_{xzm,z} + \sigma_{xm,x} - \bar{m}\tau_{xym} - \rho\omega^2 u_m) + \delta v_m(\tau_{yzm,z} + \tau_{xym,x} + \bar{m}\sigma_{ym} - \rho\omega^2 v_m)$$
$$+\delta w_m(\sigma_{zm,z} + \tau_{zxm,x} - \bar{m}\tau_{yzm} - \rho\omega^2 w_m) + \delta\phi_m(D_{xm,x} - \bar{m}D_{ym} + D_{zm,z})$$
$$+\delta\sigma_{xm}(\bar{s}_{11}\sigma_{xm} + \bar{s}_{12}\sigma_{ym} + \bar{s}_{13}\sigma_{zm} + \bar{d}_{31}D_{zm} - u_{m,x}) + \delta\sigma_{ym}(\bar{s}_{12}\sigma_{xm} + \bar{s}_{22}\sigma_{ym} + \bar{s}_{23}\sigma_{zm}$$
$$+\bar{d}_{32}D_{zm} + \bar{m}v_m) - \delta\sigma_{zm}(w_{m,z} - \bar{s}_{13}\sigma_{xm} - \bar{s}_{23}\sigma_{ym} - \bar{s}_{33}\sigma_{zm} - \bar{d}_{33}D_{zm}) - \delta\tau_{yzm}(v_{m,z}$$
$$+\bar{m}w_m - \bar{s}_{44}\tau_{yzm} - \bar{d}_{24}D_{ym}) - \delta\tau_{zxm}(u_{m,z} + w_{m,x} - \bar{s}_{55}\tau_{zxm} - \bar{d}_{15}D_{xm}) + \delta\tau_{xym}(s_{66}\tau_{xym}$$
$$-v_{m,x} - \bar{m}u_m) - \delta D_{xm}(\phi_{m,x} + \bar{\epsilon}_{11}D_{xm} - \bar{d}_{15}\tau_{zxm}) - \delta D_{ym}(\bar{m}\phi_m + \bar{\epsilon}_{22}D_{ym} - \bar{d}_{24}\tau_{yzm})$$
$$-\delta D_{zm}(\phi_{m,z} - \bar{d}_{31}\sigma_{xm} - \bar{d}_{32}\sigma_{ym} - \bar{d}_{33}\sigma_{zm} + \bar{\epsilon}_{33}D_{zm})]\mathrm{d}z\mathrm{d}x\mathrm{d}t = 0,$$
$$\forall \quad \delta u_{im}, \delta\phi_m, \delta\sigma_{im}, \delta\tau_{ijm}, \delta D_{im} \tag{4.18}$$

where $\bar{m} = m\pi/b$.

Further, Eq. (4.18) is PDE in (x and z) which is converted to ODE in (x and y) by applying the mixed-field multi-term EKM proposed by Kumari et al. [151]. In this method, the field variables

$$\mathbf{X} = [\, u \quad v \quad w \quad \sigma_x \quad \sigma_y \quad \sigma_z \quad \tau_{xy} \quad \tau_{yz} \quad \tau_{zx} \quad \phi \quad D_x \quad D_y \quad D_z \,]_m^{\mathrm{T}} \tag{4.19}$$

are expressed as the sum of n terms consisting of products of separable functions of ξ_1 and ζ. Thus, the solution of the lth variable X_l of $\mathbf{X}$ for the kth layer takes the form:

$$X_l(\xi_1, \zeta) = \sum_{i=1}^{n} f_l^i(\xi_1) g_l^i(\zeta) \quad \text{for} \quad l = 1, 2, \ldots, 13 \tag{4.20}$$

where the repeated index l does not mean summation here. Functions $f_l^i(\xi_1)$ are valid for all layers, whereas $g_l^i(\zeta)$ correspond to kth layer. These are determined iteratively as follows.

4.3.1 First Iteration Step

In the first step, functions $f_l^i(\xi_1)$ are considered as known, while $g_l^i(\zeta)$ are determined for each layer. As mentioned earlier, in the EKM, the initial trial functions are not required to satisfy the prescribed boundary conditions. Here, in the first iteration, we assume f_l^i as

$$f_2^i(\xi_1) = f_3^i(\xi_1) = f_4^i(\xi_1) = f_5^i(\xi_1) = f_6^i(\xi_1) = f_8^i(\xi_1) = f_{10}^i(\xi_1) = f_{12}^i(\xi_1) = f_{13}^i(\xi_1) = \sin i\pi\xi_1$$
$$f_1^i(\xi_1) = f_7^i(\xi_1) = f_9^i(\xi_1) = f_{11}^i(\xi_1) = \cos i\pi\xi_1. \tag{4.21}$$

From Eq. (4.20), the variation δX_l in this case is obtained as

$$\delta X_l = \sum_{i=1}^{n} f_l^i(\xi_1)\delta g_l^i \tag{4.22}$$

Functions $g_l^i(\zeta)$ are divided into two groups

$$\bar{\mathbf{G}} = [\, g_1^1 \dots g_1^n \quad g_2^1 \dots g_2^n \quad g_3^1 \dots g_3^n \quad g_6^1 \dots g_6^n \quad g_8^1 \dots g_8^n \quad g_9^1 \dots g_9^n \quad g_{10}^1 \dots g_{10}^n \quad g_{13}^1 \dots g_{13}^n \,]^{\mathrm{T}}$$
$$\hat{\mathbf{G}} = [\, g_4^1 \dots g_4^n \quad g_5^1 \dots g_5^n \quad g_7^1 \dots g_7^n \quad g_{11}^n \dots g_{11}^n \quad g_{12}^n \dots g_{12}^n \,]^{\mathrm{T}} \tag{4.23}$$

where $\bar{\mathbf{G}}$ contains the $8n$ primary variables that appear in Eqs. (4.12)-(4.13), while $\hat{\mathbf{G}}$ contains the remaining $5n$ dependent variables. After substituting Eqs. (4.20) and (4.22) into the variational expansion Eq. (4.18), its dependence on ξ_1 is eliminated by performing the integration over ξ_1 direction on the known functions of ξ_1. Since the variations δg_l^i are arbitrary, the coefficients of δg_l^i in the resulting expression must vanish individually. This process yields $8n$ ODEs of first order and $5n$ linear algebraic equations for g_l^i for the kth layer:

$$\mathbf{M}\bar{\mathbf{G}}_{,\zeta} = \bar{\mathbf{A}}\bar{\mathbf{G}} + \hat{\mathbf{A}}\hat{\mathbf{G}} \tag{4.24}$$

$$\mathbf{K}\hat{\mathbf{G}} = \tilde{\mathbf{A}}\bar{\mathbf{G}} \tag{4.25}$$

where $\mathbf{M}$, $\bar{\mathbf{A}}$, $\hat{\mathbf{A}}$, $\mathbf{K}$ and $\tilde{\mathbf{A}}$ are $8n \times 8n$, $8n \times 8n$, $8n \times 5n$, $5n \times 5n$ and $5n \times 8n$ matrices. Defining $\langle \dots \rangle_a = a \int_0^1 (\dots) d\xi_1$, the nonzero terms of the above matrices of Eqs. (4.24)-(4.25) are given below.

$$M_{i_1 j_1} = M_{j_6 i_6} = \langle f_9^i f_1^j \rangle_a, \quad M_{i_2 j_2} = M_{j_5 i_5} = \langle f_8^i f_2^j \rangle_a, \; M_{i_3 j_3} = M_{j_4 i_4} = \langle f_6^i f_3^j \rangle_a$$
$$M_{i_7 j_7} = M_{j_8 i_8} = \langle f_{13}^i f_{10}^j \rangle_a, \; \bar{A}_{i_1 j_3} = \tfrac{-t}{a} \langle f_9^i f_{3,\xi_1}^j \rangle_a, \qquad \bar{A}_{i_1 j_6} = t\bar{s}_{55} \langle f_9^i f_9^j \rangle_a$$
$$\hat{A}_{i_1 j_4} = t\bar{d}_{15} \langle f_9^i f_{11}^j \rangle_a, \qquad \bar{A}_{i_2 j_3} = -\bar{m}t \langle f_8^i f_3^j \rangle_a, \qquad \bar{A}_{i_2 j_5} = t\bar{s}_{44} \langle f_8^i f_8^j \rangle_a$$
$$\hat{A}_{i_2 j_5} = t\bar{d}_{24} \langle f_8^i f_{12}^j \rangle_a, \qquad \bar{A}_{i_3 j_4} = t\bar{s}_{33} \langle f_6^i f_6^j \rangle_a, \qquad \bar{A}_{i_3 j_8} = t\bar{d}_{33} \langle f_6^i f_{13}^j \rangle_a$$

$$
\begin{array}{lll}
\hat{A}_{i_3j_1} = t\bar{s}_{13}\langle f_6^i f_4^j\rangle_a, & \hat{A}_{i_3j_2} = t\bar{s}_{23}\langle f_6^i f_5^j\rangle_a, & \bar{A}_{i_4j_5} = \bar{m}t\langle f_3^i f_8^j\rangle_a \\
\bar{A}_{i_4j_6} = \frac{-t}{a}\langle f_3^i f_{9,\xi_1}^j\rangle_a, & \hat{A}_{i_5j_2} = -\bar{m}t\langle f_2^i f_5^j\rangle_a, & \hat{A}_{i_5j_3} = \frac{-t}{a}\langle f_2^i f_{7,\xi_1}^j\rangle_a \\
\hat{A}_{i_6j_1} = \frac{-t}{a}\langle f_1^i f_{4,\xi_1}^j\rangle_a, & \hat{A}_{i_6j_3} = \bar{m}t\langle f_1^i f_7^j\rangle_a, & \bar{A}_{i_7j_4} = t\bar{d}_{33}\langle f_{13}^i f_6^j\rangle_a \\
\bar{A}_{i_7j_8} = -t\bar{\epsilon}_{33}\langle f_{13}^i f_{13}^j\rangle_a, & \hat{A}_{i_7j_1} = t\bar{d}_{31}\langle f_{13}^i f_4^j\rangle_a, & \hat{A}_{i_7j_2} = t\bar{d}_{32}\langle f_{13}^i f_5^j\rangle_a \\
\hat{A}_{i_8j_4} = \frac{-t}{a}\langle f_{10}^i f_{11,\xi_1}^j\rangle_a, & \hat{A}_{i_8j_5} = t\bar{m}\langle f_{10}^i f_{12}^j\rangle_a, & K_{i_1j_1} = \bar{s}_{11}\langle f_4^i f_4^j\rangle_a \\
K_{i_1j_2} = \bar{s}_{12}\langle f_4^i f_5^j\rangle_a, & K_{i_2j_1} = K_{i_1j_2}, & K_{i_2j_2} = \bar{s}_{22}\langle f_5^i f_5^j\rangle_a, \\
K_{i_3j_3} = s_{66}\langle f_7^i f_7^j\rangle_a, & K_{i_4j_4} = \bar{\epsilon}_{11}\langle f_{11}^i f_{11}^j\rangle_a, & K_{i_5j_5} = \bar{\epsilon}_{22}\langle f_{12}^i f_{12}^j\rangle_a \\
\tilde{A}_{i_1j_1} = \frac{1}{a}\langle f_4^i f_{1,\xi_1}^j\rangle_a, & \tilde{A}_{i_1j_4} = -\bar{s}_{13}\langle f_4^i f_6^j\rangle_a, & \tilde{A}_{i_1j_8} = -\bar{d}_{31}\langle f_4^i f_{13}^j\rangle_a \\
\tilde{A}_{i_2j_2} = -\bar{m}\langle f_5^i f_2^j\rangle_a, & \tilde{A}_{i_2j_4} = -\bar{s}_{23}\langle f_5^i f_6^j\rangle_a, & \tilde{A}_{i_2j_8} = -\bar{d}_{32}\langle f_5^i f_{13}^j\rangle_a, \\
\tilde{A}_{i_3j_1} = \bar{m}\langle f_7^i f_1^j\rangle_a, & \tilde{A}_{i_3j_2} = \frac{1}{a}\langle f_7^i f_{2,\xi_1}^j\rangle_a, & \tilde{A}_{i_4j_6} = \bar{d}_{15}\langle f_{11}^i f_9^j\rangle_a \\
\tilde{A}_{i_4j_7} = -\frac{1}{a}\langle f_{11}^i f_{10,\xi_1}^j\rangle_a, & \tilde{A}_{i_5j_5} = \bar{d}_{24}\langle f_{12}^i f_8^j\rangle_a, & \tilde{A}_{i_5j_7} = -\bar{m}\langle f_{12}^i f_{10}^j\rangle_a \\
\bar{A}_{i_4j_3} = -\rho\omega^2 t\langle f_3^i f_3^j\rangle_a, & \bar{A}_{i_5j_2} = -\rho\omega^2 t\langle f_2^i f_2^j\rangle_a, & \bar{A}_{i_6j_1} = -\rho\omega^2 t\langle f_1^i f_1^j\rangle_a
\end{array}
\tag{4.26}
$$

Eliminating $\hat{\mathbf{G}}$ from Eq. (4.24) using Eq. (4.25) yields

$$\bar{\mathbf{G}}_{,\zeta} = \mathbf{A}\bar{\mathbf{G}} \tag{4.27}$$

where $\mathbf{A} = \mathbf{M}^{-1}[\bar{\mathbf{A}} + \hat{\mathbf{A}}\mathbf{K}^{-1}\tilde{\mathbf{A}}]$. Equation Eq. (4.27) represents a system of $8n$ homogeneous first order ODEs with constant coefficients. Its complementary solution is of the form $\bar{\mathbf{G}}_{\mathbf{c}}(\zeta) = e^{\lambda\zeta}\mathbf{Y}$, which on substitution in the homogeneous part of Eq. (4.27) yields an eigenvalue problem

$$\mathbf{A}\mathbf{Y} = \lambda\mathbf{Y} \tag{4.28}$$

Hence, the exponent λ and $\mathbf{Y}$ are the $8n$ eigenvalue and eigenvector pairs of matrix $\mathbf{A}$. The eigenvalues λ can be either real or occur in complex conjugate pairs. The general solution of Eq. (4.27) is

$$\bar{\mathbf{G}}(\zeta) = \sum_{i=1}^{8n} \mathbf{F}_i(\zeta)C_i \tag{4.29}$$

where $\mathbf{F}_i(\zeta)$ are column vector of functions corresponding to the eigenpair λ_i and Y_i. After applying the traction free boundary condition at the top and bottom of the plate and satisfying

the interface continuity conditions, equation Eq. (4.29) yields

$$\sum_{i=1}^{8n} \mathbf{K_d}_i(\zeta) C_i = \mathbf{0} \tag{4.30}$$

where, the coefficient matrix $\mathbf{K_d}$ depends on $\omega = \omega_m$. For non-trivial solution, it's determinant is zero and ω can be obtained by finding roots of the equation $|det(\mathbf{K_d})|$=0 using bisection method. The undamped natural frequencies $\omega_{01} = \omega_m$ are obtained using the procedure of Kapuria and Achary [101]. After obtaining the desired natural frequency, Eq. (4.30) is solved for determining the unknown constants by solving the linear algebraic equations and then from solving Eq. (4.29) the modal displacements, electric variables and stresses are obtained.

4.3.2 Second Iteration Step

Now that g_l^i's have been obtained in the previous step, these are considered as known, and new estimates of f_l^i are determined. In this case, the variation $\delta\mathbf{X}$ is obtained from Eq. (4.20) as

$$\delta X_l = \sum_{i=1}^{n} g_l^i(\zeta) \delta f_l^i \tag{4.31}$$

Similar to the thickness direction, $f_l^i(\xi_1)$ are divided into two groups : (i) $\bar{\mathbf{F}}$ containing $8n$ primary variables that appear in the boundary conditions (4.15), and (ii) $\hat{\mathbf{F}}$ containing the remaining $5n$ variables:

$$\begin{aligned}
\bar{\mathbf{F}} &= [\, f_1^1 \ldots f_1^n \quad f_2^1 \ldots f_2^n \quad f_3^1 \ldots f_3^n \quad f_4^1 \ldots f_4^n \quad f_7^1 \ldots f_7^n \quad f_9^1 \ldots f_9^n \quad f_{10}^1 \ldots f_{10}^n \quad f_{11}^1 \ldots f_{11}^n \,]^{\mathrm{T}} \\
\hat{\mathbf{F}} &= [\, f_5^1 \ldots f_5^n \quad f_6^1 \ldots f_6^n \quad f_8^1 \ldots f_8^n \quad f_{12}^1 \ldots f_{12}^n \quad f_{13}^1 \ldots f_{13}^n \,]^{\mathrm{T}}
\end{aligned} \tag{4.32}$$

Equations (4.20) and (4.31) are substituted into Eq. (4.18), and this time, it is integrated over the thickness direction ζ. Since the variations δf_l^i are arbitrary, their coefficients are individually equated to zero, which yields the following system of differential-algebraic equations for f_l^i:

$$\mathbf{N}\bar{\mathbf{F}}_{,\xi_1} = \bar{\mathbf{B}}\bar{\mathbf{F}} + \hat{\mathbf{B}}\hat{\mathbf{F}} \tag{4.33}$$

$$\mathbf{L}\hat{\mathbf{F}} = \tilde{\mathbf{B}}\bar{\mathbf{F}} \tag{4.34}$$

where $\mathbf{N}$, $\bar{\mathbf{B}}$, $\hat{\mathbf{B}}$, $\mathbf{L}$ and $\tilde{\mathbf{B}}$ are matrices of size $8n \times 8n$, $8n \times 8n$, $8n \times 5n$, $5n \times 5n$ and $5n \times 8n$, respectively. Using the notation $\langle \ldots \rangle_h = \sum_{k=1}^{L} t^{(k)} \int_0^1 (\ldots)^{(k)} \, d\zeta$ for integration across the

laminate thickness, the nonzero elements of matrices $\mathbf{N}$, $\bar{\mathbf{B}}$, $\hat{\mathbf{B}}$, $\mathbf{L}$ and $\tilde{\mathbf{B}}$ of Eqs. (4.33)-(4.34) are given below

$$
\begin{aligned}
&N_{i_1j_1} = N_{j_4i_4} = \langle g_4^i g_1^j\rangle_h, \quad N_{i_2j_2} = N_{j_5i_5} = \langle g_7^i g_2^j\rangle_h, \; N_{i_3j_3} = N_{j_6i_6} = \langle g_9^i g_3^j\rangle_h \\
&N_{i_7j_7} = N_{j_8i_8} = \langle g_{10}^i g_{11}^j\rangle_h, \; \bar{B}_{i_1j_4} = a\langle \bar{s}_{11} g_4^i g_4^j\rangle_h, \qquad \hat{B}_{i_1j_1} = a\langle \bar{s}_{12} g_4^i g_5^j\rangle_h \\
&\hat{B}_{i_1j_2} = a\langle \bar{s}_{13} g_4^i g_6^j\rangle_h, \qquad \hat{B}_{i_1j_5} = \langle \bar{d}_{31} g_4^i g_{13}^j\rangle_h, \qquad \bar{B}_{i_2j_1} = -a\bar{m}\langle g_7^i g_1^j\rangle_h \\
&\bar{B}_{i_2j_5} = a\langle s_{66} g_7^i g_7^j\rangle_h, \qquad \bar{B}_{i_3j_1} = -a\langle g_9^i \tfrac{g_{1,\zeta}^j}{t}\rangle_h, \qquad \bar{B}_{i_3j_6} = a\langle \bar{s}_{55} g_9^i g_9^j\rangle_h \\
&\bar{B}_{i_3j_8} = a\langle \bar{d}_{15} g_9^i g_{11}^j\rangle_h, \qquad \bar{B}_{i_4j_5} = a\bar{m}\langle g_1^i g_7^j\rangle_h, \qquad \bar{B}_{i_4j_6} = a\langle \tfrac{g_{1,\zeta}^i}{t} g_9^j\rangle_h \\
&\hat{B}_{i_5j_1} = -a\bar{m}\langle g_2^i g_5^j\rangle_h, \qquad \hat{B}_{i_5j_3} = a\langle \tfrac{g_{2,\zeta}^i}{t} g_8^j\rangle_h, \qquad \hat{B}_{i_6j_2} = -a\langle g_3^i \tfrac{g_{6,\zeta}^j}{t}\rangle_h \\
&\hat{B}_{i_6j_3} = a\bar{m}\langle g_3^i g_8^j\rangle_h, \qquad \bar{B}_{i_7j_8} = -a\langle \bar{\epsilon}_{11} g_{11}^i g_{11}^j\rangle_h, \; \bar{B}_{i_7j_6} = a\langle \bar{d}_{15} g_{11}^i g_9^j\rangle_h \\
&\hat{B}_{i_8j_4} = a\bar{m}\langle g_{10}^i g_{12}^j\rangle_h, \qquad \hat{B}_{i_8j_5} = -a\langle g_{10}^i \tfrac{g_{13,\zeta}^j}{t}\rangle_h, \qquad L_{i_1j_1} = \langle \bar{s}_{22} g_5^i g_5^j\rangle_h \\
&L_{i_1j_2} = \langle \bar{s}_{23} g_5^i g_6^j\rangle_h, \qquad L_{i_1j_5} = \langle \bar{d}_{32} g_5^i g_{13}^j\rangle_h, \qquad L_{j_2i_1} = L_{i_1j_2} \\
&L_{i_2j_2} = \langle \bar{s}_{33} g_6^i g_6^j\rangle_h, \qquad L_{i_2j_5} = \langle \bar{d}_{33} g_6^i g_{13}^j\rangle_h, \qquad L_{i_3j_3} = \langle \bar{s}_{44} g_8^i g_8^j\rangle_h \\
&L_{i_3j_4} = \langle \bar{d}_{24} g_8^i g_{12}^j\rangle_h, \qquad L_{i_4j_3} = L_{i_3j_4}, \qquad L_{i_4j_4} = -\langle \bar{\epsilon}_{22} g_{12}^i g_{12}^j\rangle_h \\
&L_{i_5j_1} = \langle \bar{d}_{32} g_{13}^i g_5^j\rangle_h, \qquad L_{i_5j_2} = \langle \bar{d}_{33} g_{13}^i g_6^j\rangle_h, \qquad L_{i_5j_5} = -\langle \bar{\epsilon}_{33} g_{13}^i g_{13}^j\rangle_h \\
&\tilde{B}_{i_1j_2} = -\bar{m}\langle g_5^i g_2^j\rangle_h, \qquad \tilde{B}_{i_1j_4} = -\langle \bar{s}_{12} g_5^i g_4^j\rangle_h, \qquad \tilde{B}_{i_2j_3} = \langle g_6^i \tfrac{g_{3,\zeta}^j}{t}\rangle_h, \\
&\tilde{B}_{i_2j_4} = -\langle \bar{s}_{13} g_6^i g_4^j\rangle_h, \qquad \tilde{B}_{i_3j_3} = \bar{m}\langle g_8^i g_3^j\rangle_h, \qquad \tilde{B}_{i_3j_2} = \langle g_8^i \tfrac{g_{2,\zeta}^j}{t}\rangle_h \\
&\tilde{B}_{i_4j_7} = \bar{m}\langle g_{12}^i g_{10}^j\rangle_h, \qquad \tilde{B}_{i_5j_4} = -\langle \bar{d}_{31} g_{13}^i g_4^j\rangle_h, \qquad \tilde{B}_{i_5j_7} = \langle g_{13}^i \tfrac{g_{10,\zeta}^j}{t}\rangle_h \\
&\bar{B}_{i_4j_1} = -a\rho\omega^2\langle g_1^i g_1^j\rangle_h, \qquad \bar{B}_{i_5j_2} = -a\rho\omega^2\langle g_2^i g_2^j\rangle_h, \qquad \bar{B}_{i_6j_3} = -a\rho\omega^2\langle g_3^i g_3^j\rangle_h
\end{aligned}
\tag{4.35}
$$

Equations (4.33) and (4.34) are of the same nature as Eqs. (4.24)-(4.25), and are solved following the same procedure. The solution involves $8n$ constants, which are determined from the boundary conditions given by Eq. (4.15), expressed in terms of f_l^i. The two steps described in Sec. 4.3.1 and Sec. 4.3.2 complete one iteration. The iterations are continued till the desired level of convergence is achieved.

4.4 RESULTS AND DISCUSSION

The efficacy of the present 3D EKM approach is validated by comparing with the 3D exact results for simply supported case and with 3D FE results for other boundary conditions. Four configurations of plate (a), (b), (c) and (d) as shown in Fig. 4.2 are considered for numerical study. The material codings (mat.1, mat.2, mat.3...) enumerated in Fig. 4.2 and Fig. 4.6 are as per mentioned in Table 4.1.

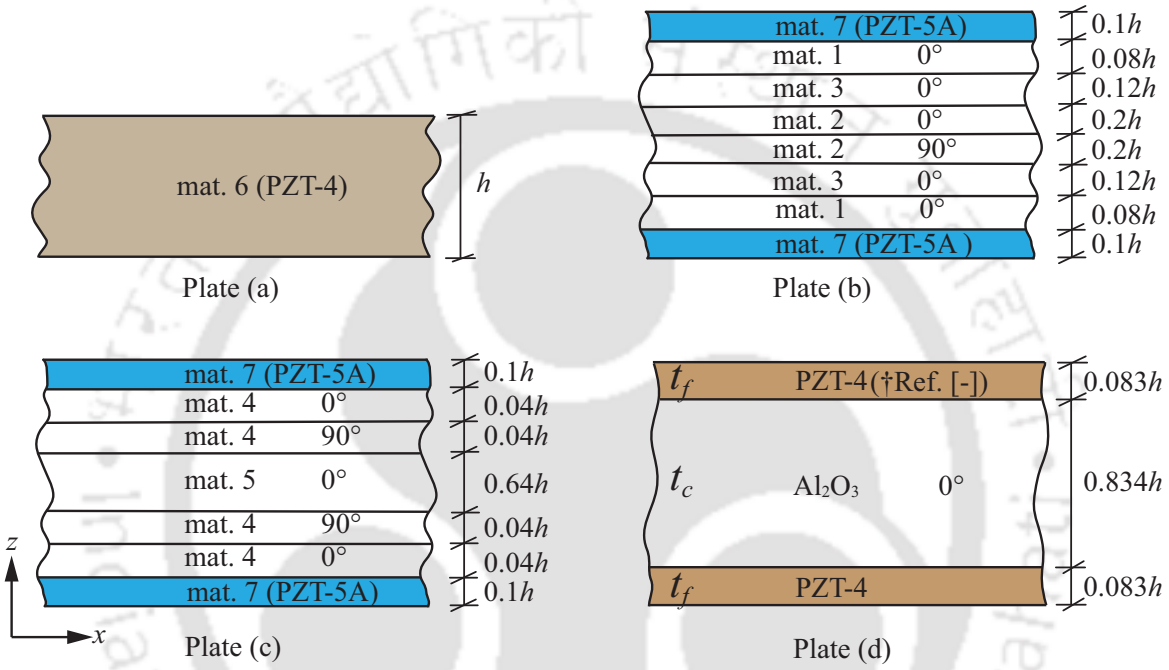

Figure 4.2: Configurations of piezoelectric plate (a), smart composite plate (b), (d) and sandwich plate (c).†Ref.[165]

Unless mentioned otherwise, the natural frequency $\bar{\omega}_m$, the modal displacements, stresses and electrical state variables are non-dimensionalized as:

$$\bar{\omega}_m = \omega a S \sqrt{\rho_0 / Y_0}$$

$$(\bar{u},\, \bar{v},\, \bar{w}) = (u, v, w)/\max(u, v, w)$$

$$(\bar{\sigma}_x,\, \bar{\sigma}_y,\, \bar{\sigma}_z,\, \bar{\tau}_{zx},\, \bar{\tau}_{yz}) = (\sigma_x,\, \sigma_y,\, \sigma_z,\, \tau_{zx},\, \tau_{yz}) S\, h / Y_0 \max(u, v, w)$$

$$\bar{D}_z = D_z S\, h / d_0\, Y_0 \max(u, v, w)$$

$$\bar{\phi} = \phi\, d_0 / \max(u, v, w)$$

where $S(= a/h)$ denote the span-to-thickness ratio and $\max(u, v, w)$ denote the largest value of u, v and w through the thickness for a particular mode. Y_0=81.3 GPa for plate (a), 6.9 GPa for

plate (b) and (c) and 380.7 GPa for plate (d). ρ_0=1 kg/m^3 for plate (a), 1578 kg/m^3 for plate (b), 1000 kg/m^3 for plate (c), 4000 kg/m^3 for plate (d) and 7600 kg/m^3 for plate (e). $d_0 = d_{33}$ pm/V for respective plates wherever applicable.

The 3D FE solution is obtained using the ABAQUS software [161]. In the 3D FE analysis, 20-node hexahedral solid elements of type C3D20RE for piezo-layers and C3D20R for elastic layers with reduced integration are used. The convergence study of the 3D FE solution for a typical case of a thick (S=5) hybrid sandwich plate (g) is presented in Table 4.2 considering three different mesh sizes ($40 \times 40 \times 20$), ($50 \times 50 \times 20$) and ($60 \times 60 \times 20$), respectively. The mesh discretization presented inside the parenthesis are along the width, length, and thickness of the plate respectively and is as shown in Fig. 4.3. It can be observed from the table that for simply supported case convergence in frequencies is observed for the whole five significant digits while for C-C and C-F convergence is observed up to four significant digits and in some frequencies up to five significant digits. Hence, it is fair to consider ($50 \times 50 \times 20$) mesh size

Table 4.1: Material properties

		Ref.[149]					PZT-4	PZT-5A	Ref.[151]
Property	Unit	Mat.1	Mat.2	Mat.3	Mat.4	Mat.5	Mat.6	Mat.7	Mat.8
Y_1	GPa	6.9	224.25	172.5	131.1	0.0002208	81.3	61.0	181
Y_2	GPa	6.9	6.9	6.9	6.9	0.0002001	81.3	61.0	10.3
Y_3	GPa	6.9	6.9	6.9	6.9	2.76	64.5	53.2	10.3
G_{12}	GPa	1.38	56.58	3.45	3.588	0.01656	30.6	22.6	7.17
G_{23}	GPa	1.38	1.38	1.38	2.3322	0.4554	25.6	21.1	2.87
G_{31}	GPa	1.38	56.58	3.45	3.588	0.5451	25.6	21.1	7.17
ν_{12}		0.25	0.25	0.25	0.32	0.99	0.329	0.35	0.28
ν_{13}		0.25	0.25	0.25	0.32	3×10^{-5}	0.432	0.38	0.28
ν_{23}		0.25	0.25	0.25	0.49	3×10^{-5}	0.432	0.38	0.33
ρ	kg/m^3	1578	1578	1578	1000	70	1	7600	1578
d_{31}	pm/V						d_{31}^6	-171	
d_{32}	pm/V						d_{32}^6	-171	
d_{33}	pm/V						d_{33}^6	374	
d_{15}	pm/V						496.875	584	
d_{24}	pm/V						496.875	584	
η_{11}	nF/m						13.0537	15.3	
η_{22}	nF/m						13.0537	15.3	
η_{33}	nF/m						11.505	15.0	

$d_{31}^6 = d_{32}^6 = -123.0474784747847, d_{33}^6 = 289.0604422323293$

without compromising the accuracy and stability which we have adopted for all the test cases in the present investigation.

Table 4.2: Natural frequency (Hz) convergence study of 3D FE solution of a typical thick (S=5) hybrid sandwich plate (g)

		Mesh size (width× length× thickness)		
BCs	Mode	(40 × 40 × 20)	(50 × 50 × 20)	(60 × 60 × 20)
S-S	1	378.21	378.21	378.21
	2	643.80	643.80	643.80
	3	660.19	660.19	660.19
C-C	1	409.89	409.82	409.80
	2	659.07	659.05	659.04
	3	720.18	720.12	720.07
C-F	1	273.71	273.70	273.70
	2	430.08	430.08	430.08
	3	504.70	504.69	504.67

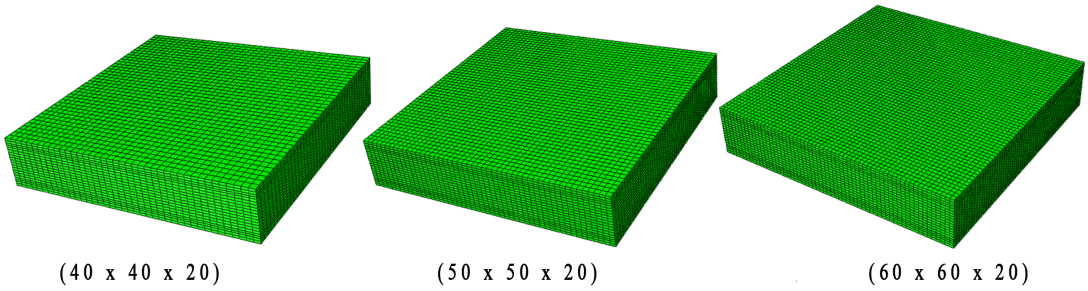

Figure 4.3: 3D FE mesh discretization of a thick (S=5) hybrid sandwich plate (g) for convergence study.

4.4.1 Validation with 3D Exact Results for Simply Supported (S-S) Case

The plate (a) with all round simply supported boundary conditions is considered for analysis in this section. The top and bottom surfaces of the plate are both kept either in closed circuit condition or in open circuit condition. The natural frequencies for m=1 are presented for S value of 1 and 4 with a=1 m and compared with 3D exact [166] solutions in Table 4.3. The present 3D EKM results show excellent match with the 3D exact solution.

Table 4.3: Natural frequencies of simply supported (S-S) square hybrid single layer piezoelectric plate under closed circuit (CC) and open circuit condition for S=1 and 4

Mode		Close circuit		Open Circuit	
sequence	S	Present	3D Exact[166]	Present	3D Exact[166]
1	1	713062.7	713061.0	724602.0	724602.0
2		777020.5	777021.0	777020.5	777021.0
3		889901.3	889902.0	912911.4	912912.0
4		925431.5	925431.0	925431.5	925431.0
5		1243817.9	1243819.0	1270594.7	1270594.0
6		1270594.7	1270594.0	1293505.0	1293504.0
1	4	96929.9	96929.9	98231.7	98231.7
2		194254.8	194255.0	194254.8	194255.0
3		327662.5	327663.0	355110.0	355110.0
4		538884.4	538885.0	538884.4	538885.0
5		609185.3	609186.0	690766.8	690767.0
6		958922.3	958922.0	960103.9	960103.0

The through-thickness distributions of in-plane displacement ($\bar{u}$), deflection ($\bar{w}$) and electric potential ($\bar{\phi}$) for first and third modes are shown in Fig. 4.4 for S=1 for both closed and open circuit conditions. Here, the electric potential is normalized by dividing with its largest value only i.e $\bar{\phi} = \phi/\max(\phi)$. For CC case, the plot is compared against the 3D exact solution of Heyliger and Saravanos [166] and for OC case the plot is compared against 3D exact solution of Kapuria and Achary [101] as it is not available in Ref. [166]. In both the cases the plotted entities of the present results are matching exactly with the referred solution. The 3D exact results, for the OC case, are obtained using the computer program developed by Kapuria and Achary [101].

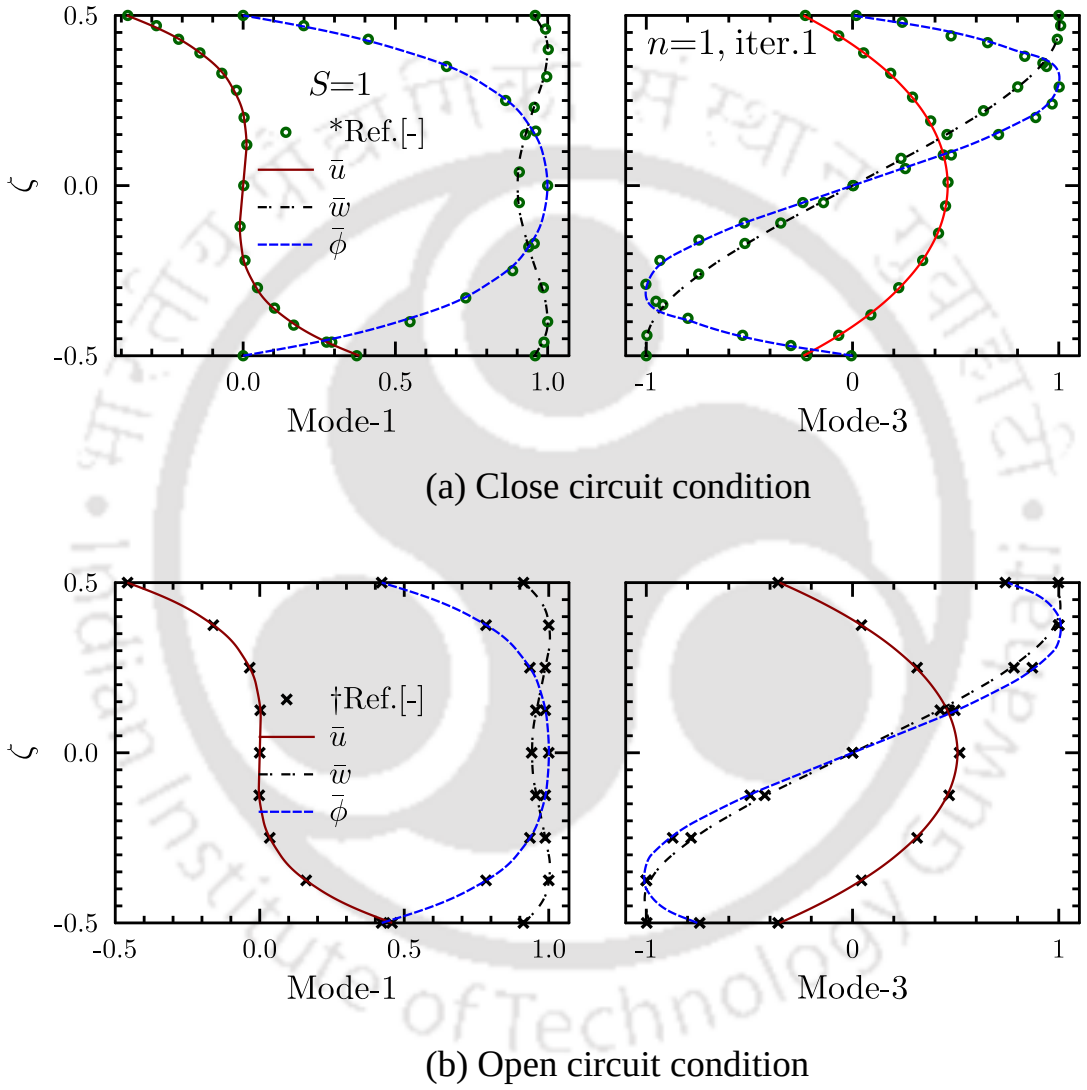

Figure 4.4: Validation of $\bar{u}$, $\bar{w}$ and $\bar{\phi}$ for mode 1 and 3 of an all round simply supported single layer piezoelectric plate (S=1) for both close and open circuit condition. *Ref.[166]; †Ref.[101]

The natural frequencies for four S values 5, 10, 20 and 1000 are presented in Table 4.4 for a square hybrid plate (b) of highly unsymmetrical lay-up and hybrid sandwich plate (c). The natural frequencies are compared with the 3D exact [167] results for S=5, 10, 20 and also with the additional results for S=1000 which are validated using the computer program of Kapuria and Achary [101]. It is observed that the present EKM results are exactly matching with the 3D exact [101, 167] results for thick to thin plates.

Table 4.4: Natural frequencies $\bar{\omega}_{mn}$ of simply supported (S-S) hybrid plate (b) and hybrid sandwich plate (c) with different S values

		Plate (b)		Plate (c)	
S	Entity	Present	3D Exact[167]	Present	3D Exact[167]
5	$\bar{\omega}_{11}$	7.4148	7.4148	4.5233	4.5233
	$\bar{\omega}_{21}$	14.714	14.714	7.8958	7.8958
	$\bar{\omega}_{22}$	18.643	18.643	10.292	10.292
	$\bar{\omega}_{31}$	23.621	23.621	11.837	11.837
10	$\bar{\omega}_{11}$	10.034	10.034	7.3390	7.3390
	$\bar{\omega}_{21}$	22.397	22.397	13.880	13.880
	$\bar{\omega}_{22}$	29.659	29.659	18.093	18.093
	$\bar{\omega}_{31}$	37.741	37.741	21.231	21.231
20	$\bar{\omega}_{11}$	11.418	11.418	9.7440	9.7440
	$\bar{\omega}_{21}$	29.024	29.024	21.357	21.357
	$\bar{\omega}_{22}$	40.137	40.137	29.356	29.356
	$\bar{\omega}_{31}$	53.580	53.580	35.693	35.693
1000	$\bar{\omega}_{11}$	12.050	12.050	11.337	11.337
	$\bar{\omega}_{21}$	33.615	33.615	28.836	28.836
	$\bar{\omega}_{22}$	48.197	48.198	45.336	45.336
	$\bar{\omega}_{31}$	69.932	69.932	58.690	58.690

4.4.2 Validation for Other Boundary Conditions

The comparison of natural frequencies of a hybrid sandwich plate (c) for C-S and C-C cases are presented in Table 4.5 for three different S values i.e. 5, 10 and 20. The hybrid sandwich plate has PZT-5A layers at top and bottom, graphite-epoxy faces of cross-ply lay-up and a soft core. The side surfaces and interfaces of both the PZT layers along with the top surface of the top PZT layer are grounded. The bottom surface of the bottom PZT layer is kept in open circuit condition. Since no analytical solution is available for the present case therefore present results are compared with the 3D FE results. In Table 4.5 the present results show a very good agreement with the 3D FE results of ABAQUS.

Table 4.5: Natural flexural frequencies $\bar{\omega}_m$ of a square hybrid sandwich plate (c) for boundary conditions C-S and C-C (n=1, iter.3)

		C-S		C-C	
S	Entity	Present	3D FE	Present	3D FE
5	$\bar{\omega}_1$	4.5990	4.6952	4.7716	4.9014
	$\bar{\omega}_2$	7.7312	7.7855	7.7759	7.8821
	$\bar{\omega}_3$	7.9946	8.2421	8.1539	8.6125
	$\bar{\omega}_4$	10.370	10.553	10.497	10.841
	$\bar{\omega}_5$	11.846	11.897	11.864	11.965
10	$\bar{\omega}_1$	7.7032	7.7892	8.1126	8.2908
	$\bar{\omega}_2$	13.356	13.411	13.489	13.587
	$\bar{\omega}_3$	14.129	14.385	14.397	14.879
	$\bar{\omega}_4$	18.232	18.432	18.396	18.782
	$\bar{\omega}_5$	20.182	20.227	20.216	20.306
20	$\bar{\omega}_1$	10.929	10.997	12.269	12.414
	$\bar{\omega}_2$	20.866	20.931	21.322	21.470
	$\bar{\omega}_3$	22.697	22.889	23.955	24.340
	$\bar{\omega}_4$	30.081	30.255	30.823	31.159
	$\bar{\omega}_5$	33.570	33.770	33.902	33.999

The results in Table 4.6 are presented for a three layer square hybrid plate (d) with aluminum oxide (Al_2O_3) core comparing with the analytical results those given in Ref. [165]. The following material properties are considered for this plate as given in Ref. [165]:

$[(C_{11}, C_{12}, C_{33}, C_{13}, C_{55}), (e_{31}, e_{33}, e_{15}), (\eta_{11}, \eta_{33}), \rho] =$

PZT-4: [(132, 71, 115, 73, 26) GPa, (-4.1, 14.1, 10.5) C/m^2, (7.124, 5.841) nF/m, 7500 kg/m^3]

Al_2O_3: [(460.2, 174.7, 509.5, 127.4, 126.9) GPa, 4000 kg/m^3]

where C_{ij} and e_{ij} are the stiffness coefficients and piezoelectric stress constants. In the table, t_f and t_c denote the face and core thickness, respectively. The frequencies are computed for boundary conditions S-S, C-C and F-F with the major piezoelectric surfaces either in closed circuit (CC) or open circuit (OC) condition. Depending on the total plate thickness, which in case of here is $(2t_f + t_c)$, the results are presented for four different S values i.e. 16.67, 14.29, 8.34 and 7.14. It is evident from the table that the present computed frequencies agree well with the analytical solution of Farsangi et al. [165] for simple supported and free-free cases. The deviation is more significant for thick plates as observed for C-C case owing to the 2D approach (FSDT theorem) of Farsangi et al. [165].

Table 4.6: Comparison of first three natural frequencies (Hz) for C-C and F-F for square hybrid plate (d) for different S values

				Mode sequences					
				1st		2nd		3rd	
BCs	t_c	t_f	EBCs	Present	Ref.[165]	Present	Ref.[165]	Present	Ref.[165]
S-S	0.05	0.005	CC	423.138	422.966	1040.276	1038.436	1637.615	1633.073
			OC	430.028	429.818	1056.790	1054.813	1663.015	1658.196
		0.01	CC	405.880	405.858	995.583	992.919	1564.153	1556.567
			OC	419.071	418.993	1026.702	1024.066	1611.309	1604.047
	0.1	0.01	CC	818.358	816.534	1930.069	1918.659	2934.954	2910.463
			OC	831.037	829.094	1957.660	1945.644	2974.161	2948.553
		0.02	CC	782.559	778.274	1833.640	1810.841	2775.467	2727.761
			OC	806.219	802.005	1882.677	1860.773	2842.598	2797.491
C-C	0.05	0.005	CC	614.011	609.652	1146.421	1139.314	1422.047	1415.781
			OC	622.394	619.187	1163.075	1156.901	1442.594	1436.811
		0.01	CC	591.517	583.692	1087.983	1087.968	1352.764	1348.827
			OC	606.859	601.821	1120.721	1121.272	1386.773	1388.307
	0.1	0.01	CC	1147.362	1128.191	2080.422	2060.096	2486.073	2456.099
			OC	1158.738	1143.582	2102.651	2087.428	2514.855	2484.766
		0.02	CC	1093.007	1068.626	1974.881	1939.224	2357.679	2299.904
			OC	1108.143	1097.013	2017.612	1989.419	2359.680	2351.255
F-F	0.05	0.005	CC	206.766	206.189	338.674	337.986	766.857	763.342
			OC	208.927	208.514	340.229	339.685	774.197	771.475
		0.01	CC	198.969	198.324	325.650	325.041	736.322	730.608
			OC	202.989	202.751	328.507	328.241	749.741	746.136
	0.1	0.01	CC	404.720	404.375	651.027	649.789	1440.733	1421.432
			OC	408.611	408.708	654.024	652.670	1452.443	1435.764
		0.02	CC	388.322	387.512	621.593	620.529	1372.490	1341.602
			OC	396.977	395.673	627.900	625.835	1368.923	1368.417

4.4.3 Some New Benchmark Results

4.4.3.1 Single Layer Piezoelectric Plate (a)

First three frequencies for a very thick (S=1) piezoelectric plate (a) are presented in Table 4.7 for m=1 for non-simply supported boundary conditions (C-C, C-S, C-F and F-F) with top and bottom open circuit condition. The through-thickness distributions of in-plane displacements ($\bar{u}$, $\bar{v}$), transverse deflection ($\bar{w}$) and electric potential ($\bar{\phi}$) for mode-1 and mode-3 are presented in Fig. 4.5 for C-C, C-F and F-F boundary conditions and are compared with the 3D FE solution of ABAQUS. In the figure, the numbers within the parentheses denote the corresponding frequencies which are mentioned in Table 4.7. Here the electric potential is also normalized by dividing with its largest value only. It can be observed from Fig. 4.5 that the first modes for all the boundary conditions are flexural modes. The third mode for C-C is an inplane stretching mode ($\bar{u}$ maximum) in x direction whereas for C-F and F-F the third modes are thickness stretching modes ($\bar{w}$ varies from -1 to 1).

Table 4.7: First three frequencies of a thick (S=1) piezoelectric plate (a) for m=1 with open circuit condition (n=1. iter. 3)

	Boundary conditions			
Mode Sequence	C-C	C-S	C-F	F-F
1	735973.0	729634.5	468799.0	417230.1
2	927205.0	775038.9	700069.2	491310.2
3	1102446.9	930042.1	777898.7	736189.7

4.4.3.2 Piezoelectric Bimorph Plate (e)

A rectangular piezoelectric bimorph plate (e) consisting of two identical layers of PZT-4 piezometric with poling along z-direction is considered here. The material properties of PZT-4 considered here is taken as given in Ref. [149]:

$[(C_{11}, C_{22}, C_{33}, C_{12}, C_{23}, C_{31}, C_{44}, C_{55}, C_{66}]$ = [139, 139, 115, 77.8, 74.3, 74.3, 25.6, 25.6, 30.6] GPa

$[(e_{31}, e_{32}, e_{33}, e_{15}, e_{24}), (\eta_{11}, \eta_{11}, \eta_{33})]$ = [(-5.2, -5.2, 15.1, 12.7, 12.7) C/m^2, (13.06, 13.06, 11.51) nF/m]

and ρ=7600 kg/m^3. The interface between the two PZT layers is grounded. The natural frequencies $\bar{\omega}_m (= \omega a S\sqrt{\rho/Y_2})$ are obtained for the plate of span-to-thickness ratio, $S = 10$, for (i) top, bottom close circuit ($\phi = 0$) , (ii) top, bottom open circuit conditions (D_z=0) and (iii)

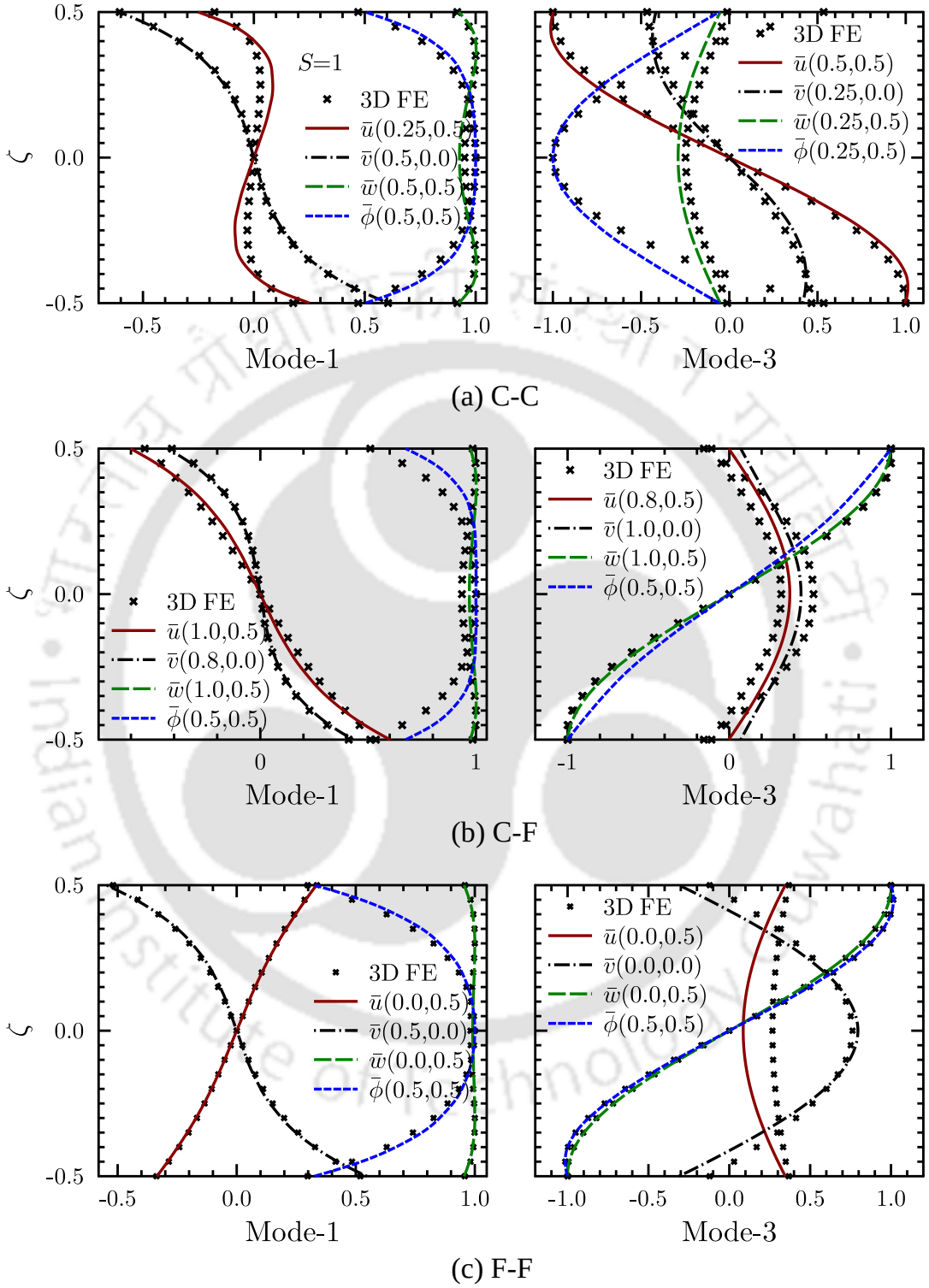

Figure 4.5: Through-thickness distributions of in-plane displacements, deflection and electric potential for C-C, C-F and F-F boundary conditions for first and third modes.

top close, bottom open circuit conditions.

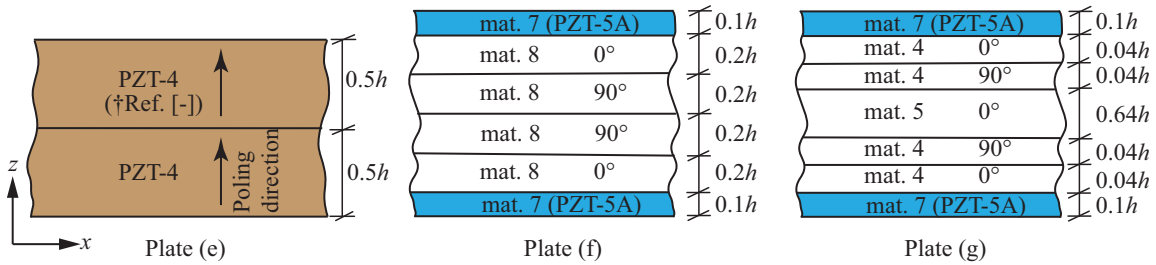

Figure 4.6: Configurations of bimorph plate (e), smart composite plate (f) and smart sandwich plate (g). †Ref.[149]

The flexural natural frequencies for the first six modes determined by the present 3D EKM for S-S case are presented in Table 4.8 and are compared with the 3D exact results of Kapuria and Achary [101] confirming exact match. Here for S-S case the side surfaces at ξ_1= 0, 1 are also grounded. In the Fig. 4.7, the displacements, stresses and electrical variables of simply supported bimorph plate of case (iii) for the first mode ($\bar{\omega}_m$ = 6.084) are presented along with the 3D exact [101] solution and found to establish an exact match.

Table 4.8: Non-dimensional flexural natural frequencies $\bar{\omega}_m$ of piezoelectric bimorph plate (e) with S-S boundary conditions for S=10

Mode	top,bottom close		top, bottom open		top close, bottom open	
Sequence	3D EKM	3D Exact[101]	3D EKM	3D Exact[101]	3D EKM	3D Exact[101]
1	5.937	5.937	6.250	6.250	6.084	6.084
2	14.109	14.109	14.684	14.684	14.381	14.381
3	21.589	21.589	22.280	22.280	21.918	21.918
4	26.264	26.264	26.984	26.984	26.609	26.609
5	32.891	32.891	33.608	33.608	33.235	33.235
6	41.123	41.123	41.789	41.789	41.444	41.444

The flexural natural frequencies for the first ten modes determined by the present 3D EKM are produced in Table 4.9 for F-F case. The side surfaces at ξ_1= 0, 1 of the plate are kept in OC condition for the cases (ii) and (iii). The 3D FE results obtained from ABAQUS are also presented for comparing the relative accuracy. The percentage difference (% diff.) is calculated as: % diff. = (3D EKM frequency - 3D FE frequency)/3D EKM frequency. A maximum difference of 1.58% is noted for the sixth frequency in case (i) for plate aspect ratio, b/a=2.

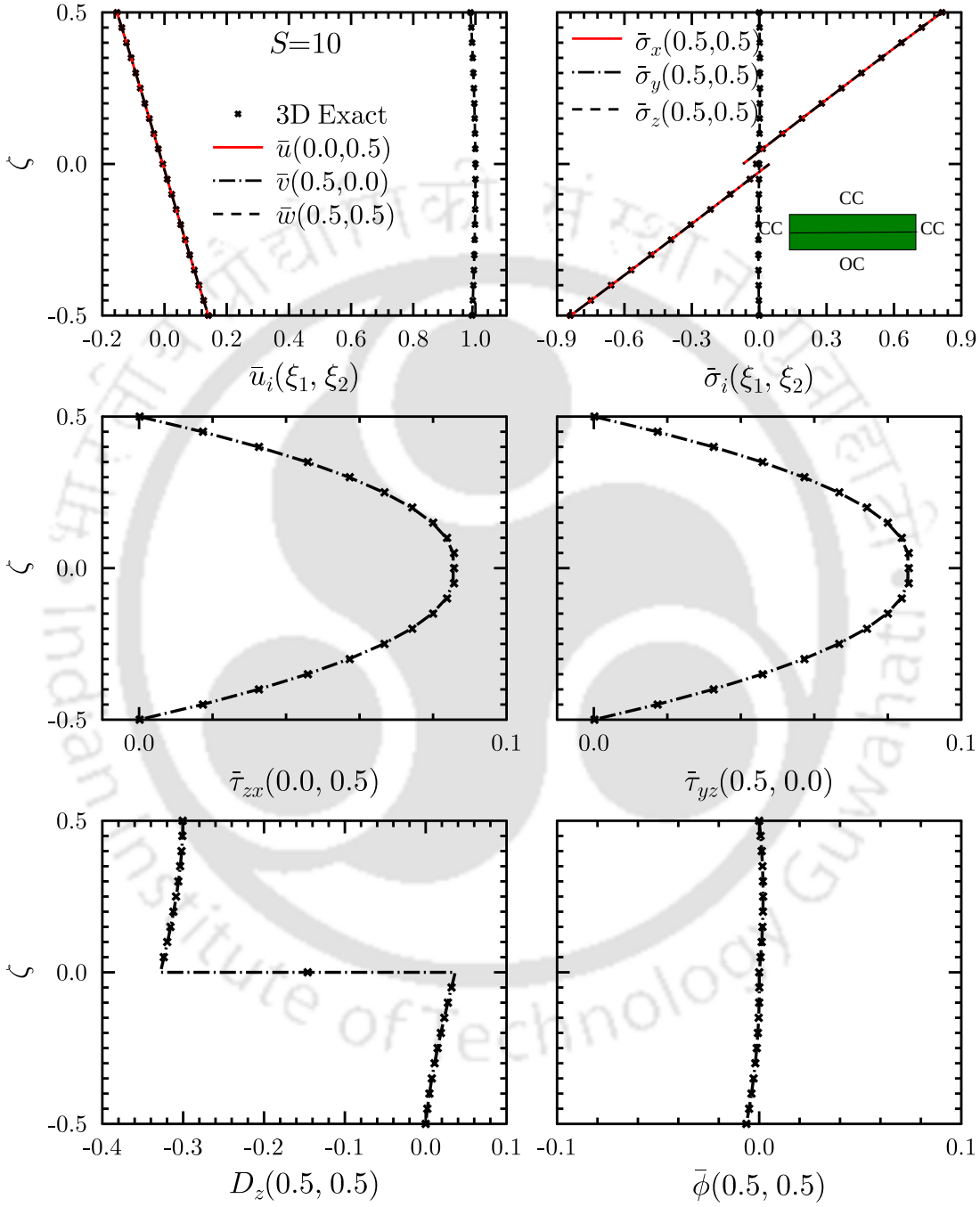

Figure 4.7: Through-thickness distributions of in-plane displacements, transverse deflection, stresses and electrical variables for simply supported (S-S) bimorph plate (e) for the first mode ($\bar{\omega}_m = 6.084$) for top close and bottom open condition.

Table 4.9: Non-dimensional flexural natural frequencies $\bar{\omega}_m$ of piezoelectric bimorph plate (e) with F-F boundary conditions for S=10

		top, bottom close			top, bottom open			top close, bottom open		
b/a	Entity	Present	3D FE	% diff.	Present	3D FE	% diff.	Present	3D FE	% diff.
1	$\bar{\omega}_1$	2.905	2.904	-0.03	3.007	3.008	0.02	2.957	2.953	0.14
	$\bar{\omega}_2$	4.649	4.647	-0.04	4.708	4.710	0.04	4.684	4.678	0.13
	$\bar{\omega}_3$	10.490	10.371	-1.15	10.784	10.718	-0.62	10.522	10.532	-0.09
	$\bar{\omega}_4$	11.195	11.182	-0.12	11.557	11.543	-0.12	11.389	11.356	0.29
	$\bar{\omega}_5$	13.005	13.012	0.05	13.283	13.269	-0.11	13.248	13.139	0.82
	$\bar{\omega}_6$	18.968	18.923	-0.24	19.571	19.338	-1.20	19.248	19.123	0.65
	$\bar{\omega}_7$	20.564	20.405	-0.78	21.158	21.108	-0.24	20.587	20.735	-0.72
	$\bar{\omega}_8$	23.522	23.492	-0.13	24.044	24.022	-0.09	23.763	23.753	0.04
	$\bar{\omega}_9$	25.088	25.058	-0.12	25.48	25.460	-0.08	25.278	25.264	0.05
	$\bar{\omega}_{10}$	28.485	28.305	-0.64	28.779	28.930	0.52	28.540	28.601	-0.21
2	$\bar{\omega}_1$	0.729	0.725	-0.55	0.749	0.748	-0.13	0.737	0.736	0.13
	$\bar{\omega}_2$	1.985	1.984	-0.05	1.994	1.994	0.00	1.990	1.988	0.10
	$\bar{\omega}_3$	2.905	2.904	-0.03	3.007	3.008	0.03	2.958	2.953	0.17
	$\bar{\omega}_4$	4.649	4.647	-0.04	4.708	4.710	0.04	4.684	4.678	0.14
	$\bar{\omega}_5$	6.454	6.446	-0.12	6.650	6.675	0.37	6.575	6.555	0.30
	$\bar{\omega}_6$	7.850	7.728	-1.58	8.137	8.089	-0.59	7.985	7.891	1.18
	$\bar{\omega}_7$	8.317	8.314	-0.04	8.481	8.469	-0.14	8.387	8.390	-0.03
	$\bar{\omega}_8$	10.490	10.371	-1.15	10.784	10.718	-0.62	10.554	10.532	0.21
	$\bar{\omega}_9$	11.195	11.182	-0.12	11.557	11.543	-0.12	11.389	11.356	0.29
	$\bar{\omega}_{10}$	13.005	13.012	0.05	13.283	13.269	-0.11	13.152	13.140	0.10

4.4.3.3 Smart Composite Plate (f)

The benchmark frequencies of first ten flexural modes of a square smart composite plate (f) of top and bottom PZT-5A layers bonded on symmetric cross-ply graphite-epoxy (mat.8) substrate subjected to different sets of boundary conditions are presented in Table 4.10 for S values of 5, 10 and 20. All the side surfaces of piezoelectric layers, piezo-elastic interfaces and the outer surface of the top piezoelectric layer are grounded ($\phi = 0$) whereas the outer surface of the bottom piezoelectric layer is kept in open circuit condition. It is observed that the boundary conditions affect the lower mode frequencies significantly for the thick, moderately thick and thin plates, while its diminishing effect is observed at higher modes. For instance, the percentage difference in the natural frequency in first mode between C-C and F-F is 48.92% calculated with respect to C-C frequency while it is 24.54% at the tenth mode for the thick plate, it is 60.89% and 26.62% at first and tenth mode for moderately thick plate and for the thin plate the difference is 69.93% and 34.37% at the first and tenth mode frequencies. Similar trend can be ascertained for other cases of boundary conditions also. The mode shapes for first three flexural frequencies of thick plates for various boundary conditions are illustrated in Fig. 4.8. In the figure, the numerical figures side by to the mode numbers denote the corresponding dimensionless frequencies.

Table 4.10: The first ten non-dimensional flexural frequencies ($\bar{\omega}_m$) of smart composite plate (f) for different sets of boundary conditions

S	BCs	Mode sequences									
		1	2	3	4	5	6	7	8	9	10
5	S-S	7.181	13.594	13.821	18.367	20.931	21.632	24.523	24.884	28.817	29.448
	C-C	7.887	14.018	14.150	18.713	21.680	21.460	25.162	24.981	29.488	29.925
	C-S	7.476	13.901	13.838	18.514	21.160	21.656	24.708	25.057	28.890	29.513
	C-F	4.715	9.449	12.284	15.409	16.202	20.582	20.570	22.746	23.434	26.774
	F-F	4.028	5.514	11.314	11.851	13.081	17.234	17.745	20.330	21.135	22.581
10	S-S	9.369	19.614	21.236	28.724	34.047	35.019	40.796	40.876	49.491	50.098
	C-C	11.589	20.427	23.266	29.903	34.352	36.461	41.391	41.954	50.215	50.675
	C-S	10.551	20.000	22.251	29.292	34.187	35.716	41.076	41.375	50.156	50.047
	C-F	5.651	13.601	16.956	22.849	26.523	31.843	33.382	36.450	40.121	44.519
	F-F	4.532	6.706	16.120	16.659	17.666	25.695	30.240	31.422	32.679	37.183
20	S-S	10.433	22.930	27.833	37.474	43.185	51.659	54.923	59.448	68.796	73.865
	C-C	15.723	25.333	34.516	42.574	44.202	57.712	57.814	64.273	69.431	77.225
	C-S	12.830	24.007	31.336	40.042	43.650	54.750	56.289	61.887	69.065	75.548
	C-F	6.059	17.450	19.164	28.383	37.857	39.798	46.499	47.271	62.376	62.516
	F-F	4.727	7.169	18.352	19.542	20.958	31.527	39.071	41.063	41.412	50.680

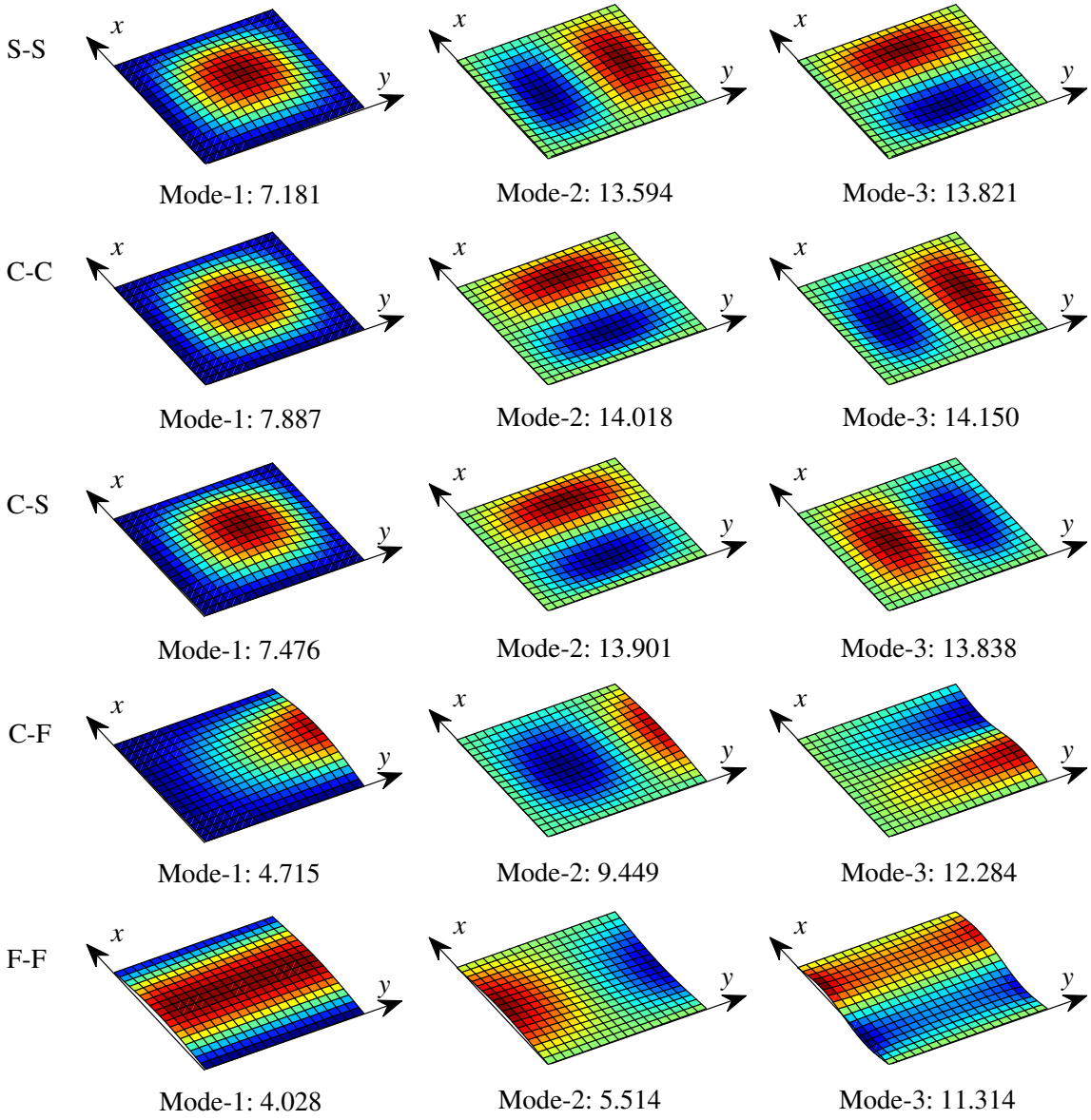

Figure 4.8: First three flexural mode shapes with the frequencies for thick (S=5) smart composite plate (f) subjected to arbitrary boundary conditions (S-S, C-C, C-S, C-F, F-F).

4.4.3.4 Smart Sandwich Plate (g)

The natural frequencies for flexural modes of a seven layer soft core smart square sandwich plate (g) is presented in Table 4.11 for plates of different span-to-thickness ratios (S=5, 10, 20) and subjected to arbitrary boundary conditions. The smart sandwich plate has PZT-5A layers embedded to the top and bottom surface of graphite-epoxy (mat.4) faces sandwiching a soft-core material (mat.5). Similar electrical boundary conditions as considered for composite plate (f) are taken for this case also. The mode shapes for first three flexural frequencies of thick plates for various boundary conditions are illustrated in Fig. 4.9. The numerical figures side by to the mode numbers denote the corresponding frequencies.

Table 4.11: The first ten non-dimensional flexural frequencies ($\bar{\omega}_m$) of smart sandwich plate (g) for different sets of boundary conditions

S	BCs	Mode sequences									
		1	2	3	4	5	6	7	8	9	10
5	S-S	4.523	7.700	7.896	10.292	11.837	11.950	13.871	13.875	16.626	16.750
	C-C	4.772	7.776	8.154	10.497	11.864	12.394	14.026	14.332	16.763	17.357
	C-S	4.599	7.721	7.995	10.370	11.846	12.129	13.935	14.038	16.755	16.935
	C-F	3.219	5.885	6.850	8.690	9.588	11.208	11.694	12.584	13.854	15.055
	F-F	2.794	3.902	6.609	7.269	7.480	9.881	10.946	11.053	11.650	13.039
10	S-S	7.339	13.252	13.880	18.093	20.154	21.231	23.895	24.428	27.772	28.993
	C-C	8.113	13.489	14.397	18.396	20.216	21.631	24.055	24.752	27.790	29.506
	C-S	7.703	13.356	14.129	18.232	20.182	21.410	23.875	24.573	27.782	29.359
	C-F	4.788	9.755	11.668	15.063	16.736	18.956	20.634	21.574	24.166	26.214
	F-F	4.234	5.864	11.235	11.997	12.614	17.032	18.631	19.200	19.735	23.067
20	S-S	9.744	20.459	21.357	29.356	33.561	35.693	40.446	41.712	47.411	50.707
	C-C	12.269	21.322	23.955	30.813	33.902	37.504	41.200	42.993	47.558	52.073
	C-S	10.929	20.866	22.697	30.081	33.570	36.610	40.831	42.347	47.482	51.444
	C-F	6.265	14.087	17.759	23.676	27.021	31.393	34.199	36.181	41.449	44.651
	F-F	5.240	7.433	16.521	17.073	18.732	26.312	30.519	30.995	32.943	37.890

The effect of varying piezo-layer thickness (h_p=0.02, 0.05 and 0.25) on the natural frequencies of a thick (S=5) sandwich plate is presented in Table 4.12 for different boundary conditions. It is observed that the increase in piezo-layer thickness have suppressing effect on the natural frequency. This inference is important and can serve as a vital input in the designing of hybrid sandwich structures.

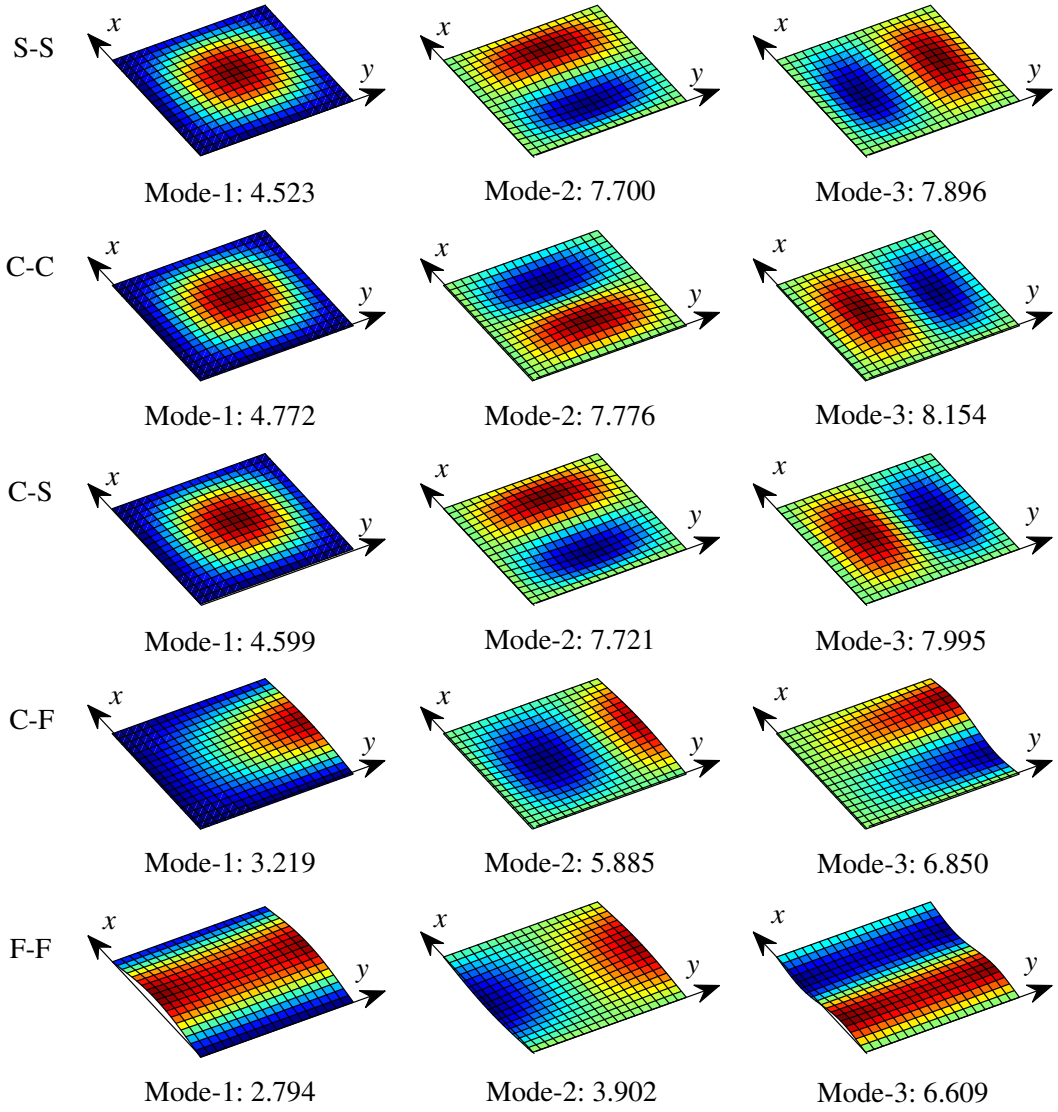

Figure 4.9: First three flexural mode shapes with the frequencies for thick (S=5) smart sandwich plate (g) subjected to arbitrary boundary conditions (S-S, C-C, C-S, C-F, F-F).

4.4.3.5 Effect of Adhesive Thickness on the Natural Frequency of a Bimorph Plate

The natural frequencies are presented for a square bimorph plate bonded with epoxy adhesive with adhesive thickness, t_a= 0, 0.02, and 0.04 for different boundary conditions, the configuration of which is shown in Fig. 4.10. The interfaces, side surfaces and top piezoelectric surfaces are grounded ($\bar{\phi} = 0$). The bottom piezoelectric surface is kept open (D_z=0). The plate is made of PZT-4 material, the properties of which are taken from Ref. [149] and are reproduced

Table 4.12: The first ten non-dimensional flexural frequencies ($\bar{\omega}_m$) of smart sandwich plate (g) for different sets of boundary conditions with varying piezo-layer thickness (h_p) and S=5

		Mode Sequences									
(h_p)	BCs	1	2	3	4	5	6	7	8	9	10
0.02	S-S	7.275	12.107	13.004	16.235	17.619	19.088	20.693	21.427	23.481	24.971
	C-C	7.783	12.250	13.092	16.310	17.629	19.138	20.739	23.348	25.013	25.094
	C-S	7.455	12.171	13.056	16.271	17.637	19.101	20.713	21.448	23.485	24.990
	C-F	5.214	9.327	10.603	13.623	15.447	16.671	18.372	18.769	21.676	22.483
	F-F	4.572	5.662	10.506	11.565	11.944	15.565	16.438	17.260	17.342	20.274
0.05	S-S	5.636	9.368	9.829	12.458	13.828	14.423	16.174	16.419	18.810	19.217
	C-C	5.886	9.426	9.927	12.540	13.840	14.518	16.226	16.530	18.812	19.601
	C-S	5.734	9.391	9.999	12.493	13.833	14.468	16.195	16.466	18.811	19.278
	C-F	4.016	7.215	8.323	10.581	11.736	13.076	14.110	14.742	16.360	17.564
	F-F	3.509	4.660	8.059	9.063	9.170	12.056	12.875	13.125	13.616	15.789
0.25	S-S	3.871	7.492	7.517	10.579	12.863	12.865	15.495	15.507	19.584	19.666
	C-C	4.477	7.775	8.819	11.504	13.017	16.134	17.007	19.676	21.074	21.834
	C-S	4.084	7.590	8.058	10.969	12.924	13.720	15.778	16.190	19.623	20.463
	C-F	2.664	5.304	6.541	8.514	9.511	11.991	12.399	13.666	15.523	17.105
	F-F	2.293	3.295	6.319	7.053	9.534	10.593	11.825	12.352	13.533	14.530

in Sec. 4.4.3.2. The properties of epoxy adhesive is taken from Ref. [168] and are given as follows: Modulus of elasticity, Y_a= 4.39 GPa, Poisson's ratio, ν =0.34 and density, ρ_a=2500 kg/m^3.

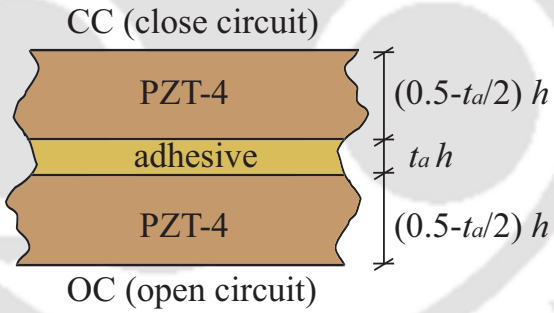

Figure 4.10: Configuration of bimorph plate with adhesive layer.

The lowest five flexural natural frequencies for thick (S=5) bimorph plate with adhesive thicknesses t_a=0.0, 0.02 and 0.04 are presented in Table 4.13 for boundary conditions S-S, C-C, C-S, C-F and F-F. It is observed that as the adhesive layer thickness increases the natural frequencies decrease for all types of boundary conditions and decrement is more pronounced at higher modes as can be observed from Fig. 4.11 where the frequencies are plotted against the mode numbers for C-C, C-S, C-F and F-F cases. It is due the fact that adhesive being a lower elastic modulus material acts as vibration suppressor upon increasing its layer thickness.

Table 4.14 presents the effect of adhesive elastic modulus on the natural frequency of thick piezoelectric bimorph plate for adhesive layer thickness, t_a=0.04 for S-S and C-F cases. As observed from table the plate natural frequencies decrease upon increasing adhesive modulus. For simply supported case there is a 4.69% and 6.52% decrease in the fundamental frequency upon increasing the adhesive modulus two times and three times, respectively. For C-F case the decrement is 3.71% and 5.10% in the fundamental frequency. When we increase the adhesive elastic modulus up to three times w.r.t its original, its contribution increases but still it is very soft (1/8 times of PZT modulus) as compared to PZT. Therefore, overall, it helps to reduce the natural frequency of plate and below 10%. The effect of adhesive density on plate natural frequency is investigated and is presented in Table 4.15. It shows that the plate natural frequency increases on increasing the adhesive density. A maximum increment of 1.35% is observed for the fundamental frequency in case of C-F. As adhesive density become 3 times of the original density, which is equal to the density of PZT-4A material, but elastic modulus of adhesive is 20 times less than that of PZT-4A. So slight increase in natural frequency is observed with the increment of density.

Table 4.13: First five flexural frequencies ($\bar{\omega}_m$) of a thick (S=5) square bimorph plate for different adhesive thickness (t_a) and boundary conditions.

BCs	Entity	$t_a = 0.0$	$t_a = 0.02$	$t_a = 0.04$
S-S	$\bar{\omega}_1$	5.480	5.239	5.049
	$\bar{\omega}_2$	11.804	10.957	10.387
	$\bar{\omega}_3$	16.966	15.559	14.707
	$\bar{\omega}_4$	20.011	18.279	17.283
	$\bar{\omega}_5$	24.163	22.010	20.848
C-C	$\bar{\omega}_1$	6.626	6.406	6.012
	$\bar{\omega}_2$	12.247	11.272	10.654
	$\bar{\omega}_3$	13.609	12.323	11.617
	$\bar{\omega}_4$	17.813	16.241	15.368
	$\bar{\omega}_5$	20.048	18.290	17.144
C-S	$\bar{\omega}_1$	6.156	5.786	5.508
	$\bar{\omega}_2$	12.007	11.097	10.505
	$\bar{\omega}_3$	12.318	11.643	10.914
	$\bar{\omega}_4$	17.388	15.889	15.019
	$\bar{\omega}_5$	20.072	18.130	17.292
C-F	$\bar{\omega}_1$	3.447	3.336	3.245
	$\bar{\omega}_2$	7.679	7.459	7.0768
	$\bar{\omega}_3$	10.026	9.359	8.894
	$\bar{\omega}_4$	13.649	12.553	11.860
	$\bar{\omega}_5$	14.989	13.693	12.917
F-F	$\bar{\omega}_1$	2.780	2.712	2.668
	$\bar{\omega}_2$	4.240	4.096	3.976
	$\bar{\omega}_3$	9.059	8.664	8.306
	$\bar{\omega}_4$	9.566	8.958	8.534
	$\bar{\omega}_5$	10.835	10.120	9.597

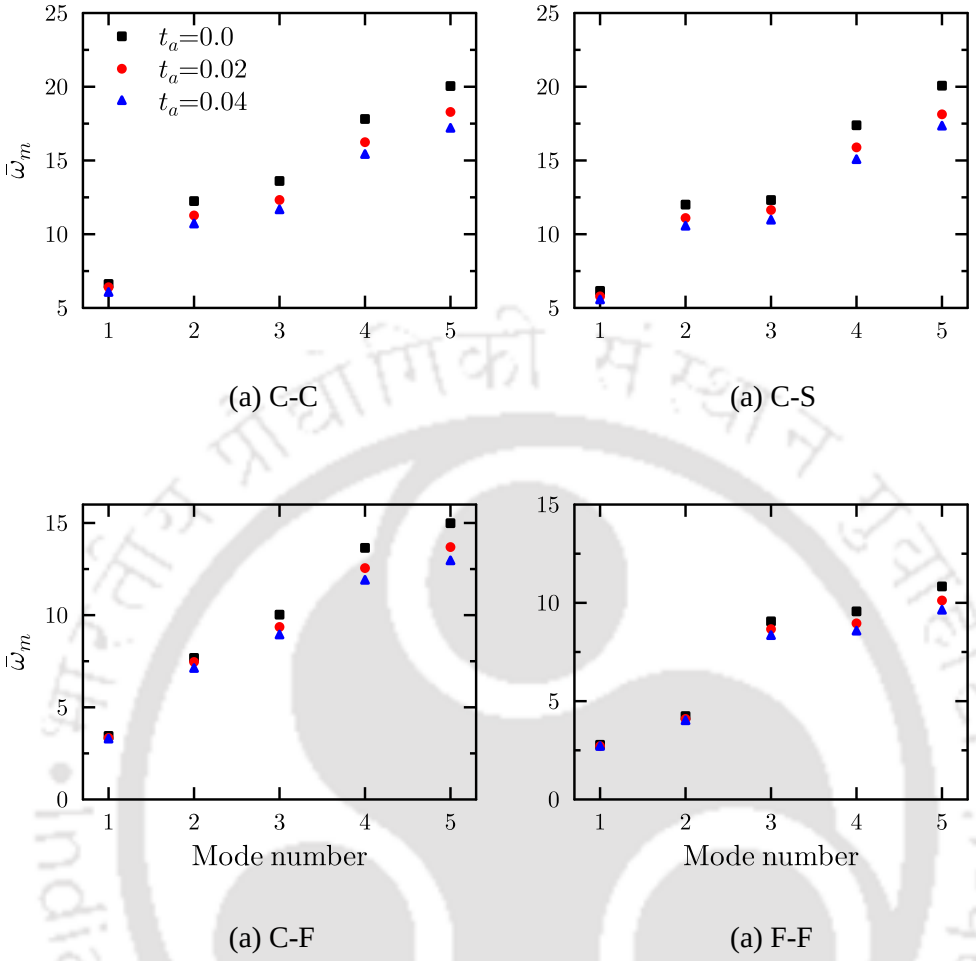

Figure 4.11: Effect of adhesive thickness (t_a) on the natural frequencies of thick bimorph plate for C-C, C-S, C-F and F-F boundary conditions.

Table 4.14: Natural flexural frequencies $\bar{\omega}_m$ for a thick (S=5) square bimorph plate for S-S and C-F cases with adhesive thickness (t_a=0.04) for varying adhesive elastic modulus Y_a.

S-S			C-F		
Y_a	$2Y_a$	$3Y_a$	Y_a	$2Y_a$	$3Y_a$
$\bar{\omega}_m$	% decrease		$\bar{\omega}_m$	% decrease	
5.049	-4.69	-6.52	3.245	-3.71	-5.10
10.387	-6.49	-9.31	7.034	-5.32	-7.37
14.707	-6.76	-9.92	8.894	-6.27	-8.92
17.283	-6.76	-9.90	11.860	-6.89	-10.01
20.848	-6.40	-9.64	12.917	-5.83	-10.41

Table 4.15: Natural flexural frequencies $\bar{\omega}_m$ for a thick (S=5) square bimorph plate for S-S and C-F cases with adhesive thickness (t_a=0.04) for varying adhesive density ρ_a.

S-S			C-F		
ρ_a	$2\rho_a$	$3\rho_a$	ρ_a	$2\rho_a$	$3\rho_a$
$\bar{\omega}_m$	% increase		$\bar{\omega}_m$	% increase	
5.049	0.66	1.32	3.245	0.68	1.35
10.387	0.66	1.31	7.077	0.59	1.18
14.707	0.66	1.31	8.894	0.65	1.30
17.283	0.66	1.31	11.860	0.63	1.25
20.848	0.66	1.30	12.917	0.65	1.29

4.5 CONCLUSIONS

In this work 3D piezoelasticity solution for the free vibration of hybrid laminated plates is developed using multi-term EKM. The versatility of the present 3D EKM is verified by extensive validation of its results for piezoelectric plate, smart composite and sandwich plates with the 3D exact and approximate solutions and with the 3D FE results of ABAQUS wherever 3D analytical results are not available and found to agree well.

- Benchmark natural frequencies are presented for very thick ($S = 1$) single layer piezoelectric plate for different non-simply supported boundary conditions. The plots of state variables ($\bar{u}, \bar{v}, \bar{w}, \bar{\phi}$) for the first and third modes are observed to agree well with 3D FE results.

- The results for bimorph plate with different electrical boundary (close and open circuit) conditions and aspect ratios (b/a=1 and 2) show good agreement with 3D FE results of ABAQUS.

- The benchmark natural frequencies for smart composite and sandwich plates subjected to various boundary conditions and span-to-thickness ratios are presented. It is observed that different boundary conditions influence natural frequencies more significantly at lower modes than at higher modes.

- It is observed that increasing the piezo-layer thickness significantly reduces the natural frequency as seen for a thick ($S = 5$) sandwich plate: 22.53% and 46.80% reduction in

the fundamental frequency for all round simply supported case for piezo-layer thickness, h_p=0.05 and 0.25 respectively with respect to h_p=0.02.

- Using adhesives as binding agent reduces the frequency response of piezoelectric bimorph plates. The increase of adhesive thickness lowers the natural frequencies for all types of boundary conditions.It is due the fact that adhesive being a lower elastic modulus material acts as vibration suppressor upon increasing its layer thickness

- The increase in adhesive elastic modulus reduces the natural frequencies of the bimorph plate. When we increase the adhesive elastic modulus up to three times w.r.t its original, its contribution increases but still it is very soft (1/8 times of PZT modulus) as compared to PZT. Therefore, overall, it helps to reduce the natural frequency of plate and below 10%

- The denser adhesives help in increasing the natural frequencies as can be seen for simply supported and free-free cases. As adhesive density become 3 times of the original density, which is equal to the density of PZT-4A material, but elastic modulus of adhesive is 20 times less than that of PZT-4A. So slight increase in natural frequency is observed with the increment of density.

Chapter 5

Advanced 2D Zig-zag Piezolaminate Theory for the Free Vibration of Levy-type Hybrid Plates

5.1 INTRODUCTION

Two dimensional (2D) laminate theories which are traditionally being used for analysis of plates for its simplicity and versatility with some compromise concerning the accuracy are still remain popular because the 3D analytical piezoelasticity solutions are difficult to obtain and constricted to some particular shapes and geometry whereas the finite element implementation of 3D approaches are computationally too involved and inefficient for such purposes that often it prove to be prohibitive for practical problems. The improved zig-zag theory (IZIGT) seems the best one of such 2D theories proposed by Kapuria [148] for hybrid plates. The accuracy of such advanced 2D theories are assessed by comparing their results with the 3D solutions, especially for simply supported boundary case; but such an assessment is unable to present a clear picture about the sharp variation of the boundary layer stresses as no boundary layer effect is observed in simply-supported case [2] whereas it does develop in case of clamped and free edge boundary conditions. This boundary layer effect also known as free edge effect which occurs near free edges due to a mismatch in material properties between plies is responsible for delamination failure of the composite laminates. These effects become more complex for piezolaminated plates due to presence of electromechanical coupling. In this Chapter, static bending of Levy-type hybrid plates based on zig-zag theory [150] is extended to the free vibration case for the first time.

5.2 MATHEMATICAL MODELLING

5.2.1 Geometry

Let us consider, a multilayered orthotropic rectangular plate integrated with piezoelectric layers of dimensions ($a \times b \times h$) along x, y and z-axis, respectively as illustrated in Fig. 5.1. The principal material direction x_3 is parallel to reference axis z whereas other material directions x_1 and x_2 can make angle φ to the inplane reference axes x, y which in case of cross-ply lay-up is either 0^0 or 90^0. The plies are numbered from the bottom (1st layer) to top (Lth layer). The z coordinate of the bottom and top surface of kth ply is denoted as $z = z_{k-1}$ and $z = z_k$, respectively. The plate is subjected to hard simply supported along x-axis (i.e $x = 0$ and $x = a$) while along y-axis (i.e y=-$b/2$ and y=+$b/2$), any combination among clamped, free and simply supported boundary conditions can be applied. The midplane (x-y) of the plate is chosen as a reference plane ($z = 0$).

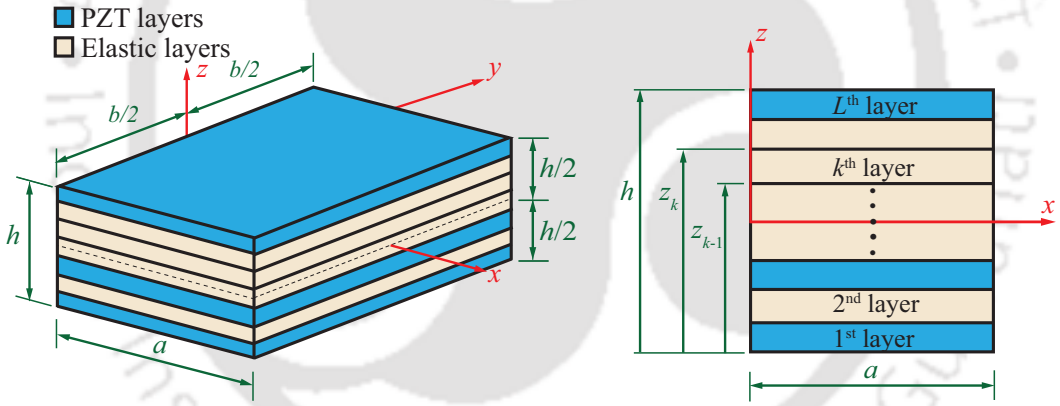

Figure 5.1: Geometry and coordinate system of a hybrid plate.

5.2.2 The Strain-Displacement and Constitutive Relations

The linear strain displacement relations of the orthotropic laminate with respect to the plate axis system (x-y-z) are considered as:

$$\begin{aligned} \varepsilon_x &= u_{x,x}, & \varepsilon_y &= u_{y,y}, & \gamma_{xy} &= u_{x,y} + u_{y,x} \\ \gamma_{yz} &= u_{y,z} + w_{,y}, & \gamma_{zx} &= u_{x,z} + w_{,x}, & & \end{aligned} \tag{5.1}$$

The linear constitutive equations of the cross-ply piezoelectric laminate with the assumption that the transverse normal stress $\sigma_z \simeq 0$ can be written as:

$$\begin{bmatrix}\sigma_1\\ \sigma_2\\ \tau_{12}\end{bmatrix} = \begin{bmatrix}Q_{11} & Q_{12} & 0\\ Q_{12} & Q_{22} & 0\\ 0 & 0 & Q_{66}\end{bmatrix}\begin{bmatrix}\varepsilon_1\\ \varepsilon_2\\ \gamma_{12}\end{bmatrix} - \begin{bmatrix}\hat{e}_{31}\\ \hat{e}_{32}\\ 0\end{bmatrix} E_3$$

$$\begin{bmatrix}\tau_{31}\\ \tau_{23}\end{bmatrix} = \begin{bmatrix}Q_{55} & 0\\ 0 & Q_{44}\end{bmatrix}\begin{bmatrix}\gamma_{31}\\ \gamma_{23}\end{bmatrix} - \begin{bmatrix}\hat{e}_{15} & 0\\ 0 & \hat{e}_{24}\end{bmatrix}\begin{bmatrix}E_1\\ E_2\end{bmatrix}$$

$$\begin{bmatrix}D_1\\ D_2\end{bmatrix} = \begin{bmatrix}\hat{e}_{15} & 0\\ 0 & \hat{e}_{24}\end{bmatrix}\begin{bmatrix}\gamma_{31}\\ \gamma_{23}\end{bmatrix} + \begin{bmatrix}\hat{\eta}_{11} & 0\\ 0 & \hat{\eta}_{22}\end{bmatrix}\begin{bmatrix}E_1\\ E_2\end{bmatrix} \tag{5.2}$$

$$D_3 = \begin{bmatrix}\hat{e}_{31} & \hat{e}_{32} & 0\end{bmatrix}\begin{bmatrix}\varepsilon_1\\ \varepsilon_2\\ \gamma_{12}\end{bmatrix} + \hat{\eta}_{33}E_3$$

$$\varepsilon_3 = s_{13}\sigma_1 + s_{23}\sigma_2 + d_{33}E_3$$

σ_1, σ_2, τ_{12} and ε_1, ε_2, γ_{12} are the inplane stress and strain components, respectively, τ_{13}, τ_{23} and γ_{13}, γ_{23} denote the transverse shearing stress and strain components, and E_i and D_i, $(i = x, y, z)$ denote the electric field and electric displacement components, respectively. Q_{ij}, $\hat{e}_{ij}$ and $\hat{\eta}_{ij}$ are the reduced elastic stiffnesses, piezoelectric stress constants and electric permittivities, respectively, which can be expressed in terms of the engineering material constants, namely, Young's moduli, shear moduli G_{ij}, Poisson's ratio ν_{ij}, piezoelectric strain constant d_{ij} and electric permitivities η_{ij} as given as follows:

$$\begin{aligned}
&Q_{11} = Y_1/(1-\nu_{12}\nu_{21}),\ \ Q_{12} = \nu_{12}Y_2/(1-\nu_{12}\nu_{21}),\ \ Q_{22} = Y_2/(1-\nu_{12}\nu_{21}),\\
&Q_{44} = G_{23},\ \ Q_{55} = G_{31},\ \ Q_{66} = G_{12},\\
&\hat{e}_{31} = Q_{11}d_{31} + Q_{12}d_{32},\ \ \hat{e}_{32} = Q_{12}d_{31} + Q_{22}d_{32},\ \ \hat{e}_{24} = Q_{44}d_{24},\ \ \hat{e}_{15} = Q_{55}d_{15}\\
&\hat{\eta}_{11} = \eta_{11},\ \ \hat{\eta}_{22} = \eta_{22},\ \ \hat{\eta}_{33} = \epsilon_{33} - d_{31}\hat{e}_{31} - d_{32}\hat{e}_{32}
\end{aligned} \tag{5.3}$$

For the basis x, y, z with $x_3 = z$ and x_1, x_2 at an angle φ to the in-plane axes x, y, the constitutive equations (5.2) transform to

$$\sigma = \begin{bmatrix}\sigma_x\\ \sigma_y\\ \tau_{xy}\end{bmatrix} = \begin{bmatrix}\bar{Q}_{11} & \bar{Q}_{12} & \bar{Q}_{16}\\ \bar{Q}_{12} & \bar{Q}_{22} & \bar{Q}_{26}\\ \bar{Q}_{16} & \bar{Q}_{26} & \bar{Q}_{66}\end{bmatrix}\begin{bmatrix}\varepsilon_x\\ \varepsilon_y\\ \gamma_{xy}\end{bmatrix} - \begin{bmatrix}\bar{e}_{31}\\ \bar{e}_{32}\\ \bar{e}_{36}\end{bmatrix} E_z$$

$$\tau = \begin{bmatrix}\tau_{zx}\\ \tau_{yz}\end{bmatrix} = \begin{bmatrix}\bar{Q}_{55} & \bar{Q}_{45}\\ \bar{Q}_{45} & \bar{Q}_{44}\end{bmatrix}\begin{bmatrix}\gamma_{zx}\\ \gamma_{yz}\end{bmatrix} - \begin{bmatrix}\bar{e}_{15} & \bar{e}_{25}\\ \bar{e}_{14} & \bar{e}_{24}\end{bmatrix}\begin{bmatrix}E_x\\ E_y\end{bmatrix}$$

$$D = \begin{bmatrix}D_x\\ D_y\end{bmatrix} = \begin{bmatrix}\bar{e}_{15} & \bar{e}_{14}\\ \bar{e}_{25} & \bar{e}_{24}\end{bmatrix}\begin{bmatrix}\gamma_{zx}\\ \gamma_{yz}\end{bmatrix} + \begin{bmatrix}\bar{\eta}_{11} & \bar{\eta}_{12}\\ \bar{\eta}_{21} & \bar{\eta}_{22}\end{bmatrix}\begin{bmatrix}E_x\\ E_y\end{bmatrix} \tag{5.4}$$

$$D_z = [\,\bar{e}_{31} \quad \bar{e}_{32} \quad \bar{e}_{36}\,] \begin{bmatrix} \varepsilon_x \\ \varepsilon_y \\ \gamma_{xy} \end{bmatrix} + \bar{\eta}_{33} E_z$$

$$\varepsilon_z = \bar{s}_{13}\sigma_x + \bar{s}_{23}\sigma_y + \bar{s}_{36}\tau_{xy} + \bar{d}_{33} E_z$$

where

$$\begin{aligned}
\bar{Q}_{11} &= c^4 Q_{11} + 2c^2 s^2 (Q_{12} + 2Q_{66}) + s^4 Q_{22}, \\
\bar{Q}_{22} &= s^4 Q_{11} + 2c^2 s^2 (Q_{12} + 2Q_{66}) + c^4 Q_{22}, \\
\bar{Q}_{12} &= c^2 s^2 (Q_{11} + Q_{22} - 4Q_{66}) + (s^4 + c^4) Q_{12}, \\
\bar{Q}_{16} &= c^3 s (Q_{11} - Q_{12} - 2Q_{66}) + cs^3 (Q_{12} - Q_{22} + 2Q_{66}), \\
\bar{Q}_{26} &= c^3 s (Q_{12} - Q_{22} + 2Q_{66}) + cs^3 (Q_{11} - Q_{12} - 2Q_{66}), \\
\bar{Q}_{66} &= c^2 s^2 (Q_{11} - 2Q_{12} + Q_{22}) + (c^2 - s^2)^2 Q_{66}, \\
\bar{Q}_{44} &= c^2 Q_{44} + s^2 Q_{55}, \\
\bar{Q}_{45} &= cs (Q_{55} - Q_{44}), \\
\bar{Q}_{55} &= s^2 Q_{44} + c^2 Q_{55}, \\
\bar{s}_{13} &= c^2 s_{13} + s^2 s_{23}, \\
\bar{s}_{23} &= s^2 s_{13} + c^2 s_{23}, \\
\bar{s}_{36} &= 2cs (s_{13} - s_{23}) \\
\bar{d}_{33} &= d_{33} \\
\bar{e}_{31} &= c^2 \hat{e}_{31} + s^2 \hat{e}_{32} \\
\bar{e}_{32} &= s^2 \hat{e}_{31} + c^2 \hat{e}_{32} \\
\bar{e}_{36} &= cs (\hat{e}_{31} - \hat{e}_{32}) \\
\bar{e}_{14} &= \bar{e}_{25} = cs (\hat{e}_{15} - \hat{e}_{24}) \\
\bar{e}_{15} &= c^2 \hat{e}_{15} + s^2 \hat{e}_{24} \\
\bar{e}_{24} &= s^2 \hat{e}_{15} + c^2 \hat{e}_{24} \\
\bar{\eta}_{11} &= c^2 \hat{\eta}_{11} + s^2 \hat{\eta}_{22} \\
\bar{\eta}_{22} &= s^2 \hat{\eta}_{11} + c^2 \hat{\eta}_{22} \\
\bar{\eta}_{33} &= \hat{\eta}_{33}
\end{aligned} \tag{5.5}$$

where $s = \sin\varphi$, $c = \cos\varphi$. Equation (5.4) is used to develop the 2D theories for piezoelectric plates in this chapter. The constitutive equations for the elastic plates are obtained as a special case of Eq. (5.4) with the piezoelectric constants being zero. For cross-ply lay-up φ is either 0° or 90° and hence the elements (5.5) of matrices of Eq. (5.4) will be reduced accordingly.

Electric potential ϕ is approximated as a piecewise quadratic between n_ϕ points at $z = z_\phi^j$ across the thickness of the laminate as given in Ref. [150]:

$$\phi(x, y, z, t) = \Psi_\phi^j(z)\phi^j(x, y, t) + \Psi_c^q(z)\phi_c^q(x, y, t) \tag{5.6}$$

where $\phi^j(x, y, t)$ $[= \phi(x, y, z_\phi^j, t)]$ represents prescribed electric potential at the piezoelectric layer surfaces/inter-faces at $z = z_\phi^j$ with $j \in [1, 2, \ldots, n_\phi]$. The quadratic component of electric potential is denoted by $\phi_c^q(x, y, t)$ at $z = (z_\phi^q + z_\phi^{q+1})/2$ with $q \in [1, 2, \ldots, n_\phi - 1]$. Here $z = z_\phi^j$ is the z-coordinate of j^{th} point from bottom for discretizing ϕ. The summation convention is used for repeated indices j and q. $\Psi_\phi^j(z)$ is a piecewise linear function and $\Psi_c^q(z)$ is a quadratic function, which are given as

$$\Psi_c^q(z) = \left\{ \begin{array}{ll} 4(z_\phi^{q+1} - z)(z - z_\phi^q)/(z_\phi^{q+1} - z_\phi^q)^2 & \text{if } \; z_\phi^q \le z \le z_\phi^{q+1} \\ 0 & \text{otherwise} \end{array} \right\} \tag{5.7}$$

The deflection w contains two components, one for mechanical deformation and other for electrical deformation, then finally improved approximation of deflection is expressed as

$$w(x,y,z,t) = w_0(x,y,t) - \bar{\Psi}^j_\phi(z)\phi^j(x,y,t) - \bar{\Psi}^q_c(z)\phi^q_c(x,y,t) \tag{5.8}$$

where $\bar{\Psi}^j_\phi(z) = \int_0^z \bar{d}_{33}\Psi^j_{\phi,z}(z)\,dz$ and $\bar{\Psi}^q_c(z) = \int_0^z \bar{d}_{33}\Psi^q_{c,z}(z)\,dz$.

As per zig-zag assumption, the inplane displacements u_x and u_y are expressed by taking cubic variation in z over the entire laminate thickness and a local layerwise linear variation considering discontinuity in slopes $u_{x,z}$ and $u_{y,z}$ (a subscript comma denotes differentiation) at the layer interfaces:

$$\mathbf{u}(x,y,z,t) = \mathbf{u_k}(x,y,t) - z\mathbf{w}_{0d}(x,y,t) + z\boldsymbol{\psi}_k(x,y,t) + z^2\boldsymbol{\xi}(x,y,t) + z^3\boldsymbol{\eta}(x,y,t) \tag{5.9}$$

where

$$\mathbf{u} = \begin{bmatrix} u_x \\ u_y \end{bmatrix}, \quad \mathbf{w}_{0d} = \begin{bmatrix} w_{0,x} \\ w_{0,y} \end{bmatrix}, \quad \mathbf{u_k} = \begin{bmatrix} u_{kx} \\ u_{ky} \end{bmatrix}, \quad \boldsymbol{\psi}_k = \begin{bmatrix} \psi_{kx} \\ \psi_{ky} \end{bmatrix}, \quad \boldsymbol{\xi} = \begin{bmatrix} \xi_x \\ \xi_y \end{bmatrix}, \quad \boldsymbol{\eta} = \begin{bmatrix} \eta_x \\ \eta_y \end{bmatrix} \tag{5.10}$$

$\mathbf{u}_k$ is the translation component of the k^{th} layer and $\boldsymbol{\psi}_k$ is its shear rotation components which has piecewise linear variation across the layers. $\boldsymbol{\xi}$ and $\boldsymbol{\eta}$ are the quadratic and cubic terms in z, representing the global cubic variation across the thickness.

Using the $2(L-1)$ number of conditions, each for the continuity of $\mathbf{u}$ and the transverse shear stresses τ_{ij} $(i,j = x,\ y,\ z)$ at the layer interfaces and the four shear traction-free conditions at the top and bottom surfaces at $z = z_0, z_L$, the $(4L+4)$ variables $\mathbf{u}_k$, $\boldsymbol{\psi}_k$, ξ and $\boldsymbol{\eta}$ in Eq. (5.9) are expressed in terms of $\mathbf{u_0}$, $\psi_\mathbf{0}$ and $\boldsymbol{\phi}^j$ to yield

$$\mathbf{u}(x,y,z,t) = \mathbf{u_0}(x,y,t) - z\mathbf{w_{0_d}}(x,y,t) + \mathbf{R}^k(z)\boldsymbol{\psi}_0(x,y,t) + \bar{\mathbf{R}}^{kj}(z)\boldsymbol{\phi}^j_d \tag{5.11}$$

where $\boldsymbol{\phi}^j_d = [\phi^j_{,x}, \phi^j_{,y}]^{\mathrm{T}}$, and $\mathbf{R}^k(z)$ and $\bar{\mathbf{R}}^{kj}(z)$ are 2×2 matrices of layerwise functions of z of the form

$$\mathbf{R}^k(z) = \hat{\mathbf{R}}^k_1 + z\hat{\mathbf{R}}^k_2 + z^2\hat{\mathbf{R}}_3 + z^3\hat{\mathbf{R}}_4 \tag{5.12}$$

$$\bar{\mathbf{R}}^{\mathbf{kj}}(\mathbf{z}) = \bar{\mathbf{R}}^{kj}_1 + z\bar{\mathbf{R}}^{kj}_2 + z^2\bar{\mathbf{R}}^j_3 + z^3\bar{\mathbf{R}}^j_4 \qquad (j = 1, 2, \ldots\ n_\phi) \tag{5.13}$$

$\hat{\mathbf{R}}^k_1, \hat{\mathbf{R}}^k_2, \hat{\mathbf{R}}_3, \hat{\mathbf{R}}_4, \bar{\mathbf{R}}^{kj}_1, \bar{\mathbf{R}}^{kj}_2, \bar{\mathbf{R}}^j_3, \bar{\mathbf{R}}^j_4$ are 2×2 coefficient matrices dependent on the material properties and the lay-up which are given as follows:

$$\bar{\mathbf{R}}^{kj}_1 = \mathbf{R}^{kj}_1 - \hat{\mathbf{R}}^k_1\mathbf{R}^{k_0 j}_2, \qquad \bar{\mathbf{R}}^{kj}_2 = \mathbf{R}^{kj}_2 - \hat{\mathbf{R}}^k_2\mathbf{R}^{k_0 j}_2$$

$$\bar{\mathbf{R}}_3^j = \mathbf{R}_3^j - \hat{\mathbf{R}}_3\mathbf{R}_2^{k_0 j}, \qquad \bar{\mathbf{R}}_4^j = \mathbf{R}_4^j - \hat{\mathbf{R}}_4\mathbf{R}_2^{k_0 j}$$
$$\mathbf{R}_1^{kj} = \hat{\mathbf{R}}_2^{kj} - \hat{\mathbf{R}}_2^{k_0 j}, \qquad \hat{\mathbf{R}}_2^{kj} = \sum_{i=2}^{k} z_{i-1}(\mathbf{R}_2^{(i-1)j} - \mathbf{R}_2^{ij})$$

$$\begin{aligned}
&\mathbf{R}_2^{kj} = \mathbf{a}_1^k\mathbf{R}_3^j + \mathbf{a}_2^k\mathbf{R}_4^j + (\hat{\mathbf{Q}}^k)^{-1}[\mathbf{C}_{3j}^k - \hat{\mathbf{e}}^k\Psi_\phi^j(z_k)] + \bar{\Psi}_\phi^j(z_k)\mathbf{I_2}\\
&\mathbf{R}_3^j = -\boldsymbol{\Delta}^{-1}(2z_0^2\mathbf{C}_{3j}^L + 4\mathbf{C}_2^L\mathbf{C}_5^j), \qquad \mathbf{R}_4^j = \boldsymbol{\Delta}^{-1}(4z_0\mathbf{C}_{3j}^L + 4\mathbf{C}_1^L\mathbf{C}_5^j)/3\\
&\mathbf{C}_{3j}^k = \sum_{i=1}^{k}[\hat{\mathbf{e}}^i\{\Psi_\phi^j(z_i) - \Psi_\phi^j(z_{i-1})\} - \hat{\mathbf{Q}}^i\{\bar{\Psi}_\phi^j(z_i) - \bar{\Psi}_\phi^j(z_{i-1})\}]\\
&\mathbf{C}_5^j = \bar{\Psi}_\phi^j(z_0)\mathbf{I_2} - (\hat{\mathbf{Q}}^1)^{-1}\hat{\mathbf{e}}^1\Psi_\phi^j(z_0)
\end{aligned} \tag{5.14}$$

and the matrices $\hat{\mathbf{R}}_1^k$, $\hat{\mathbf{R}}_2^k$, $\hat{\mathbf{R}}_3$, $\hat{\mathbf{R}}_4$, $\mathbf{a}_1^k$, $\mathbf{a}_2^k$, $\boldsymbol{\Delta}$, $\mathbf{C}_1^L$ and $\mathbf{C}_2^L$ corresponding to the elastic case are as given below.

$$\begin{aligned}
&(\hat{\mathbf{R}}_1^k,\ \hat{\mathbf{R}}_2^k,\ \hat{\mathbf{R}}_3,\ \hat{\mathbf{R}}_4) = [\mathbf{R}_2^{k_0}]^{-1}(\mathbf{R}_1^k,\ \mathbf{R}_2^k,\ \mathbf{R}_3,\ \mathbf{R}_4)\\
&\mathbf{R}_1^k = \bar{\mathbf{R}}_2^k - \bar{\mathbf{R}}_2^{k_0}, \qquad \bar{\mathbf{R}}_2^k = \sum_{i=2}^{k} z_{i-1}(\mathbf{R}_2^{i-1} - \mathbf{R}_2^i)\\
&\mathbf{R}_2^k = \mathbf{a}_1^k\mathbf{R}_3 + \mathbf{a}_2^k\mathbf{R}_4, \qquad \mathbf{R}_3 = 4\boldsymbol{\Delta}^{-1}\mathbf{C}_2^L\\
&\mathbf{R}_4 = -4\boldsymbol{\Delta}^{-1}\mathbf{C}_1^L/3, \qquad \mathbf{a}_1^k = 2[(\hat{\mathbf{Q}}^k)^{-1}\mathbf{C}_1^k - z_k\mathbf{I_2}]\\
&\mathbf{a}_2^k = 3[2(\hat{\mathbf{Q}}^k)^{-1}\mathbf{C}_2^k - z_k^2\mathbf{I_2}], \qquad \mathbf{C}_1^k = \sum_{i=1}^{k}\hat{\mathbf{Q}}^i(z_i - z_{i-1})\\
&\mathbf{C}_2^k = \sum_{i=1}^{k}\hat{\mathbf{Q}}^i(z_i^2 - z_{i-1}^2)/2, \qquad \boldsymbol{\Delta} = 4z_0^2\mathbf{C}_1^L - 8z_0\mathbf{C}_2^L
\end{aligned} \tag{5.15}$$

In the smeared ITOT, the layerwise terms $\mathbf{u}_k$ and $\boldsymbol{\psi}_k$ in Eq. (5.9) are replaced by $\mathbf{u}_0$ and $\boldsymbol{\psi}_0$. After satisfying the traction free condition at the top and bottom surfaces, $\mathbf{u}$ can be expressed using Eq. (5.11) by replacing layerwise matrix functions $\mathbf{R}^k(z)$ and $\bar{\mathbf{R}}^{kj}(z)$ with the global functions $\mathbf{R}(z)$ and $\bar{\mathbf{R}}(z)$ for all layers

$$\mathbf{R}(z) = [z - 4z^3/3h^2]\mathbf{I}_2, \tag{5.16}$$
$$\bar{\mathbf{R}}(z) = [z^2/2h - 2z^3/3h^2]\mathbf{I}_2\tilde{e}^1 + [-z^2/2h + 2z^3/3h^2]\mathbf{I}_2\tilde{e}^L \tag{5.17}$$

where $\mathbf{I}_2$ is a 2×2 unity matrix. Matrix $\tilde{e}^k$ for the k^{th} layer is given by $\tilde{e}^k = [\hat{Q}^k]^{-1}\hat{e}^k$.

Substituting Eqs. (5.8) and (5.11) into the linear strain-displacement relations, and Eq. (5.6) into electric field-potential relations, the strain and electric field components $\boldsymbol{\varepsilon}$, $\boldsymbol{\gamma}$, $\mathbf{E}$ and E_z can

be expressed as

$$\boldsymbol{\varepsilon} = \boldsymbol{\varepsilon}^0 + z\boldsymbol{\kappa}^0 + \boldsymbol{\Phi}^k(z)\boldsymbol{\psi}_{0_d} + \boldsymbol{\Phi}^{kj}(z)\boldsymbol{\phi}^j_{dd}, \qquad \boldsymbol{\gamma} = \mathbf{R}^k_{,z}\boldsymbol{\psi}_0 + (\bar{\mathbf{R}}^{kj}_{,z} - \bar{\Psi}^j_{\phi}\mathbf{I_2})\boldsymbol{\phi}^j_d$$
$$\mathbf{E} = -\Psi^j(z)\boldsymbol{\phi}^j_d - \Psi^q_c(z)\boldsymbol{\phi}^q_{c_d}, \qquad E_z = -\Psi^j_{,z}\phi^j - \Psi^q_{c,z}\phi^q_c \tag{5.18}$$

with

$$\begin{aligned}
\boldsymbol{\varepsilon}^0 &= [\, u_{0x,x} \quad u_{0y,y} \quad u_{0x,y}+u_{0y,x} \,]^{\mathrm{T}}, \quad \boldsymbol{\kappa}^0 = -[\, w_{0,xx} \quad w_{0,yy} \quad 2w_{0,xy} \,]^{\mathrm{T}} \\
\boldsymbol{\psi}_{0_d} &= [\, \psi_{0x,x} \quad \psi_{0x,y} \quad \psi_{0y,x} \quad \psi_{0y,y} \,]^{\mathrm{T}}, \; \boldsymbol{\phi}^j_{dd} = [\, \phi^j_{,xx} \quad \phi^j_{,xy} \quad \phi^j_{,yx} \quad \phi^j_{,yy} \,]^{\mathrm{T}} \\
\boldsymbol{\Phi}^k &= \begin{bmatrix} R^k_{11} & 0 & R^k_{12} & 0 \\ 0 & R^k_{21} & 0 & R^k_{22} \\ R^k_{21} & R^k_{11} & R^k_{22} & R^k_{12} \end{bmatrix}, \qquad \boldsymbol{\Phi}^{kj} = \begin{bmatrix} \bar{R}^{kj}_{11} & 0 & \bar{R}^{kj}_{12} & 0 \\ 0 & \bar{R}^{kj}_{21} & 0 & \bar{R}^{kj}_{22} \\ \bar{R}^{kj}_{21} & \bar{R}^{kj}_{11} & \bar{R}^{kj}_{22} & \bar{R}^{kj}_{12} \end{bmatrix} \\
\phi^q_{cd} &= [\, \phi^q_{c,x} \quad \phi^q_{c,y} \,]^{\mathrm{T}}
\end{aligned} \tag{5.19}$$

where R^k_{ip} denotes (i,p)th term of $\mathbf{R}^k$, $\bar{\mathbf{R}}^{kj}_{ip}$ denotes $(i,p)^{th}$ term of $\bar{\mathbf{R}}^{kp}$.

5.2.3 Governing Differential Equations and Boundary Conditions

The Extended Hamilton principle for the piezoelectric medium can be expressed, using the notation $\langle \ldots \rangle = \sum_{k=1}^{L} \int_{z^+_{k-1}}^{z^-_k} (\ldots)\, dz$ for integration across the thickness, as

$$\begin{aligned}
&\int_0^t \int_A [\langle \rho\ddot{u}_x\delta u_x + \rho\ddot{u}_y\delta u_y + \rho\ddot{w}\delta w + \sigma_x\delta\varepsilon_x + \sigma_y\delta\varepsilon_y + \tau_{xy}\delta\gamma_{xy} + \tau_{yz}\delta\gamma_{yz} + \tau_{zx}\delta\gamma_{zx} + D_x\delta\phi_{,x} \\
&+D_y\delta\phi_{,y} + D_z\delta\phi_{,z}\rangle - p^1_z\delta w(x,y,z_0,t) - p^2_z\delta w(x,y,z_L,t) + D_z(x,y,z_0,t)\delta\phi^1 - D_z(x,y,z_L,t)\delta\phi^{n_\phi} \\
&-q_{j_i}\delta\phi^{j_i}]\, dAdt - \int_0^t \int_{\Gamma_L} \langle \sigma_n\delta u_n + \tau_{ns}\delta u_s + \tau_{nz}\delta w + D_n\delta\phi \rangle\, dsdt = 0
\end{aligned} \tag{5.20}$$

for all $\delta u_0, \delta w_0, \delta\psi_0, \delta\phi^j, \delta$ and ϕ^q_c, where A and Γ_L are the reference plane surface area of the plate and the boundary curve of the midplane, respectively having normal $\bar{n}$ and tangent $\bar{s}$ to the planes. The plate is subjected to pressure loading with p^1_z and p^2_z on bottom and top surfaces, respectively. Further plate is subjected to electric potential loading ϕ^{j_i} at interfaces and surfaces of piezolayers and total number of such prescribed potentials is $\bar{n}_\phi$. At the piezo-interfaces, electric displacement D_z will be discontinuous, so the jump in electric displacement D_z across the interface $z = z^{j_i}_\phi$ is denoted as q_{j_i}. The variational equation is expressed in terms of $\delta u_0,\ \delta w_0, \delta\psi_0, \delta\phi^j$ and $\delta\phi^q_c$ to yield the governing equations and boundary conditions.

5.2.3.1 *Inertia Matrices*

Eq. (5.11) and Eq. (5.8) for u, w can be expressed as

$$u = f_1(z)\bar{u}_1, \qquad w = f_2(z)\bar{u}_2, \tag{5.21}$$

$$\delta u = f_1(z)\delta\bar{u}_1, \qquad \delta w = f_2(z)\delta\bar{u}_2 \tag{5.22}$$

with

$$\bar{u}_1 = \begin{bmatrix} u_0^T & -w_{0_d}^T & \psi_0^T & \phi_d^{jT} \end{bmatrix}^T = [\, u_{0x} \quad u_{0y} \quad -w_{0x} \quad -w_{0y} \quad \psi_{0x} \quad \psi_{0y} \quad \phi^j_{,x} \quad \phi^j_{,y} \,]^T,$$
$$\bar{u}_2 = [\, w_0 \quad -\phi^j \quad -\phi^q \,]^T, \quad f_1(z) = [\, I_2 \quad zI_2 \quad R^k(z) \quad \bar{R}^{kj}(z) \,]^T, \quad f_2(z) = [\, 1 \quad \bar{\psi}^j_\phi \quad \bar{\psi}^q_c \,]^T,$$

where elements with index j means a sequence of elements with $j = 1$ to n_ϕ. The inertia terms in Eq. (5.20) can be expressed as

$$\begin{aligned} \langle \rho\delta u^T \ddot{u} + \rho\delta w\ddot{w} \rangle &= \langle \rho\delta\bar{u}_1^T f_1^T(z) f_1(z)\ddot{\bar{u}}_1 + \rho\delta\bar{u}_2^T f_2^T(z) f_2(z)\ddot{\bar{u}}_2 \\ &= \delta\bar{u}_1^T(I\ddot{\bar{u}}_1) + \delta\bar{u}_2^T(\bar{I}\ddot{\bar{u}}_2) \end{aligned} \tag{5.23}$$

where the inertia matrices I and $\bar{I}$ are defined as

$$I = \langle \rho f_1^T(z) f_1(z) \rangle, \qquad \bar{I} = \langle \rho f_2^T(z) f_2(z) \rangle \tag{5.24}$$

$$I = \begin{bmatrix} I_{11} & 0 & I_{13} & 0 & I_{15} & I_{16} & I_{17}^{j'} & I_{18}^{j'} \\ 0 & I_{22} & 0 & I_{24} & I_{25} & I_{26} & I_{27}^{j'} & I_{28}^{j'} \\ I_{31} & 0 & I_{33} & 0 & I_{35} & I_{36} & I_{37}^{j'} & I_{38}^{j'} \\ 0 & I_{42} & 0 & I_{44} & I_{45} & I_{46} & I_{47}^{j'} & I_{48}^{j'} \\ I_{51} & I_{52} & I_{53} & I_{54} & I_{55} & I_{56} & I_{57}^{j'} & I_{58}^{j'} \\ I_{61} & I_{62} & I_{63} & I_{64} & I_{65} & I_{66} & I_{67}^{j'} & I_{68}^{j'} \\ I_{71}^{j} & I_{72}^{j} & I_{73}^{j} & I_{74}^{j} & I_{75}^{j} & I_{76}^{j} & I_{77}^{jj'} & I_{78}^{jj'} \\ I_{81}^{j} & I_{82}^{j} & I_{83}^{j} & I_{84}^{j} & I_{85}^{j} & I_{86}^{j} & I_{87}^{jj'} & I_{88}^{jj'} \end{bmatrix} = I^T, \quad \bar{I} = \begin{bmatrix} \bar{I}_{33} & \bar{I}_{36}^{j'} & \bar{I}_{37}^{q'} \\ \bar{I}_{63}^{j} & \bar{I}_{66}^{jj'} & \bar{I}_{67}^{jq'} \\ \bar{I}_{73}^{q} & \bar{I}_{76}^{qj'} & \bar{I}_{77}^{qq'} \end{bmatrix} \tag{5.25}$$

5.2.3.2 *Stress and Electric Displacement Resultants*

Substituting Eq. (5.6), Eq. (5.8) and Eq. (5.11) for ϕ, w and $\mathbf{u}$, and Eq. (5.18) for $\boldsymbol{\varepsilon}$, $\boldsymbol{\gamma}$, $\mathbf{E}$ and E_z into Eq. (5.20) yields

$$\begin{aligned} &\int_0^t [\int_\Omega [\delta\bar{u}_1^T I\ddot{\bar{u}}_1 + \delta\bar{u}_2^T\bar{I}\ddot{\bar{u}}_2 + \delta\bar{\boldsymbol{\varepsilon}}_1^{\mathrm{T}}\mathbf{F_1} + \delta\bar{\boldsymbol{\varepsilon}}_2^{\mathrm{T}}\mathbf{F_2} + \delta\bar{\boldsymbol{\varepsilon}}_3^{\mathrm{T}}\mathbf{F_3} + \delta\bar{\boldsymbol{\varepsilon}}_4^{\mathrm{T}}\mathbf{F_4} - P_3\delta w_0 - P_\phi^j\delta\phi^j]dA \\ &- \int_{\Gamma_L} [N_n\delta u_{0_n} + N_{ns}\delta u_{0_s} - M_n\delta w_{0,n} + (V_n + M_{ns,s})\delta w_0 + P_n\delta\psi_{0_n} + P_{ns}\delta\psi_{0_s} \\ &+ (H_n^j - V_{\phi_n}^j - S_{ns,n}^j)\delta\phi^j + \delta\phi^j_{,n}S_n^j + (\tilde{H}_n^q - \tilde{V}_{\phi_n}^q)\delta\phi_c^q]ds\,]dt \\ &- \sum_i \Delta M_{ns}(s_i)\delta w_0(s_i) - \Delta S_{ns}^j(s_i)\delta\phi^j(s_i) = 0 \end{aligned} \tag{5.26}$$

where the boundary has corners at $s = s_i$. In this equation, $\bar{\boldsymbol{\varepsilon}}_1$, $\bar{\boldsymbol{\varepsilon}}_2$, $\bar{\boldsymbol{\varepsilon}}_3$ and $\bar{\boldsymbol{\varepsilon}}_4$ are the generalized strains given by

$$\begin{aligned} \bar{\boldsymbol{\varepsilon}}_1 &= \begin{bmatrix} \boldsymbol{\varepsilon}_0^{\mathrm{T}} & \boldsymbol{\kappa}_0^{\mathrm{T}} & \boldsymbol{\psi}_{0_d}^{\mathrm{T}} & \boldsymbol{\phi}_{dd}^{j\mathrm{T}} \end{bmatrix}^{\mathrm{T}}, & \bar{\boldsymbol{\varepsilon}}_2 &= \begin{bmatrix} \boldsymbol{\psi}_0^{\mathrm{T}} & \boldsymbol{\phi}_d^{j\mathrm{T}} & \boldsymbol{\phi}_{c_d}^{q\mathrm{T}} \end{bmatrix}^{\mathrm{T}} \\ \bar{\boldsymbol{\varepsilon}}_3 &= [\, \phi^j_{,x} \quad \phi^j_{,y} \quad \phi^q_{c,_x} \quad \phi^q_{c,_y} \,]^{\mathrm{T}}, & \bar{\boldsymbol{\varepsilon}}_4 &= [\, \phi^j \quad \phi_c^q \,]^{\mathrm{T}} \end{aligned} \tag{5.27}$$

$\mathbf{F}_1$ and $\mathbf{F}_2$ are the stress resultants, and $\mathbf{F}_3$ and $\mathbf{F}_4$ denote the electric displacement resultants, defined by

$$\begin{array}{l} \mathbf{F}_1 = \left[\begin{array}{cccc} \mathbf{N}^{\mathrm{T}} & \mathbf{M}^{\mathrm{T}} & \mathbf{P}^{\mathrm{T}} & \mathbf{S}^{j\mathrm{T}} \end{array}\right]^{\mathrm{T}} = \left[\begin{array}{c} \langle \mathbf{f}_1^{\mathrm{T}}(z)\boldsymbol{\sigma}\rangle \end{array}\right], \mathbf{F}_3 = \left[\begin{array}{cc} \mathbf{H}^{j\mathrm{T}} & \tilde{\mathbf{H}}^{q\mathrm{T}} \end{array}\right]^{\mathrm{T}} = \left[\begin{array}{c} \langle \mathbf{f}_3^{\mathrm{T}}(z)\mathbf{D}\rangle \end{array}\right] \\ \mathbf{F}_2 = \left[\begin{array}{ccc} \mathbf{Q}^{\mathrm{T}} & \bar{\mathbf{Q}}^{j\mathrm{T}} & \tilde{\mathbf{Q}}^{q\mathrm{T}} \end{array}\right]^{\mathrm{T}} = \left[\begin{array}{c} \langle \mathbf{f}_2^{\mathrm{T}}(z)\boldsymbol{\tau}\rangle \end{array}\right], \qquad \mathbf{F}_4 = \left[\begin{array}{cc} G^j & \tilde{G}^q \end{array}\right]^{\mathrm{T}} = \left[\begin{array}{c} \langle \mathbf{f}_4^{\mathrm{T}}(z)D_z\rangle \end{array}\right] \end{array} \tag{5.28}$$

with

$$\begin{array}{lll} \mathbf{N} = \left[\begin{array}{cccc} N_x & N_y & N_{xy} \end{array}\right]^{\mathrm{T}}, & \mathbf{M} = \left[\begin{array}{cccc} M_x & M_y & M_{xy} \end{array}\right]^{\mathrm{T}}, & \mathbf{Q} = \left[\begin{array}{cccc} Q_x & Q_y \end{array}\right]^{\mathrm{T}} \\ \mathbf{P} = \left[\begin{array}{cccc} P_x & P_{yx} & P_{xy} & P_y \end{array}\right]^{\mathrm{T}}, & \mathbf{S}^j = \left[\begin{array}{cccc} S_x^j & S_{yx}^j & S_{xy}^j & S_y^j \end{array}\right]^{\mathrm{T}}, & \bar{\mathbf{Q}}^j = \left[\begin{array}{cccc} \bar{Q}_x^j & \bar{Q}_y^j \end{array}\right]^{\mathrm{T}} \\ \tilde{\mathbf{Q}}^q = \left[\begin{array}{cccc} \tilde{Q}_x^q & \tilde{Q}_y^q \end{array}\right]^{\mathrm{T}}, & \mathbf{H}^j = \left[\begin{array}{cccc} H_x^j & H_y^j \end{array}\right]^{\mathrm{T}}, & \tilde{\mathbf{H}}^q = \left[\begin{array}{cccc} \tilde{H}_x^q & \tilde{H}_y^q \end{array}\right]^{\mathrm{T}} \end{array} \tag{5.29}$$

and

$$\begin{array}{l} \mathbf{f}_1(z) = \left[\begin{array}{cccc} \mathbf{I_3} & z\mathbf{I_3} & \boldsymbol{\Phi}^k(z) & \boldsymbol{\Phi}^{kj}(z)\mathbf{I_4} \end{array}\right], \qquad \mathbf{f}_3(z) = \left[\begin{array}{cc} \Psi^j(z)\mathbf{I_2} & \Psi_c^q(z)\mathbf{I_2} \end{array}\right] \\ \mathbf{f}_2(z) = \left[\begin{array}{ccc} \mathbf{R}_{,z}^k(z) & \mathbf{R}_{,z}^{kj}(z) - \bar{\Psi}_\phi^j(z)\mathbf{I_2} & -\bar{\Psi}_c^q\mathbf{I_2} \end{array}\right], \mathbf{f}_4(z) = \left[\begin{array}{cc} \Psi_{,z}^j(z) & \Psi_{c,z}^q(z) \end{array}\right] \end{array} \tag{5.30}$$

where $\mathbf{I_n}$ is a $n \times n$ unity matrix. P_3 and P_ϕ^j are the mechanical and electric loads defined as

$$P_3 = p_z^1 + p_z^2, \qquad P_\phi^j = -p_z^1\bar{\Psi}_\phi^j(z_0) - p_z^2\bar{\Psi}_\phi^j(z_L) + D_{z_L}\delta_{jn_\phi} - D_{z_0}\delta_{j1} + q_{j_i}\delta_{jj_i} \tag{5.31}$$

where δ_{ij} is Kronecker's delta. The generalized stress resultants $\mathbf{F}_1$, $\mathbf{F}_2$, $\mathbf{F}_3$ and $\mathbf{F}_4$ can be expressed in terms of the displacement and potential variables by substituting the expressions of $\boldsymbol{\sigma}, \boldsymbol{\tau}, \mathbf{D}$ and D_z from Eq. (5.2) into Eq. (5.28) and using Eqs. (5.6), (5.8) and (5.11):

$$\mathbf{F}_1 = \mathbf{A}\bar{\boldsymbol{\varepsilon}}_1 + \boldsymbol{\beta}\bar{\boldsymbol{\varepsilon}}_4, \qquad \mathbf{F}_2 = \bar{\mathbf{A}}\bar{\boldsymbol{\varepsilon}}_2 + \bar{\boldsymbol{\beta}}\bar{\boldsymbol{\varepsilon}}_3, \quad \mathbf{F}_3 = \bar{\boldsymbol{\beta}}^{\mathrm{T}}\bar{\boldsymbol{\varepsilon}}_2 - \bar{\mathbf{E}}\bar{\boldsymbol{\varepsilon}}_3, \qquad \mathbf{F}_4 = \boldsymbol{\beta}^{\mathrm{T}}\bar{\boldsymbol{\varepsilon}}_1 - \hat{\mathbf{E}}\bar{\boldsymbol{\varepsilon}}_4 \tag{5.32}$$

with

$$\begin{array}{lll} \mathbf{A} = \langle \mathbf{f}_1^{\mathrm{T}}(z)\bar{\mathbf{Q}}\mathbf{f}_1(z)\rangle, & \bar{\mathbf{A}} = \langle \mathbf{f}_2^{\mathrm{T}}(z)\hat{\mathbf{Q}}\mathbf{f}_2(z)\rangle & \boldsymbol{\beta} = \langle \mathbf{f}_1^{\mathrm{T}}(z)\bar{\mathbf{e}}_3^{\mathrm{T}}\mathbf{f}_4(z)\rangle \\ \bar{\boldsymbol{\beta}} = \langle \mathbf{f}_2^{\mathrm{T}}(z)\hat{\mathbf{e}}\mathbf{f}_3(z)\rangle, & \bar{\mathbf{E}} = \langle \mathbf{f}_3^{\mathrm{T}}(z)\hat{\boldsymbol{\eta}}\mathbf{f}_3(z)\rangle, & \hat{\mathbf{E}} = \langle \mathbf{f}_4^{\mathrm{T}}(z)\bar{\eta}_{33}\mathbf{f}_4(z)\rangle \end{array} \tag{5.33}$$

where $\mathbf{A}$ and $\bar{\mathbf{A}}$ are $[(10+4n_\phi)\times(10+4n_\phi)]$ and $[(2+2n_\phi+2n_\phi^q)\times(2+2n_\phi+2n_\phi^q)]$ stiffness matrices with $n_\phi^q = n_\phi - 1$; $\boldsymbol{\beta}$ and $\bar{\boldsymbol{\beta}}$ are $[(10+4n_\phi)\times(n_\phi+n_\phi^q)]$ and $[4n_\phi\times(2n_\phi+2n_\phi^q)]$ electro-mechanical coupling matrices, and $\bar{\mathbf{E}}$ and $\hat{\mathbf{E}}$ are $[(2n_\phi + 2n_\phi^q)\times(2n_\phi + 2n_\phi^q)]$ and $[(n_\phi + n_\phi^q)\times(n_\phi + n_\phi^q)]$ dielectric matrices of hybrid plate. The explicit forms of Eqs. (5.32) are given as follows:

$$\begin{bmatrix} N_x \\ N_y \\ N_{xy} \\ M_x \\ M_y \\ M_{xy} \\ P_x \\ P_{yx} \\ P_{xy} \\ P_y \\ S_x^j \\ S_{yx}^j \\ S_{xy}^j \\ S_y^j \end{bmatrix} = \begin{bmatrix} A_{11} & A_{12} & \dots & A_{1,10} & A_{1,11}^{j'} & A_{1,12}^{j'} & A_{1,13}^{j'} & A_{1,14}^{j'} \\ A_{21} & A_{22} & \dots & A_{2,10} & A_{2,11}^{j'} & A_{2,12}^{j'} & A_{2,13}^{j'} & A_{2,14}^{j'} \\ \vdots & \vdots & \vdots & \vdots & \vdots & \vdots & \vdots & \vdots \\ A_{10,1} & A_{10,2} & \dots & A_{10,10} & A_{10,11}^{j'} & A_{10,12}^{j'} & A_{10,13}^{j'} & A_{10,14}^{j'} \\ A_{11,1}^{j} & A_{11,2}^{j} & \dots & A_{11,10}^{j} & A_{11,11}^{jj'} & A_{11,12}^{jj'} & A_{11,13}^{jj'} & A_{11,14}^{jj'} \\ A_{12,1}^{j} & A_{12,2}^{j} & \dots & A_{12,10}^{j} & A_{12,11}^{jj'} & A_{12,12}^{jj'} & A_{12,13}^{jj'} & A_{12,14}^{jj'} \\ A_{13,1}^{j} & A_{13,2}^{j} & \dots & A_{13,10}^{j} & A_{13,11}^{jj'} & A_{13,12}^{jj'} & A_{13,13}^{jj'} & A_{13,14}^{jj'} \\ A_{14,1}^{j} & A_{14,2}^{j} & \dots & A_{14,10}^{j} & A_{14,11}^{jj'} & A_{14,12}^{jj'} & A_{14,13}^{jj'} & A_{14,14}^{jj'} \end{bmatrix} \begin{bmatrix} u_{0_x,x} \\ u_{0_y,y} \\ u_{0_x,y} + u_{0_y,x} \\ -w_{0,xx} \\ -w_{0,yy} \\ -2w_{0,xy} \\ \psi_{0_x,x} \\ \psi_{0_x,y} \\ \psi_{0_y,x} \\ \psi_{0_y,y} \\ \phi_{,xx}^{j'} \\ \phi_{,xy}^{j'} \\ \phi_{,yx}^{j'} \\ \phi_{,yy}^{j'} \end{bmatrix}$$

$$+\begin{bmatrix} \beta_{11}^{j'} & \beta_{12}^{q'} \\ \beta_{21}^{j'} & \beta_{22}^{q'} \\ \vdots & \vdots \\ \beta_{10,1}^{j'} & \beta_{10,2}^{q'} \\ \beta_{11,1}^{j'} & \beta_{11,2}^{q'} \\ \beta_{12,1}^{j'} & \beta_{12,2}^{q'} \\ \beta_{13,1}^{j'} & \beta_{13,2}^{q'} \\ \beta_{14,1}^{j'} & \beta_{14,2}^{q'} \end{bmatrix} \begin{bmatrix} \phi^{j'} \\ \phi_c^{q'} \end{bmatrix} \tag{5.34}$$

$$\begin{bmatrix} Q_x \\ Q_y \\ \bar{Q}_x^j \\ \bar{Q}_y^j \\ \tilde{Q}_x^q \\ \tilde{Q}_y^q \end{bmatrix} = \begin{bmatrix} \bar{A}_{11} & \bar{A}_{12} & \bar{A}_{13}^{j'} & \bar{A}_{14}^{j'} & \bar{A}_{15}^{q'} & \bar{A}_{16}^{q'} \\ \bar{A}_{21} & \bar{A}_{22} & \bar{A}_{23}^{j'} & \bar{A}_{24}^{j'} & \bar{A}_{25}^{q'} & \bar{A}_{26}^{q'} \\ \bar{A}_{31}^{j} & \bar{A}_{32}^{j} & \bar{A}_{33}^{jj'} & \bar{A}_{34}^{jj'} & \bar{A}_{35}^{jq'} & \bar{A}_{36}^{jq'} \\ \bar{A}_{41}^{j} & \bar{A}_{42}^{j} & \bar{A}_{43}^{jj'} & \bar{A}_{44}^{jj'} & \bar{A}_{45}^{jq'} & \bar{A}_{46}^{jq'} \\ \bar{A}_{51}^{q} & \bar{A}_{52}^{q} & \bar{A}_{53}^{qj'} & \bar{A}_{54}^{qj'} & \bar{A}_{55}^{qq'} & \bar{A}_{56}^{qq'} \\ \bar{A}_{61}^{q} & \bar{A}_{62}^{q} & \bar{A}_{63}^{qj'} & \bar{A}_{64}^{qj'} & \bar{A}_{65}^{qq'} & \bar{A}_{66}^{qq'} \end{bmatrix} \begin{bmatrix} \psi_{0x} \\ \psi_{0y} \\ \phi_{,x}^{j'} \\ \phi_{,y}^{j'} \\ \phi_{c,x}^{q'} \\ \phi_{c,y}^{q'} \end{bmatrix} + \begin{bmatrix} \bar{\beta}_{11}^{j'} & \bar{\beta}_{12}^{j'} & \bar{\beta}_{13}^{q'} & \bar{\beta}_{14}^{q'} \\ \bar{\beta}_{21}^{j'} & \bar{\beta}_{22}^{j'} & \bar{\beta}_{23}^{q'} & \bar{\beta}_{24}^{q'} \\ \bar{\beta}_{31}^{jj'} & \bar{\beta}_{32}^{jj'} & \bar{\beta}_{33}^{jq'} & \bar{\beta}_{34}^{jq'} \\ \bar{\beta}_{41}^{jj'} & \bar{\beta}_{42}^{jj'} & \bar{\beta}_{43}^{jq'} & \bar{\beta}_{44}^{jq'} \\ \bar{\beta}_{51}^{qj'} & \bar{\beta}_{52}^{qj'} & \bar{\beta}_{53}^{qq'} & \bar{\beta}_{54}^{qq'} \\ \bar{\beta}_{61}^{qj'} & \bar{\beta}_{62}^{qj'} & \bar{\beta}_{63}^{qq'} & \bar{\beta}_{64}^{qq'} \end{bmatrix} \begin{bmatrix} \phi_{,x}^{j'} \\ \phi_{,y}^{j'} \\ \phi_{c,x}^{q'} \\ \phi_{c,y}^{q'} \end{bmatrix} \tag{5.35}$$

$$\begin{bmatrix} H_x^j \\ H_y^j \\ \tilde{H}_x^q \\ \tilde{H}_x^q \end{bmatrix} = \begin{bmatrix} \bar{\beta}_{11}^{j} & \bar{\beta}_{21}^{j} & \bar{\beta}_{31}^{j'j} & \bar{\beta}_{41}^{j'j} & \bar{\beta}_{51}^{q'j} & \bar{\beta}_{61}^{q'j} \\ \bar{\beta}_{12}^{j} & \bar{\beta}_{22}^{j} & \bar{\beta}_{32}^{j'j} & \bar{\beta}_{42}^{j'j} & \bar{\beta}_{52}^{q'j} & \bar{\beta}_{62}^{q'j} \\ \bar{\beta}_{13}^{q} & \bar{\beta}_{23}^{q} & \bar{\beta}_{33}^{j'q} & \bar{\beta}_{43}^{j'q} & \bar{\beta}_{53}^{q'q} & \bar{\beta}_{63}^{q'q} \\ \bar{\beta}_{14}^{q} & \bar{\beta}_{24}^{q} & \bar{\beta}_{34}^{j'q} & \bar{\beta}_{44}^{j'q} & \bar{\beta}_{54}^{q'q} & \bar{\beta}_{64}^{q'q} \end{bmatrix} \begin{bmatrix} \psi_{0x} \\ \psi_{0y} \\ \phi_{,x}^{j'} \\ \phi_{,y}^{j'} \\ \phi_{c,x}^{q'} \\ \phi_{c,y}^{q'} \end{bmatrix} - \begin{bmatrix} \bar{E}_{11}^{jj'} & \bar{E}_{12}^{jj'} & \bar{E}_{13}^{jq'} & \bar{E}_{14}^{jq'} \\ \bar{E}_{21}^{jj'} & \bar{E}_{22}^{jj'} & \bar{E}_{23}^{jq'} & \bar{E}_{24}^{jq'} \\ \bar{E}_{31}^{qj'} & \bar{E}_{32}^{qj'} & \bar{E}_{33}^{qq'} & \bar{E}_{34}^{qq'} \\ \bar{E}_{41}^{qj'} & \bar{E}_{42}^{qj'} & \bar{E}_{43}^{qq'} & \bar{E}_{44}^{qq'} \end{bmatrix} \begin{bmatrix} \phi_{,x}^{j'} \\ \phi_{,y}^{j'} \\ \phi_{c,x}^{q'} \\ \phi_{c,y}^{q'} \end{bmatrix} \tag{5.36}$$

$$\begin{bmatrix} G^j \\ \tilde{G}^q \end{bmatrix} = \begin{bmatrix} \beta_{11}^{j} & \beta_{21}^{j} & \cdots & \beta_{10,1}^{j} & \beta_{11,1}^{j'j} & \beta_{12,1}^{j'j} & \beta_{13,1}^{j'j} & \beta_{14,1}^{j'j} \\ \beta_{12}^{q} & \beta_{22}^{q} & \cdots & \beta_{10,2}^{q} & \beta_{11,2}^{q} & \beta_{12,2}^{j'q} & \beta_{13,2}^{j'q} & \beta_{14,2}^{j'q} \end{bmatrix} \begin{bmatrix} u_{0x,x} \\ u_{0y,y} \\ u_{0x,y} + u_{0y,x} \\ -w_{0,xx} \\ -w_{0,yy} \\ -2w_{0,xy} \\ \psi_{0x,x} \\ \psi_{0x,y} \\ \psi_{0y,x} \\ \psi_{0y,y} \\ \phi_{,xx}^{j'} \\ \phi_{,xy}^{j'} \\ \phi_{,yx}^{j'} \\ \phi_{,yy}^{j'} \end{bmatrix} - \begin{bmatrix} \hat{E}_{11}^{jj'} & \hat{E}_{12}^{jq'} \\ \hat{E}_{21}^{qj'} & \hat{E}_{22}^{qq'} \end{bmatrix} \begin{bmatrix} \phi^{j'} \\ \phi_c^{q'} \end{bmatrix} \tag{5.37}$$

The area integral in Eq. (5.26) is expressed in terms of $\delta u_{0_x}, \delta u_{0_y}, \delta w_0, \delta\psi_{0_x}, \delta\psi_{0_y}, \delta\phi_c^q$ and $\delta\phi^j$, by using Green's theorem if required, and the terms involving $\delta u_{0_x}, \delta u_{0_y}, \delta\psi_{0_x}, \delta\psi_{0_y}, \delta w_{0,x}$, $\delta w_{0,y}$, $\delta\phi_c^q$ and $\delta\phi^j$ in the integrand of Γ_L are expressed in terms of components n, s. It yields

the following coupled equations of equilibrium for the laminated piezoelectric plate

$$
\begin{aligned}
&-I_{11}\ddot{u}_{0x}+I_{13}\ddot{w}_{0,x}-I_{15}\ddot{\psi}_{0x}-I^{j'}_{17}\ddot{\phi}^{j'}_{,x}+N_{x,x}+N_{xy,y}=0,\\
&-I_{22}\ddot{u}_{0y}+I_{24}\ddot{w}_{0,y}-I_{26}\ddot{\psi}_{0y}-I^{j'}_{28}\ddot{\phi}^{j'}_{,y}+N_{xy,x}+N_{y,y}=0,\\
&-I_{31}\ddot{u}_{0x,x}+I_{33}\ddot{w}_{0,xx}-I_{35}\ddot{\psi}_{0x,x}-I^{j'}_{37}\ddot{\phi}^{j'}_{,xx}-I_{42}\ddot{u}_{0y,y}+I_{44}\ddot{w}_{0,yy}-I_{46}\ddot{\psi}_{0y,y}-I^{j'}_{48}\ddot{\phi}^{j'}_{,yy}-\bar{I}_{33}\ddot{w}_0+\bar{I}^{j'}_{36}\ddot{\phi}^{j'}\\
&+\bar{I}^{q'}_{37}\ddot{\phi}^{q'}_{c}+M_{x,xx}+2M_{xy,xy}+M_{y,yy}+P_3=0,\\
&-I_{51}\ddot{u}_{0x}+I_{53}\ddot{w}_{0,x}-I_{55}\ddot{\psi}_{0x}-I^{j'}_{57}\ddot{\phi}^{j'}_{,x}+P_{x,x}+P_{yx,y}-Q_x=0,\\
&-I_{62}\ddot{u}_{0y}+I_{64}\ddot{w}_{0,y}-I_{66}\ddot{\psi}_{0y}-I^{j'}_{68}\ddot{\phi}^{j'}_{,y}+P_{xy,x}+P_{y,y}-Q_y=0,\\
&\bar{I}^{q}_{73}\ddot{w}-\bar{I}^{qj'}_{76}\ddot{\phi}^{j}-\bar{I}^{qq'}_{77}\ddot{\phi}^{q}_{c}+\tilde{Q}^{q}_{x,x}+\tilde{Q}^{q}_{y,y}+\tilde{H}^{q}_{x,x}+\tilde{H}^{q}_{y,y}-\tilde{G}^{q}=0,\\
&I^{j}_{71}\ddot{u}_{0x,x}-I^{j}_{73}\ddot{w}_{0,xx}+I^{j}_{75}\ddot{\psi}_{0x,x}+I^{jj'}_{77}\ddot{\phi}^{j'}_{,xx}+I^{j}_{82}\ddot{u}_{0y,y}-I^{j}_{84}\ddot{w}_{0,yy}+I^{j}_{86}\ddot{\psi}_{0y,y}+I^{jj'}_{88}\ddot{\phi}^{j'}_{,yy}+\bar{I}^{j'}_{63}\ddot{w}_0-\bar{I}^{jj'}_{66}\ddot{\phi}^{j}\\
&-\bar{I}^{q'}_{67}\ddot{\phi}^{q}_{c}+Q^{j}_{x,x}+Q^{j}_{y,y}+H^{j}_{x,x}+H^{j}_{y,y}-S^{j}_{x,xx}-2S^{j}_{xy,yx}-S^{j}_{y,yy}-G^{j}+P^{j}_{\phi}=0
\end{aligned}
\tag{5.38}
$$

for $j=1,2,\dots n_\phi$ and $q=1,2,\dots n^q_\phi$,. Using the fundamental Lemma of Variational principals in Eq. (5.26), coefficients of $\delta u_{0n}, \delta u_{0s}$, $\delta w_0, \delta w_{0,n}, \delta\psi_{0n}$, $\delta\psi_{0s}$, $\delta\phi^j$, $\delta\phi^j_{,n}$ and $\delta\phi^q_c$ in the boundary integral equated to zero since these variations are arbitrary:

$u_{0n}=\bar{u}_{0n}$ or $\bar{N}_n=N_n=N_xn_x^2+N_yn_y^2+2N_{xy}n_xn_y$,

$u_{0s}=\bar{u}_{0s}$ or $\bar{N}_s=N_s=N_xn_xs_x+N_yn_ys_y+N_{xy}(n_xs_y+n_ys_x)$,

$w_0=\bar{w}_0$ or $(\bar{V}_n+\bar{M}_{ns,s})=(-I_{31}\ddot{u}_{0x}+I_{33}\ddot{w}_{0,x}-I_{35}\ddot{\psi}_{0x}-I^{j'}_{37}\phi^j_{,x})n_x-(I_{42}\ddot{u}_{0y}+I_{44}\ddot{w}_{0,x}$
$-I_{46}\ddot{\psi}_{0y}-I^{j'}_{48}\ddot{\phi}^{j'}_{,y})n_y+(M_{x,x}+M_{xy,y})n_x+(M_{xy,x}+M_{y,y})n_y+M_{ns,s}$,

$w_{0,n}=\bar{w}_{0,n}$ or $\bar{M}_n=M_n=M_xn_x^2+M_yn_y^2+2M_{xy}n_xn_y$,

$\psi_{0n}=\bar{\psi}_{0n}$ or $P_n=P_xn_x^2+(P_{xy}+P_{yx})n_xn_y+P_yn_y^2$,

$\psi_{0s}=\bar{\psi}_{0s}$ or $\bar{P}_{ns}=P_{ns}=P_xn_xs_x+P_xyn_xs_y+P_yxn_ys_x+P_yn_ys_y$,

$\phi^j=\bar{\phi}^j$ or $(\bar{H}^j-\bar{V}^j_{\phi_n}-\bar{S}^j_{ns,s})=I^j_{71}\ddot{u}_{0x}-I^j_{73}\ddot{w}_{0,x}+I^j_{75}\ddot{\psi}_{0x}+I^{jj'}_{77}\ddot{\phi}^{j'}_{,x})n_x+(I^j_{82}\ddot{u}_{0y}-I^j_{84}\ddot{w}_{0,y}$
$+I^j_{86}\ddot{\psi}_{0y}+I^{jj'}_{88}\ddot{\phi}^{j'}_{,y})n_y+Q^j_xn_x+\bar{Q}^j_yn_y+H^j_xn_x+H^j_yn_y-(S^j_{x,x}+S^j_{yx,y})n_x$
$-(S^j_{y,y}+S^j_{xy,x})n_y-S^j_{ns,s}$,

$\phi^j_{,n}=\bar{\phi}^j_{,n}$ or $\bar{S}^j_n=S^j_n=S^j_xn_x^2+(S^j_{xy}+S^j_{yx})n_xn_y+S^j_yn_y^2$

$\phi^q_c=\bar{\phi}^q_c$ or $\bar{\tilde{H}}^q_n-\bar{\tilde{V}}^q_{\phi n}=\tilde{H}^q_n-\tilde{V}^q_{\phi n}$

and at corners s_i :

$$w_0(s_i)=\bar{w}_0(s_i) \quad \text{or} \quad \Delta M_{ns}(s_i)=\Delta\bar{M}_{ns}(s_i),$$

$$\phi^j(s_i) = \bar{\phi}^j(s_i) \quad \text{or} \quad \Delta S^j_{ns}(s_i) = \Delta \bar{S}^j_{ns}(s_i) \tag{5.39}$$

The electromechanical boundary conditions at the edges $y = \mp b/2$, considered for the present study, are

1. Mechanical

   Hard-simply supported (S) : $N_y = 0,\ u_{0x} = 0,\ w_0 = 0,\ M_y = 0,\ P_y = 0,\ \psi_{0x} = 0$

   Hard-clamped (C) : $u_{0y} = 0,\ u_{0x} = 0,\ w_0 = 0,\ w_{0,y} = 0,\ \psi_{0y} = 0,\ \psi_{0x} = 0$ (5.40)

   Free (F) : $N_y = 0,\ N_{yx} = 0,\ V_y + M_{yx,x} = 0,\ M_y = 0,\ P_y = 0,\ P_{yx} = 0$

2. Electric

   Close circuit condition (CC) : $\phi^q_c = 0$

   Open circuit condition (OC) : $\tilde{H}^q_y - \tilde{V}^q_{\phi y} = 0$ (5.41)

5.2.4 Levy-type Solution

For the Levy-type solution, we consider a cross-ply plate for which $\bar{Q}_{16} = \bar{Q}_{26} = \bar{Q}_{45} = \bar{e}_{14} = \bar{e}_{25} = \bar{e}_{36} = \bar{\eta}_{12} = 0$. Also, the applied pressure loading p^i_z and electric potential ϕ^j at surfaces of the piezoelectric layers are considered to be independent of the $y-$ coordinate. For this case, $\phi_{,y} = 0$ and the last equation of the family of Eqs. (5.38) reduces to

$$\begin{aligned} I^{q'}_{73}\ddot{u}_{0x,x} - I^j_{73}\ddot{w}_{0,xx} + I^j_{75}\ddot{\psi}_{0x,x} + I^{jj'}_{77}\ddot{\phi}^{j'}_{,xx} + \bar{I}^{j'}_{63}\ddot{w}_0 - \bar{I}^{jj'}_{66}\ddot{\phi}^j - \bar{I}^{q'}_{67}\ddot{\phi}^q_c \\ + Q^j_{x,x} + H^j_{x,x} - S^j_{x,xx} - G^j + P^j_\phi = 0 \end{aligned} \tag{5.42}$$

and the boundary conditions involving ϕ^j in Eq. (5.39) do not exist. The supports at $x = 0,\ a$ are hard-simply supported (S-S), and under close circuit condition (CC):

$$N_x = 0, \quad u_{0y} = 0, \quad w_0 = 0, \quad M_x = 0, \quad P_x = 0, \quad \psi_{0y} = 0, \quad \phi^q_c = 0 \tag{5.43}$$

For the cross-ply laminate, the loading as well as the solution, satisfying the boundary condition in Eq. (5.43), can be expanded in terms of Fourier series in x:

$$\begin{aligned} &(u_{0y},\ w_0,\ \psi_{0y},\ N_x,\ N_y,\ M_x,\ M_y,\ P_x,\ P_y,\ S^j_x,\ G^j,\ \tilde{G}^q,\ \phi^j,\ \phi^q_c,\ p^i_z,\ Q_y,\ \tilde{Q}_y,\ \tilde{H}^q_y) = \\ &\sum_{m=1}^{\infty} \Re[(u_{0ym},\ w_{0m},\ \psi_{0ym}, N_{xm},\ N_{ym},\ M_{xm},\ M_{ym},\ P_{xm},\ P_{ym},\ S^j_{xm},\ G^j_m,\ \tilde{G}^q_m, \\ &\phi^j_m,\ \phi^q_{cm},\ p^i_{zm},\ Q_{ym},\ \tilde{Q}_{ym},\ \tilde{H}^q_{ym})e^{i\omega t}] \sin m\pi\xi \end{aligned}$$

$$(u_{0x},\, \psi_{0_x},\, N_{xy},\, M_{xy},\, P_{xy},\, Q_x,\, \bar{Q}^j_x,\, H^j_x,\, \tilde{Q}^q_x,\, \tilde{H}^q_x) =$$
$$\sum_{m=1}^{\infty} \Re[(u_{0x_m},\, \psi_{0_{x_m}},\, N_{xy_m}, M_{xy_m},\, P_{xy_m},\, Q_{x_m},\, \bar{Q}^j_{x_m},\, H^j_{x_m},\, \tilde{Q}^q_{x_m},\, \tilde{H}^q_{x_m})e^{i\omega t}] \cos m\pi\xi \quad (5.44)$$

where $\Re[...]$ is the real part of the complex number $(...)_m$ and $\xi = x/a$.

A mixed formulation approach is followed to get the solution in y direction. Unlike in displacement formulation approach where the entire governing equations at the end are expressed in terms of the displacement and electric potential variables, the advantage of the mixed formulation approach is that it naturally leads to first order differential governing equations and the boundary conditions in terms of the mixed primary variables which consists of displacements, stress resultants and electrical state variables. Thus, the solution in the y direction is developed in terms of 12 mechanical and $2n^q_\phi$ electrical primary variables given by

$$\mathbf{X_m} = [u_{0x_m}\ u_{0y_m}\ w_{0_m}\ w_{0,y_m}\ \psi_{0x_m}\ \psi_{0y_m}\ N_{y_m}\ N_{xy_m}\ (V_{y_m} + M_{xy,x_m})\ M_{y_m}$$
$$P_{y_m}\ P_{yx_m}\ (\tilde{Q}^q_y + \tilde{H}^q_y)_m\ \phi^q_{c_m}]^{\mathrm{T}} \quad (5.45)$$

which appear in the boundary conditions at edges $y = \mp b/2$. Using Eq. (5.45) in the equilibrium equations (5.38) and the plate constitutive equations (5.32) yields the following system of $12+2n^q_\phi$ first order ODEs and n_ϕ algebraic equations for the variables $\mathbf{X_m}$ for each Fourier component m:

$$\mathbf{H}^m\mathbf{X}_{m,y} = \mathbf{K}^m\mathbf{X}_m + \mathbf{P}^m + \mathbf{C}^m\mathbf{\Phi}^m \quad (5.46)$$

$$\mathbf{F}^m\mathbf{\Phi}^m = \mathbf{H}^m_\phi\mathbf{X}_{m,y} + \mathbf{K}^m_\phi\mathbf{X}_m - \mathbf{P}^m_\phi \quad (5.47)$$

where $\mathbf{\Phi}^m = [\,\phi^1 \quad \phi^2 \quad \dots \quad \phi^{n_\phi}\,]^{\mathrm{T}}_m$, $\mathbf{P}^m_\phi = [\,P^1_\phi \quad P^2_\phi \quad \dots \quad P^{n_\phi}_\phi\,]^{\mathrm{T}}_m$, and

$$\mathbf{H}^m = \begin{bmatrix}
A_{3,3} & 0 & 0 & 0 & A_{3,8} & 0 & 0 & 0 & 0 & 0 & 0 & 0 & 0 & 0 \\
0 & A_{2,2} & 0 & -A_{2,5} & 0 & A_{2,10} & 0 & 0 & 0 & 0 & 0 & 0 & 0 & 0 \\
0 & 0 & 1 & 0 & 0 & 0 & 0 & 0 & 0 & 0 & 0 & 0 & 0 & 0 \\
0 & A_{5,2} & 0 & -A_{5,5} & 0 & A_{5,10} & 0 & 0 & 0 & 0 & 0 & 0 & 0 & 0 \\
A_{8,3} & 0 & 0 & 0 & A_{8,8} & 0 & 0 & 0 & 0 & 0 & 0 & 0 & 0 & 0 \\
0 & A_{10,2} & 0 & -A_{10,5} & 0 & A_{10,10} & 0 & 0 & 0 & 0 & 0 & 0 & 0 & 0 \\
0 & 0 & 0 & 0 & 0 & 0 & 1 & 0 & 0 & 0 & 0 & 0 & 0 & 0 \\
0 & \bar{m}A_{1,2} & 0 & -\bar{m}A_{1,5} & 0 & \bar{m}A_{1,10} & 0 & 1 & 0 & 0 & 0 & 0 & 0 & 0 \\
0 & -\bar{m}^2A_{4,2} & 0 & \bar{m}^2A_{4,5} & 0 & -\bar{m}^2A_{4,10} & 0 & 0 & 1 & 0 & 0 & 0 & 0 & 0 \\
-2\bar{m}A_{6,3} & 0 & 0 & 0 & -2\bar{m}A_{6,8} & 0 & 0 & 0 & 0 & 1 & 0 & 0 & 0 & 0 \\
-\bar{m}A_{9,3} & 0 & 0 & 0 & -\bar{m}A_{9,8} & 0 & 0 & 0 & 0 & 0 & 1 & 0 & 0 & \Gamma_1 \\
0 & \bar{m}A_{7,2} & 0 & -\bar{m}A_{7,5} & 0 & \bar{m}A_{7,10} & 0 & 0 & 0 & 0 & 0 & 1 & 0 & 0 \\
0 & -\beta^{q'}_{22} & 0 & \beta^{q'}_{52} & 0 & -\beta^{q'}_{10,2} & 0 & 0 & 0 & 0 & 0 & 0 & 1 & 0 \\
0 & 0 & 0 & 0 & 0 & 0 & 0 & 0 & 0 & 0 & 0 & 0 & 0 & \Gamma_2
\end{bmatrix}$$

$$\mathbf{K}^m = [\,\mathbf{K}^a \quad \mathbf{K}^b\,]$$

$$\mathbf{K}^a = \begin{bmatrix}
0 & -\bar{m}A_{3,3} & 0 & 2\bar{m}A_{3,6} & 0 & -\bar{m}A_{3,9} \\
\bar{m}A_{2,1} & 0 & -\bar{m}^2A_{2,4} & 0 & \bar{m}A_{2,7} & 0 \\
0 & 0 & 0 & 1 & 0 & 0 \\
\bar{m}A_{5,1} & 0 & -\bar{m}^2A_{5,4} & 0 & \bar{m}A_{5,7} & 0 \\
0 & -\bar{m}A_{8,3} & 0 & 2\bar{m}A_{8,6} & 0 & -\bar{m}A_{8,9} \\
\bar{m}A_{10,1} & 0 & -\bar{m}^2A_{10,4} & 0 & \bar{m}A_{10,7} & 0 \\
0 & 0 & 0 & 0 & 0 & 0 \\
\bar{m}^2A_{1,1} & 0 & -\bar{m}^3A_{1,4} & 0 & \bar{m}^2A_{1,7} & 0 \\
-\bar{m}^3A_{4,1} & 0 & \bar{m}^4A_{4,4} & 0 & -\bar{m}^3A_{4,7} & 0 \\
0 & 2\bar{m}^2A_{6,3} & 0 & -4\bar{m}^2A_{6,6} & 0 & 2\bar{m}^2A_{6,9} \\
0 & \bar{m}^2A_{9,3} & 0 & -2\bar{m}^2A_{9,6} & 0 & \bar{m}^2A_{9,9} + \bar{A}_{22} \\
\bar{m}^2A_{7,1} & 0 & -\bar{m}^3A_{7,4} & 0 & \bar{m}^2A_{7,7} + \bar{A}_{11} & 0 \\
-\bar{m}\beta^{q'}_{12} & 0 & \bar{m}\beta^{q'}_{42} & 0 & \bar{m}\bar{A}^q_{51} + \bar{m}\bar{\beta}^{q'}_{13} - \bar{m}\beta^{q'}_{7,2} & 0 \\
0 & 0 & 0 & 0 & 0 & \bar{A}^q_{62} + \bar{\beta}^{q'}_{24}
\end{bmatrix}$$

with

$$\bar{m} = m\pi/a, \quad \Gamma_1 = -\bar{A}^{q'}_{26} - \bar{\beta}^{q'}_{24}, \quad \Gamma_2 = -\bar{A}^{qq'}_{66} - \bar{\beta}^{qq'}_{64} - \bar{\beta}^{q'q}_{64} + \bar{E}^{qq'}_{44}$$

The non-zero elements of K^b part of K^m are

$$K_{1,8} = K_{2,7} = K_{4,10} = K_{5,12} = K_{6,11} = K_{10,9} = 1, \quad K_{7,8} = \bar{m},$$

$$K_{2,12+2q'} = -\beta^{q'}_{22}, \qquad K_{4,12+2q'} = -\beta^{q'}_{52}, \qquad K_{6,12+2q'} = -\beta^{q'}_{10,2}$$

$$K_{8,12+2q'} = -\bar{m}\beta^{q'}_{12}, \qquad K_{9,12+2q'} = \bar{m}^2\ \beta^{q'}_{42}, \qquad K_{12+2q,11+2q'} = -1$$

$$K_{12,12+2q'} = \bar{m}\bar{A}^{q'}_{15} + \bar{m}\bar{\beta}^{q'}_{13} - \bar{m}\beta^{q'}_{7,2}, \qquad K_{11+2q,5} = \bar{m}\bar{A}^{q}_{51} + \bar{m}\bar{\beta}^{q}_{13} - \bar{m}\beta^{q}_{7,2}$$

$$K_{11+2q,12+2q'} = \bar{m}^2\bar{A}^{qq'}_{55} + \bar{m}^2\bar{\beta}^{qq'}_{43} + \bar{m}^2\bar{\beta}^{q'q}_{43} - \bar{m}^2\bar{E}^{qq'}_{33} - \hat{E}^{qq'}_{22}$$

The nonzero elements of matrices $\mathbf{P}^m$ and $\mathbf{C}^m$

$$P^m_9 = -P_3, \qquad C^m_{2,j'} = \bar{m}^2 A^{j'}_{2,11} - \beta^{j'}_{21}, \quad C^m_{4,j'} = \bar{m}^2 A^{j'}_{5,11} - \beta^{j'}_{51}$$

$$C^m_{6,j'} = \bar{m}^2 A^{j'}_{10,11} - \beta^{j'}_{10,1}, \qquad C^m_{8,j'} = \bar{m}^3 A^{j'}_{1,11} - \bar{m}\beta^{j'}_{11}$$

$$C^m_{9,j'} = -\bar{m}^4 A^{j'}_{4,11} + \bar{m}^2\beta^{j'}_{41}, \qquad C^m_{12,j'} = \bar{m}^3 A^{j'}_{7,11} - \bar{m}\beta^{j'}_{7,1} + \bar{m}\beta^{j'}_{11} + \bar{m}\bar{A}^{j'}_{13}$$

$$C^m_{12+q,j'} = \bar{m}^2\bar{A}^{qj'}_{53} + \bar{m}^2\bar{\beta}^{qj'}_{51} + \bar{m}^2\bar{\beta}^{qj'}_{33} - \bar{m}^2\bar{E}^{qj'}_{31} - \bar{m}^2\beta^{j'q}_{11,2} - \hat{E}^{qj'}_{21}$$

Matrices $\mathbf{H}^m_\phi$, $\mathbf{K}^m_\phi$ and $\mathbf{F}^m$ are given by

$$\mathbf{H}^m_{\phi j} = [\,0 \quad -\bar{m}^2 A^j_{11,2} + \beta^j_{21} \quad 0 \quad \bar{m}^2 A^j_{11,5} - \beta^j_{51} \quad 0 \quad -\bar{m}^2 A^j_{11,10} + \beta^j_{10,1} \quad 0 \quad 0 \quad 0 \quad 0 \quad 0 \quad 0 \quad 0 \quad 0\,]$$

$$\mathbf{K}^m_{\phi j} = [\,\bar{m}^3 A^j_{11,1} - \bar{m}\beta^j_{11} \quad 0 \quad -\bar{m}^4 A^j_{11,4} + \bar{m}^2\beta^j_{41} \quad 0 \quad \Gamma^j_3 \quad 0 \quad 0 \quad 0 \quad 0 \quad 0 \quad 0 \quad 0 \quad 0 \quad \Gamma^j_4\,]$$

$$\mathbf{F}^m_{jj'} = [-\bar{m}^4 A^{jj'}_{11,11} + \bar{m}^2(\beta^{jj'}_{11,1} + \beta^{j'j}_{11,1}) - \bar{m}^2\bar{A}^{jj'}_{33} - \bar{m}^2(\bar{\beta}^{jj'}_{31} + \bar{\beta}^{j'j}_{31}) + \bar{m}^2\bar{E}^{jj'}_{11} + \hat{E}^{jj'}_{11}\,]$$

where

$$\Gamma^j_3 = \bar{m}^3 A^j_{11,7} + \bar{m}\bar{A}^j_{31} + \bar{m}\bar{\beta}^j_{11} - \bar{m}\beta^j_{7,1}$$

$$\Gamma^j_4 = -\bar{m}^2\beta^{jq'}_{11,2} + \bar{m}^2\bar{A}^{jq'}_{35} + \bar{m}^2\bar{\beta}^{q'j}_{51} - \bar{m}^2\bar{E}^{jq'}_{13} - \hat{E}^{jq'}_{12} + \bar{m}^2\bar{\beta}^{jq'}_{33}$$

The non-zero elements from dynamic terms with addition to the above

$$K^m_{7,2} = -\omega^2 I_{22} \qquad K^m_{7,4} = \omega^2 I_{24}, \qquad K^m_{7,6} = -\omega^2 I_{26}, \qquad K^m_{8,1} = -\omega^2 I_{11},$$

$$K^m_{8,3} = \bar{m}\omega^2 I_{13}, \qquad K^m_{8,5} = -\omega^2 I_{15}, \qquad K^m_{9,1} = \bar{m}\omega^2 I_{31}, \qquad K^m_{9,3} = -\bar{m}^2\omega^2 I_{33} - \omega^2\bar{I}_{33},$$

$$K^m_{9,5} = \bar{m}\omega^2 I_{35}, \qquad K^m_{9,12+2q} = \omega^2\bar{I}^q_{37}, \qquad K^m_{10,2} = -\omega^2 I_{42}, \qquad K^m_{10,4} = \omega^2 I_{44},$$

$$K^m_{10,6} = -\omega^2 I_{46}, \qquad K^m_{11,2} = -\omega^2 I_{62}, \qquad K^m_{11,4} = \omega^2 I_{64}, \qquad K^m_{11,6} = -\omega^2 I_{66},$$

$$K^m_{11+2q,3} = \omega^2\bar{I}^q_{73}, \qquad K^m_{11+2q,12+2q} = -\omega^2\bar{I}^{qq'}_{77}, \qquad K^m_{12,1} = -\omega^2 I_{51}, \qquad K^m_{12,3} = \bar{m}\omega^2 I_{53},$$

$$K^m_{12,5} = -\omega^2 I_{55}, \qquad C^m_{8,j} = -\bar{m}\omega^2 I^{j'}_{17}, \qquad C^m_{9,j} = \bar{m}^2\omega^2 I^{j'}_{37} + \omega^2\bar{I}^j_{36}, \quad C^m_{12,j} = -\bar{m}\omega^2 I^{j'}_{57},$$

$$C^m_{11+2q,j} = -\omega^2\bar{I}^{jq}_{76}, \qquad H^m_{\phi j}(j,2) = \omega^2 I^j_{82}, \qquad H^m_{\phi j}(j,4) = -\omega^2 I^j_{84}, \quad H^m_{\phi j}(j,6) = \omega^2 I^j_{86},$$

$$K^m_{\phi j}(j,1) = -\bar{m}\omega^2 I^j_{71}, \qquad K^m_{\phi j}(j,3) = \bar{m}^2\omega^2 I^j_{73} + \omega^2\bar{I}^{j'}_{63}, \qquad K^m_{\phi j}(j,5) = -\bar{m}\omega^2 I^j_{75},$$

$$K^m_{\phi j}(j,12+2q) = -\omega^2\bar{I}^{q'}_{67}, \qquad F^m_{jj'} = \bar{m}^2\omega^2\bar{I}^{jj'}_{66} + \bar{m}^2\omega^2 I^{jj'}_{72a}$$

Equation (5.47) is an algebraic equation. In a general actuation-sensory response, some of the piezoelectric layers act as sensors wherein the induced electric potential is unknown, and

others as actuators where voltage is prescribed. $\mathbf{\Phi}^m$ is partitioned into a set of unknown (sensor) output voltages $\mathbf{\Phi}_s^m$ at locations $z = z_\phi^j$ where $\mathbf{\Phi}^m$ is not prescribed and a set of known input actuation voltages $\mathbf{\Phi}_a^m$ at the actuated surfaces $z = z_\phi^{j_i}$, i.e. $\mathbf{\Phi}^m = \begin{bmatrix} \mathbf{\Phi}_s^m \\ \mathbf{\Phi}_a^m \end{bmatrix}$. The corresponding matrices $\mathbf{F}^m, \mathbf{H}_\phi^m, \mathbf{K}_\phi^m$ and $\mathbf{P}_\phi^m$ are also partitioned accordingly. Accordingly, Eq. (5.47) can be partitioned as

$$\begin{bmatrix} \mathbf{F}_{ss}^m & \mathbf{F}_{sa}^m \\ \mathbf{F}_{sa}^m & \mathbf{F}_{aa}^m \end{bmatrix} \begin{bmatrix} \mathbf{\Phi}_s^m \\ \mathbf{\Phi}_a^m \end{bmatrix} = \begin{bmatrix} \mathbf{H}_{\phi s}^m \\ \mathbf{H}_{\phi a}^m \end{bmatrix} \mathbf{X}_{m,y} + \begin{bmatrix} \mathbf{K}_{\phi s}^m \\ \mathbf{K}_{\phi a}^m \end{bmatrix} \mathbf{X}_m - \begin{bmatrix} \mathbf{P}_{\phi s}^m \\ \mathbf{P}_{\phi a}^m \end{bmatrix} \tag{5.48}$$

which is solved for $\mathbf{\Phi}_s^m$ as

$$\mathbf{\Phi}_s = \mathbf{F}_{ss}^{-1} \left[\mathbf{H}_{\phi s}^m \mathbf{X}_{m,y} + \mathbf{K}_{\mathbf{\Phi}_s}^m \mathbf{X}_m - \mathbf{F}_{sa}^m \mathbf{\Phi}_a^m - \mathbf{P}_{\phi s}^m \right] \tag{5.49}$$

Substituting $\mathbf{\Phi}_s^m$ from Eq. (5.49) into the partitioned equation (5.46) yields

$$\tilde{\mathbf{H}}^m \mathbf{X}_{m,y} = \tilde{\mathbf{K}}^m \mathbf{X}_m + \tilde{\mathbf{P}}^m \tag{5.50}$$

where

$$\begin{aligned} \tilde{\mathbf{H}}^m &= \mathbf{H}^m - \mathbf{C}_s^m (\mathbf{F}_{ss}^m)^{-1} \mathbf{H}_{\phi s}^m, \qquad \tilde{\mathbf{K}}^m = \mathbf{K}^m + \mathbf{C}_s^m (\mathbf{F}_{ss}^m)^{-1} \mathbf{K}_{\phi s}^m \\ \tilde{\mathbf{P}}^m &= \mathbf{P}^m + \mathbf{C}_a^m \mathbf{\Phi}_a^m - \mathbf{C}_s^m (\mathbf{F}_{ss}^m)^{-1} \mathbf{P}_{\phi s}^m - \mathbf{C}_s^m (\mathbf{F}_{ss}^m)^{-1} \mathbf{F}_{sa}^m \mathbf{\Phi}_a^m \end{aligned} \tag{5.51}$$

For free vibration case $\tilde{\mathbf{P}}^m$ in Eq. (5.50) will be zero. So Eq. (5.49) reduces to

$$\begin{aligned} &\tilde{\mathbf{H}}^m \mathbf{X}_{m,y} = \tilde{\mathbf{K}}^m \mathbf{X}_m \\ \Rightarrow\ &\mathbf{X}_{m,y} - \left[\tilde{\mathbf{H}}^m \right]^{-1} \tilde{\mathbf{K}}^m \mathbf{X}_m = 0 \end{aligned} \tag{5.52}$$

The general solution of the non-homogeneous, linear ODEs with constant coefficients given by Eq. (5.50) is obtained as the sum of the complementary and particular solutions $\mathbf{X}_m^c$ and $\mathbf{X}_m^p$. Let the complementary solution be $\mathbf{X}_m^c = e^{\lambda y} \mathbf{Y}_m$. The homogeneous part of Eq. (5.50) i.e. Eq. (5.52) yields

$$\tilde{\mathbf{K}}^m \mathbf{Y}_m = \lambda \tilde{\mathbf{H}}^m \mathbf{Y}_m \Longrightarrow \tilde{\mathbf{M}}^m \mathbf{Y}_m = \lambda \mathbf{Y}_m \tag{5.53}$$

with $\tilde{\mathbf{M}}^m = (\tilde{\mathbf{H}}^m)^{-1} \tilde{\mathbf{K}}^m$. Hence λ and $\mathbf{Y}_m$ are eigenvalue and eigenvector pairs of the $(12 + 2n_\phi^q) \times (12 + 2n_\phi^q)$ real matrix $\tilde{\mathbf{M}}^m$. The eigenvalues and eigenvectors are obtained by the QR algorithm after first reducing to Hessenberg form. The complementary solution is the sum of $(12 + 2n_\phi^q)$ solutions for the $(12 + 2n_\phi^q)$ eigenvalues of $\tilde{\mathbf{M}}^m$.

The eigenvalues of the real matrix $\mathbf{M}^m$ are either real or occur in complex conjugate pairs. For complex conjugate eigenvalues $\lambda = \alpha \pm i\beta$ with the complex eigenvector $\mathbf{Y}_{m1}$ corresponding to $\alpha + i\beta$, the complementary solution in terms of real arbitrary constants C_1^m and C_2^m is

$$\mathbf{X}_m^c = \mathbf{F}_1^m(y)C_1^m + \mathbf{F}_2^m(y)C_2^m \tag{5.54}$$

with

$$\mathbf{F}_1^m = e^{\alpha y}[\Re(\mathbf{Y}_{m1})\cos(\beta y) - \Im(\mathbf{Y}_{m1})\sin(\beta y)], \quad \mathbf{F}_2^m = e^{\alpha y}[\Re(\mathbf{Y}_{m1})\sin(\beta y) + \Im(\mathbf{Y}_{m1})\cos(\beta y)]$$

where $\Re$ and $\Im$ indicate the real and imaginary parts of a complex number. The complementary solution for distinct real eigenvalue $\lambda = p$ with eigenvector $\mathbf{Y}_{m3}$, in terms of arbitrary constant C_3^m, is

$$\mathbf{X}_m^c = \mathbf{F}_3^m(y)C_3^m \qquad \text{with} \qquad \mathbf{F}_3^m(y) = \mathbf{Y}_{m3}e^{py} \tag{5.55}$$

The complementary solution for repeated eigenvalues require special treatment. For example, for a double eigenvalue μ of $\mathbf{M}^m$ with eigenvector $\mathbf{Y}_{m4}$, the complementary solution is given by [169]:

$$\mathbf{X}_m^c = \mathbf{Y}_{m4}e^{\mu y}C_4^m + (y\mathbf{Y}_{m4} + \mathbf{Z}_{m4})e^{\mu y}C_5^m \tag{5.56}$$

where $\mathbf{Z}_{m4}$ is a solution of $(\mathbf{M}^m - \mu\mathbf{I})\mathbf{Z}_{m4} = \mathbf{Y}_{m4}$. Thus, the general solution of Eq. (5.50) is

$$\mathbf{X}_m = \sum_{j=1}^{12+2n_\phi^q} \mathbf{F}_j^m(y)\mathbf{D}_j^m + \mathbf{X}_m^p \tag{5.57}$$

where the functions $\mathbf{F}_j^m(y)$ are of the forms given by Eq. (5.54) or Eq. (5.55) depending on the nature of eigenvalue, λ_j of $\tilde{\mathbf{M}}^m$.

The particular solution $\mathbf{X}_m^p$ depends on the form of the function $\tilde{\mathbf{P}}^m(y)$. In this study, p_z^i and ϕ^j are independent of y coordinate, for which $\tilde{\mathbf{P}}^m$ is a constant and the particular solution is given by

$$\mathbf{X}_m^p = -(\tilde{\mathbf{K}}^m)^{-1}\tilde{\mathbf{P}}^m \tag{5.58}$$

The $(6 + n_\phi^q)$ boundary conditions each at the edges $y = \mp b/2$ yield $(12 + 2n_\phi^q)$ linear algebraic equations for the $(12 + 2n_\phi^q)$ arbitrary constants $\mathbf{D}_j^m$ in the general solution (5.57). After solving for $\mathbf{D}_j^m$, the variables $\mathbf{X}_m$ are obtained from Eq. (5.57). Now substituting the

obtained solution $\mathbf{X}_m$ into Eq. (5.49), gives the sensory potential $\mathbf{\Phi}_s^m$. The displacements, stress resultants, electric potential, stresses and electric displacement at any point of the plate can be computed by using Eqs. (5.44), (5.8), (5.11), (5.27) and (5.4) by taking a finite number of terms, say M, in the Fourier series. A convergence study will determine the appropriate value of M to be used for the given distribution of mechanical and potential loads along $x-$direction.

The transverse shear stresses are obtained by the Cauchy's equilibrium equations as

$$\tau_{zx} = -\int_{-h/2}^{z} (\sigma_{x,x} + \tau_{xy,y})dz, \qquad \tau_{yz} = -\int_{-h/2}^{z} (\sigma_{y,y} + \tau_{xy,x})dz \tag{5.59}$$

For free vibration case the particular solution part ($\mathbf{X}_m^p$) will not be there in Eq. (5.57) making it a homogeneous algebraic equation and its coefficient matrix $\mathbf{F}_j^m$ depends on ω. For non-trivial solution, its determinant is zero. First ω is bracketed taking initial guess and can be found by root finding of the equation $\det(\mathbf{F}_j^m) = 0$ using the bisection method. This methodology was adopted by Heyliger and Saravanos [166], but as reported by them this method leads to roots which do not satisfy the condition of zero transverse shear stresses at the bottom and top surfaces. This problem has been overcome by adopting the method used by Kapuria and Achary [101].

For elastic case the deflection w in Eq.(5.8) contains only the mechanical deformation whereas for piezoelectric case it contains additional electrical deformation terms along with the mechanical. Hence, the 2D theories are termed as ZIGT and TOT for elastic case while they are called IZIGT and ITOT for piezoelectric case.

Chapter 6

Assessment of Advanced 2D Piezolaminate Theories

6.1 INTRODUCTION

In this Chapter, analytical solutions of zig-zag theory (ZIGT) and its smeared counterpart improved third-order theory (ITOT) are obtained for elastic/hybrid rectangular plates and are compared with 3D elasticity/piezoelasticity solution obtained by 3D EKM [151, 159].

In Sec. 6.2, the free vibration response of elastic laminated rectangular plates are presented and the effect of different boundary conditions, inplane modulus ratios, span-to-thickness ratios and laminate lay-ups on the plate natural frequencies are investigated. The 2D elasticity results are assessed for its accuracy by comparing its results with the 3D EKM [159] results presented in Chapter 3 and also with other first and higher order theory results. In Sec. 6.3, the static response of single layer piezoelectric and hybrid sandwich plates under electromechanical loading is presented and assessed in comparison with the 3D piezoelasticity solution based on EKM [151] presented in Chapter 2. Further, the 2D IZIGT and ITOT free vibration response of hybrid composite and sandwich plates are assessed in comparison with the 3D EKM solution presented in Chapter 4 in Sec. 6.4. The effect of various electromechanical boundary conditions on the plate natural frequencies of hybrid plates are investigated.

6.2 FREE VIBRATION OF ELASTIC LAMINATED PLATES

The best way to assess the accuracy of 2D theories is by comparing with the 3D analytical solutions which do not make any a priori assumptions of field variables through the thickness. Hence, The effectiveness of the present ZIGT in estimating the free vibration behaviours has been investigated for Levy type cross-ply plates by comparison with the other 2D and 3D solutions. The TOT solution can also be obtained using the same number of displacement state variables without requiring any shear correction factor and hence the TOT results are also compared. Unless mentioned otherwise, the non-dimensional frequency parameter $\bar{\omega}$ considered in the present analysis is as follows: $\bar{\omega} = \omega_m a S \sqrt{\rho_0/Y_2}$, where ω_m is the calculated frequency, S is the span-to-thickness ratio, ρ_0 is the mass density in Kg/m^3 and E_2 is the minor elastic modulus in N/m^2. The dimensionless material parameters used in the present investigation are as follows: $Y_1/Y_2 = 40, Y_2 = Y_3 = 6.9\,\text{GPa}, G_{12} = G_{13} = 0.6Y_2, G_{23} = 0.5Y_2, \nu_{23} = \nu_{13} = \nu_{12} = 0.25$. Any modification to the material constants mentioned above is clearly specified in the relevant places. The plates are designated as per the boundary conditions subjected on the edges at $y = \mp b/2$. A C-S plate, for instance, designates a plate subjected to clamped (C) boundary condition at $y = -b/2$ and simply supported (S) at $y = b/2$. For comparison purpose, the EKM results are transformed to Levy model coordinate system as shown in Fig. 6.1. Hence, the laminate sequence in Ref. [159] is altered to match with the present model.

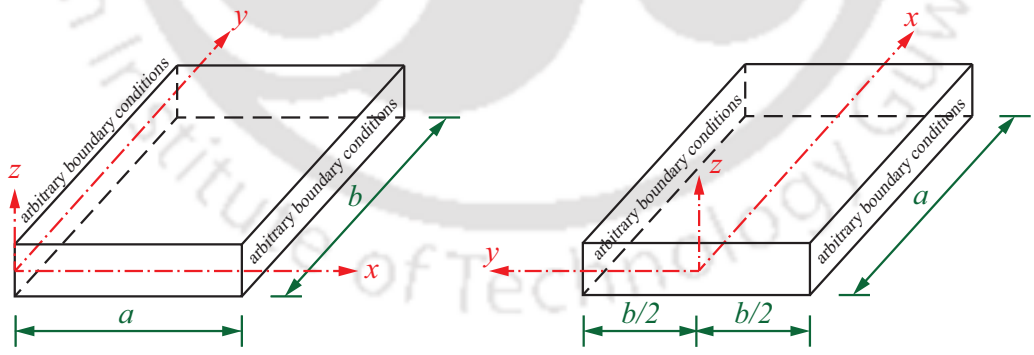

Figure 6.1: Coordinate systems of EKM and Levy solutions.

The percentage errors are calculated with respect to the reference results and is as follows: % error = [((2D frequency)-(reference frequency))/(reference frequency)]×100. The modal displacement and stresses are non-dimesionalized as:

$$\bar{v} = \frac{u_{0y}}{\max(w_0)}; \qquad (\bar{\sigma}_y, \bar{\tau}_{yz}) = \frac{Sh(\sigma_y, \tau_{yz})}{Y_0 \times \max(w_0)} \tag{6.1}$$

6.2.1 Validation

The accuracy of the present ZIGT result has been verified by direct comparison with the 3D exact [101] and 3D EKM [159] results for all round simply supported (S-S) case in Table 6.1 and with the results of FSDT [170] and third order shear deformation theory (TSDT) [171] for other type of boundary conditions in Table 6.2. In Table 6.1, the dimensionless fundamental natural frequencies ($\bar{\omega}$) of an un-symmetric two layer [90°/0°] and a symmetric four layer [90°/0°/0°/90°] lay-up cross-ply laminated plates subjected to S-S boundary conditions are presented for S value of (5, 10, 20, 50, 100) and are compared against the reference 3D EKM and 3D exact results. As can be seen from the table that for thin plates the 2D theories have predicted frequencies quite accurately, but for thicker plates, these theories over predict the frequencies. The maximum error being 7.74% for ZIGT and 6.58% for TOT in case of the two-layered thick plate (S=5). The error percentage is 1.33% and 0.99%, respectively, for ZIGT and TOT for the four-layered thick plate. The flexural fundamental frequency of Levy-type single layer isotropic plate is presented in Table 6.2 and are compared with the TSDT [171] and FSDT [170] results for different types of boundary conditions. For this table, the frequency parameter $\bar{\omega} = (\omega_m a^2)\sqrt{\rho_0 h/D_1}$ where $D_1 = Eh^3/12(1-\nu^2)$ is the flexural rigidity of the plate. The isotropic material constants are E= 6.9 GPa and Poisson's ratio, ν=0.3. The results are presented for square and rectangular plates for S= 5 and 10. It is observed from the table that the ZIGT results are in excellent agreement with the TSDT [171] results for all type of boundary conditions, whereas the FSDT results except for S-S case are erroneous as compared to the higher order theory results.

Hereafter, the dimensionless natural frequencies of 3D EKM are given for reference whereas the percentage errors of the present ZIGT and TOT are given for ready assessment.

Table 6.1: Comparison of fundamental natural frequencies for all-round simply-supported (S-S) boundary conditions

Laminate scheme	Theory	S				
		5	10	20	50	100
90°/0°	ZIGT	9.187	10.606	11.116	11.277	11.301
	TOT	9.087	10.568	11.105	11.275	11.300
	3D EKM [159]	8.526	10.336	11.036	11.263	11.297
	3D Exact [101]	8.526	10.336	11.036	11.263	11.297
90°/0°/0°/90°	ZIGT	10.830	15.125	17.652	18.673	18.836
	TOT	10.787	15.107	17.647	18.672	18.836
	3D EKM [159]	10.682	15.068	17.635	18.669	18.835
	3D Exact [101]	10.682	15.068	17.635	18.669	18.835

Table 6.2: Fundamental natural frequency, $\bar{\omega} = (\omega_m a^2)\sqrt{\rho_0 h/D_1}$ of square and rectangular single layer isotropic plate for S=5 and 10.

b/a	S	Theory	S-S	C-C	S-C	F-C	F-S	F-F
1	5	ZIGT	17.447	22.526	19.763	11.370	10.697	8.983
		TSDT [171]	17.452	22.536	19.770	11.374	10.700	8.984
		FSDT [170]	17.449	21.584	19.388	11.573	10.921	9.082
	10	ZIGT	19.060	26.703	22.396	12.249	11.371	9.441
		TSDT [171]	19.065	26.708	22.402	12.252	11.374	9.442
		FSDT [170]	19.065	26.333	22.270	12.366	11.474	9.482
2	5	ZIGT	11.369	12.291	11.780	9.659	9.571	9.089
		TSDT [171]	11.372	12.294	11.783	9.661	9.573	9.090
		FSDT [170]	11.371	12.177	11.736	9.741	9.652	9.150
	10	ZIGT	12.065	13.272	12.591	10.199	10.086	9.551
		TSDT [171]	12.068	13.275	12.594	10.200	10.087	9.555
		FSDT [170]	12.067	13.239	12.580	10.237	10.122	9.577

6.2.2 Assessment

In this section, the veracity of ZIGT and TOT in predicting free vibration characteristics are assessed against the 3D EKM solution for multilayered composite and sandwich plates. The lowest five flexural frequencies for an un-symmetric two layer [90°/0°] laminated thick (S=5) plate is presented in Table 6.3 for different combination of boundary conditions. The material parameters considered for this table are as follows: $Y_1/Y_2 = 30, G_{12}/Y_2 = G_{13}/Y_2 = 0.5, G_{23}/Y_2 = 0.35, \nu_{12} = \nu_{13} = 0.3, \nu_{23} = 0.49$ with Y_2=6.9 GPa. It is observed from the table that at lower modes, the % error for S-S case is less as compared to other boundary conditions. The C-C boundary support shows the highest % error i.e. 18.3% and 17.5% for ZIGT and TOT,

respectively.

Table 6.3: Lowest five flexural frequencies $\bar{\omega}_m = \omega h\sqrt{\rho_0/Y_2}$ for a two layer [90°/0°] laminated composite plate (S=5) and the corresponding % error of ZIGT and TOT frequencies (material parameters: $Y_1/Y_2 = 30, G_{12}/Y_2 = G_{13}/Y_2 = 0.5, G_{23}/Y_2 = 0.35, \nu_{12} = \nu_{13} = 0.3, \nu_{23} = 0.49$)

BCs	Theory	Mode sequences				
		1	2	3	4	5
S-S	3D EKM [159]	0.3117	0.6361	0.6361	0.8532	1.0185
	ZIGT (% error)	6.23	5.72	13.7	4.14	17.1
	TOT (% error)	4.33	5.72	13.7	4.14	13.1
C-C	3D EKM [159]	0.3782	0.6664	0.6772	0.8819	1.0345
	ZIGT (% error)	15.9	16.4	18.3	0.76	15.3
	TOT (% error)	11.4	11.2	17.5	0.76	14.1
C-F	3D EKM [159]	0.2328	0.4260	0.5942	0.7107	0.7784
	ZIGT (% error)	6.67	4.28	13.5	13.6	19.2
	TOT (% error)	4.77	4.28	7.97	9.36	13.6
S-F	3D EKM [159]	0.2179	0.3984	0.4320	0.5893	0.6970
	ZIGT (% error)	6.60	5.05	14.5	11.7	8.12
	TOT (% error)	4.69	3.95	9.21	7.86	12.5
F-F	3D EKM [159]	0.2073	0.2438	0.5138	0.5763	0.6120
	ZIGT (% error)	7.33	4.82	7.31	16.9	13.6
	TOT (% error)	5.22	3.30	5.28	11.9	9.10

The effect of the span-to-thickness ratio (S) on the fundamental natural frequencies of a three-layer [90°/0°/90°] rectangular plate for boundary conditions C-C, S-C, S-S, F-C, F-S and F-F is presented in Table 6.4. As observed in Table 6.4, here also, the % error with respect to 3D EKM frequency is maximum for C-C boundary condition irrespective of plate span-to-thickness ratios (S=2, 5, 10). As S value increases, the frequency % error decreases: for S-S case it reduces to 0.03%, whereas for C-C case it reduces to 3.83% for moderately thick (S=10) plate in case of ZIGT prediction.

Effect of inplane elastic modulus ratio (Y_1/Y_2) on the fundamental natural frequency of an unsymmetrical four layer [90°/0°/90°/0°] moderately thick (S=10) plate is presented in Table 6.5. It is observed from the table that as the ratio (Y_1/Y_2) decreases thereby making the plate material closer to isotropic condition, the error percentage of 2D theories is decreased, for instance, for (Y_1/Y_2)=40, the ZIGT and TOT % errors are 1.83% and 2.38% respectively, while for (Y_1/Y_2)=2 the corresponding errors decreased to -0.14% and -0.11%. Hence, it suggests that the 2D theories perform well for plates made of isotropic materials. The ZIGT results are more

closer to 3D EKM results than the TOT results for (Y_1/Y_2)=40, 20, 10 and for (Y_1/Y_2)=2, the TOT results seem superior than ZIGT.

Table 6.4: Effect of span-to-thickness ratio (S) on the fundamental natural frequencies of a three layer [90°/0°/90°] laminated composite plate: (material parameters: $Y_1/Y_2 = 40, Y_2 = Y_3 = 6.9\,\text{GPa}, G_{12} = G_{13} = 0.6Y_2, G_{23} = 0.5Y_2, \nu_{13} = \nu_{12} = 0.25, \nu_{23} = 0.49$)

Theory	S	C-C	S-C	S-S	F-C	F-S	F-F
3D EKM [159]	2	5.331	5.201	5.192	3.481	3.072	2.715
HSDT [75] (% error)		-0.48	-2.51	-0.77	3.50	4.79	7.30
ZIGT (% error)		34.0	18.9	5.47	9.21	4.35	5.99
TOT (% error)		26.7	14.5	3.30	6.94	2.73	3.73
3D EKM [159]	5	11.426	10.679	10.246	5.810	4.401	3.911
HSDT [75] (% error)		-0.05	-2.64	-0.88	1.19	2.36	3.03
ZIGT (% error)		6.11	5.75	0.53	3.20	2.25	2.95
TOT (% error)		6.11	4.57	0.19	2.59	1.66	2.21
3D EKM [159]	10	19.660	17.108	14.702	7.135	4.876	4.241
HSDT [75] (% error)		0.15	-1.00	-0.29	0.37	0.69	1.72
ZIGT (% error)		3.83	2.17	0.03	0.89	0.76	0.77
TOT (% error)		3.14	1.81	0.00	0.76	0.59	0.57

Table 6.5: Effect of inplane modulus ratio (Y_1/Y_2) on the fundamental natural frequency of an unsymmetrical four layer [90°/0°/90°/0°] laminated composite plate(S=10).

Theory	Y_1/Y_2	S-S	C-C	C-S	C-F
3D EKM [159]	40	0.14501	0.18652	0.16490	0.10875
ZIGT (% error)		1.83	5.30	3.58	1.98
TOT (% error)		2.38	6.37	4.40	-6.32
3D EKM [159]	20	0.11653	0.16088	0.13738	0.08638
ZIGT (% error)		0.79	2.97	1.75	0.57
TOT (% error)		1.10	3.72	2.26	0.86
3D EKM [159]	10	0.09438	0.13627	0.11337	0.06869
ZIGT (% error)		0.22	0.98	0.49	-0.41
TOT (% error)		0.38	1.44	0.78	-0.26
3D EKM [159]	2	0.06719	0.09641	0.07992	0.04628
ZIGT (% error)		-0.14	-1.94	-1.08	-3.41
TOT (% error)		-0.11	-1.85	-1.02	-3.38

The percentage errors of the lowest eight flexural frequencies for a three-layer [90°/0°/90°] composite laminated plate is presented in Table 6.6 for S-S and C-C cases with S= 10 and 20 along with the reference 3D EKM results. The non-dimensional frequency parameter $\bar{\omega} = (\omega_n a^2/\pi^2)\sqrt{\rho_0 h/D_2}$, where $D_2 = E_2 h^3/12(1-\nu_{12}\nu_{21})$. Here in the table, we can see, the 2D theories predict quite accurate results for S-S case and the error percentage is more for C-C

case with maximum error 7.36% for the moderately thick plate. The TOT results come more accurate as compared to the ZIGT results both for S-S and C-C cases.

Table 6.6: Lowest eight natural frequencies, $\bar{\omega} = (\omega_m a^2/\pi^2)\sqrt{\rho_0 h/D_2}$ of the 3D EKM with the % errors of ZIGT and TOT results for a three ply [90°/0°/90°] laminated plate for S-S and C-C boundary conditions

BCs	S	Theory	Mode sequences							
			1	2	3	4	5	6	7	8
S-S	10	3D EKM [159]	5.154	7.606	12.276	13.100	14.355	17.399	18.087	21.355
		FSDT [71] (% error)	0.22	1.98	5.21	-0.39	0.14	2.24	7.82	-1.42
		ZIGT (% error)	0.07	1.50	3.94	0.36	0.64	2.03	5.72	0.58
		TOT (% error)	0.04	1.11	2.89	0.09	0.31	1.35	4.08	-0.22
	20	3D EKM [159]	6.131	8.841	14.845	19.320	20.618	23.287	24.202	30.426
		FSDT [71] (% error)	0.12	0.53	1.79	0.18	0.23	3.36	0.59	1.98
		ZIGT (% error)	0.01	0.41	1.46	0.03	0.07	2.69	0.35	1.50
		TOT (% error)	0.01	0.31	1.12	0.02	0.04	2.05	0.21	1.11
C-C	10	3D EKM [159]	5.796	9.019	13.363	13.830	15.147	18.521	19.487	21.535
		FSDT [71] (% error)	1.30	4.82	-0.17	7.58	1.27	3.82	8.95	-1.21
		ZIGT (% error)	0.97	3.91	0.51	6.14	1.53	3.42	7.36	-0.27
		TOT (% error)	0.74	3.05	0.21	4.77	1.02	2.52	5.66	-1.05
	20	3D EKM [159]	6.867	11.040	18.001	19.578	21.675	26.230	26.827	33.205
		FSDT [71] (% error)	0.33	1.87	3.68	0.21	0.58	1.75	5.34	3.44
		ZIGT (% error)	0.21	1.55	3.05	0.06	0.37	1.35	4.37	2.81
		TOT (% error)	0.16	1.22	2.41	0.04	0.27	1.04	3.43	2.81

The ZIGT and TOT frequency percentage errors for the lowest five flexural frequencies are presented in Table 6.7 with respect to the 3D EKM results for a five layered sandwich plate [90°/0°/Core/0°/90°] under five boundary conditions (S-S, C-C, C-S, C-F and F-F) for $S = 5, 10$ and 20. The material constants those follow are considered for face and core layers, Face: $Y_1 = 181\,\text{GPa}, Y_2 = Y_3 = 10.3\,\text{GPa}, G_{12} = G_{13} = 7.17\,\text{GPa}, G_{23} = 2.87\,\text{GPa}, \nu_{12} = \nu_{13} = 0.28, \nu_{23} = 0.33, \rho = 1578\,\text{kg/m}^3$, Core: $Y_1 = Y_2 = 0.276\,\text{GPa}, Y_3 = 3.45\,\text{GPa}, G_{13} = G_{23} = 0.414\,\text{GPa}, G_{12} = 0.1104$ GPa, $\nu_{12} = 0.25$, $\nu_{13} = \nu_{23} = 0.02$ and $\rho = 1000\,\text{kg/m}^3$. The frequency parameter $\bar{\omega} = \omega_m a S\sqrt{\rho_0/Y_2}$, where $\rho_0 = 1578\,\text{kg/m}^3$ and $Y_2 = 10.3\,\text{GPa}$. From Table 6.7, it is clear that the frequency increases with the increase in S value i.e. the thinner the plate, higher the plate frequency. The lowest frequencies are noted for F-F boundary case, while the highest frequencies are noted for C-C boundary case for all the plates. It is to observe that ZIGT predicts quite accurate results for S-S and F-F boundary conditions, but for other type of boundary conditions it gives more errors and the maximum (4.41%) being for C-C boundary

case. It is observed that for sandwich plate ZIGT predicts superior results than TOT for all types of boundary conditions and plate categories.

The distributions of inplane displacement $\bar{v}$, normal stress $\bar{\sigma}_y$ and shear stress $\bar{\tau}_{yz}$ for S-S boundary condition are illustrated in Fig. 6.2 for moderately thick (S=10) and thick (S=5) sandwich plates for the first mode (m=1). The ZIGT and TOT predictions are compared with the 3D exact and 3D EKM predictions and found that ZIGT has fairly accurate predictions while the TOT overpredicts $\bar{v}$ for the thick plate and $\bar{\tau}_{yz}$ for both thick and moderately thick plates. Figure 6.3 displays the variation of displacement and stress variables for (a) C-C and (b) C-F boundary conditions. From the figures, it is observed that ZIGT and TOT predict erroneous results while the ZIGT predictions are superior to the TOT predictions.

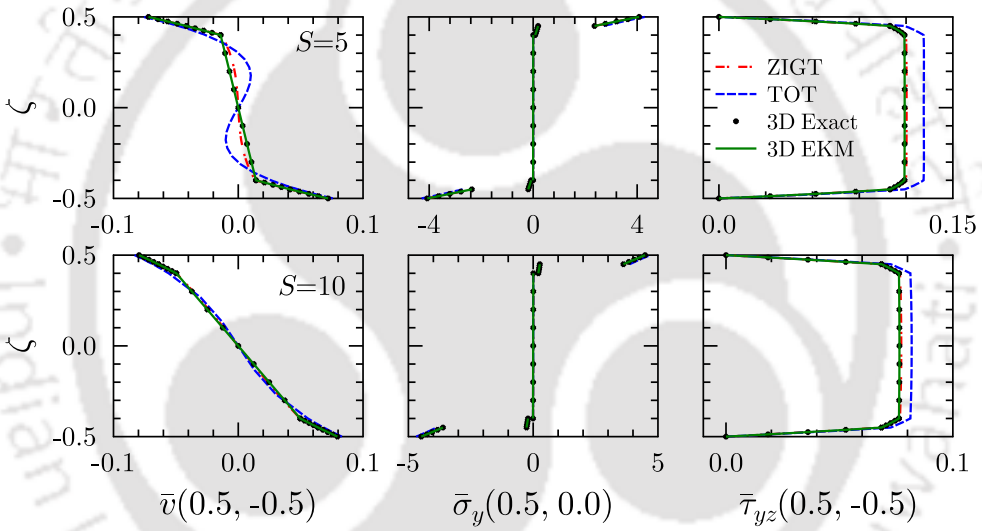

Figure 6.2: Distributions $\bar{v}$, $\bar{\sigma}_y$ and $\bar{\tau}_{yz}$ for the first mode of all round simply supported (S-S) square sandwich plate.

Table 6.7: The % errors of lowest five flexural natural frequencies of ZIGT and TOT with respect to 3D EKM for a square sandwich plate under five different boundary conditions for S=5, 10 and 20

S	Mode	S-S			C-C			C-S			C-F			F-F		
		3D EKM [159]	ZIGT %error	TOT %error	3D EKM [159]	ZIGT %error	TOT %error	3D EKM [159]	ZIGT %error	TOT %error	3D EKM [159]	ZIGT %error	TOT %error	3D EKM [159]	ZIGT %error	TOT %error
5	1	4.807	0.07	7.03	5.041	2.29	8.99	4.876	1.53	8.41	3.605	0.51	9.09	3.181	0.12	9.94
	2	7.921	0.09	-2.21	8.036	1.00	10.8	7.958	0.66	10.5	6.162	2.32	8.09	3.829	0.29	8.21
	3	8.367	0.14	5.77	8.397	4.41	9.53	8.388	2.20	7.59	7.232	0.26	7.10	6.997	0.29	10.7
	4	10.479	0.14	7.87	10.507	2.89	10.2	10.497	1.46	9.01	8.890	1.36	10.0	7.637	0.25	2.47
	5	11.505	0.13	3.57	11.564	0.59	3.04	11.525	0.41	3.39	10.278	1.01	5.88	7.972	0.51	5.90
10	1	7.677	0.04	4.36	8.821	1.30	6.14	8.201	0.82	5.46	5.597	0.25	5.39	4.951	0.14	4.69
	2	14.164	0.05	8.78	14.702	0.55	9.09	14.406	0.34	8.99	10.323	1.22	5.56	5.791	0.13	5.41
	3	15.078	0.08	4.66	15.469	2.25	6.91	15.296	1.18	5.81	13.005	0.55	6.66	12.728	0.07	8.98
	4	19.228	0.07	7.03	19.508	1.51	8.39	19.381	0.79	7.71	15.915	0.70	8.54	13.146	0.15	3.90
	5	21.437	0.07	5.06	21.726	0.31	3.67	21.567	0.21	4.43	18.388	1.34	5.82	13.486	0.12	2.86
20	1	9.849	0.02	1.73	13.453	0.58	3.33	11.569	0.30	2.50	7.009	0.19	2.18	6.193	0.01	0.68
	2	21.707	0.03	5.27	23.338	0.42	5.52	22.460	0.16	5.31	14.973	0.55	2.93	7.249	0.09	2.23
	3	23.314	0.04	2.68	26.275	1.05	4.64	24.875	0.63	3.79	20.240	0.15	3.59	17.551	0.04	1.73
	4	30.711	0.03	4.35	32.819	0.77	5.41	31.811	0.40	4.88	24.870	0.32	5.18	19.823	-1.01	4.59
	5	36.632	0.05	3.49	37.517	0.18	1.05	37.031	0.11	2.37	29.958	0.53	3.69	20.765	0.08	0.95

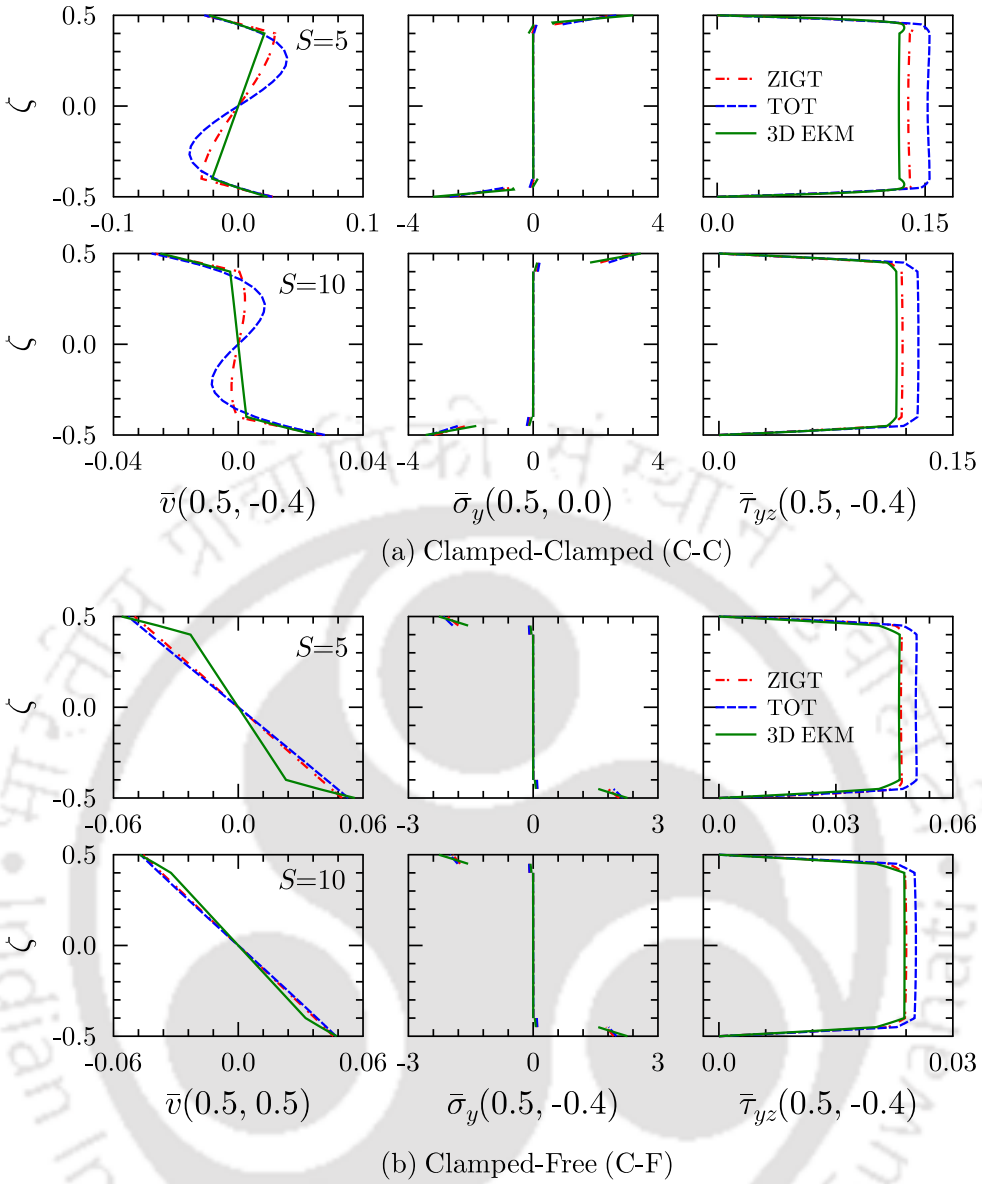

(a) Clamped-Clamped (C-C)

(b) Clamped-Free (C-F)

Figure 6.3: Distributions $\bar{v}$, $\bar{\sigma}_y$ and $\bar{\tau}_{yz}$ for the first modes of square sandwich plate for C-C and C-F boundary conditions.

6.3 STATIC ANALYSIS OF RECTANGULAR HYBRID PLATES

The results of IZIGT and ITOT are assessed both for single layer piezoelectric plate (a) and hybrid sandwich plate (b), as shown in Fig. 6.4, for various boundary conditions under electrical and mechanical loadings. The interfaces between the PFRC layers with the host laminate in the hybrid plate are grounded ($\phi = 0$). The material properties are listed in Table 2.3.

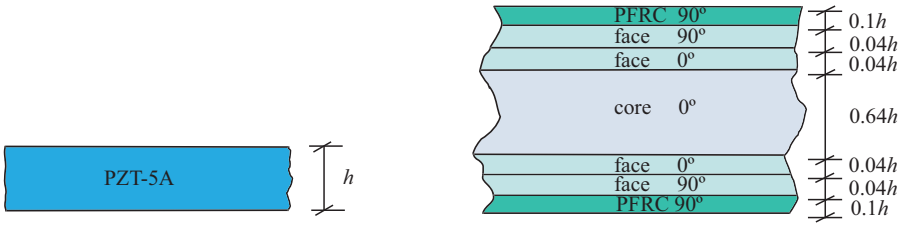

Piezoelectric plate (a) Hybrid sandwich plate (b)

Figure 6.4: Configurations of piezoelectric plate (a) and hybrid sandwich plate (b).

The plate is subjected to the following load cases,

1. Pressure $p_2 = p_0 \sin(\pi y/b)$ acting on top surface.

2. Actuation potentials of $\phi_1 = \phi_2 = \phi_0 \sin(\pi y/b)$ applied on both top and bottom surfaces.

The results are nondimensionalized as follows:

Load case 1.

$$(\bar{v}, \bar{w}, \bar{\phi}) = 100(Sv, w, 10^4 \phi d_0 S^2) Y_0/p_0 h S^4; \quad (\bar{\sigma}_x, \bar{\sigma}_y, \bar{\tau}_{yz}, \bar{\tau}_{zx}) = (\sigma_x, \sigma_y, S\tau_{yz}, S\tau_{zx}) h/p_0 S^2$$

$$(\bar{D}_x, \bar{D}_y) = (D_x, D_y)/d_0 p_0 S$$

Load case 2.

$$(\bar{v}, \bar{w}) = (Sv, w) Y_0/S^2 d_0 \phi_0; \quad (\bar{\sigma}_x, \bar{\sigma}_y, \bar{\tau}_{yz}, \bar{\tau}_{zx}) = (\sigma_x, \sigma_y, S\tau_{yz}, S\tau_{zx}) h/Y_0 d_0 \phi_0$$

where $S = a/h, d_0 = 374.0 \times 10^{-12} mV^{-1}, Y_0 = 10.3GPa$ for plate (a) and for plate (b) $d_0 = 100.0 \times 10^{-12} mV^{-1}$. The plates are designated in terms of their mechanical boundary conditions at the edges at $y = \mp b/2$. For example, a plate which is clamped (C) at $y/b = -0.5$ and free (F) at $y/b = 0.5$, is called a C-F plate. The response of the piezoelectric plate (a) is obtained for the pressure load case, while the hybrid sandwich plate (b) is analyzed for both pressure and potential load cases.

The longitudinal variations of displacements, stresses, sensory potential and electrical displacements at z-locations where they are large, are plotted in Fig. 6.5 for the square thick ($S = 5$) piezoelectric plate under clamped-clamped (C-C) boundary conditions along y-axis. The 3D FE (ABAQUS) results are also plotted for verification of the results obtained by 3D EKM. It is

observed that the two-term EKM solution is in excellent agreement with 3D FE solution for all the response entities. The displacements are accurately predicted by the IZIGT over the range and are in good agreement with 3D EKM. The error in the value of $\bar{\sigma}_y$ is more than that of the $\bar{\sigma}_x$ near the clamped edge. Similar trend is observed for shear stresses, in which $\bar{\tau}_{yz}$ is the least accurate near the edge. Electric displacements $\bar{D}_x$ and $\bar{D}_y$ and electric potential ϕ is also not accurately predicted by IZIGT near the clamped edge. It has been found that for the simply supported case, all the entities are accurately predicted by IZIGT and ITOT.

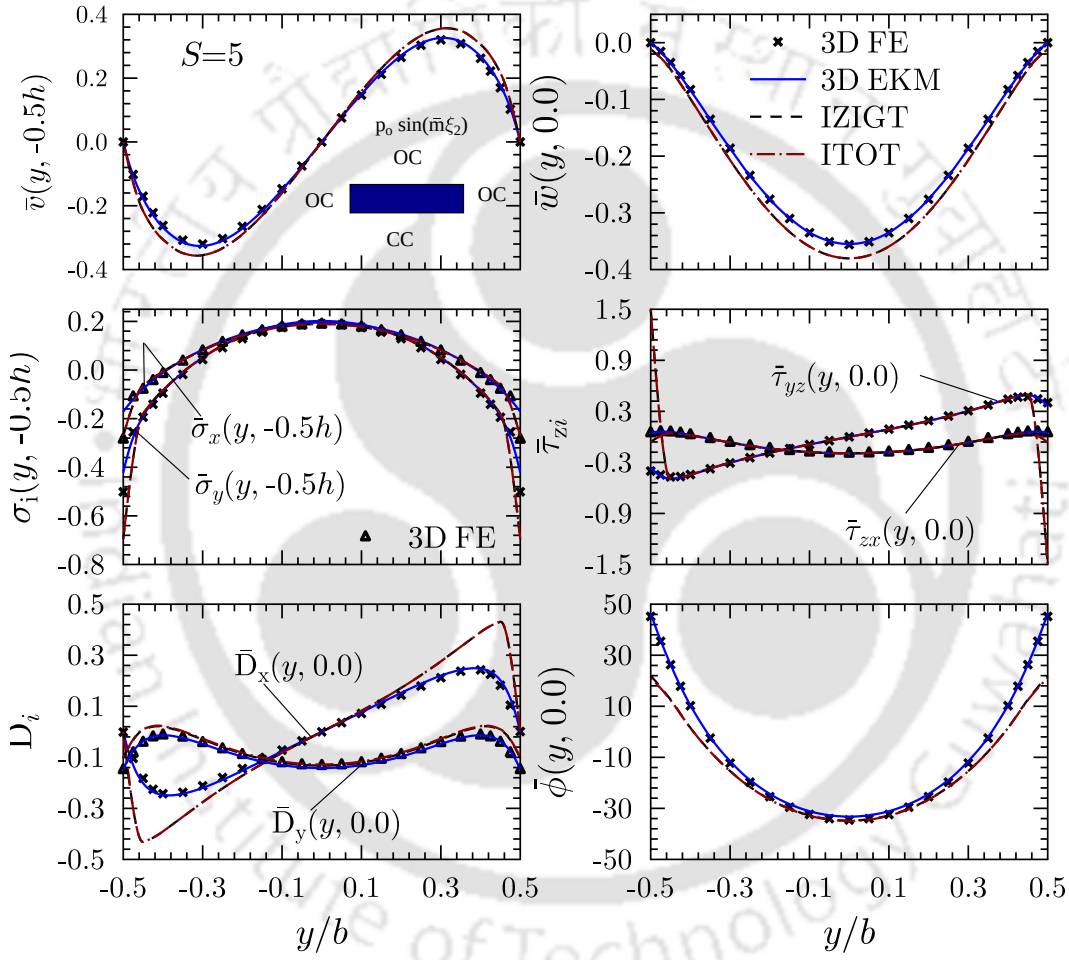

Figure 6.5: Longitudinal variations of displacements, stresses, electric potential and electric displacements for square piezoelectric plate (a) under pressure loading.

Figure 6.6 shows the longitudinal variation of $\bar{w}, \bar{\sigma}_y, \bar{\tau}_{yz}$ and electric displacement $\bar{D}_z$ under pressure loading for sandwich plate (b) with clamped-free (C-F) and clamped-simply supported (C-S) boundary conditions. Transverse deflection $\bar{w}$ is accurately predicted by IZIGT for both C-F and C-S cases whereas ITOT under predicts the deflection with large error. In-plane normal stress $\bar{\sigma}_y$ is predicted very accurately by the IZIGT as compared to the ITOT in the interior

part of the plate but near the clamped support, prediction is poor by both the theories. Both the theories give inaccurate results for the transverse shear stress and electric displacement near the clamped-supports.

Longitudinal variations of deflection, stresses and electric displacement under potential loading for moderately thick sandwich plate with C-F and C-S boundary conditions are presented in Fig. 6.6. For C-F case, IZIGT produces accurate results for whole range except at the boundaries (clamped and free supports) whereas ITOT gives erroneous prediction of stresses even in the interior part of the plate. For C-S case, IZIGT over predict the deflection whereas ITOT under predict it. A mismatch in normal stress value is observed by both the theories in the interior as well as at boundaries of the plates. Both the theories fail to satisfy the boundary conditions at the edge (i.e. zero stress at free and simply supported edge).

Longitudinal variations of $\bar{v}, \bar{w}, \bar{\sigma}_x, \bar{\sigma}_y, \bar{\tau}_{zx}$ and $\bar{\tau}_{yz}$ under potential loading with free-free (F-F) support conditions is plotted in Fig. 6.7 for moderately thick sandwich plate. Transverse displacement is very accurately predicted by both IZIGT and ITOT whereas a slight mismatch is observed for in-plane displacement near the free support. The results of IZIGT are in close agreement with 3D EKM for both in-plane normal and transverse shear stresses. However, ITOT results are erroneous even in the interior part of the plate specifically for $\bar{\sigma}_x$. Transverse shear stresses are accurately predicted both by IZIGT and ITOT except at the edge. For transverse shear $\bar{\tau}_{zx}$ at the free edge, both IZIGT and ITOT under predict almost four times less than the exact value predicted by 3D EKM. This high value of free edge stresses which cause delamination in the structures are not predicted by these two-dimensional theories.

Through-thickness variations of transverse shear stresses τ_{zx} and τ_{yz} at three location of y/b $(0.025, 0.05,$ and $0.1)$ are plotted in Fig. 6.8. It is observed that IZIGT produces more close predictions of the stresses as compared to ITOT. However, both the theories produce erroneous results at the piezo-interface and through the core in the sandwich.

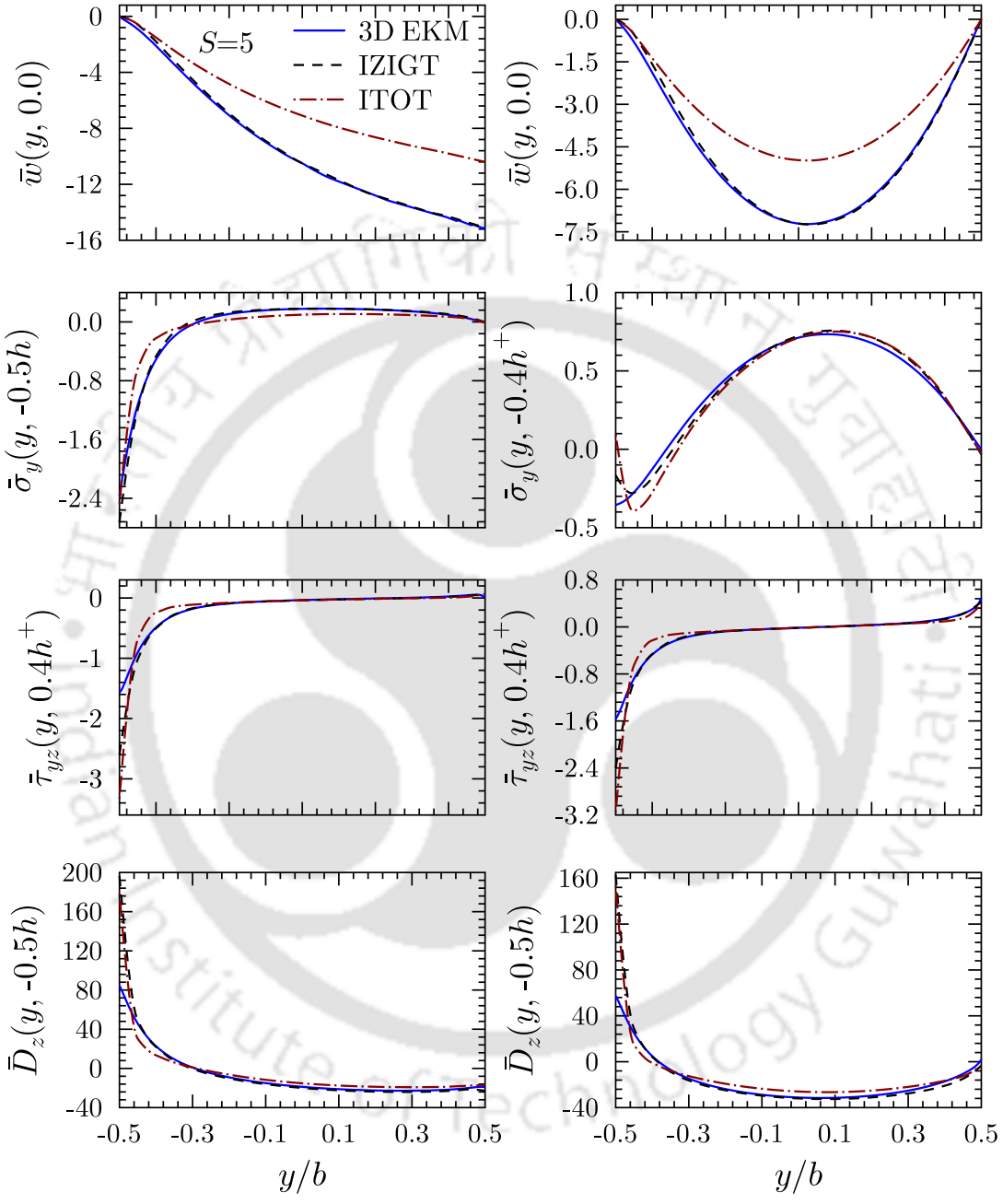

(a) C-F (b) C-S

Figure 6.6: Longitudinal variation of deflection, stresses and electric displacement under pressure loading for sandwich plate (b) under top and bottom close circuit conditions

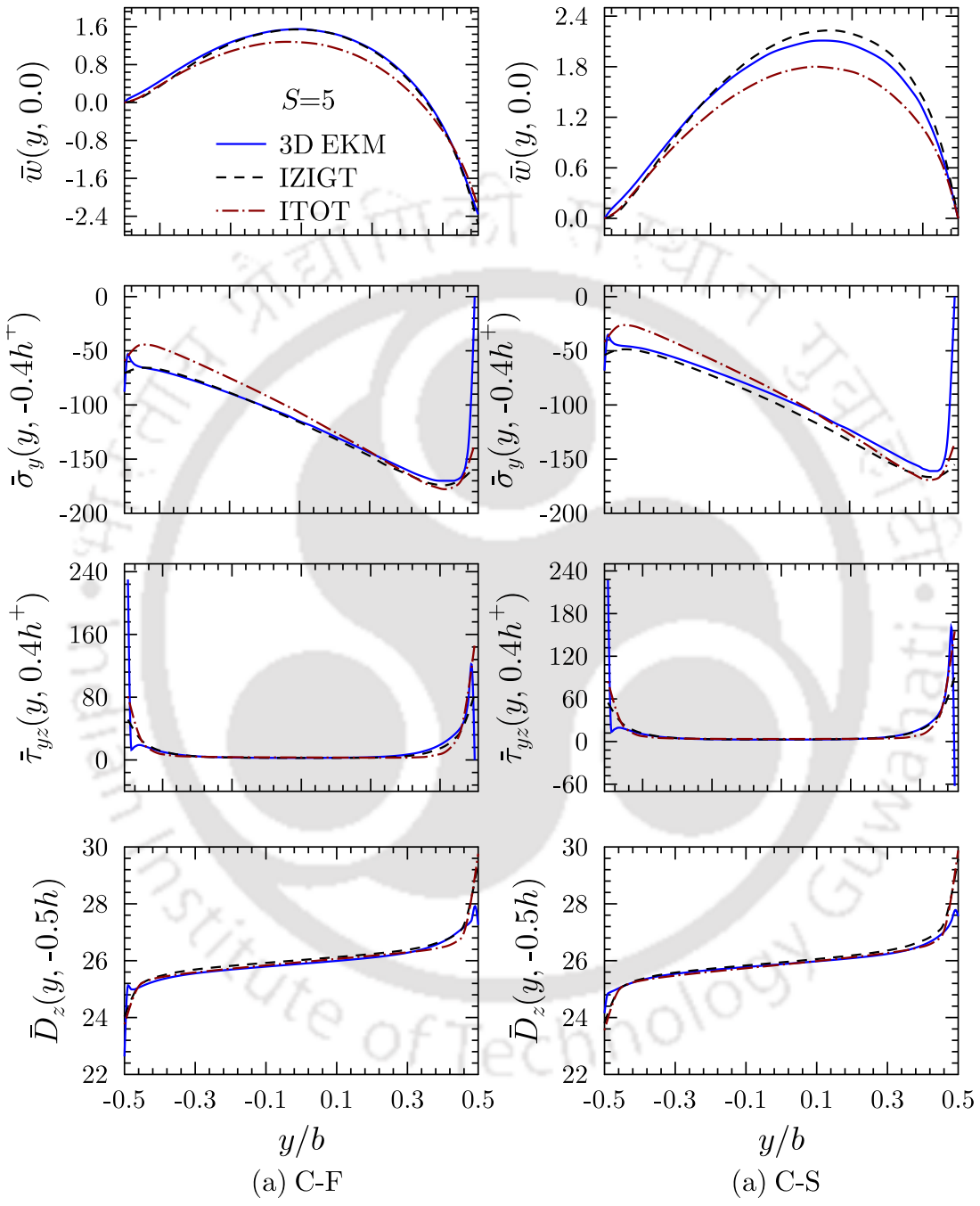

Figure 6.7: Longitudinal variation of deflection, stresses and electric displacements under potential loading for sandwich plate (b) under top and bottom close circuit conditions

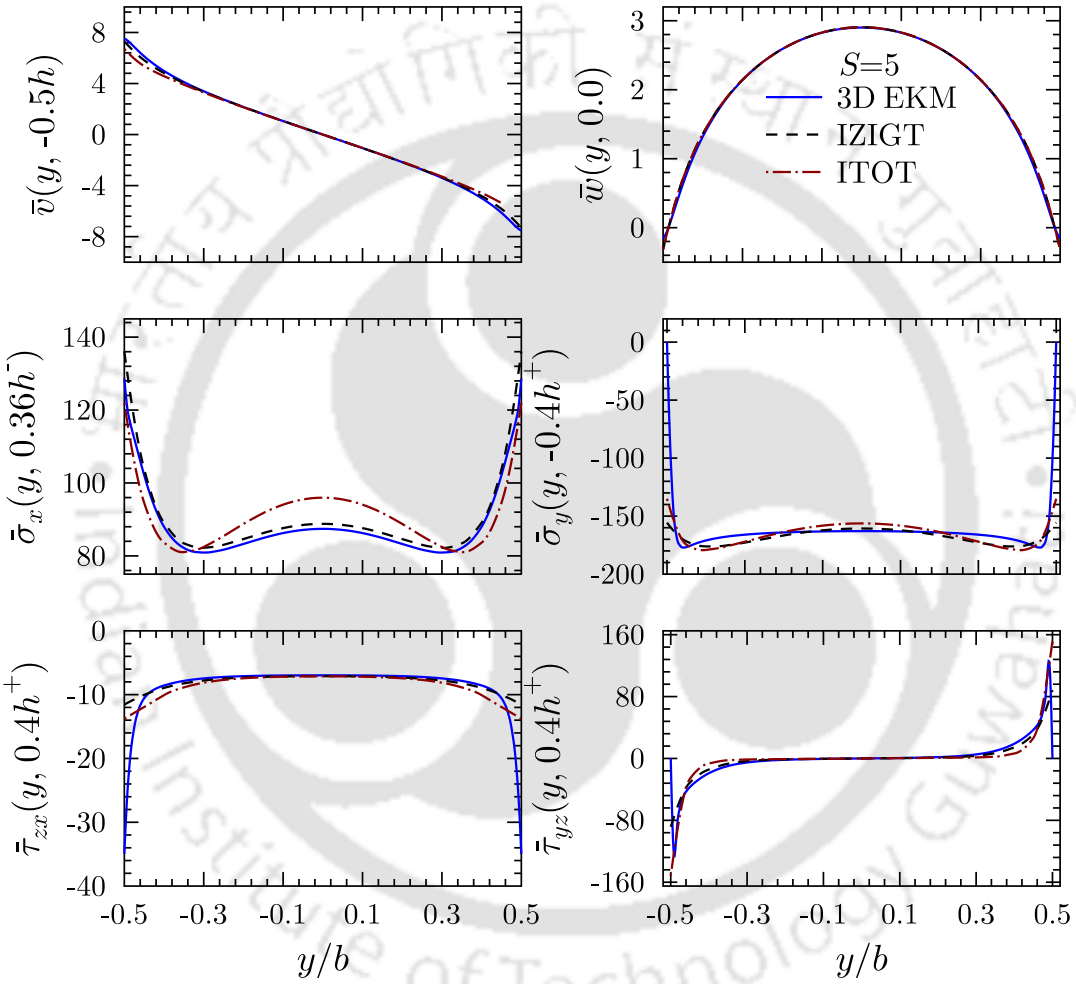

Figure 6.8: Longitudinal variation of displacements and stresses under potential loading for sandwich plate (b) with F-F boundary conditions under top and bottom close circuit conditions

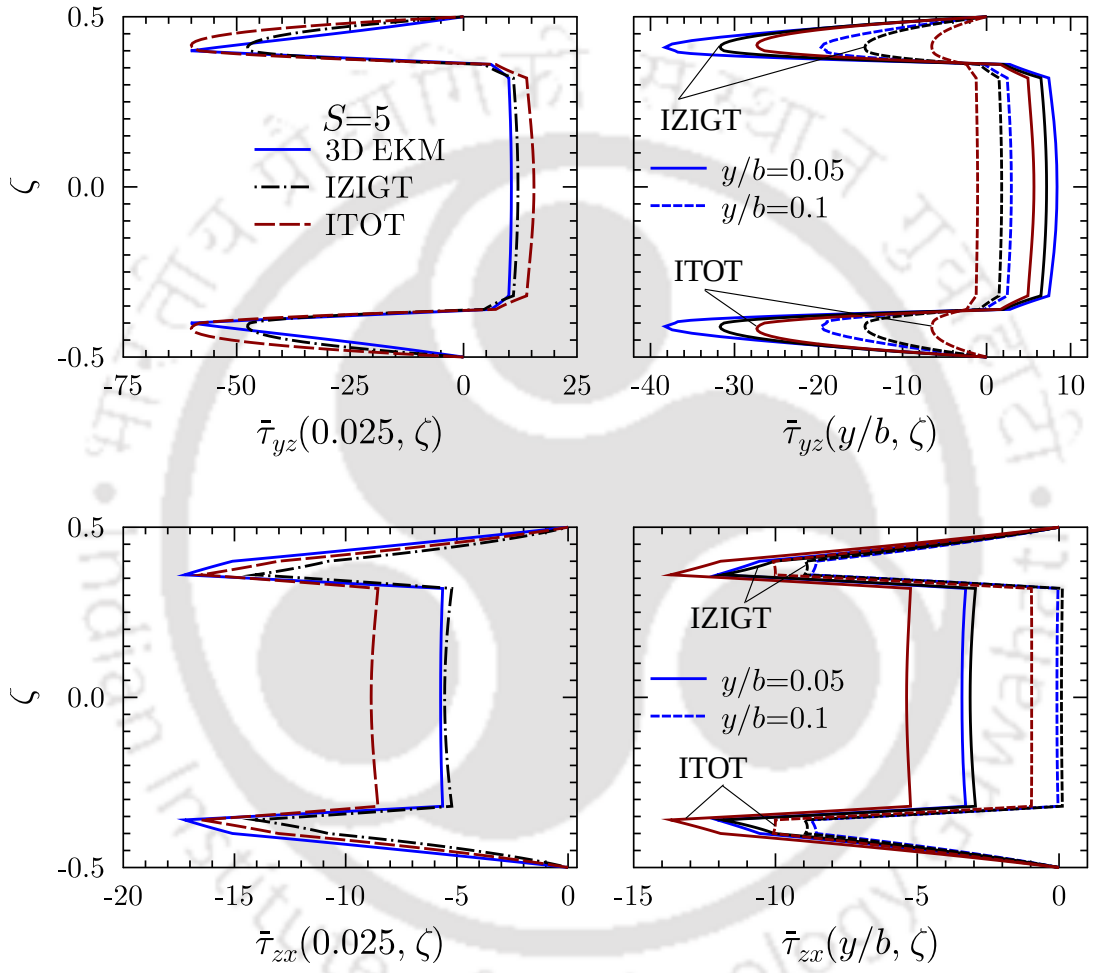

Figure 6.9: Through-thickness variation of transverse shear stresses under potential loading for sandwich plate (b) with free-free boundary conditions under top and bottom close circuit conditions

6.4 FREE VIBRATION ANALYSIS OF RECTANGULAR HYBRID PLATES

In this section, the accuracy of the 2D theories in free vibration of hybrid plates is assessed by comparing the results with 3D piezoelasticity EKM solutions presented in Chapter 4. Unless mentioned otherwise, the non-dimensional frequency parameter $\bar{\omega}$ considered in the present analysis is as follows: $\bar{\omega} = \omega_m a S \sqrt{\rho_0 / Y_2}$, where ω_m is the calculated frequency, $S = a/h$, is the span-to-thickness ratio, ρ_0 is the mass density in Kg/m^3 and Y_2 is the minor elastic modulus in N/m^2.

6.4.1 Validation

The frequencies predicted by the advanced 2D theories IZIGT and ITOT are compared with the 3D exact and 3D EKM results for validation purpose. Table 6.8 presents the frequencies for hybrid sandwich plate (Fig. 6.10) for S-S boundary condition. The material properties of all the layers are given in Table 4.1. The piezoelectric-elastic layer interfaces along with the top surface of the top piezoelectric layer are electrically grounded and the bottom surface of the bottom piezoelectric layer is kept in open circuit condition. As can be seen from the table that IZIGT results are more closer to accurate 3D results while the ITOT results are far away from the accurate 3D results. As we move from thick to thin plates the accuracy of the 2D theories increase and for plate with S=1000, 2D theories almost predict accurate results.

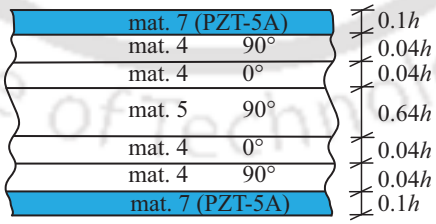

Figure 6.10: Configurations of smart composite plate.

Table 6.8: Natural flexural frequencies of simply supported (S-S) hybrid plate (b) with different S values

S	Entity	IZIGT	ITOT	3D EKM[164]	3D Exact[167]
5	ω_{11}	4.4866	5.5113	4.5233	4.5233
	ω_{21}	7.9003	9.6754	7.8958	7.8958
	ω_{22}	10.377	12.550	10.292	10.292
	ω_{31}	12.078	14.375	11.837	11.837
10	ω_{11}	7.2033	8.2553	7.3390	7.3390
	ω_{21}	13.733	16.464	13.880	13.880
	ω_{22}	17.947	22.044	18.093	18.093
	ω_{31}	21.114	25.814	21.231	21.231
20	ω_{11}	9.4685	10.016	9.7440	9.7440
	ω_{21}	21.250	23.174	21.357	21.357
	ω_{22}	28.813	33.021	29.356	29.356
	ω_{31}	35.169	40.690	35.693	35.693
1000	ω_{11}	10.931	10.931	11.337	11.337
	ω_{21}	27.837	27.839	28.836	28.836
	ω_{22}	43.715	43.720	45.336	45.336
	ω_{31}	56.723	56.734	58.690	58.690

6.4.2 Assessment

The accuracy of the advanced 2D theories IZIGT and ITOT are assessed with a comparison to 3D piezoelasticity based EKM solution for hybrid composite (a) and sandwich plate (b), as shown in Fig. 6.11, in predicting the free vibration response. The material properties of the plates mentioned in Fig. 6.11 are given in Table 4.1. All the plates considered are having a span, a=1m. The interfaces between the piezoelectric layer and elastic substrate and the top surface of the top piezoelectric layer are electrically grounded (ϕ=0). The bottom surface of the bottom piezoelectric layer is kept electrically open (D_z=0).

The lowest five flexural frequencies in percentage errors with respect to the 3D EKM results of hybrid composite plate (a) are presented for S value of 5, 10 and 20 for various boundary conditions in Table 6.9. It is seen from the table that the prediction of natural frequencies by IZIGT and ITOT are highly erroneous. However, IZIGT results are in overall superior than the ITOT results for all types of boundary conditions. Similarly, the lowest five flexural frequencies for hybrid sandwich plate (b) are presented in Table 6.10 for S= 5, 10 and 20 for various boundary conditions. In this case also the IZIGT predictions are far superior than the ITOT predictions. The ITOT predictions are highly erroneous and the error percentage is highest for C-C boundary condition.

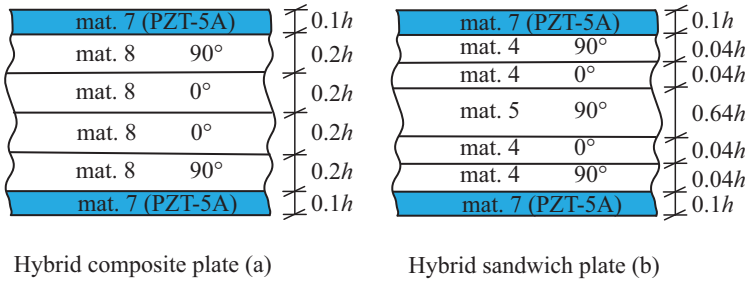

Figure 6.11: Configurations of smart composite plate (a) and smart sandwich plate (b).

6.5 CONCLUSIONS

The assessment of 2D zigzag and third order theories for the free vibration of elastic laminated and static/free vibration of hybrid laminated plates have been carried out for different cross-ply lay-ups and electromechanical boundary conditions. The analysis reveals that:

- The 2D theories predict accurate frequencies for the simply supported case, but for other boundary conditions, 2D theories predict erroneous results even in the first mode frequency. The percentage error is observed maximum for C-C boundary condition for all plate configurations. The error in the ZIGT results for natural frequencies is large for thicker plates.
- It is observed that TOT produces better natural frequencies than ZIGT for symmetric laminates, but for unsymmetrical laminated and sandwich plates, ZIGT predicts the frequency for different boundary conditions within 3% error with respect to 3D elasticity solution while TOT gives 10 % error.

Table 6.9: The percentage errors of lowest five flexural natural frequencies of IZIGT and ITOT with respect to 3D EKM for a square hybrid composite plate (a) under five different boundary conditions for S=5, 10 and 20

		S-S			C-C			C-S			C-F			F-F		
S	Mode	3D EKM [164]	IZIGT % error	ITOT % error	3D EKM [164]	IZIGT % error	ITOT % error	3D EKM [164]	IZIGT % error	ITOT % error	3D EKM [164]	IZIGT % error	ITOT % error	3D EKM [164]	IZIGT % error	ITOT % error
5	1	7.181	-1.84	2.29	7.887	2.73	5.66	7.476	0.70	4.38	4.715	2.12	3.92	4.028	-1.13	-0.34
	2	13.594	-1.03	4.52	14.018	1.64	4.02	13.901	0.78	3.61	9.449	3.37	6.93	5.514	1.97	4.42
	3	13.821	-0.10	3.08	14.150	6.53	7.81	13.838	2.89	6.49	12.284	1.71	3.43	11.314	6.72	8.15
	4	18.367	-0.28	4.58	18.713	4.29	6.55	18.514	2.00	5.68	15.409	2.16	5.62	11.851	0.99	6.11
	5	20.931	0.47	3.84	21.680	3.87	6.11	21.160	4.98	6.02	16.202	5.82	9.03	13.081	1.73	4.31
10	1	9.369	-2.32	-0.27	11.589	3.22	7.37	10.551	-0.57	2.61	5.651	0.95	1.97	4.532	-0.29	-1.20
	2	19.614	-2.15	-0.30	20.427	-0.52	1.80	20.000	-1.40	0.68	13.601	2.43	5.96	6.706	-0.51	0.52
	3	21.236	-1.40	3.64	23.266	2.24	6.93	22.251	0.63	5.60	16.956	-1.29	-0.21	16.120	-0.84	-0.01
	4	28.724	-1.84	2.29	29.903	0.70	4.38	29.292	-0.50	3.46	22.849	-0.33	2.33	16.659	-0.34	2.55
	5	34.047	-1.05	0.90	34.352	-0.52	1.45	34.187	-0.79	1.18	26.523	1.64	6.39	17.666	2.27	3.71
20	1	10.433	-2.54	-1.87	15.723	-0.81	1.57	12.830	-1.49	-0.02	6.059	0.68	1.08	4.727	-2.18	-2.09
	2	22.930	-2.92	-2.25	25.333	-1.19	0.30	24.007	-2.16	-1.15	17.450	-0.93	0.87	7.169	-0.82	-0.42
	3	27.833	-1.61	0.75	34.516	0.51	4.45	31.336	-0.81	2.39	19.164	-0.95	-0.95	18.352	-2.28	-1.97
	4	37.474	-2.32	-0.27	42.574	-1.43	1.73	40.042	-1.97	0.66	28.383	-1.14	0.33	19.542	-1.04	0.06
	5	43.185	-2.58	-1.71	44.202	-1.74	-0.58	43.650	-2.20	-1.21	37.857	-0.58	2.69	20.958	-1.45	-0.90

Table 6.10: The percentage errors of lowest five flexural natural frequencies of IZIGT and ITOT with respect to 3D EKM for a square hybrid sandwich plate (b) under five different boundary conditions for S=5, 10 and 20

		S-S			C-C			C-S			C-F			F-F		
		3D EKM	IZIGT	ITOT	3D EKM	IZIGT	ITOT	3D EKM	IZIGT	ITOT	3D EKM	IZIGT	ITOT	3D EKM	IZIGT	ITOT
S	Mode	[164]	% error	% error	[164]	% error	% error	[164]	% error	% error	[164]	% error	% error	[164]	% error	% error
5	1	4.523	-0.81	21.8	4.772	3.00	24.7	4.599	1.77	24.2	3.219	1.40	23.8	2.794	-0.58	23.1
	2	7.700	0.06	23.4	7.776	1.88	24.4	7.721	1.09	24.1	5.885	2.90	22.8	3.902	0.59	20.0
	3	7.896	0.06	22.5	8.154	7.27	25.8	7.995	3.88	24.7	6.850	0.77	25.1	6.609	0.05	25.0
	4	10.292	0.83	21.9	10.497	5.24	23.8	10.370	3.11	23.1	8.690	3.40	24.7	7.269	1.89	22.4
	5	11.837	2.05	19.4	11.864	3.13	20.0	11.846	2.59	19.8	9.588	4.99	24.0	7.480	1.15	24.0
10	1	7.339	-1.85	12.5	8.113	1.24	19.4	7.703	-0.30	16.1	4.788	3.79	17.4	4.234	-0.99	11.7
	2	13.252	-1.18	21.5	13.489	-0.16	22.9	13.356	-0.63	22.2	9.755	0.81	17.3	5.864	-0.02	12.7
	3	13.880	-1.06	18.6	14.397	3.03	23.4	14.129	1.13	21.3	11.668	-3.73	19.3	11.235	-0.75	22.9
	4	18.093	-0.81	21.8	18.396	1.77	24.2	18.232	0.52	23.1	15.063	0.44	22.3	11.997	-0.38	14.4
	5	20.154	-0.73	24.6	20.216	-0.16	25.2	20.182	-0.45	24.9	16.736	2.13	21.7	12.614	-0.10	22.0
20	1	9.744	-2.83	2.79	12.269	-0.80	9.67	10.929	-1.79	6.06	6.265	-0.05	5.10	5.240	-1.45	3.00
	2	20.459	-2.11	10.7	21.322	-1.16	12.7	20.866	-1.68	11.6	14.087	-0.24	8.83	7.433	-0.47	4.83
	3	21.357	-2.05	8.51	23.955	0.26	15.5	22.697	-0.83	12.2	17.759	-0.91	8.48	16.521	-1.43	5.49
	4	29.356	-1.85	12.5	30.813	-0.30	16.1	30.081	-1.06	14.3	23.676	-0.89	12.7	17.073	-1.22	11.6
	5	33.561	-1.57	9.76	33.902	-1.18	18.3	33.558	-0.90	9.77	27.021	-0.42	12.8	18.732	1.14	14.1

- As the inplane elastic modulus ratio decreases, thereby making the plate material closer to isotropic condition, the frequency percentage errors of 2D theories with respect to the 3D EKM also decrease.

- The comparison of displacement and stresses for sandwich plate shows that ZIGT predicts quite accurately than the TOT for S-S case, but for C-C and C-F cases both theories estimate highly erroneous results. The displacement profile predicted by TOT is far from the exact prediction.

- Stresses predicted by the IZIGT and also by ITOT are not accurate in the close vicinity of the clamped support in the pressure load case, and near the clamped, soft-simply supported and free supports in case of potential loading case.

- 2D theories also prove to be inefficient in predicting stress which does not satisfy the zero stress condition at the simply supported and free edges for potential loading case.

- The natural frequencies predicted by the 2D theories for hybrid composite and sandwich plates are highly erroneous. For hybrid composite and sandwich plates IZIGT results are superior than the ITOT results in overall for all type of boundary conditions. For sandwich plates ITOT results are highly erroneous.

The natural frequencies tabulated in this chapter will be handy for the research community to evaluate the accuracy of the different finite element models and 2D laminate theories. The present zig-zag theory can be recommended for dynamic analysis of composite and sandwich plates for its firmness, accuracy and reasonable computational efficiency.

Chapter 7

Conclusions

7.1 CONCLUSIONS FROM THE PRESENT WORK

The major outcomes of this research work and the scope for future research are summarized in this Chapter. Here, the major conclusions are encapsulated as follows:

1. The static coupled 3D piezoelasticity solution for edge effects in Levy-type rectangular piezolaminated plates using the mixed field extended Kantorovich method under pressure as well as electric potential loading reveals that:

   (i) The 3D EKM solution converges within just two/three terms in the trial functions, for both single layer piezoelectric and hybrid plates under electromechanical loading.

   (ii) The present method is accurate in predicting the free edge stresses near the edges which is established by comparing its order of singularity at the interface of a long bi-material strip with the available analytical solution.

   (iii) The nature of through-thickness distributions of displacements and stresses change depending on the x-location and thickness ratio. The distribution of in-plane stresses in the piezoelectric layer is dependent on the aspect ratio (b/a).

   (iv) It is revealed that the load transfer takes place over a small range from the edge of the actuator, leading to a very large interlaminar shear stress near the edge. The nature of its variation along the interface is similar for the simply-supported and free edge conditions. The simply supported and the free edges show a singularity in the peel stress $\bar{\sigma}_z$ which may lead to de-bonding, whereas the clamped edge does not show the same behaviour.

(v) The use of adhesive as binding agent between layers in piezolaminated composites helped to smoothen the interlaminar stress concentrations for pressure loading, but for potential loading case, the interfacial and central values of interlaminar stresses slightly increase with adhesive layer thickness. The low elastic modulus adhesives significantly reduce the interlaminar stresses for both pressure and potential load cases.

2. The 3D free vibration analysis of Levy-type elastic laminated plates using multi-term extended Kantorovich method for various boundary conditions led to following conclusions:

   (i) It can predict natural frequencies for very thick plates accurately for symmetric and un-symmetric laminates as compared with the 3D exact solution.

   (ii) As the in-plane modulus ratio Y_1/Y_2 increases (keeping Y_2 constant) the frequency parameter increase significantly because the overall plate stiffness increases.

   (iii) Thickness stretching mode generally occurs at higher modes as seen to occur at eighth mode for S-S and C-C case for thick sandwich plate $S = 5$.

   (iv) The benchmark natural frequencies, mode shapes, stresses and displacements profiles presented for composite and sandwich plates would serve as valuable assets for further scientific investigation and assessment of numerical 3D solutions and 2D theories.

   (v) Using adhesive as binding agent in composite plates lowers the frequency response. As the adhesive thickness increases, the frequency of the plate decreases. There is significant decrement in the natural frequencies of plates at higher modes.

   (vi) Increasing the adhesive modulus, increases the plate natural frequency thereby stabilize the structures whereas as the variation of adhesive density has negligible effect on plate natural frequency.

3. The results of the 3D piezoelasticity solution for the free vibration analysis of Levy-type piezolaminated plates using the EKM for arbitrary boundary conditions leads to the following inferences.

   (i) The benchmark natural frequencies presented herein for hybrid bimorph plates, hybrid test plates with cross-ply composite and sandwich substrates cover a wide range

of possible cases, which would be useful for assessing numerical 3D solutions and 2D theories for hybrid plates.

(ii) The varying piezoelectric layer thickness has significant effect on the natural frequencies of thick hybrid sandwich plates. The thicker piezoelectric layers help drop the plate natural frequencies, while on the other hand the thin piezoelectric layers raise the fundamental frequencies thereby stabilize the structure.

(iii) Using adhesives as binding agent reduces the natural frequencies of piezoelectric bimorph plates. The increase of adhesive thickness lowers the natural frequencies for all types of boundary conditions. The increase in adhesive elastic modulus reduces the natural frequencies of the bimorph plate. The denser adhesives facilitate increasing the natural frequencies as can be seen for S-S and F-F cases.

4. Assessment of the advanced 2D laminate theories with the 3D elasticity/piezoelasticity solution for static and free vibration response of Levy-type rectangular elastic and piezo-laminated plates for different mechanical and electrical boundary conditions reveal that:

(i) The error in the prediction of natural frequencies of elastic composite plates by ZIGT and TOT are large for thicker plates. For thin plates 2D theories predict natural frequencies quite accurately.

(ii) Displacement and stress assessment show that ZIGT results are more closer to the accurate 3D solution than the TOT results.

(iii) The TOT results are marginally superior than the ZIGT for elastic composite laminated plates, but for sandwich plates ZIGT yields marginally accurate results than the TOT. The 2D theories are quite accurate and competent for thin plates, but for thick plates 2D theories may not be recommended for practical design and analysis.

(iv) From the predictions of static piezoelasticity response it is observed that the IZIGT and ITOT are not able to predict the sharp variation of stresses at the edges or at the piezo-elastic layer interface accurately as have been observed for C-S, C-F and F-F boundary conditions. However, IZIGT predictions are superior than the ITOT predictions in all the cases investigated.

(v) Stresses predicted by the IZIGT and also by ITOT are not accurate in the close vicinity of the clamped support in the pressure load case, and near the clamped,

soft-simply supported and free supports in case of potential loading case.

(vi) The prediction of natural frequencies of hybrid plates by both the IZIGT and ITOT are highly erroneous with IZIGT results being superior in overall than the ITOT results. For hybrid sandwich plates ITOT predictions of natural frequencies are highly erroneous.

7.2 FUTURE SCOPE OF WORK

The multi-term multi-field 3D EKM which has been used for the static and free vibration analysis of elastic/hybrid rectangular plates can be extended on the following aspects for the future studies:

1. The present 3D elasticity/piezoelasticity solution can be extended to the thermoelectromechanical analysis of elastic/hybrid plates of different plate geometry incorporating geometrical complexity.
2. Buckling and transient vibration analysis of Levy-type rectangular plate can be developed based on the 3D EKM.
3. The present 3D EKM can be extended to develop methodologies to analyze the stress singular problems.
4. Methods can be developed to analyze the static and dynamic behaviour of shell structures based on 3D EKM.
5. The effect of presence of electrodes on piezoelectric layers on the static and dynamic response of plate can be studied in future.

In the present work, the material damping is not considered. The present work can be extended by considering material damping/ shunting the piezoelectric layers for effective vibration control. Loss factor associated to stiffness and mass can be considered to calculate the effective damping coefficient (extra matrix corresponding to damping matrix). Viscoelastic material model may be used for analyzing the material damping and its effect on vibration can be studied.

Bibliography

[1] K Uchino. *Ferroelectric Devices*. Marcel Dekker Inc, New York, 2000.

[2] M Karama, M Touratier, and A Idlbi. An evaluation of the edge solution for a higher-order laminated plate theory. *Composite Structures*, 25:495–502, 1993.

[3] R B Pipes and N J Pagano. Interlaminar stresses in composite laminates under uniform axial extension. *Journal of Composite Materials*, 4(4):538–548, 1970.

[4] T Hayashi. Analytical study of interlaminar shear stresses in a laminated composite plate. *Transactions of the Japan Society for Aeronautical and Space Sciences*, 10:43–48, 1967.

[5] W Kaplan. Review of Approximate methods of higher analysis by L. V. Kantorovich and V. I. Krylov. *Bulletin of the American Mathematical Society*, 66(3):146–147, 1960. doi: 10.1090/S0002-9904-1960-10408-9.

[6] L V Kantorovich and V I Krylov. *Approximate Methods of Higher Analysis*. Interscience Publishers, New York, 1958.

[7] A D Kerr. An extension of the Kantorovich method. *Quarterly of Applied Mathematics*, 26(2):219–229, 1968.

[8] E A Shahrbabaki and A Alibeigloo. A review of the literature on finite element modelling of composite plates. *Shock and Vibration Digest*, 17:3–8, 1985.

[9] R K Kapania and S Raciti. Recent advances in analysis of laminated beams and plates, Part I: Shear effects and buckling. *AIAA Journal*, 27:923–934, 1989.

[10] R K Kapania and S Raciti. Recent advances in analysis of laminated beams and plates, Part II: Vibration and wave propagation. *AIAA Journal*, 27:935–946, 1989.

[11] E Carrera. Developments, ideas and evaluations based upon Reissner's mixed variational theorem in the modelling of multi layered plates and shells. *Applied Mechanics Reviews*, 54:301–329, 2001.

[12] K M Liew, Y Xiang, and S Kitipornchai. Research on thick plate vibration: A literature survey. *Journal of Sound and Vibration*, 180(1):163–173, 1995.

[13] Y Y Yu. Some recent advances in linear and nonlinear dynamical modeling of elastic and piezoelectric plates. *Journal of Intelligent Material Systems and Structures*, 6:237–254, 1995.

[14] C Y K Chee, L Tong, and G P Steven. A review on the modeling of piezoelectric sensors and actuators incorporated in intelligent structures. *Journal of Intelligent Material Systems and Structures*, 9:3–19, 1998.

[15] D A Saravanos and P Heyliger. Mechanics and computational models for laminated piezoelectric beams, plates and shells. *Applied Mechanics Reviews*, 98:1547–1557, 1999.

[16] S V Gopinathan, V V Varadan, and V K Vardhan. A review and critique of theories for piezoelectric laminates. *Smart Materials and Structures*, 10:229–239, 2000.

[17] T R Tauchert, F Ashida, N Noda, S Adali, and V Verijenko. Developments in thermopiezoelasticity with relevance to smart composite structures. *Composite Structures*, 48 (1):31–38, 2000.

[18] C P Wu, K H Chiu, and Y M Wang. A review on the three-dimensional analytical approaches of multilayered and functionally graded piezoelectric plates and shells. *Computers, Materials & Continua*, 8(2):93–132, 2008.

[19] S Kapuria, P Kumari, and J K Nath. Efficient modeling of smart piezoelectric composite laminates: a review. *Acta Mechanica*, 214(1):31–48, 2010.

[20] C P Wu and Y C Liu. A review of semi-analytical numerical methods for laminated composite and multilayered functionally graded elastic/piezoelectric plates and shells. *Composite Structures*, 147:1–15, 2016.

[21] P Singhatanadgid and T Singhanart. The Kantorovich method applied to bending, buckling, vibration, and 3D stress analyses of plates: A literature review. *Mechanics of Advanced Materials and Structures*, 2017. doi: 10.1080/15376494.2017.1365984.

[22] A S Sayyad and Y M Ghugal. On the free vibration analysis of laminated composite and sandwich plates: A review of recent literature with some numerical results. *Composite Structures*, 129:177–201, 2015.

[23] S Hanagud, M W Obal, and A J Calises. Optimal vibration control by the use of piezoceramic sensors and actuators. *Journal of Guidance, Control, and Dynamics*, 15(5):1199–1206, 1992.

[24] A Baz and S Poh. Performance of an active control systemwith piezoelectric actuators. *Journal of Sound and Vibration*, 126(2):327–43, 1988.

[25] D H Robbins and J N Reddy. Analysis of piezoelectrically actuated beams using a layerwise displacement theory. *Computers and Structures*, 41(2):265–279, 1991.

[26] T R Tauchert. Piezothermoelastic behavior of a laminated plate. *Journal of Thermal Stresses*, 15(1):25–37, 1992.

[27] K Chandrashekhara and A N Agarwal. Active vibration control of laminated composite plates using piezoelectric devices: A finite element approach. *Journal of Intelligent Material Systems and Structures*, 4(4):496–508, 1993.

[28] R C Batra, X Q Liang, and J S Yang. The vibration of a simply supported rectangular elastic plate due to piezoelectric actuators. *International Journal of Solids and Structures*, 33(11):1597–1618, 1996.

[29] H S Tzou and J P Zhong. Electromechanics and vibrations of piezoelectric shell distributed systems. *Journal of Dynamic Systems, Measurement and Control, Transactions of the ASME*, 115(3):506–517, 1993.

[30] M C Ray, R Bhattacharya, and B Samanta. Exact solutions for static analysis of intelligent structures. *AIAA Journal*, 31(9):1684–1691, 1993.

[31] M C Ray, K M Rao, and B Samanta. Exact solution for static analysis of an intelligent structure under cylindrical bending. *Computers and Structures*, 47(6):1031–1042, 1993.

[32] P Bisegna and F Maceri. An exact three-dimensional solution for simply supported rectangular piezoelectric plates. *Journal of Applied Mechanics, Transactions ASME*, 63(3): 628–638, 1996.

[33] R Chandra and I Chopra. Structural modeling of composite beams with induced-strain actuators. *AIAA Journal*, 31(9):1692–1701, 1993.

[34] P Heyliger. Static behavior of laminated elastic/piezoelectric plates. *AIAA Journal*, 32 (12):2481–2484, 1994.

[35] H S Tzou and H Q Fu. A study of segmentation of distributed piezoelectric sensors and actuators, part i: Theoretical analysis. *Journal of Sound and Vibration*, 172(2):247–259, 1994.

[36] K Ghosh and R C Batra. Shape control of plates using piezoceramic elements. *AIAA Journal*, 33(7):1354–1357, 1995.

[37] K Xu, A K Noor, and Y Y Tang. Three-dimensional solutions for coupled thermoelectroelastic response of multilayered plates. *Computer Methods in Applied Mechanics and Engineering*, 126(3-4):355–371, 1995.

[38] D A Saravanos and D A Hopkins. Local stresses in composite plates with piezoelectric actuators and sensors using a discrete-layer theory. 1995.

[39] F Ashida and N Noda. Control of thermally induced normal elastic displacement of an isotropic plate bonded to a piezoelectric ceramic plate. *Transactions of the Japan Society of Mechanical Engineers, Part A*, 63(613):1947–1954, 1997.

[40] P C Dumir, G P Dube, , and S Kapuria. Exact piezoelastic solution of simply-supported orthotropic circular cylindrical panel in cylindrical bending. *International Journal of Solids and Structures*, 34(6):685–702, 1997.

[41] S Kapuria and P Kumari. Multiterm extended Kantorovich method for three dimensional elasticity solution of laminated plates. *Journal of Applied Mechanics*, 79(6):061018, 2012.

[42] N J Pagano and R B Pipes. Some observations on interlaminar strength of composite laminates. *International Journal of Mechanical Sciences*, 15:679–688, 1973.

[43] E F Crawley and J D Luis. Use of piezoelectric actuators as elements of intelligent structures. *AIAA Journal*, 25(10):1373–1385, 1987.

[44] V Giurgiutiu and G Bottai-Santoni. Extension of the shear-lag solution for structurally attached ultrasonic active sensors. *AIAA Journal*, 47:1980–1983, 2009.

[45] P Tong and T H H Pian. On the convergence of the finite element method for problems with singularity. *International Journal of Solids and Structures*, 9(3):313–321, 1973.

[46] H Y Sheng, H Wang, and J Q Ye. State space solution for thick laminated piezoelectric plates with clamped and electric open-circuited boundary conditions. *International Journal of Mechanical Sciences*, 49(7):806–818, 2007.

[47] C Mittelstedt and W Becker. Free-edge effects in composite laminates. *Applied Mechanics Reviews*, 60(5):217–224, 2007.

[48] S S Vel and R C Batra. Cylindrical bending of laminated plates with distributed and segmented piezoelectric actuators/sensors. *AIAA Journal*, 38:857–867, 2000.

[49] S S Vel and R C Batra. Three-dimensional analytical solution for hybrid multilayered piezoelectric plates. *Journal of Applied Mechanics*, 67(3):558–567, 2000.

[50] M Tahani and A Andakhshideh. Interlaminar stresses in thick rectangular laminated plates with arbitrary laminations and boundary conditions under transverse loads. *Composite Structres*, 94:1793–1804, 2012.

[51] G Flanagan. An efficient stress function approximation for free-edge stresses in lamitates. *International Journal of Solids and Structures*, 31:941–952, 1994.

[52] B Huang and H S Kim. Free-edge interlaminar stress analysis of piezo-bonded composite laminates under symmetric electric excitation. *International Journal of Solids and Structures*, 51(6):1246–1252, 2014.

[53] A D Kerr. An extended Kantorovich method for the solution of eigenvalue problems. *International Journal of Solids and Structures*, 5(6):559–572, 1969.

[54] M Dalaei and A D Kerr. Natural vibration analysis of clamped rectangular orthotropic plates. *Journal of Sound and Vibration*, 189(3):399–406, 1996.

[55] K Naumenko, J Altenbach, H Altenbach, and V K Naumenko. Closed and approximate analytical solutions for rectangular Mindline plates. *Acta Mechanica*, 147:153–172, 2001.

[56] V Ungbhakorn and N Wattanasakulpong. Bending analysis of symmetrically laminated rectanular plates with arbitrary edge supports by the extended Kantorovich method. *Thammasat International Journal of Science and Technology*, 11:33–44, 2006.

[57] I Shufrin, O Rabinovitch, and M Eisenberger. A semi-analytical approach for the non-linear large deflection analysis of laminated rectangular plates under general out-of-plane loading. *International Journal of Non-Linear Mechanics*, 43:328–340, 2008.

[58] M M Aghdam and M Mohammadi. Bending analysis of thick orthotropic sector plates with various loading and boundary conditions. *Composite Structres*, 88:212–218, 2009.

[59] A M Naserian-Nik and M Tahani. Analytical solutions for bending analysis of rectangular laminated plates with arbitrary lamination and boundary conditions. *Journal of Mechanical Science and Technology*, 23:2253–2267, 2009.

[60] F Alijani and M M Aghdam. A semi-analytical solution for stress analysis of moderately thick laminated cylindrical shells with various boundary conditions. *Composite Structres*, 89:534–550, 2009.

[61] A Fereidoon, A Mohyeddin, M Sheikhi, and H Rahmani. Bending analysis of functionally graded annular sector plates by extended Kantorovich method. *Composites Part B: Engineering*, 43:2172–2179, 2012.

[62] A Bigdeli and M M Aghdam. A semianalytical solution for the bending of clamped laminated doubly curved or spherical panels. *Journal of Mechanics of Materials and Structures*, 5:855–873, 2010.

[63] R A Rahbar and H H Rostami. A semi-analytical technique for bending analysis of cylindrical panels with general loading and boundary conditions. *Journal of Mechanical Science and Technology*, 26:1711–1718, 2012.

[64] E A Lucy and H Abramovich. Piezolaminated plates-Highly accurate solution based on the extended Kantorovich method. *Composite Structres*, 84:241–247, 2008.

[65] M Tahani and A M Naserian-Nik. Bending analysis of piezolaminated rectangular plates under electromechanical loadings using multi-term extended Kantorovich method. *Mechanics of Advanced Materials and Structures*, 20(6):415–433, 2013.

[66] S Kapuria and P Kumari. Extended Kantorovich method for three-dimensional elasticity solution of laminated composite structures in cylindrical bending. *Journal of Applied Mechanics*, 78(6):061004, 2011.

[67] S Kapuria and P Kumari. Extended Kantorovich method for coupled piezoelasticity solution of piezolaminated plates showing edge effects. *Proceedings of the Royal Society A: Mathematical, Physical and Engineering Sciences*, 469(2151):20120565, 2013.

[68] P Kumari, S Kapuria, and R K N D Rajapakse. Three-dimensional extended Kantorovich solution for Levy-type rectangular laminated plates with edge effects. *Composite Structres*, 107:167–176, 2013.

[69] A W Leissa. *Vibration of Plates*. NASA SP-160, Washington, D.C.: Office of Technology Utilization, 1969.

[70] R D Mindlin. *An Introduction to the Mathematical Theory of Vibrations of Elastic Plates*. World Scientific Publishing Co. Pte. Ltd., Singapore, 2006.

[71] K M Liew. Solving the vibration of thick symmetric laminates by Reissner/Mindlin plate theory and the p-Ritz method. *Journal of Sound and Vibration*, 198(3):343–360, 1996.

[72] J N Reddy. Free vibration of antisymmetric, angle ply laminated plates including transverse shear deformation by the finite element method. *Journal of Sound and Vibration*, 66(4):565—-576, 1979.

[73] A K Noor and W S Burton. Stress and free vibration analyses of multilayered composite plates. *Composite Structures*, 11(3):183—-204, 1989.

[74] A M Naserian-Nik and M Tahani. Free vibration analysis of moderately thick rectangular laminated composite plates with arbitrary boundary conditions. *Structural Engineering and Mechanics*, 35(2):217–240, 2010.

[75] A A Khdeir and L Librescu. Analysis of symmetric cross-ply laminated elastic plates using a higher-order theory: Part II-Buckling and free vibration. *Composite Structures*, 9: 259–277, 1988.

[76] C P Wu and W Y Chen. Vibration and stability of laminated plates based on a local high order plate theory. *Journal of Sound Vibration*, 177(4):503–520, 1994.

[77] H Matsunaga. Vibration and stability of cross-ply laminated composite plates according to a global higher-order plate theory. *Composite Structures*, 48(4):231–244, 2000.

[78] J N Reddy. *Mechanics of Laminated Composite Plates and Shells: Theory and Analysis*. CRC Press, 2003.

[79] M S Qatu. *Vibration of Laminated Shells and Plates*. Elsevier Ltd., UK, 2004.

[80] H Zuo, Z Yang, X Chen, Y Xie, and H Miao. Analysis of laminated composite plates using wavelet finite element method and higher-order plate theory. *Composite Structures*, 131: 248–258, 2015.

[81] F A Fazzolari, M Boscolo, and J R Banerjee. An exact dynamic stiffness element using a higher order shear deformation theory for free vibration analysis of composite plate assemblies. *Composite Structures*, 96:262–278, 2013.

[82] M Boscolo and J R Banerjee. Layer-wise dynamic stiffness solution for free vibration analysis of laminated composite plates. *Journal of Sound and Vibration*, 333(1):200–227, 2014.

[83] Y Qu, G Yuan, S Wu, and G M State. A three-dimensional free vibration analysis of cross-ply laminated rectangular plates with clamped edges. *European Journal of Mechanics-A/Solids*, 42:376—-394, 2013.

[84] Y Qu, S Wu, H Li, and G Meng. Three-dimensional free and transient vibration analysis of composite laminated and sandwich rectangular parallelepipeds: Beams, plates and solids. *Composites Part B: Engineering*, 73:96—-110, 2015.

[85] S Srinivas, C V J Rao, and A K Rao. An exact analysis for vibration of simply-supported homogeneous and laminated thick rectangular plates. *Journal of Sound and Vibration*, 12 (2):187—-199, 1970.

[86] S Srinivas and A K Rao. Bending, vibration and buckling of simply supported thick orthotropic rectangular plates and laminates. *International Journal of Solids and Structures*, 6(11):1463–1481, 1970.

[87] A K Noor. Free vibrations of multilayered composite plates. *AIAA Journal*, 11(7):1038—-1039, 1973.

[88] J Fan and J Ye. An exact solution for the statics and dynamics of laminated thick plates with orthotropic layers. *International Journal of Solids and Structures*, 26(5-6):655–662, 1990.

[89] A Messina. Three-dimensional free vibration analysis of cross-ply laminated rectangular plates through 2D and exact models. *Mechanics of Advanced Materials and Structures*, 19 (4):250–264, 2012.

[90] W Q Chen and C F Lü. 3D free vibration analysis of cross-ply laminated plates with one pair of opposite edges simply supported. *Composite Structures*, 69(1):77–87, 2005.

[91] C F Lu, W Q Chen, and J W Saho. Semi-analytical three-dimensional elasticity solutions for generally laminated composite plates. *European Journal of Mechanics - A/Solids*, 27: 899–917, 2008.

[92] J Z Zhang, T Y Ng, and K M Liew. Three-dimensional theory of elasticity for free vibration analysis of composite laminates via layerwise differential quadrature modelling. *International Journal for Numerical Methods in Engineering*, 57(13):1819–1844, 2003.

[93] S A Eftekhari and A A Jafari. A simple and accurate mixed FE-DQ formulation for free vibration of rectangular and skew Mindlin plates with general boundary conditions. *Meccanica*, 48(5):1139–1160, 2013.

[94] E Hanukah and S Givli. Free vibration of an isotropic elastic skewed parallelepiped - a closed form study. *European Journal of Mechanics, A/Solids*, 53:131–142, 2015.

[95] S Kapuria and N Dhanesh. Three-dimensional extended Kantorovich solution for accurate prediction of interlaminar stresses in composite laminated panels with interfacial imperfections. *Journal of Engineering Mechanics*, 141(4):Art. No. 04014140, 2015.

[96] E I Bespalova. Determining the natural frequencies of an elastic parallelepiped by the advanced Kantorovich-Vlasov method. *International Applied Mechanics*, 47(4):410–421, 2011.

[97] B Huang, J Wang, J Du, Y Guo, T Ma, and L Yi. Extended Kantorovich method for local stresses in composite laminates upon polynomial stress functions. *Acta Mechanica Sinica*, 32(5):854–865, 2016.

[98] A Messina and E Carrera. Three-dimensional free vibration of multi-layered piezoelectric plates through approximate and exact analyses. *Journal of Intelligent Material Systems and Structures*, 26(5):489–504, 2015.

[99] K Xu, A K Noor, and Y Y Tang. Three-dimensional solutions for free vibrations of initially-stressed thermoelectroelastic multilayered plates. *Computer Methods in Applied Mechanics and Engineering*, 141(1-2):125–139, 1997.

[100] E Pan and P Heyliger. Free vibrations of simply supported and multilayered magneto-electro-elastic plates. *Journal of Sound and Vibration*, 252(3):429–442, 2002.

[101] S Kapuria and G G S Achary. Exact 3D piezoelasticity solution of hybrid cross-ply plates with damping under harmonic electro-mechanical loads. *Journal of Sound and Vibration*, 282(3-5):617–634, 2005.

[102] P Kumari, J K Nath, P C Dumir, and S Kapuria. 2D exact solutions for flat hybrid piezoelectric and magnetoelastic angle-ply panels under harmonic load. *Smart Materials and Structures*, 16(5):1651–1661, 2007.

[103] S M Balabaev and N F Ivina. A three-dimensional analysis of natural vibrations of rectangular piezoelectric transducers. *Russian Journal of Nondestructive Testing*, 15(10): 602–606, 2014.

[104] Z Zhang, C Feng, and K M Liew. Three-dimensional vibration analysis of multilayered piezoelectric composite plates. *International Journal of Engineering Science*, 44(7):397–408, 2006.

[105] R Vaghefi, G H Baradaran, and H Koohkan. Three-dimensional static analysis of thick

functionally graded plates by using meshless local Petro-Galerkin (MLPG) method. *Engineering Analysis with Boundary Elements*, 34(6):564–573, 2010.

[106] F Nazari, M H Abolbashari, and S M Hosseini. Three-dimensional natural frequency analysis of sandwich plates with functionally graded core using hybrid meshless local Petro-Galerkin method and artificial neural network. *Computer Modeling in Engineering & Sciences*, 105(4):271—-299, 2015.

[107] G Qing, J Qiu, and Y Liu. A semi-analytical solution for static and dynamic analysis of plates with piezoelectric patches. *International Journal of Solids and Structures*, 43(6): 1388–1403, 2006.

[108] M Feri, A Alibeigloo, and A A P Zanoosi. Three dimensional static and free vibration analysis of cross-ply laminated plate bonded with piezoelectric layers using differential quadrature method. *Meccanica*, 51(4):921–937, 2016.

[109] P Cupial. Three-dimensional perturbation solution of the natural vibrations of piezoelectric rectangular plates. *Journal of Sound and Vibration*, 351:143—-160, 2015.

[110] A Messina and E Carrera. Three-dimensional analysis of freely vibrating multilayered piezoelectric plates through adaptive global piecewise-smooth functions. *Journal of Intelligent Material Systems and Structures*, 27(20):2862–2876, 2016.

[111] G M Kulikov and S V Plotnikova. Three-dimensional exact analysis of piezoelectric laminated plates via a sampling surfaces method. *International Journal of Solids and Structures*, 50(11-12):1916–1929, 2013.

[112] E I Bespalova. Vibrations of polygonal plates with various boundary conditions. *International Applied Mechanics*, 43(5):526–533, 2007.

[113] A Joodaky, I Joodaky, M Hedayati, R Masoomi, and E B Farahani. Deflection and stress analysis of thin FGM skew plates on Winkler foundation with various boundary conditions using extended Kantorovich method. *Composites Part B: Engineering*, 51:191–196, 2013.

[114] A Joodaky and I Joodaky. A semi-analytical study on static behavior of thin skew plates on Winkler and Pasternak foundations. *International Journal of Mechanical Sciences*, 100: 322–327, 2015.

[115] M M Aghdam, N Shahmansouri, and M Mohammadi. Extended Kantorovich method for static analysis of moderately thick functionally graded sector plates. *Mathematics and Computers in Simulation*, 86:118–130, 2012.

[116] F Fallah and A Khakbaz. On an extended Kantorovich method for the mechanical behavior of functionally graded solid/annular sector plates with various boundary conditions. *Acta Mechanica*, 228(7):2655–2674, 2017.

[117] A Fereidoon, A Mohyeddin, M Sheikhi, and H Rahmanid. Bending analysis of functionally graded annular sector plates by extended Kantorovich method. *Composites Part B: Engineering*, 43(5):2172–2179, 2012.

[118] A S Sayyad and Y M Ghugal. On the free vibration analysis of laminated composite and sandwich plates: A review of recent literature with some numerical results. *Composite Structures*, 129:177–201, 2015.

[119] M F Caliri Jr., A J M Ferreira, and V Tita. A review on plate and shell theories for laminated and sandwich structures highlighting the finite element method. *Composite Structures*, 156:63–77, 2016.

[120] A S Sayyad and Y M Ghugal. Bending, buckling and free vibration of laminated composite and sandwich beams: A critical review of literature. *Composite Structures*, 171:486–504, 2017.

[121] A W Leissa. The free vibration of rectangular plates. *Journal of Sound and Vibration*, 31 (3):257–293, 1973.

[122] A W Leissa and J H Kang. Exact solutions for vibration and buckling of an SS-C-SS-C rectangular plate loaded by linearly varying in-plane stresses. *International Journal of Mechanical Sciences*, 44(9):1925–1945, 2002.

[123] E Reissner. The effect of transverse shear deformation on the bending of elastic plates. *Journal of Applied Mechanics*, 12(2):69–77, 1945.

[124] R D Mindlin. Influence of rotary inertia and shear on flexural motions of isotropic elastic plates. *Journal of Applied Mechanics*, 18(1):31–38, 1951.

[125] J N Reddy and A A Khdeir. Levy type solution for symmetrically laminated rectangular paltes using first order shear deformation theory. *Journal of Applied Mechanics*, 54:740–742, 1987.

[126] A A Khdeir. An exact approach to the elastic state of stress of shear deformable antisymmetric angle-ply laminated plates. *Composite Structures*, 11:245–258, 1989.

[127] A A Khdeir. Free vibration and buckling of symmetric cross-ply laminated plates by an exact method. *Journal of Sound and Vibration*, 126(3):447–461, 1988.

[128] W C Chen and W H Liu. Deflections and free vibrations of laminated plates-Levy type solutions. *International Journal of Mechanical Sciences*, 32:779–793, 1990.

[129] Y Xiang and G W Wei. Exact solutions for buckling and vibration of stepped rectangular Mindlin plates. *International Journal of Solids and Structures*, 41(1):279–294, 2004.

[130] S H Hashemi and M Arsanjani. Exact characteristic equations for some of classical boundary conditions of vibrating moderately thick rectangular plates. *International Journal of Solids and Structures*, 42(3-4):819–853, 2005.

[131] A J M Ferreira, C M C Roque, and R M N Jorge. Free vibration analysis of symmetric laminated composite plates by FSDT and radial basis functions. *Computer Methods in Applied Mechanics and Engineering*, 194(39):4265–4278, 2005.

[132] A J M Ferreira, L M S Castro, and S Bertoluzza. A high order collocation method for the static and vibration analysis of composite plates using a first-order theory. *Composite Structures*, 89(3):424–432, 2009.

[133] H T Thai and D H Choi. A simple first-order shear deformation theory for laminated composite plates. *Composite Structures*, 106:754–763, 2013.

[134] T Kant and K Swaminathan. Analytical solutions for free vibration of laminated composite and sandwich plates based on a higher-order refined theory. *Composite Structures*, 51(1): 73–85, 2001.

[135] S S Akavci and A H Tanrikulu. Buckling and free vibration analyses of laminated composite plates by using two new hyperbolic shear-deformation theories. *Mechanics of Composite Materials*, 44(2):145–154, 2008.

[136] K Swaminathan and S S Patil. Analytical solutions using a higher order refined computational model with 12 degrees of freedom for the free vibration analysis of antisymmetric angle-ply plates. *Composite Structures*, 82(2):209–216, 2008.

[137] N E Meiche, A Tounsi, N Ziane, I Mechab, and E A A Bedia. A new hyperbolic shear deformation theory for buckling and vibration of functionally graded sandwich plate. *International Journal of Mechanical Sciences*, 53(4):237–247, 2011.

[138] J L Mantari, A S Oktem, and S C Guedes. Static and dynamic analysis of laminated composite and sandwich plates and shells by using a new higher-order shear deformation theory. *Composite Structures*, 94(1):37–49, 2011.

[139] A Mahi, E A A Bedia, and A Tounsi. A new hyperbolic shear deformation theory for bending and free vibration analysis of isotropic functionally graded sandwich and laminated composite plates. *Applied Mathematical Modelling*, 39(9):2489–2508, 2015.

[140] B Brank. On boundary layer in the Mindlin plate model: Levy plates. *Thin-Walled Structures*, 46:451–465, 2008.

[141] A A Khdeir and J N Reddy. Analytical solution of refined plate theories of cross-ply composite laminates. *Journal Of Pressure Vessel Technology*, 113:570–578, 1991.

[142] A S Abdelnaser and M P Sing. Random response of antisymmetric angle-ply composite plates with Levy boundary conditions. *Composites Part B: Engineering*, 3:817–833, 1993.

[143] H Matsunaga. Vibration and stability of angle-ply laminated composite plates subjected to in-plane stresses. *International Journal of Mechanical Sciences*, 43(8):1925–1944, 2001.

[144] M Tahani and A Nosier. Edge effects of uniformly loaded cross-ply composite laminates. *Materials & Design*, 24(8):647–658, 2003.

[145] P Umasree and K Bhaskar. Analytical solutions for flexure of clamped rectangular cross ply plates using an accurate zig-zag type higher-order theory. *Composite Structures*, 74: 426–439, 2006.

[146] A H Akbarzadeh, M Abbasi, S K Hosseini Zad, and M R Eslami. Dynamic analysis of functionally graded plates using the hybrid Fourier-Laplace transform under thermomechanical loading. *Mechanica*, 46:1373—-1392, 2011.

[147] M Izadi and M Tahani. Analysis of interlaminar stresses in general cross-ply laminates with distributed piezoelectric actuators. *Composite Structures*, 92:757–768, 2010.

[148] S Kapuria. A coupled zig-zag third order theory for piezoelectric hybrid cross-ply plates. *Journal of Applied Mechanics*, 71:604–614, 2004.

[149] S Kapuria and S D Kulkarni. An efficient quadrilateral element based on improved zigzag theory for dynamic analysis of hybrid plates with electroded piezoelectric actuators and sensors. *Journal of Sound and Vibration*, 315(1-2):118–145, 2008.

[150] S Kapuria and P Kumari. Boundary layer effects in Levy-type rectangular piezoelectric composite plates using a coupled efficient layerwise theory. *European Journal of Mechanics-A/Solids*, 36:122–140, 2012.

[151] P Kumari, S Behera, and S Kapuria. Coupled three-dimensional piezoelasticity solution for edge effects in Levy-type rectangular piezolaminated plates using mixed field extended Kantorovich method. *Composite Structures*, 140:491–505, 2016.

[152] A R Akisanya and N A Fleck. Interfacial cracking from the free edge of a long bi-material strip. *International Journal of Solids and Structures*, 34(13):1645–1665,, 1997.

[153] Seiji Ioka, Keiji Masuda, and Shiro Kubo. Singular stress field near the edge of interface of bonded dissimilar materials with an interlayer. *International Journal of Solids and Structures*, 44(18):6232–6238, 2007.

[154] S Kapuria, S Sengupta, and P C Dumir. Three-dimensional piezothermoelastic solution for shape control of cylindrical panel. *Journal of Thermal Stresses*, 20(1):67–85, 1997.

[155] ABAQUS. *STANDARD User's Manual*. Version 6.9-1:2009, 2009.

[156] P Heyliger. Exact solution for simply supported laminated piezoelectric plates. *Journal of Applied Mechanics*, 64:299–306, 1997.

[157] S Kapuria, P C Dumir, and S Sengupta. Three-dimensional solution for shape control of a simply supported rectangular hybrid plate. *Journal of Thermal Stresses*, 22(2):159–176, 1999.

[158] V Giurgiutiu. Tuned lamb wave excitation and detection with piezoelectric wafer active sensors for strucctural health monitoring. *Journal of Intelligent Material Systems and Structures*, 16:291–305, 2005.

[159] P Kumari and S Behera. Three-dimensional free vibration analysis of Levy-type laminated plates using multi-term extended Kantorovich method. *Composite Part B: Engineering*, 116:224–238, 2017.

[160] R M Jones. *Mechanics of Composite Materials*. Taylor & Francis, Inc., London, 1999.

[161] ABAQUS. *STANDARD User's Manual*. Version 6.13-1:2013, 2013.

[162] A Nosier, R K Kapania, and J N Reddy. Free vibration analysis of laminated plates using a layerwise theory. *AIAA Journal*, 31(12):2335–2346, 1993.

[163] K N Cho, C W Bert, and A G Striz. Free vibrations of laminated rectangular plates analyzed by higher order individual-layer theory. *Journal of Sound and Vibration*, 145(3): 429–442, 1991.

[164] S Behera and P Kumari. Analytical piezoelasticity solution for natural frequencies of Levy-type piezolaminated plates. *Revised manuscript submitted to European Journal of Computational Mechanics*, 2017.

[165] M A A Farsangi, A R Saidi, and R C Batra. Analytical solution for free vibrations of moderately thick hybrid piezoelectric laminated plates. *Journal of Sound and Vibration*, 332(22):5981–5998, 2013.

[166] P Heyliger and D A Saravanos. Exact free vibration analysis of laminated plates with embedded piezoelectric layers. *The Journal of the Acoustical Society of America*, 98:1547–1557, 1995.

[167] S Kapuria and G G S Achary. A coupled zigzag theory for the dynamics of piezoelectric hybrid cross-ply plates. *Archive of Applied Mechanics*, 75(1):42–57, 2005.

[168] R Gunes, M K Apalak, and M Yildirim. Free vibration analysis of an adhesively bonded functionally graded tubular single lap joint. *The Journal of Adhesion*, 87(9):902–925, 2011.

[169] E Kreyszig. *Advanced Engineering Mathematics*. Wiley India (P) Ltd, New Delhi, 1999.

[170] H Tai Thai, T K Nguyen, T P Vo, and T Ngo. A new simple shear deformation plate theory. *Composite Structures*, 171:277–285, 2017.

[171] S H Hashemi, M Fadaee, and H R D Taher. Exact solutions for free flexural vibration of lévy-type rectangular thick plates via third-order shear deformation plate theory. *Applied Mathematical Modelling*, 35(2):708–727, 2011.

Brief Biodata of the Author

Susanta Behera was born in the year 1983 in the village Thala situated in Baleswar District of Odisha State. He graduated in Mechanical Engineering from Indira Gandhi Institute of Technology, Sarang, Odisha in the year 2007 and then successively worked in Birla Tyre as management trainee and in Orissa Enginerring College (OEC), Bhubaneswar as a faculty. In July of 2011, he joined in IIT Guwahati to pursue his Master Degree in Machine Design specialization in the Department of Mechanical Engineering. After the completion of M. Tech., he immediately joined for Ph.D. program in the same institute IIT Guwahati in July, 2013, and this research work is carried out during this period.

List of Publications from the Thesis

[1] Coupled three-dimensional piezoelasticity solution for edge effects in Levy-type rectangular piezolaminated plates using mixed field extended Kantorovich method, *Composite Structures* **140**, 491–505, 2016.

[2] Three-dimensional free vibration analysis of levy-type laminated plates using multi-term extended Kantorovich method, *Composites Part B: Engineering* **116**, 224–238, 2017.

[3] Analytical piezoelasticity solution for natural frequencies of Levy-type piezolaminated plates, *Submitted to European Journal of Computational Mechanics.*

[4] Free vibration of Levy-type rectangular laminated plates using efficient zig-zag theory, *Advances in Computational Design* **3(3)**, 213–232, 2018.

[5] Assessment of coupled third order zig-zag theory for the free vibration analysis of Levy-type rectangular cross-ply hybrid composite plates, *Under preparation.*

[6] Accurate estimation of interlaminar stresses for the adhesively bonded piezolaminated plates, *Proc.* 4th Asian Conference on Mechanics of Functional Materials and Structures (ACMFMS 2014), Osaka Institute of Technology, Nara, Japan, 10-13 October, 2014.

[7] Assessment of IZIGT for boundary layer effects in levy-type smart piezolaminated plate, *Proc.* 5th International Congress on Computational Mechanics and Simulation (ICCMS 2014), CSIR-SERC, Chennai, India, 10-13 December, 2014.

[8] Natural frequency of orthotropic laminated plate using extended Kantorovich method, *Proc.* 60th Congress of Indian Society of Theoretical and Applied Mechanics (ISTAM 2015), MNIT, Jaipur, India, 16-19 December, 2015.

[9] Accurate estimation of the influence of adhesive bonding on the free vibration of laminated plates, *Proc.* 2nd International Conference on Mechanics of Composites (MechComp2016), FEUP, Porto, Portugal, 11-14 July, 2016.

[10] Free vibration analysis of piezoelectric plate using mixed-field extended Kantorovich method, *Proc.* 3rd Indian Conference on Applied Mechanics (INCAM 2017), MNNIT Allahabad, India, 5 -7 July, 2017.

[11] Effect of adhesive thickness on the free vibration of arbitrary supported smart plates, *Proc.* 13th International Conference on Vibration Problems (ICOVP 2017), IIT Guwahati, India, 29th November-2nd December, 2017.

[12] Free vibration analysis of levy-type hybrid plates using three-dimensional extended kantorovich method, *Proc.* 2nd International Conference on Structural Integrity (ICONS 2018), IIT Madras, India, 14-17th December, 2018.*Accepted.*